A Conceptual aircraft design methodology for parallel hybrid-electric powertrains

Prediction of engine performance and electric component integration

Jonas Kaminski

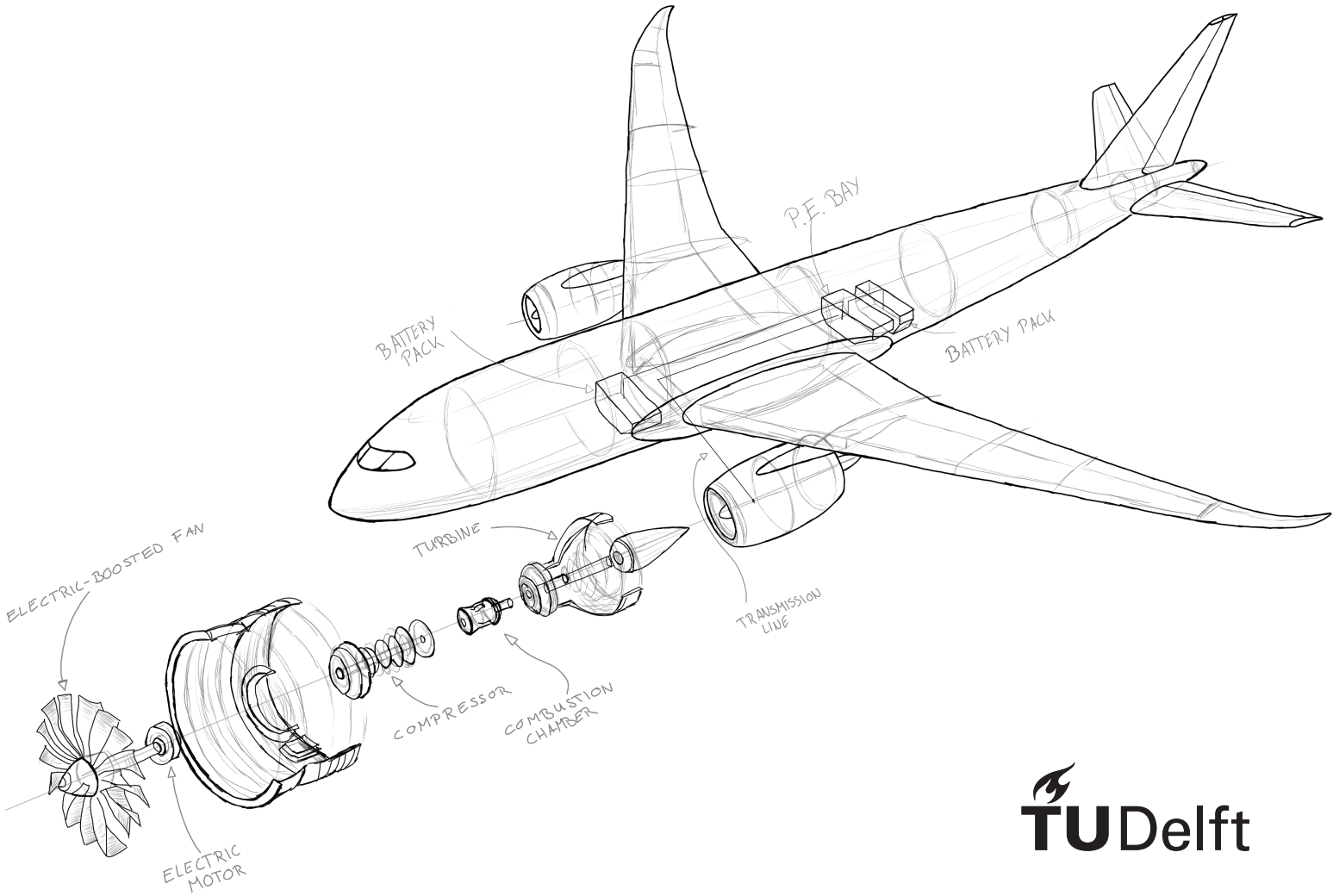

TU Delft

Title image inspired by:[a]

[a] https://www.modelon.com/wp-content/uploads/2020/03/Boosted-Turbofan-Banner-1.png [accessed: 23.06.2020]

A Conceptual aircraft design methodology for parallel hybrid-electric powertrains

Prediction of engine performance and electric component integration

by

Jonas Kaminski

to obtain the degree of Master of Science
at the Delft University of Technology,
to be defended publicly on August 12, 2022 at 1:30pm

Student number:	4171004		
Thesis supervisor:	Dr. ir. R. Vos,	TU Delft	
External Project Supervisor	M.Sc. D. Silberhorn	DLR	
Thesis committee:	Dr. ir. G. La Rocca	TU Delft	Chair
	Dr. ir. M.F.M. Hoogreef	TU Delft	Responsible Thesis Supervisor
	Dr. F. Yin	TU Delft	Examiner

An electronic version of this thesis is available at `http://repository.tudelft.nl/`.

TU Delft

Preface

After my internship at the DLR, my supervisor and I sat down to think of a possible topic for a master thesis to continue our successful collaboration. My enthusiasm for not only aviation, but also to help contribute to meet the challenges of climate change, motivated me to study the potential of hybrid-electric propulsion for the final stage of my master's degree.
Together with my future supervisors at both the TU Delft and the DLR, we agreed on an initial thesis topic to investigate what technology levels would be required for the electric components of a "boosted turbofan" hybrid-electric aircraft concept, such that the resulting aircraft would achieve an overall fuel saving compared to an equivalent conventional turbofan design. This was a twist on the typical research studies, which always assumed a specific available technology level for a given future timeframe. By changing the focus from the available to the required performance of the electric components, the predicted timeframe of introduction into service could be continuously updated as new developments were published.
While working on the thesis, it became apparent that the scope was set too large, as the plan included the development of the necessary sizing methodology that fit the thesis' needs, the creation of two dedicated design tools with an acceptable robustness for the automated generation of various hybrid-electric aircraft concepts, and conducting the actual research study of assessing the required performance assumptions for all included electric components.
We agreed on a new version of the thesis topic, that shifted the focus to the development of the sizing methodology. While still including the creation of the dedicated design tools, this new topic no longer required the extensive research into the necessary component technology levels. The result is presented in this report, an extensive documentation of the challenging work I set out to achieve, and have finally completed.

Foremost, I would like to thank my supervisors, Roelof Vos at the TU Delft, and first Matthias Strack and then Daniel Silberhorn at the DLR, for all their help during this project. It was hard work with many challenges, but I could always count on them to guide and encourage me. Furthermore I want to thank Maurice Hoogreef, who took over as my thesis supervisor for the last weeks while I was preparing for my defence. His help in finalising this project was invaluable. Finally, my heartfelt gratitude goes to my parents, Marina and Odin, and my girlfriend Silvana, for their continued patience and never-ending support.

Jonas Kaminski
Hamburg, July 2022

Abstract

The increasing demand for environmentally friendly air travel has lead to high demand in the investigation of alternate aircraft concepts that help reduce the consumption of fossil fuels. One such concept that has seen intensive study is the implementation of a hybrid-electric propulsion system to partially replace fuel as the energy carrier. As such a propulsion system fundamentally differs from a conventional turbofan, the methods used during the conceptual design of new aircraft have to be significantly adapted to correctly reflect these changes. While various hybrid-electric sizing methodologies exist in literature, a gap was identified for a novel methodology that offers both a high-detail prediction of the resulting hybrid-electric engine performance and an extensive estimation of the mass and position of all necessary components in the hybrid powertrain.

An initial analysis of the methodologies available in published literature provides the starting point for the project. It revealed that the engine performance prediction aspect of all evaluated methodologies can be categorised as following one of two approaches: an "abstract" approach that introduces the hybrid-electric propulsion system in the constraint analysis during the initial sizing, and a "high-detail" approach which focusses on providing a more detailed prediction of the engine performance by creating a more accurate model to be used during the later stages of the conceptual design process. The methods to estimate the added mass due to the electrification of the propulsion system followed the same principle in all publications; the mass of the hybrid-electric powertrain was obtained by individually estimating the mass of the constituent components. While most methodologies used simple methods for the component mass estimation, some included highly detailed model, however the increased accuracy came at the cost of being limited to one specific version of the respective component.

Using the gained insights from the analysis of the published methodologies, a new methodology was devised that aimed to integrate itself into the gap in the existing methods.
The engine performance prediction methodology is based on manipulating user-supplied origin performance maps that represent the fan and engine core performance respectively. Using a set of design sizing points which specify the desired point performance at various points in the flight envelope, these origin performance maps are individually scaled such that the resulting combined performance would abide by all prescribed requirements. Based on the choice of what type of engine configuration is desired, these scaled origin performance maps are then accessed via interpolation to generate a single performance map that represents a coherent hybrid-electric engine design.
Concerning the estimation of the added mass, an electric component sizing methodology was developed that sizes all components in a parallel hybrid-electric powertrain individually. For the sizing of the electric motors, power management and distribution system, circuit protection devices, and the thermal management system, simple models based on the component's specific power are used. The battery sizing is separated into an initial battery system sizing, which determines the optimal number and combination of individual battery packs, such that both the power and energy requirements can be achieved with the given battery pack limitations. Subsequently, the individual battery packs are sized, accounting for either the power or energy requirements being critical. Finally, the transmission lines connecting all electric components are sized automatically. A flexible cable model is used to specify the performance of the desired conductor, and the path taken is approximated as a series of step along the aircraft body axes. The position of each component is assigned based on defined knowledge rules. For the first four component types, a relative position is prescribed: the electric motors inside the respective engine; the PMAD and circuit protection devices inside the power electronics bay; and the thermal management system at the wing-fuselage intersection. The individual battery packs are positioned inside the available cargo space of the fuselage, alternating between the aft and forward fuselage. Each transmission line's equivalent point mass position is computed as the centroid of the assigned line path.

To enable an easy integration into conceptual design processes, both parts of the methodology were implemented into a dedicated design tool. By using the CPACS standard as data interface, these tools offer an inher-

ent compatibility with any other tools that employ this standard. Additionally, two rudimentary conceptual design workflows that support the generation of example aircraft concepts were created. These workflows contain an overall aircraft design tool ("openAD") for concept synthesis, the created engine performance prediction tool, a mission simulation tool ("AMC") to compute the fuel and electric energy requirements, and in the case of a hybrid-electric aircraft concept also the created component sizing tool.

For the verification of the devised methodology, a series of case studies was performed, each providing confirmation of a different part of the devised methodology. In the first case study, the underlying principle of the engine performance prediction was validated by generating example conventional turbofan aircraft concepts that matched the selected reference A320neo's performance. The second case study verified the methodologies' capabilities of sizing a hybrid-electric aircraft concept by generating an example "boosted turbofan" configuration. It's engine performance was qualitatively analysed and matched the expectations, and the estimated increase in the design masses due to the hybrid-electric propulsion system matched with the results of a comparable study from published literature. A third case study investigated the methodology's compatibility with external constraints by prescribing a fixed initial cruise altitude. While the observed increase in design masses was unexpectedly large, the cause was identified to lie in the definition of the prescribed design sizing points. Nonetheless, the observed change in the predicted engine performance correctly reflected the expected changes due to a different active design point, and the individual component mass estimates accurately captured the increase due to the larger demand of stored electric energy. Finally, a fourth case study was performed to investigate the methodology's sensitivity to the provided input data and to demonstrate the unique battery sizing method by re-creating the example concept of the third case study but with an increased specific energy for the battery packs. The resulting example concept exhibited the exact same engine performance behaviour except at a lower magnitude due to the reduced design masses. From the comparison of the two example concepts it could be deduced that the increase in battery specific energy translated into a significant reduction in required battery mass and the correspondingly lighter design. The evaluation of the battery sizing method additionally revealed only an insignificant increase compared to methods that do not consider individual battery pack capacity limitations. Including these constraints into the sizing resulted in an increase in battery mass of only 3–4 %, while enabling a much more accurate estimation of the mass added due to the transmission lines.

Extended Summary

An analysis of the published literature on hybrid-electric sizing methodologies for the conceptual design phase revealed that while the individual methods differed greatly, all methodologies identified the three points where a deviation from the established sizing procedure was required: the prediction of the performance of the hybrid-electric propulsion system (HEPS), the estimation of the mass added due to the electrical propulsion components, and a numeric mission simulation to assess the required amount of fuel and electric energy for a design mission. Although the last point is typically included in any modern conceptual design workflow, it becomes a necessity for the design of HEPS aircraft concepts due to the additional degree of freedom introduced by the dual-energy propulsion system.
The various methodologies' approach to predicting the HEPS engine performance could generally be differentiated into two categories; an abstract approach wherein the initial sizing constraint analysis was adapted to incorporate a dual power source, and a high-fidelity approach which use sophisticated engine analysis tools to either directly analyse the engine performance during each step of the mission simulation, or to create performance maps to be used to predict the resulting engine performance. The latter option was identified as the most promising for the novel sizing methodology, as it fulfilled both the requirements for a high detail performance prediction and limited computational costs. Additionally, it allows for an *inside out* approach to the performance estimation, where the mission simulation tool can access the available performance of a coherent HEPS engine, instead of the *outside in* approach used in the published methodologies, which derives the momentary engine performance during each time step of the mission simulation from the current propulsive power requirements. This also allows the de-coupling of the performance prediction and the mission simulation, enabling the use of any established simulation tools.
Concerning the estimation of the added mass due to the hybrid-electric propulsion system, all published methodologies indicated that a component-based approach was required. Although the methodologies varied in which electric components were considered, at minimum the battery and electric motors were included. The exact methods used to estimate the mass of individual components were often omitted but it was suggested that a simple model consisting of an assumed specific power and the corresponding maximum power encountered by the component were to be used. This same approach was selected for the devised component sizing methodology, with the added aspiration to include not only the component mass but also it's position to allow an assessment of not only the direct impact of the additional mass but also the consequence to the change in the aircraft's balance. To achieve a complete representation of the propulsion system, all relevant electrical components were to be included in the component sizing, with the battery system and the transmission line components being represented by more detailed component models.

Based on the insights gained from the analysis of the published literature, two independent sizing methodologies were devised to address the engine performance prediction and electric component sizing respectively. These methodologies are independent of each other, and can thus be used interchangeably with other equivalent methodologies.
Due to scope limitations, the devised engine performance prediction methodology is only valid for conventional and *parallel* HEPS turbofan configurations, and is based on combining user-provided fan and engine core performance maps into a single coherent engine performance map. Using an arbitrarily large number of prescribed design sizing points, the two provided origin performance maps are individually scaled such that the resulting performance covers all defined point performance requirements. The coherent engine performance map is then generated by interpolating the scaled fan and engine core origin performance maps at the desired sample points — using the altitude, Mach number, and total produced thrust as state variables to define the operating condition — to cover the entire operating envelope. Depending on the methods governing these interpolations, the generated performance map can represent different engine configurations, such as a "boosted turbofan" or a constant power-split ratio. By using performance maps both as starting point and end result, the performance prediction methodology can simultaneously be highly detailed and extremely versatile. Each performance parameter present in the provided origin performance maps can be included in the final engine performance map, appropriately scaled to correctly represent the desired configuration. This allows an easy assessment of secondary engine performance characteristics such as the produced emissions.

The second aspect covered in the devised design methodology is the sizing of the electric powertrain components. As learned from the analysed literature, the electric components of a hybrid-electric propulsion system must be individually sized. To properly represent the propulsion system, and to enable the accurate assessment as to relative importance of different electric component types and impact of changing input assumptions, the devised component sizing methodology incorporates methods to estimate both mass and position of all electric components, not only the battery and electric motors. To allow for sufficient flexibility to represent different variations of the same component type (e.g. different electric motor architectures), the various component models were kept abstract, with four types sized purely based on a prescribed specific power (electric motors, PMAD, circuit protection, and TMS). The battery is represented as a system of interconnected battery packs, with the sizing methodology addressing both the optimal number of connected battery packs and the sizing of the individual packs in terms of mass, volume, position, and final performance capabilities. Finally, the transmission line components used to transfer the electric power between components is separated into dedicated models for the cable conductors, and the combined transmission line connecting distinct components. The component sizing methodology is simultaneously robust to variations in the input data and flexible, supporting the use of two separate battery pack models.

To enable the use of the devised methodology to generate the required example concepts for the verification, two design tools were created that allowed an easy integration into a conceptual design workflow. Both tools use the CPACS standard as data interface, as this allows for an inherent compatibility with many existing design tools. Furthermore, both tools were programmed in a modular structure. This eases any potential adaptation of the existing methods, and facilitates implementation of new methods for additional component models.
The design tool implementing the engine performance prediction methodology consists of three major processes: the scaling of the provided origin performance maps, the generation of the coherent engine performance map via interpolation, and the post-processing procedures. The first processes is an iterative loop wherein both origin performance maps are scaled such that the combined performance corresponds to the determined active design sizing point. For the origin fan performance map this is governed by the produced fan thrust, whereas the origin engine core performance map is scaled according to the required shaft power output. In the second process, the scaled origin performance maps are combined into a single map. Here the modular structure of the tool allows a very easy addition of further *parallel* hybrid-electric performance map types, as each type is implemented as an isolated procedure using the scaled maps as input. Currently, only "augmented" (representing a "boosted turbofan" configuration) and "active" (representing a constant power-split ratio) performance map types are supported. Finally, the post-processing operations allow for extending the generated performance map and computing additional data. In the current state, the post-processing includes the addition of a vector detailing the corresponding electric power draw; the scaling of the fan diameter based upon the assumption of a constant disc loading; the computation of the engine core mass, either from a mass specified in the origin engine core performance map and the effective scaling facotor, or from a prescribed specific engine core power; and the generation of plots to visualise the resulting engine performance map. While the created design tool proved a reliable implementation of the devised methodology, and further provides useful additional features, it could be further improved by utilising multi-core processing. Particularly during the generation of the combined performance map, a process characterised by repeated execution of the same interpolation, this could reduce the tool runtime significantly.
The second created design tool implemented the electric component sizing methodology and automatically sizes all required components, not only for the prescribed requirements but also accounting for the inter-component compatibility. This automation is not limited to the mass estimation, the computation of the component positions is also automated, including geometrical calculations based on the aircraft data stored in the CPACS file. Besides the straight forward application of the stored equations for the general electric components (electric motor, PMAD, circuit protection, TMS), the tool also supports a two-type battery system without restriction on the number of battery packs[b]. Each battery pack is sized as an independent object including a rough estimation of the outer dimensions. This also allows the sizing of the transmission lines to properly reflect the different lengths, as each battery pack is individually positioned. Upon completion of the sizing of the electric components, the individual component efficiencies are used to updated the estimated overall HEPS powertrain efficiency, using average values to account for variations within the same component type. The tool also includes individual mass scaling factors for each component type to allow for

[b] Note, that an excessive amount will cause a computation error, as the available space for battery packs inside the fuselage is exceeded. However, due to the associated massive amount of added mass, this would correspond to an infeasible design anyway.

a calibration of the results to the specific needs of the user. Additionally, mass breakdown plots can be generated to visualise the impact of the sized electric powertrain on the aircraft design masses, and to assess the impact of different component types. The second design tool benefited even more from its modular structure, making the implementation of new component models extremely easy and allowing for the adaptation of existing methods without complication. Although dependent on the estimation of the outer geometry, the positioning method of the battery pack could easily be extended to allow for a placement inside an external pod without impacting the sizing method.

In preparation of the case studies to verify the results obtained from using the devised sizing methodology, two conceptual design workflows were created within RCE. These workflows constitute a rudimentary conceptual design process, reduced to the minimum number of design tools required. For the aircraft concept synthesis, and to update the design for the new masses determined during the design iteration, the overall aircraft design tool "openAD" was used. The two newly created design tools were used to represent the hybrid-electric sizing methodology, and the necessary mission simulation was performed using the tool "AMC", which performs a numerical simulation of the defined design mission and is capable of handling hybrid-electric propulsion systems. As a convergence criteria for the design iteration, the aircraft MTOW and OEM were used, with a convergence tolerance of 10 kg or 0.012 %. These small tolerances demonstrate the consistency of the devised sizing methodology and its design tool implementation, as the produced results must be essentially identical for multiple consecutive design iterations to reach this level of concordance.
All generated example aircraft concepts are sized based on the same TLARs, derived from the A320neo performance, requirements set by the certification specifications or the ICAO Annex 6 Part I, or to prescribe an outer geometry similar to the chosen reference aircraft. For the hybrid-electric aircraft concepts, the same performance assumptions of the electric components were used, with the exception of one concept which increased the battery specific energy by 30 %.
For the engine performance prediction, three design sizing points were defined for all concepts, with the HEPS "boosted turbofan" concept requiring one additional point performance requirement. The three main design sizing points prescribe the required performance for a static *takeoff* at sea-level; the desired engine performance at *top of climb*; and the required thrust at *mid-cruise_climb*, accounting not only for the drag to be compensated, but also for the thrust required to achieve a minimum rate of climb following a potential step-climb. In case of the "boosted turbofan" concepts, a *mid-cruise_steady* design sizing point was added, to prescribe the engine being capable of producing steady cruise thrust on engine core power alone. The desired design power-split ratios of 0.17 and 0.09 for the *takeoff* and *top of climb* design sizing points respectively were based on previous research from literature.
Analogous to using the exact same TLARs, all generated example concepts were sized for the same design mission. It is based on a typical civil transport mission for an A320neo type aircraft, featuring a 2500 nmi design range for the main mission, and includes a cruise to an alternate airport and a 30 min loiter phase. The main mission cruise is restricted to either even or odd thousands flight levels in accordance with the semicircular/hemispheric rule.

To verify that the devised sizing methodology accurately captures the effects of a hybrid-electric propulsion system, a series of four case studies were performed, each intended to prove a specific aspect of the methodology. The assessment of the various example aircraft concepts in each case study is performed via comparison to either an existing aircraft or a previously generated concept; a qualitative analysis of the produced results, particularly in case of the engine performance of the "boosted turbofan" concepts; and by investigating the application of specific methods, such as the unique determination of the number and combination of the battery packs.
The first case study aims to confirm the underlying principle of the engine performance prediction methodology, that two individually scaled fan and engine core performance maps can be combined into a single, coherent engine performance map that accurately represents the target performance. For this purpose, two conventional turbofan example concepts were created by simply prescribing a power-split ratio of 0.0 for each design sizing point. A subsequent comparison to the A320neo revealed a very close match for both concepts, with the concept sized for a fixed initial cruise altitude of 37,000 ft showing very minor differences. The payload-range diagrams confirm the similarity of the concepts, with a coinciding design range point, a very similar amount of payload-fuel displacement, and only a slightly higher range for the example concepts, likely caused by a slightly better TSFC due to the engines being sized to exactly match specification. As all design inputs for the conceptual design workflow were formulated to match the A320neo, this close resem-

blance of the concepts confirms the sizing methodology's capability of accurately predicting a conventional turbofan engine, which proves the underlying principle.
In the second case study, the sizing methodology's ability to generate hybrid-electric concepts is assessed. A "boosted turbofan" aircraft concept is generated, with the mission simulation tool being allowed to vary the initial cruise altitude (ICA) to find the optimum cruise altitude, and compared to the equivalent conventional turbofan concept. The expected increase in the design masses corresponds to the increase encountered in a published study investigating similar concepts for the same design range, and the payload-range diagrams shows the same behaviour while accounting for the increased potential for payload-fuel displacement due to the larger wing. A qualitative analysis of the predicted hybrid-electric engine performance shows a match to the characteristics expected of a "boosted turbofan", particularly the indicative "plateaus" of constant engine core power in the high thrust ranges when electric boost power is supplied. This qualitative performance analysis, combined with the power-usage profile of the design mission, proves that the sizing methodology successfully predicted the engine performance for a "boosted turbofan" HEPS configuration, and the concurrence of the increase in design masses confirms that the additional mass due to the electric powertrain components was estimated correctly, thereby verifying the component mass estimation methods.
The third case study investigates the methodology's compatibility with external constraints. Another "boosted turbofan" concept was generated, identical to the previous case study's with the exception that the ICA is fixed at 37,000 ft. This translates into a higher demand on the engine performance to achieve the required cruise thrust, and thus a heavier design. The observed increase in the concept's design masses was larger than expected, due to a temporary disruption of the mass convergence during the early steps of the design iteration. The cause for this disruption was found to be a repeated switching between the active design sizing point of the performance prediction, alternating between the *mid-cruise_steady* and *mid-cruise_climb* requirements, which resulted in a large and abrupt increase in required battery mass. Further investigation revealed the trigger for the switching to be in the definition of the *mid-cruise_climb* design sizing point, where the maximum output of the engine core was fixed using the previous iterations shaft power required for steady flight, thereby exceeding the engine core power demand of the current iteration. Despite the unexpectedly large increase in design masses, the qualitative analysis of the engine performance showed the anticipated difference to the variable ICA "boosted turbofan" concept, caused by the shift in active design sizing point from *takeoff* to *mid-cruise* conditions. The assessment of the example concept and it's changed engine performance revealed a correctly sized HEPS aircraft concepts, accurately representing the differences caused by the external constraint, which further proves the capabilities of the devised sizing methodology.
Finally, the fourth case study assesses the methodology's sensitivity to small changes in the input data. A third "boosted turbofan" example concept was generated, this time identical to the third study's concept with a fixed ICA except for a 30 % increase in the assumed battery pack specific energy. This concept shows a much reduced increase in design masses compared to the variable ICA "boosted turbofan" concept. Although it encounters the exact same disruption during the early design iteration steps, it is mitigated by the reduced battery mass increase due to the higher specific energy. The predicted engine performance and the corresponding power-usage profile is identical, albeit adjusted for the lower magnitude required by the reduced aircraft mass. The second aim of this case study was to assess the unique battery sizing methodology, both against the typical single pack methods and the non-optimised variation when not adjusting the active C-rate. It was found that representing the battery system as a set of connected individual battery packs with a limited capacity causes only insignificant increases in total battery mass. For the compared fixed ICA "boosted turbofan" battery systems, a single pack battery would result in a mass of only 300 kg less, which corresponds to about 2.9 % and 4.1 % respectively. The comparison of the sized battery system against a comparable system at maximum allowed C-rate showed a reduction by about 1000 kg, which corresponds to about 13 %. The comparison of the two example concepts clearly showed the methodology's ability to capture the impact of the change in the input assumption, and the large degree to which the mass changed indicates, that smaller changes to the input can easily be represented. Additionally, the assessment of the unique battery sizing method confirmed not only it's parity to single-pack methods, but also the proficiency in automatically determining the ideal combination of battery packs.
From the evaluation of all case studies, it can be concluded that the devised sizing methodology is verified to be used in conceptual research studies investigating parallel hybrid-electric aircraft concepts. The underlying principle is valid, the engine performance can be predicted accurately for different active design points, and the estimation of the electric components provides a detailed representation of the hybrid-electric powertrain. It correctly responds to changes in external constraints and is capable of accounting for small variations in the input data.

Contents

List of Figures

List of Tables

Nomenclature

Mathematical Operators

& Greek Symbols	**Designation**	**Unit**
A	Area	m^2
DoD	Depth of Discharge	-
E	Energy	Wh
$e_{sp.}$	specific energy	$Wh \cdot kg^{-1}$
ESAR	Energy Specific Air Range	$m \cdot J^{-1}$
F	Factor (scaling/calibration, mass penalty)	-
g	gravitational acceleration	$m \cdot s^{-2}$
H	Degree-of-Hybridisation	-
I	Current	A
l	length	m
L/D	Lift-to-Drag ratio	-
m	mass	kg
$\dot{m}$	mass flow	$kg \cdot s^{-1}$
N	Amount/Number of	-
P	Power	W
$p_{sp.}$	specific power	$W \cdot kg^{-1}$
Q	Battery Pack Capacity,	Wh
	or Heat	W
R	Range	m
RoC	Rate of Climb	$m \cdot s^{-1}$
S	Wing Reference Area	m^2
SAR	Specific Air Range	$m \cdot kg^{-1}$
T	Thrust,	N
	or Time-interval (during integration)	s
TSFC	Thrust Specific Fuel Consumption	$g \cdot kN^{-1} \cdot s^{-1}$
TSPC	Thrust Specific Power Consumption	$W \cdot N^{-1}$
V	Velocity,	$m \cdot s^{-1}$
	Voltage,	V
	or Volume	m^3
W	Weight	N
X, Y, Z	Position Coordinates along the x-, y-, and z-axis	m
η	Efficiency	-
Φ	Supplied Power Ratio	-
ϕ	Activation Ratio	-
ρ	air Density	$kg \cdot m^{-3}$
ρ_{cable}	linear density of cable	$kg \cdot m^{-1}$
ρ_{energy}	energy density (of battery)	$Wh \cdot m^{-3}$
ρ_{power}	power density (of battery)	$W \cdot m^{-3}$
ϖ	Power Control Parameter	-

Subscripts	**Designation**
0	Sea-Level condition
A/C	AirCraft
avail.	available
avg.	average
bat	battery
cb	cables
comp.	computed or component
distr.	distribution/distributed (relating to power)
ec	electric component
EC	Energy Conversion (efficiency)
eg / emg	electric (motor) generator
EL / elec.	ELectric
el. lead	electric lead (connector at end of electric cable)
EM / em	Electric Motor
env.	environment
f	fuel
FS	Front Spar
GB / gb	GearBox
GT / gt	Gas Turbine
INS	INStalled (power)
max.	maximum
mech.	mechanical
ov	OVerall (efficiency)
P	Propulsive (power)
PE bay	Power Electronics bay
PR	PRopulsive (efficiency)
RS	Rear Spar
sh	shaft (power)
sp.	specific
SUP	SUPplied (power)
term.	termination (HTS cable)
tot	total
TR	TRansmission (efficiency)
trans.	transmission/transmitted (power)
x-sec.	Cross-section

Acronyms	**Designation**
BLI	Boundary Layer Ingestion
CoG	Centre of Gravity
CPACS	Common Parametric Aircraft Configuration Schema
DDP	Deep Discharge Protection
DLR	Deutsches Zentrum für Luft- und Raumfahrt
DoE	Design of Experiments
DoH	Degree-of-Hybridisation
DP	Distributed Propulsion
EM	Electric Motor
FPR	Fan Pressure Ratio
HEP(S)	Hybrid-Electric Propulsion (System)
HEV	Hybrid-Electric Vehicle
HMS	Health Monitoring System
HTP	Horizontal Tail Plane
HTS	High-Temperature Super-conducting
ICA	Initial Cruise Altitude
(I)CE	(Internal) Combustion Engine

ICEV	Internal Combustion Engine Vehicle
LHV / FHV	Lower / Fuel Heating Value
LPC	Low Pressure Compressor
LPT	Low Pressure Turbine
MLG	Main Landing Gear
MLW / MLM	Maximum Landing Weight/Mass
MTOW / MTOM	Maximum TakeOff Weight/Mass
OAD	Overall Aircraft Design
OEI	One Engine Inoperative
OEM	Operating Empty Mass
OOP	Object-Oriented Programming
OPR	Overall Pressure Ratio
PE	Power Electronics
PMAD	Power Management And Distribution
RCE	Remote Component Environment tool
SLS	Sea-Level Static
SoA	State of the Art
SoC	State of Charge
TAS	True AirSpeed
TLAR	Top Level Aircraft Requirements
TMS	Thermal Management System
XML	eXtensible Markup Language

I

Sizing Methodology and Case Studies

1 Introduction

With the increasing demand for environmentally friendly air travel, many prominent research institutes and companies have investigated the potential benefits of (hybrid-) electric propulsion systems (HEPS) for commercial aviation [10–17]. Due to the nature of hybrid-electric propulsion, each of those studies had to make significant extensions to their design processes to allow them to use their established design tools. While various methodologies for the conceptual sizing of hybrid-electric aircraft have been published, none followed an *inside out* approach to the prediction of the engine performance. Instead, the methodologies featured a coupled performance prediction – mission simulation procedure, where the mission simulation would solve the momentary engine performance based on the current propulsive power requirements. Additionally, the importance of the subsequent mass estimation aspect is often overlooked, with the determination of the HEPS mass from the computed energy and power requirements typically restricted to a battery and electric motor mass estimate.
The following sections will provide a brief overview of the thesis report, starting with an explanation on why another hybrid-electric sizing methodology for the conceptual design process is useful in Section 1.1. In Section 1.2 the main purpose of the research study is elaborated, which allows the subsequent definition of the research objective and the scope of the study, as well as the precise formulation of the research questions in Section 1.3. Finally, Section 1.4 will provide a detailed outline of the structure of the thesis report.

1.1. Motivation for another Sizing Methodology

Conceptual engine sizing methods for conventional turbofan engines are traditionally regression-based, relating a select few design parameters to the resultant engine mass (and possibly some basic geometric dimensions) according to a large data set of existing turbofan engines [18–20]. Modern conceptual design workflows however, are able to utilise the increased computational power available nowadays to increase the level of detail of the generated aircraft concepts. This typically includes at least more in-depth aerodynamic and structural analyses of the aircraft model, the simulation of the design mission for a more accurate estimation of the fuel requirements, and a detailed estimation of the engine performance within the flight envelope to enable the mission simulation. Each of these analyses is typically provided by one or more dedicated design tools, which are connected to create a coherent aircraft design.
While this is relatively easy to achieve for a conventional turbofan engine — in no small part due to the complete separation of the power production and energy storage sub-systems — the electrification of the propulsion system requires non-trivial extensions to the established sizing methodologies. Essentially all published HEPS sizing methods follow the same philosophy for the mass estimation: estimating the individual electric component masses based on component specific mass properties, with the level of detail of the methodology reflected by the number of electric component types included. The employed methods for predicting the hybrid-electric engine performance however, can be classified as following one of two distinct philosophies.
Some suggested methods focus on a more abstract approach, wherein the established, top-level constraint analysis is adapted to allow the initial assessment of a generic, parallel or series architecture, hybrid-electric aircraft concept. Introducing the hybridisation of the propulsion system at this abstract level of the design formulation allows an investigation of a broad spectrum in the design space, enabling the comparison of many possible configurations. Correspondingly, this approach limits the level of detail to which the hybrid

propulsion system, separated from the overall aircraft performance, can be estimated. The propulsion system in these methodologies is usually represented by a set of power-requirements for various points in the mission profile, without consideration whether these power-requirements result in a coherent engine design.

Alternatively, the second approach taken by the suggested methods focusses on an in-depth, highly detailed analysis of the hybrid-electric engine integration. Methodologies following this approach typically include a high-fidelity engine design/analysis tool, either to create engine performance maps that are used as a basis for the subsequent performance prediction, or by creating a link with the mission simulation and using the tool directly to predict the performance during each simulation step. Especially those methods following the latter implementation allow for a HEPS engine performance prediction capable of simulating engine internal effects caused by the introduction of an additional power source, such as the change in turbine performance due to mechanical power added to the LPT shaft by an electric motor. However, this increased accuracy in the estimation of the engine performance requires the overall aircraft design to be much more detailed, limiting the use of these methods for vast design space exploration. Indeed, most high-fidelity engine analysis tools require highly detailed input-knowledge of the internal engine layout, as they are component based and model each engine component individually.

The novel sizing methodology developed within this project is intended to fit in between those two approaches. To provide a high level of detail in both the prediction of the resulting engine performance as well as the estimation of the resulting change in the propulsion system mass — accounting for both the mass increase due to added electric components as well as the change in the conventional turbine-engine mass due potential down-scaling — without incurring excessive computational cost or requiring detailed sub-component level input data. Such a methodology would allow an exploration of the design space (albeit limited to a specific HEPS architecture) with a high level of accuracy of the created aircraft concepts (although the final HEPS engine performance might deviate due to internal interaction effects). It could even be used in combination with some of the established methods in a workflow that switches to progressively more detailed methodologies as the current aircraft design approaches convergence.

1.2. Project Definition

The main purpose of the project is the development of a novel methodology for the conceptual design phase that allows the sizing of the hybrid-electric propulsion system for a generic transport aircraft. It is intended to generate a medium- to high-detail estimation of the hybrid-electric propulsion system at low computational costs, facilitating an easy assessment of the impact of different technology levels of the electric components. Given the intention for the new methodology to fall in between the extremes of the two types of existing HEPS sizing methodologies — offering a detailed prediction of the performance over the entire operating envelope without incurring the penalty of high computational costs and extensive input data of high-fidelity tools — three fundamental requirements were formulated.

Foremost, the methodology should not be restricted to a specific size of aircraft. While it is impossible to increase the level of detail of the predictions without introducing some kind of limitation, the new methodology should still be valid for a large range of aircraft sizes, from small regional to large long-range airliners. This mainly manifested in a later defined requirement to not use any statistical regression-based methods.

Furthermore, the new methodology must be compatible with the modern conceptual design paradigm, that is, a design workflow connecting many discipline-specific design and analysis tools working in coherence. To increase the ease with which the novel methodology can be integrated into such a design workflow, special care was taken to devise methods with a small number of required input parameters, and to create procedures that were as independent on outside interaction as possible.

Finally, largely influenced by the desire to minimise the dependency on direct interaction with other parts of the sizing process, the new methodology is required to exhibit no coupling between the engine performance prediction and the design mission simulation procedures. By preventing the need for direct interaction of the engine performance estimation and the mission simulation procedures, the design workflow can make use of established design tools to simulate the design mission. Dedicated, discipline-specific tools are usually not only more sophisticated but also much more robust, thus eliminating a further potential source of problems for the aircraft concept convergence. This of course imposes the prerequisite, that the chosen mission analysis tool is capable of handling electric power or energy flow of the engine, similar to the conventional fuel flow. Alternatively, a tool that provides a detailed output of the complete time-step data of the performed simulation would allow for a manual reconstruction of the power-use of the design mission via the generated HEPS engine performance map.

As elaborated in Chapter 2, essentially every published HEPS sizing method not relying on a dedicated engine analysis tool follows an "outside to inside power-path approach" [2]. These methods determine the *required* thrust or propulsive power at each time-step of the mission simulation from the overall aircraft requirements. The required thrust or propulsive power is then used to compute the corresponding power and energy requirement of the engine and electric components, creating a set of required power and energy point performances that the hybrid-electric propulsion system must deliver.
In contrast, the newly developed methodology adheres to a "coherent HEPS engine" approach, wherein a simplified HEPS engine is created whose performance capabilities at each point within the flight envelope are detailed. The methodology combines the known performances of a conventional engine core and fan, according to a set of either desired or required point performances, to create a coherent HEPS engine performance map. This allows the mission analysis tool to access the *available* HEPS engine performance during each time-step of the mission simulation. Essentially, instead of providing a set of power-demand points for the design of the engine, the new methodology provides an estimation of the available performance of an already sized engine. This also reflects, that a sized engine will never optimally meet the power demands of the aircraft at any point in the flight envelope exactly. Additionally, by predicting the performance of a sized HEPS engine the computational effort required for the mission simulation is reduced, as the resulting available engine performance at any point within the flight envelope can simply be interpolated without need of direct performance computations.

Ultimately, any newly devised methodology must be proven to work correctly and reliably. As it is impossible to properly validate the concepts generated according to the devised methodology — no transport aircraft with a hybrid-electric propulsion system have been produced and a comparison with published HEPS aircraft concepts is problematic due to the lack of information on the methods used to generate said concepts — a verification of the methodology's methods and an analysis of generated example concepts must suffice. For this purpose, two dedicated design tools were created, implementing the engine performance prediction and the propulsion system mass estimation aspects of the methodology respectively. These tools were integrated into a rudimentary modern conceptual design workflow, limited to an OAD (overall aircraft design) tool that governs concept generation and mass convergence, a mission simulation tool to obtain an accurate estimate on the required fuel and electric energy demand of the chosen design mission, and the two created sizing tools to predict the HEPS engine performance and the corresponding impact on the aircraft mass and balance.
The verification of the methodology is obtained via an analysis of the produced outputs from the design tools during the generation of various example aircraft concepts, both conventional and hybrid-electric following the "boosted turbofan" architecture. While the two aspects of the methodology are analysed individually — verifying that the produced conventional turbofan engine performance maps match their known behaviour and the generated "boosted turbofan" engine performance maps match the expected behaviour, as well as verifying that all electric component mass estimation and positioning methods are producing the expected output according to the determined input data — the generated example aircraft concepts are also analysed on the vehicle level. The input requirements for both methodology aspects (vehicle level point performances within the flight envelope, and power and energy requirements based on the engine performance throughout the design mission) are dependent on the evolution of the aircraft concept during the convergence-iteration, and the final aircraft concept, while not matching exactly, should still exhibit similar trends as observed in published studies.

1.3. Research Objectives, Scope, and Questions

The definition of the project discussed above provides the details for the formal definition of the research objectives and corresponding questions, as well as a proper limitation of the scope. The main objective as listed below can be separated into three consecutive tasks, addressing the formulation of a new methodology, the creation of means to apply the formulated methodology, and the assessment of the produced outputs. While the first task essentially fulfils the overall objective, the two following tasks are indirectly necessary, as they provide the proof that the devised methodology is indeed providing the required functionality. Each of the defined main tasks is further divided into sub-tasks to provide an overview of the work that has to be performed to accomplish said task.

Devise a conceptual design methodology to generate high-detail predictions for the engine performance and size the electric powertrain components of parallel hybrid-electric aircraft concepts.

I. Devise a methodology for the sizing of a parallel hybrid-electric propulsion system.
   - enable the prediction of the HEPS engine performance throughout the flight envelope *without* the need for repeated calls on high-fidelity engine analysis tools.
   - estimate the additional mass and the corresponding shift in the aircraft's centre of gravity due to the added electrical components.

II. Implement the devised sizing methodology into independent design tools, capable of being integrated into established modern conceptual design workflows.
   - create a stand-alone design tool for the prediction of the HEPS engine performance
   - create a stand-alone design tool for the estimation of the hybrid-electric propulsion system mass

III. Demonstrate that the devised methodology produces accurate and usable results.
   - create rudimentary conceptual design workflow capable of demonstrating devised methodologies.
   - generate conventional reference and example HEPS ("boosted turbofan") aircraft concepts
   - analyse produced outputs of created design tools as well as generated aircraft concepts and compare, where possible, to published aircraft data

Before formulating the official research questions to be answered by this thesis, the project scope has to be limited. Due to the general nature of the project objective and the vastness of the potential of hybrid-electric propulsion, a comprehensive set of restrictions has been formulated in Table 1.1.

Table 1.1: Comprehensive overview of the imposed limitations to the project scope and the corresponding implications for the devised design methodology.

Scope Limitation	Methodology Implication
The methodology is intended for conceptual level of detail	The necessary input parameters of the methodologies must be limited to a low level of detail.
	The employed models to represent the electric components must be completely characterised by a small set of performance parameters (efficiency, specific power/energy, etc.).
The methodology is only applicable for *parallel* hybrid-electric architectures.	The methodology formulated for the prediction of the engine performance is only compatible with direct parallel HEPS architectures.
	The methods defined for estimating the electric component masses are limited to the components expected in a parallel HEPS configuration.
	The knowledge rules defined for estimating the electric component positions within the aircraft are defined according to a parallel HEPS architecture layout.
The methodology is only valid for hybrid-electric *turbofan* aircraft	The engine performance prediction methods assume the electrification of a turbofan engine.
	A potential compatibility with turboprop engine aircraft can be achieved via adaptation of some aspects of the methodology.

Continued on next page

Table 1.1: (cont.) Comprehensive overview of the imposed limitations to the project scope and the corresponding implications for the devised design methodology.

Scope Limitation	Methodology Implication
The methodology is intended for small to moderate level degree-of-hybridisation.	The generated HEPS engine performance prediction does not allow for independent variation in conventional and electric power settings (i.e. obtain the same engine thrust with different combinations of fuel flow and electric power draw).
	Only "boosted turbofan" and constant power-split ratio hybrid-electric performance maps are implemented.
	Despite limitation, the engine performance prediction methodology is theoretically compatible with very large power-split ratios (up to essentially universally electric engine).
	The mass estimation methods are not checking the compatibility of individual electric components or the available space within the aircraft structure.
The methodology is only applicable for battery-based electric energy sources	The mass estimation methodology only implements batteries as electric energy storage devices. Alternatives (fuel cell, photovoltaic, etc.) are not considered.
	The limitation of considered electric storage device does not impact the engine performance prediction methodology.

Finally, based on the defined research objectives and the imposed scope limitations, the official research questions can be formulated. While the main research questions reflects the overall purpose of the thesis, the individual sub-questions not only refine the understanding of the task, but also act as a guide for thesis project.

How can a more detailed prediction of a parallel hybrid-electric powertrain be included in the conceptual design process without the implementation of high-fidelity, component-based engine modelling tools?

a. What aspects of the conceptual design process need to be adapted to enable the generation of a parallel HEPS aircraft design?
b. How can the performance of a parallel HEPS engine be predicted in more detail without a component-based thermodynamic engine analysis?
c. How can the mass added to the aircraft by the hybrid-electric propulsion system be estimated?
d. How can the impact of the added HEPS mass on the aircraft balance be estimated?
e. How can the newly devised methodology be integrated into established modern conceptual design workflows?
f. How can be verified that the devised methodologies provide usable and accurate results?

1.4. Thesis Structure

Due to the large scope of the thesis project, the extensive documentation of the performed work has forced the report to be split into two main parts. Part I contains the chapters detailing the academically relevant aspects of the conducted work, focussing on the novel knowledge gained, while Part II contains supplementary information and addresses the software implementation for those interested in a more in-depth overview.
As the thesis report is quite extensive, an extended summary is provided following the abstract. This summary contains a comprehensive recap of all the work conducted during the thesis project.

Chapter 1 contains the initial motivation for the thesis project; why another conceptual sizing methodology for hybrid-electric aircraft is beneficial, and provides a clear project definition, as well as an official formulation of the research objectives and questions, including a limitation of the project scope.
A concise analysis of similar conceptual sizing methodologies from recent publications is presented in Chapter 2. Six examples of such methodologies are analysed, assessing their suggested approach to the prediction of the engine performance, the integration of the necessary numerical mission simulation, and the estimation of the added HEPS mass. It also includes a brief overview of the gained insights and the implications for the development of the novel methodology.
The description of the devised methodology is presented in Chapter 3. After formulating the requirements for the methodology and analysing how to best integrate it into existing conceptual design processes, both parts of the methodology — the engine performance prediction and individual HEPS component sizing — are described in detail.
Chapter 4 addresses the verification of the devised methodology. It contains an overview of all the information necessary for replication, such as the defined Top-Level Aircraft Requirements, the used definition of the engine performance design sizing points, the design mission for which the aircraft are sized, and how the fuel and energy demand of the ground segments of the mission are updated for the changed engine performance. The verification itself is performed via four case studies, with each subsequent study providing confirmation of a different aspect of the devised methodology.
The final entry in Part I is Chapter 5. It contains the conclusions of the overall thesis project, as well as a set of recommendations for both the continued development of the methodology and potential future research studies.

Part II contains any supplementary information. The concrete integration of the devised sizing methodology into an actual conceptual design process is discussed in Chapter 6. As the only realistic option is the creation of dedicated design tools, the chapter includes first the possible placement of these tools, before providing an extensive description of the created tools themselves.
In Chapter 7 a detailed description of the design workflows used to generate the example concepts from the verification case studies in Chapter 4 is given. As the case studies required both conventional and hybrid-electric aircraft concepts, two dedicated workflows were created, both following the same setup and including a dedicated post-convergence process.
To enable a replication of the performed studies, the exact definition of the design mission using the CPACS standard is provided in Chapter 8. This includes first a brief overview of how a mission definition is structured in CPACS, and then a detailed listing of all prescribed performance parameters of the used design mission.

Finally, Part III contains the appendices. Appendix A contains additional background information. This includes a general overview of hybrid-electric propulsion systems for aviation, and a detailed discussion of the various electrical components included in the mass estimation methodology.

2

Published HEPS Sizing Methods for the Conceptual Design Phase

Studies about hybrid-electric propulsion for aviation are typically conducted by three major sources: commercial companies such as Boeing and Rolls Royce; national research institutes such as NASA, the DLR, or the NLR; and at universities such as the Delft University of Technology, the Aachen University of Applied Sciences, or the Royal Melbourne Institute of Technology. While all three sources produce papers focussed on assessing the potential benefits of hybrid-electric aircraft concepts (in terms of reduced fuel consumption and emissions or other factors), only projects from the research institutes and universities have published papers about the sizing methodologies themselves. In fact, publications discussing the potential of specific HEPS aircraft concepts, independent of author organisation, contain very limited information on the underlying sizing methods, while simultaneously including novel technologies such as boundary layer ingestion (BLI) and distributed propulsion (DP) in their concepts.

All papers focussing on the sizing methodology have identified the need to adapt two aspects of the design process: the prediction of the hybrid-electric engine performance and the estimation of the mass of the hybrid-electric propulsion system. Most published papers have included a third aspect into their methodology, a detailed point-mass mission simulation, necessitated by their choices of methods for the first two aspects.

Generally, the methods proposed for the HEPS performance prediction can be classified as following one of two approaches: an abstract approach, wherein the thrust-based constraint analysis typical for the initial conceptual design of turbofan aircraft is adapted to be power-based instead; or a high-detail approach, wherein a sophisticated, high-detail engine model (often incorporating a dedicated engine analysis tool) is implemented to simulate the exact behaviour of the specific HEPS engine.

The former is considered "abstract" because the introduction of the electrification in the constraint analysis allows these methods to be applicable to any generic HEPS concept without requiring any specific assumptions on the electric component layout besides the choice of either a *series* or *parallel* architecture. It is characterised by broader, sub-system level assumptions, which allows an investigation of a large area of the available design space at the cost of a less detailed modelling of the hybrid-electric propulsion system. The latter approach, however, is more prevalent in the literature, because the obtained high-detail predictions allow a more accurate estimation of concrete values for the fuel saving potential. A high accuracy in the predictions is essential when performing trade-offs between alternative concepts, but requires a much more detailed definition of the engine, which in turn limits the design freedom.

As the mass estimation approach featured in all published methodologies requires accurate data on the amount of total electric energy and the largest occurring power draw, the conceptual design of a hybrid-electric aircraft concept includes a detailed mission simulation by necessity. Opposed to conventional turbofan aircraft, whose energy demand can be easily estimated via the Breguet range equation, no simple equivalent exists for hybrid-electric aircraft. A few studies (i.a. Voskuijl et al. [21]) have derived an analytical extension of the Breguet equation for their HEPS sizing method, which is usually used exclusively for the first design iterations before being replaced by the typical numerical flight path simulation. It should be noted, that each study that extended their sizing methodology with a mission simulation created a process that featured a direct interaction of the mission simulation and the defined performance prediction. During each

time-step of the mission simulation, the methods call upon the performance methodology, preventing the use of established mission analysis tools.
Finally, all methods presented in the subsequent Sections 2.1 to 2.6 are limited to the aspects corresponding to the sizing of *parallel* hybrid-electric aircraft concepts. Although individual methodologies may provide the means for sizing series HEPS concepts, those aspects of the methods will not be included in this overview.

2.1. Publication: Finger, Bil, and Braun [1]

This study conducted by Finger, Bil, and Braun follows the "abstract" approach for the engine performance estimation. It provides not only a methodology for the initial sizing of generic HEPS aircraft concepts, but also includes an optimisation procedure to identify "[...] the optimal design point of [HEPS] aircraft and especially the corresponding degree of hybridization". While the particular methodology was developed for general aviation aircraft, the underlying principle can similarly be applied for transport aircraft.
The proposed engine performance prediction methodology consists of three consecutive steps: 1. create the constraint lines within the design space from the defined TLARs via conventional relations; 2. convert the thrust-based constraint relations into power-based; 3. adapt the interpretation of the constraint diagram for hybrid-electric propulsion. Steps 1. and 2. are easily achieved via the established sizing methods as well as the propulsive power and efficiency definitions. The third step should not be considered a change to the methods but rather as a novel way to use the established constraint diagram.Because the constraint analysis has used established conventional methods, the indicated power-loading values correspond to the power provided by the conventional engine. The methodology suggests that the design space considered infeasible in conventional conceptual design should be used to indicate the degree-of-hybridisation of power.
As can be seen in the Figure 2.1, at the generic design point "i" an aircraft operating entirely on the ICE engine is capable of satisfying all imposed constraints. Introducing a parallel hybrid-electric propulsion system now allows the design point to move downwards into the previously infeasible region. At 33% hybridisation of the propulsion system (triangle design point in Figure 2.1), the concept easily satisfies the cruise performance constraint on the ICE alone, but requires a small boost of the EM for the rate of climb requirement, and the full support for the takeoff distance performance.

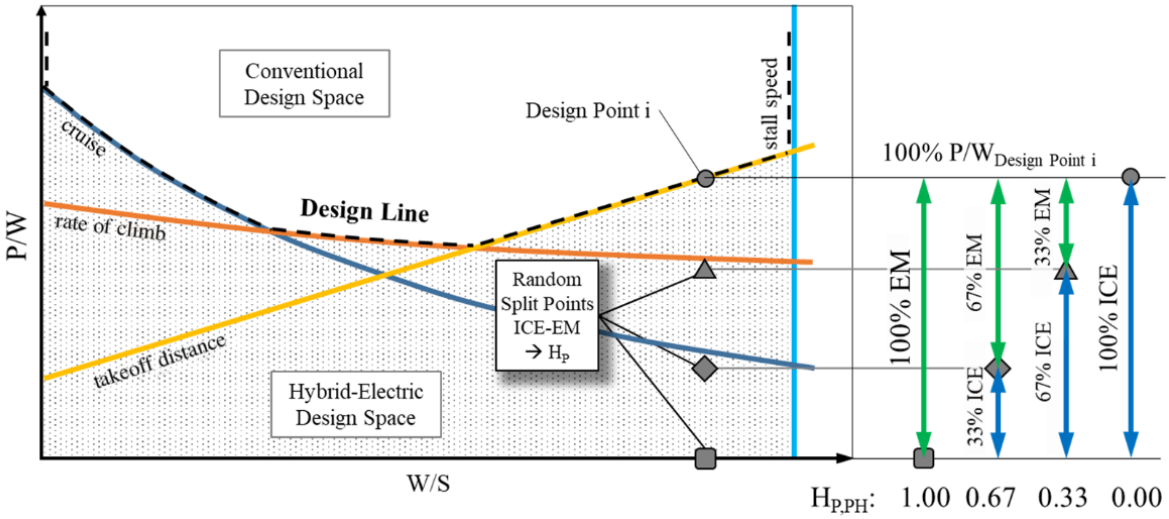

Figure 2.1: Constraint diagram illustrating the design space of a generic parallel hybrid-electric aircraft concept sized according to the methodology by Finger, Bil, and Braun.

Source: [1]

By using the constraint analysis diagram in such a way, the designer is able to identify the exact level of hybridisation required for each defined constraint. In fact, this adapted constraint analysis could be used to determine the required design input power-split values required for the methodology devised in this thesis.

As the performance prediction methodology of this publication is essentially a novel approach to the interpre-

tation of a classic power-based constraint diagram, the corresponding mass estimation methodology is build around using the obtained wing- and power-loadings as well as the selected power DoH $H_{P,PH}$. Figure 2.2, illustrating the process flow of the overall sizing methodology, illustrates the combined mission analysis and mass estimation procedure in detail.

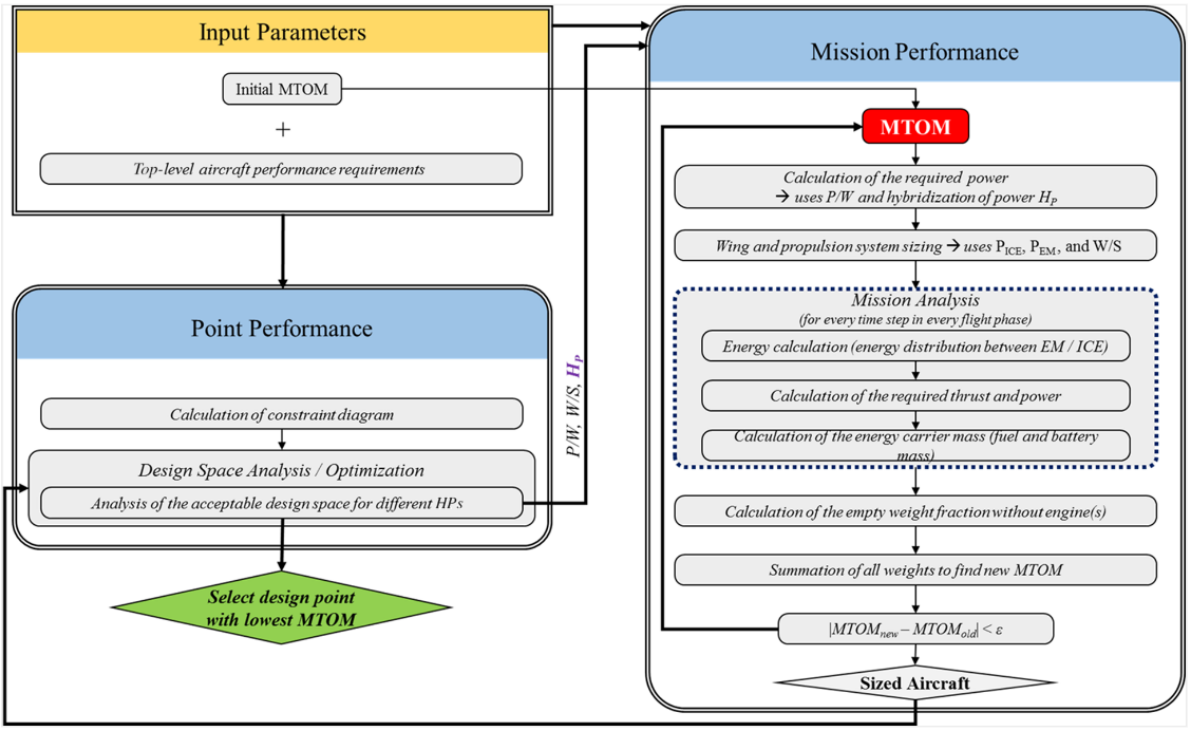

Figure 2.2: Flow chart illustrating the overall HEPS sizing methodology according to Finger et al., highlighting the mission analysis and mass estimation based on only the initial design parameters (wing- and power-loading) and the power-DoH.

Source: [1]

As can be seen in the "Mission Performance" block of Figure 2.2, the mass estimation methodology adapted the standard class-I methods as shown in Equation (2.1). It thus not only provides an estimate of the added mass of the hybrid-electric system, but also redefines the empty mass estimation.

$$MTOW = m_{empty\ w/o\ engine} + m_{propulsion\ system} + m_{fuel} + m_{battery} + m_{payload} \tag{2.1}$$

The mass estimation methodology can be separated into three mass aspects: 1) the propulsion system mass, 2) the energy carrier mass, and 3) the adapted empty mass. Once all part-masses are computed, the MTOW is updated and used as convergence criteria in the aircraft mass iteration as indicated in Figure 2.2.

Propulsion System Mass Assuming an initial MTOW value, the maximum power demanded of the propulsion system can easily be computed from the power-loading at the design point. The paper does not provide any concrete methods on how to estimate the resulting mass of a hybrid-electric propulsion system from only the maximum power and degree-of-hybridisation, as "a wide variety of different mass estimation methods can be used for this step"[1]. It is however implied to use "specific methodologies for the sizing of the propulsion system's components based on empirical and physical modeling [, which] could be based on the mass specific powers of the propulsion system components"[1].

Energy Carrier Mass The mass estimation of the energy carriers in this methodology differs from any other methodology in that it computes the aircraft's energy demand from the *required transport energy* during the whole mission, and uses the design variable of the energy-DoH to divide the energy demand. During each time-step of the mission simulation, the change in total transport energy is computed according to Equation (2.2). This also implies that the flight performance simulation is performed differently to most other

methodologies. Typically, the basic equations of motion are used to simulate the current thrust requirement of the aircraft during each time-step, which is then translated by the engine performance model into a power and finally energy demand. Here, the aircraft flight performance is assessed in an energy-based approach, removing any implications of propulsion system type.

$$\Delta E = \underbrace{\frac{m \cdot g \cdot v}{\left({}^{L}/_{D}\right)} \cdot \Delta t}_{\Delta E_{Aero.Drag}} + \underbrace{\frac{m \cdot \Delta v^2}{2}}_{\Delta E_{Kinetic}} + \underbrace{m \cdot g \cdot RoC \cdot \Delta t}_{\Delta E_{Potential}} \tag{2.2}$$

The required transport energy is then divided into energy from consumable sources (i.e. fuel) ΔE_{fuel} and non-consumable sources (e.g. batteries) $\Delta E_{battery}$ via the assumed design energy-DoH H_E. To relate the energy demand to the respective fuel and battery masses, some additional assumptions about the propulsion system powertrain must be made, particularly the component efficiencies and the combustion engines brake specific fuel consumption (BSFC). The power demand during each time-step for the combustion engine and the electric motor can then be computed via Equations (2.3) and (2.4) respectively, with the "shaft-to-thrust" efficiencies $\eta_{shaft \rightarrow Thrust,\ ICE}$ and $\eta_{shaft \rightarrow Thrust,\ EM}$ according to the efficiency chains shown in Figure 2.3a. Similarly to the propulsion mass estimation method, the paper does not provide any concrete methods for the component efficiency and ICE BSFC estimation.

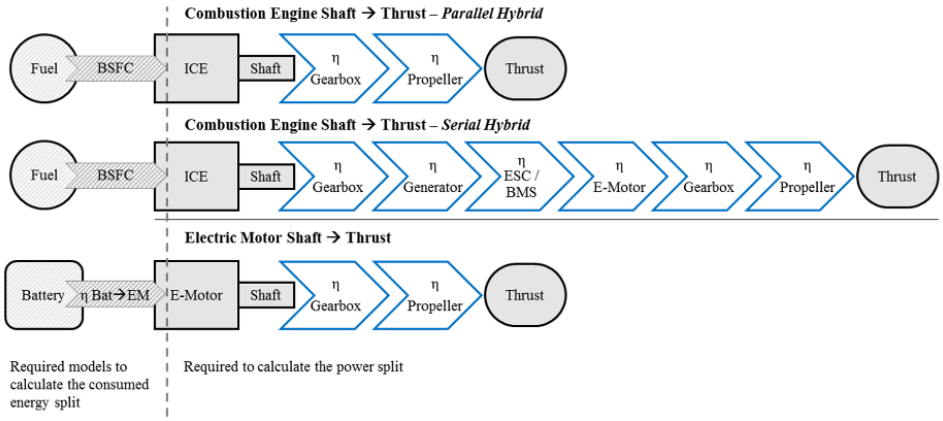

(a) Efficiency chains component breakdown from power converter to produced thrust

Source: [1]

(b) Efficiency chain from battery energy source to produced thrust

Source: [1]

Figure 2.3: Schematic overview of the various efficiency chains used in the mass estimation methodology of Finger et al.

$$P_{ICE} = \frac{\Delta E_{fuel}}{\eta_{shaft \rightarrow Thrust,\ ICE} \cdot \Delta t \cdot N_{ICE}} \tag{2.3}$$

$$P_{EM} = \frac{\Delta E_{battery}}{\eta_{shaft \rightarrow Thrust,\ EM} \cdot \Delta t \cdot N_{EM}} \tag{2.4}$$

Finally, the amount of fuel required and the increase in battery mass corresponding to the change in transport energy of the current time-step are computed by Equations (2.5) and (2.6). Both equations include a term to account for unusable energy stored (trapped fuel(tf) and deep discharge protection (ddp)) and the efficiency required for the battery mass estimation combines the entire powertrain from battery to thrust according to Figure 2.3b.

$$\Delta m_{fuel} = (1+tf) \cdot P_{ICE} \cdot N_{ICE} \cdot BSFC \cdot \Delta t \tag{2.5}$$

$$\Delta m_{battery} = (1+DDP) \cdot \frac{\Delta E_{battery}}{\eta_{battery \rightarrow Thrust} \cdot e_{sp.,\, battery}} \tag{2.6}$$

Adapted Empty Mass Traditional Class-I mass breakdowns include the engine in the empty mass estimation. Due to the introduction of the separate mass estimate for the propulsion system, a new regression analysis was performed to derive a statistical relation between MTOW and empty mass without engines. Because the publications focussed on general aviation aircraft, the obtained relation as shown in Equation (2.7) is limited for aircraft of this class. However, the same methodology can be used to derive expressions for other aircraft sizes.

$$\left(\frac{m_{empty\ w/o\ engine}}{MTOW}\right)_{Gen.\ Aviation} = 0.743 \cdot MTOW^{-0.06} \tag{2.7}$$

2.2. Publication: Zamboni, Vos, Emeneth, and Schneegans [2]

The study by Zamboni et al. combines an "abstract" performance prediction methodology based on a constraint analysis for the sizing of the propulsion system with a more in-depth breakdown of the individual powertrain component powers for the computation of the required amounts of fuel and electric energy during the mission simulation. While the methodology presented in the paper is applied to the hybridisation of turboprop aircraft, it explicitly states that "a similar approach could be used for jet-aircrafts using turbofans"[2].

Figure 2.4 depicts the overall process flow of the entire methodology, further illustrating the three identified aspects — engine performance prediction, numerical mission simulation, and component mass estimation — which separate the HEPS sizing methods from the conventional process. As stated, the performance prediction methodology is twofold, accounting for the constraint analysis used for the initial sizing as well as providing most of the methods used during the point mass analysis.

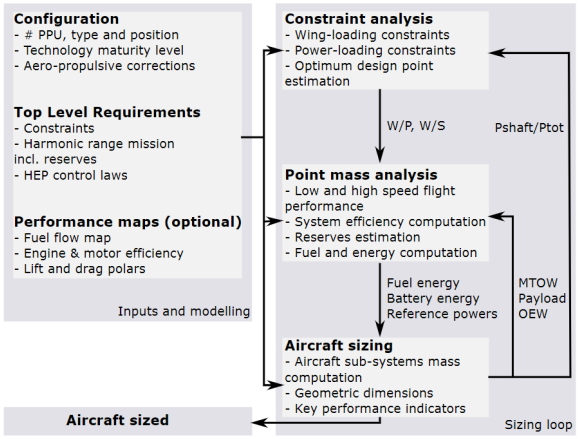

Figure 2.4: Flow chart illustrating the overall procedure for the conceptual design of a hybrid-electric aircraft according to the methodology proposed by Zamboni et at.

Source: [2]

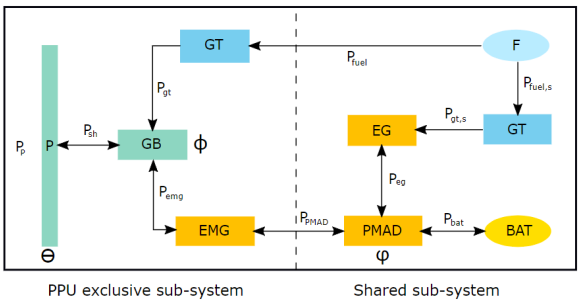

Figure 2.5: Schema of the generic propulsion power unit used in the methodology from Zamboni et al.

Source: [2]

The constraint analysis is initiated according to the established methods for the sizing of conventional aircraft. Depending on the configuration of the desired HEPS concept, this results in a constraint matching diagram relating the wing-loading to either the power-loading for turboprop, or the thrust-to-weight ratio for turbofan aircraft. As stated in the paper, during the sizing of a HEPS concept a power-based constraint diagram is preferred to a thrust-based one, because the internal components of the hybrid-electric propulsion system are sized according to their power requirements. However, although the sizing of a hybrid-electric turboprop concept is at an advantage, as "the propulsive power results are valid for conventional and hybrid electric designs alike since the underlying assumption of equilibrium of forces over a point is detached from

any definition of the propulsion system architecture"[2], both thrust- and power-based constraint diagrams must be converted into shaft power loading. The paper identified four aspects for which the constraint lines need to be corrected: 1. aero-propulsive interaction; 2. propulsive efficiency; 3. atmospheric and flight speed conditions; and 4. one engine inoperative (OEI) conditions. Factors 1. and 4. are included to account for changes due to novel technologies that may have been enabled by the hybridisation of the propulsion system, particularly distributed propulsion. As these technologies are not guaranteed to be included, they are ignored in this summary for brevity.

To correct for the propulsive efficiency, the propulsive power (turboprop) or thrust (turbofan) obtained in the constraint analysis can be related to the engine shaft power via the propeller, or in this case more accurately propulsor, efficiency. The definition provided in Equation (2.8) provides an easy conversion of both propulsive power and thrust into the desired engine shaft power.

$$\eta_P = \frac{P_p}{P_{sh}} = \frac{T \cdot V}{P_{sh}} \tag{2.8}$$

$$\Upsilon = \frac{P_{sh,\,gt}}{P_{sh,\,gt,\,0}} = \left(\frac{\rho}{\rho_0}\right)^k \tag{2.9}$$

To account for the 3. factor, the atmospheric and flight speed conditions, a "power lapse coefficient" (Equation (2.9)) is defined that simulates the degradation in performance of an air-breathing engine due to reduced air density at higher altitudes. Incorporating the power lapse coefficient, and accounting for the segment-specific degree-of-hybridisation, the sea-level based shaft power loading for the constraint analysis can be determined according to Equation (2.10).

$$\frac{W}{P_{sh,\,0}} = \frac{{}^{W}/_{P_{sh,\,gt}}}{\Upsilon} + \frac{W}{P_{sh,\,EM}} = \frac{W}{P_{sh}} \cdot \left(\frac{1 - DoH_{P,\,seg}}{\Upsilon} + DoH_{P,\,seg}\right) \tag{2.10}$$

As already apparent from the flow chart presented in Figure 2.4, the methodology presented in the publication does not explicitly state the methods used to estimate the masses of the electric components. Instead it refers to "the full report of this work"[2], which implies that the specific models used for the component mass estimation are secondary to the methods devised to provide the engine performance to the mission simulation. The following will thus present the methods used during the "point mass analysis" to compute the required fuel and battery energy demands, which will then be used by some methods to estimate the individual component masses. These methods are defined according to the powertrain component breakdown as detailed in Figure 2.5, where each component is represented by a power, re-computed during each time-step according to the required total propulsive power, and an efficiency, which is either assumed constant or obtained from a supplied performance map.
It should be noted, that the publications applies the subsequently presented methodology to the design of a turboprop aircraft concept, therefore the equations provided in the source are in relation to a propeller as propulsive device. However, as hybrid-electric propulsion systems are typically also sized according to power requirements, the only instance where the supplied equations have to be changed for HEPS turbofan implementations is in the method used to predict the propulsor efficiency.

The point mass analysis consists of a mission simulation implemented into Pacelab APD — a commercial software which offers a fully-fledged preliminary aircraft design environment used to model, analyse and optimize aircraft configurations and system architectures — which was designed to simulate a flight profile by connecting an arbitrary number of mission segments. The results of each segment specific performance computations are propagated downstream during the simulation to obtain the resulting final fuel and energy estimates.
The overall performance assessment during each time-step iteration can be separated into a three-step process, consisting of: 1) Propulsive Device Computations, 2) Propulsive System Component Power Computations, and 3) Energy and System Performance Computations. Note, that all the computations detailed below are performed *in addition to* the standard aircraft flight performance calculations using at minimum the basic equations of motion. Depending on the time resolution of the mission simulation, this may equate to a non-trivial extra computational cost for the design process.

Propulsive Device Computations Because the constraint analysis of the preceding "abstract" performance sizing methodology provides a *propulsive power* P_P requirement, a model of the propulsive device efficiency is necessary to convert this into the corresponding *shaft power* P_{sh} requirement. The model proposed by the study for a high-speed propeller was the Actuator Disk Theory, as this provided the best combination of few inputs and fast solutions for an accurate representation of the impact of altitude and flight speed on the resulting efficiency. From this theory, the expression presented in Equation (2.11) was derived to determine the propulsor efficiency, with the correction factor k_{prop} accounting for losses due to non-uniform axial velocities and residual rotational kinetic energy not captured in the computation of the theoretical efficiency. To address the variation in those losses, the correction factor itself is a function of the advance ratio J. Finally, the propeller diameter is computed from the design disk loading, an input parameter here defined as the ratio of shaft power and propeller area, to coordinate the propeller dimensions and performance.

$$\eta_P = \frac{P_P}{P_{sh}} = k_{prop} \cdot \eta_{P,\,theo.}\,, \qquad \text{with } \eta_{P,\,theo.} = \frac{2}{1+\sqrt{1+\frac{T}{\frac{1}{2}\rho\frac{\pi}{4}D^2V^2}}} \tag{2.11}$$

Propulsive System Component Computations Before discussing the equations used to determine the individual propulsion system component power requirements, the "propulsive power unit control parameters" have to be defined. These design parameters allow a time-dependent control of the power-paths in the hybrid-electric propulsion system throughout the simulated mission. The first control parameter, defined at aircraft-level to account for HEPS configurations utilising different types of propulsive units simultaneously (e.g. a parallel architecture combining a conventional turbofan/-prop engine with additional purely electric driven fans, or a concept incorporating electric driven wing-tip fans) is the *propulsive power share*. It defines the ratio of the propulsive power supplied by a specific propulsive device "i" in relation to the required total propulsive power, as defined in Equation (2.12). The second parameter, the *shaft power ratio*, is required for parallel architectures and denotes the share of the shaft power supplied by the electric motor to the propulsor shaft as stated in Equation (2.13). Consequently, the third parameter is essential for series architectures. The *electric power ratio*, defined as the ratio of consumed battery power relative to the total consumed electric power in Equation (2.14), denotes how much of the electric energy is carried on-board via batteries.

$$\Theta_i = \frac{P_{P,\,i}}{P_P} \tag{2.12}$$

$$\phi = \frac{P_{emg}}{P_{emg}+P_{gt}} \tag{2.13}$$

$$\varphi = \frac{P_{bat}}{P_{bat}+P_{eg}} \tag{2.14}$$

Using the control parameters and the propulsor efficiency defined above, the required propulsive power from the flight performance calculations can be used to determine the individual HEPS powertrain component powers. The shaft power at the gearbox P_{gb} of a propulsion unit can easily be computed via the propulsive power share as shown in Equation (2.15).

$$P_{gb} = \Theta_i \frac{P_P}{\eta_P} \tag{2.15}$$

Subsequently, the shaft power requirement at the gearbox can be used to compute the electric motor and gas turbine shaft power requirements P_{em} and P_{gt} according to the defined shaft power ratio as shown in Equations (2.16) and (2.17). Note, that the losses over the gearbox are accounted for in both equations and that the gas turbine shaft power is additionally adjusted for the loss in power due to altitude via the power lapse coefficient Υ as defined in Equation (2.9).

$$P_{em} = \varphi \frac{P_{gb}}{\eta_{gb}} \tag{2.16}$$

$$P_{gt} = \Upsilon\left(1-\varphi\right)\frac{P_{gb}}{\eta_{gb}} \tag{2.17}$$

To assess the power propagation through the electrical system, the PMAD has to be modelled. This model provides a simplified estimation of a complex connection of multiple electric components, varying according to the HEPS architecture, configuration, and design choices such as AC or DC distribution. The power at the PMAD is found via Equation (2.18), while the representative PMAD efficiency can be computed according to Equation (2.19). Note, that the power computation takes into account the efficiency of the cables, while the overall PMAD efficiency is simply the product of the individual electric component efficiencies.

$$P_{PMAD} = \frac{P_{em}}{\eta_{em} \cdot \eta_{cb}} \tag{2.18}$$

$$\eta_{PMAD} = \prod_{i=1}^{n} \eta_{ec,\,i} \tag{2.19}$$

In case of a series HEPS architecture, the shaft power demand of the gas turbine used to power the electric generator can be computed from the PMAD electric power and also related to the electric power output of the electric generator P_{eg}. Equation (2.20) computes the shaft power required of the gas turbine, accounting for losses in the electric generator (η_{eg}), the cables (η_{cb}), and the PMAD (η_{PMAD}), as well as accounting for the altitude power lapse.

$$P_{egt} = \Upsilon \left(1 - \phi\right) \frac{P_{PMAD}}{\eta_{eg} \cdot \eta_{cb} \cdot \eta_{PMAD}} = \Upsilon \frac{P_{eg}}{\eta_{eg}} \tag{2.20}$$

Finally, to enable the computation of the energy demand in the next step, the power demands from the energy carriers, P_{fuel} for the stored fuel and P_{bat} for the installed batteries, are determined in Equations (2.21) and (2.22). The fuel power relates the fuel's specific energy and mass flow to the produced gas turbine power, while the battery power accounts for the losses occurring between the power drawn from the battery and the PMAD. Note, that should multiple gas turbines and/or electric motors be installed in the propulsion system, the respective values for P_{gt} and P_{PMAD} correspond to the sum of the individual component powers.

$$P_{fuel} = \underbrace{e_{sp.,\,fuel}}_{=\,\mathrm{LHV}} \cdot \dot{m}_{fuel} = \frac{P_{gt}}{\eta_{gt}} \tag{2.21}$$

$$P_{bat} = \phi \frac{P_{PMAD}}{\eta_{bat} \cdot \eta_{cb} \eta_{PMAD}} = \frac{P_{bat}}{\eta_{bat}} \tag{2.22}$$

Energy and System Performance Computations Lastly, the aircraft's energy requirements and the overall propulsion system performance can be computed. The energy estimates obtained from the mission simulation are based on the fuel and battery powers determined during each time-step via simple Riemann trapezoidal sums over the entire mission time-steps, either by computing the incremental energy demands during each time-step, or by performing one integration over the individual time-step mass flow and battery power values. The equations provided by the authors follow the second approach, as shown in Equations (2.23) and (2.24).

$$E_{fuel} = \sum_{i=1}^{n} \left[\left(\frac{\dot{m}_{fuel,\,i} + \dot{m}_{fuel,\,i-1}}{2} \right) \cdot e_{sp.,\,fuel} \cdot (t_i - t_{i-1}) \right] \tag{2.23}$$

$$E_{bat} = \sum_{i=1}^{n} \left[\left(\frac{P_{bat,\,i} + P_{bat,\,i-1}}{2} \right) \cdot (t_i - t_{i-1}) \right] \tag{2.24}$$

The overall propulsion system performance is evaluated in terms of the overall efficiency η_{ov} and the two degrees-of-hybridisation DoH_P and DoH_E in Equations (2.25) to (2.27). The efficiency is denotes the overall efficiency of the combined propulsion system, while the DoH values provide the established assessment of the overall electrification of the propulsion system.

$$\eta_{ov} = \frac{P_P}{P_{bat} + P_{fuel}} \tag{2.25}$$

$$DoH_P = \frac{P_{em}}{P_{em} + P_{gt}} \tag{2.26}$$

$$DoH_E = \frac{E_{bat}}{E_{bat} + E_{fuel}} = \frac{E_{bat}}{E_{tot}} \tag{2.27}$$

It should be noted that the values for the fuel and battery power P_{fuel} and P_{bat}, as well as the fuel flow $\dot{m}_{fuel}$, correspond to the power/mass flow required by the sum of all components in the propulsion system.

2.3. Publication: de Vries, Brown, Vos [3]

The final performance prediction methodology following the "abstract" approach is proposed by de Vries et al. [3], and used in papers by i.a. Hoogreef et al. [22]. This methodology shows similarities to the methodology proposed by Zamboni et al. [2], in that the performance prediction is twofold, employing a constraint analysis for the initial sizing and providing a detailed component-power prediction for the mission simulation which determines the energy requirements for the mass estimation. Additionally, the method was devised specifically to include aero-propulsive effects to assess the impact of distributed propulsion on the HEPS concept. For the summary provided here, only the methods relating to the implementation of the hybridisation of the propulsion system are considered. Both these aspects can be seen in the flow chart depicting the general procedure of the methodology as shown in Figure 2.6.

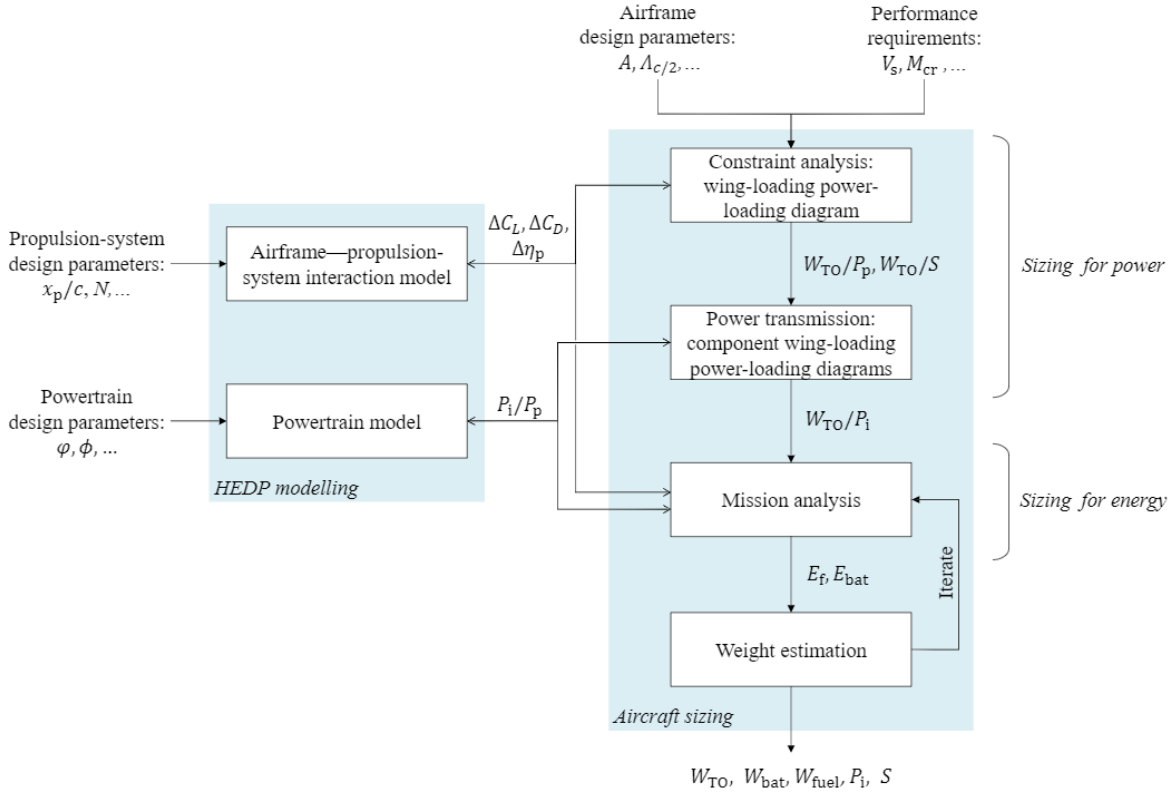

Figure 2.6: Flow chart illustrating the overall procedure for the conceptual design of a hybrid-electric aircraft according to the methodology proposed by de Vries et al.

Source: [3]

The majority of the paper is focussed on the implementation of the aero-propulsive effects and is thus not relevant for the discussion here. Excluding those effects, the methodology for the initial sizing is relatively straight forward and is essentially simply converting a conventional constraint analysis diagram from being expressed in terms of thrust-to-weight into using a power-loading via Equation (2.28). Opposed to the methodology proposed by Zamboni et al., this approach does not include the propulsor efficiency. The power-loading obtained from the constraint analysis is thus not relating the required engine shaft power, but the required propulsive power. This corresponds to the different approach both methodologies take when predicting the individual component powers during the mass estimation procedure.

$$\frac{W}{P_P} = \frac{1}{V \cdot {}^{T}/_{W}} \tag{2.28}$$

The mass estimation methodology of the hybrid-electric propulsion system is largely dominated by the methods to determine the individual component power requirements during the mission simulation. Excluding

the battery, the methodology's approach to estimating the electric component masses is that "If the specific power (kW/kg) of each component of the corresponding powertrain architecture is known, then the complete powertrain weight can be estimated for a given MTOW value, since the power required from each component is determined by its respective power-loading diagram"[3]. Consequently, this summary will again present the methodology's approach to determining the individual component powers during each time-step of the mission simulation.

Opposed to the methodology from Zamboni et al. where the powertrain equations are solved sequentially, this methodology creates a set of linear equations to be solved. The most extensive architecture supported by the methodology is illustrated in Figure 2.7, from which it is apparent that this HEPS powertrain model contains ten unknowns, requiring a set of ten equations. Applying the power balance calculations of Equation (2.29) across each component of the powertrain, seven equations can be obtained.

$$\sum P_{out} = \eta_{comp.} \sum P_{in} \tag{2.29}$$

The remaining three relations can be obtained from the power control parameters dictating the *supplied power ratio* ϕ and the *shaft power ratio* φ (Equations (2.30) and (2.31)), as well as the breakdown of the total propulsive power (Equation (2.32)).

$$\phi = \frac{P_{bat}}{P_{bat} + P_f} \tag{2.30}$$

$$\varphi = \frac{P_{s2}}{P_{s2} + P_{s1}} \tag{2.31}$$

$$P_P = P_{p1} + P_{p2} \tag{2.32}$$

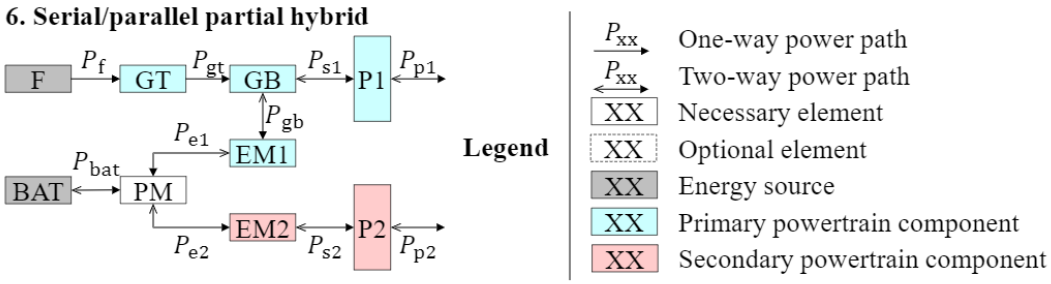

Figure 2.7: Illustration of the most extensive hybrid-electric architecture used in the publication of the sizing methodology by de Vries et al., indicating the potential included components and the possible power-paths.

Source: [3]

Combining all ten powertrain equations into a linear system results in Equation (2.33), where the first seven rows correspond to the power balance equations across the gas turbine, gearbox, primary propulsor, primary electrical machine, PMAD, secondary electrical machine, and secondary propulsor, respectively. The three subsequent rows are created from the auxiliary equations which can be altered according to the user's preference.

$$\begin{bmatrix} -\eta_{GT} & 1 & 0 & 0 & 0 & 0 & 0 & 0 & 0 & 0 \\ 0 & -\eta_{GB} & 1 & 1 & 0 & 0 & 0 & 0 & 0 & 0 \\ 0 & 0 & 0 & -\eta_{P1} & 0 & 0 & 0 & 0 & 1 & 0 \\ 0 & 0 & -\eta_{EM1} & 0 & 1 & 0 & 0 & 0 & 0 & 0 \\ 0 & 0 & 0 & 0 & -\eta_{PM} & -\eta_{PM} & 1 & 0 & 0 & 0 \\ 0 & 0 & 0 & 0 & 0 & 0 & -\eta_{EM2} & 1 & 0 & 0 \\ 0 & 0 & 0 & 0 & 0 & 0 & 0 & -\eta_{P2} & 0 & 1 \\ \phi & 0 & 0 & 0 & 0 & (1-\phi) & 0 & 0 & 0 & 0 \\ 0 & 0 & 0 & \varphi & 0 & 0 & 0 & (1-\varphi) & 0 & 0 \\ 0 & 0 & 0 & 0 & 0 & 0 & 0 & 0 & 1 & 1 \end{bmatrix} \cdot \begin{bmatrix} P_f \\ P_{gt} \\ P_{gb} \\ P_{s1} \\ P_{e1} \\ P_{bat} \\ P_{e2} \\ P_{s2} \\ P_{p1} \\ P_{p2} \end{bmatrix} = \begin{bmatrix} 0 \\ 0 \\ 0 \\ 0 \\ 0 \\ 0 \\ 0 \\ 0 \\ 0 \\ P_P \end{bmatrix} \tag{2.33}$$

Because the linear set of equations in Equation (2.33) is relatively small, it can be solved directly by inverting the coefficient matrix, provided the component efficiencies are assumed constant and not power-dependent.

As these equations have to be solved during each time-step of the mission performance simulation, this low computational cost is an advantage compared to solving them sequentially.

Fuel and Battery Sizing The amount of energy required of both the fuel and batteries can simply be computed during the mission simulation. After solving for the powertrain component powers, the incremental increase in required energy of the battery and fuel are computed according to Equations (2.34) and (2.35). The computed values correspond to exactly the amount of energy required, so any reserve values for either additional fuel or minimum state-of-charge/deep-discharge-protection should be accounted for.

$$\Delta E_{bat} = P_{bat} \cdot \Delta t \tag{2.34}$$

$$\Delta E_f = P_f \cdot \Delta t \tag{2.35}$$

The required fuel mass can simply be determined via the fuel's specific energy, while the required battery mass must account for both the energy and power requirements. The methodology suggests a simple relation of sizing the battery for the energy requirement via a specific energy $e_{sp.,\,battery}$ at pack level, and using the maximum battery power $P_{bat,\,max.}$ in combination with a specific power $p_{sp.,\,battery}$ (also at pack level). To obtain the maximum battery power, the authors suggest using the design power-loading value from the battery-power-loading diagram and the current MTOW . Another option is to select the maximum value for P_{bat} that occurred during the mission simulation when solving Equation (2.33).

Electric Powertrain Components Opposed to the battery mass estimation, all other components masses are, as stated previously,4 simply estimated based on an assumed component specific power $p_{sp.,\,comp.}$, according to Equation (2.36).

$$m_{comp.\,i} = p_{sp.,\,comp.\,i} \cdot P_{comp.\,i} \tag{2.36}$$

2.4. Publication: Pornet, Gologan, Vratny, Seitz, Schmitz, Isikveren, and Hornung [4]

This study conducted by Pornet et al. proposes a conceptual sizing methodology wherein the hybridisation of the propulsion system is introduced via a "flight performance integrated mission performance" analysis. This methodology uses a high-fidelity engine tool to generate various engine efficiency or performance maps, which are then used for the HEPS concept specific engine performance prediction, similarly to the methodology proposed by this thesis.
The overall process flow of the proposed methodology is displayed in Figure 2.8, clearly illustrating how the impact of the hybridisation is introduced via the thrust and energy tables generated by a dedicated "Energy-Power System Performance" module. This follows from the authors desire to develop "a methodology for aircraft using unconventional energy sources capable of being integrated in available sizing and performance programs"[4], which is similar to the requirement formulated for the methodology devised in this thesis.
The driving force in the development of the papers engine prediction methodology was that in "many existing aircraft performance programs, the engine performances are interfaced using look-up tables comprising the thrust and the fuel-flow characteristics according to a given engine rating"[4]. As such, the methodology to predict the engine performance summarised here defines the means to create those required thrust and energy tables, with the energy table being the equivalent to the fuel-flow tables for conventional aircraft. To account for the introduction of a battery-based hybrid-electric propulsion system, the methodology introduced the following design variables:

1. the total installed battery mass $m_{battery,\,totalinst.}$
2. the maximum installed power of the electric motor P_{maxEM}
3. the sea-level static maximum power of the combustion engine P_{SLS}
4. the power setting of the electric motor for each segment $\lambda_{EM,\,seg.}$
5. the power setting of the combustion engine for each segment λ_{CE}

Thrust tables: In contrast to the performance maps used in the methodology devised in this thesis and described in Section 3.2, the thrust tables here contain only the *maximum available* thrust at the sample

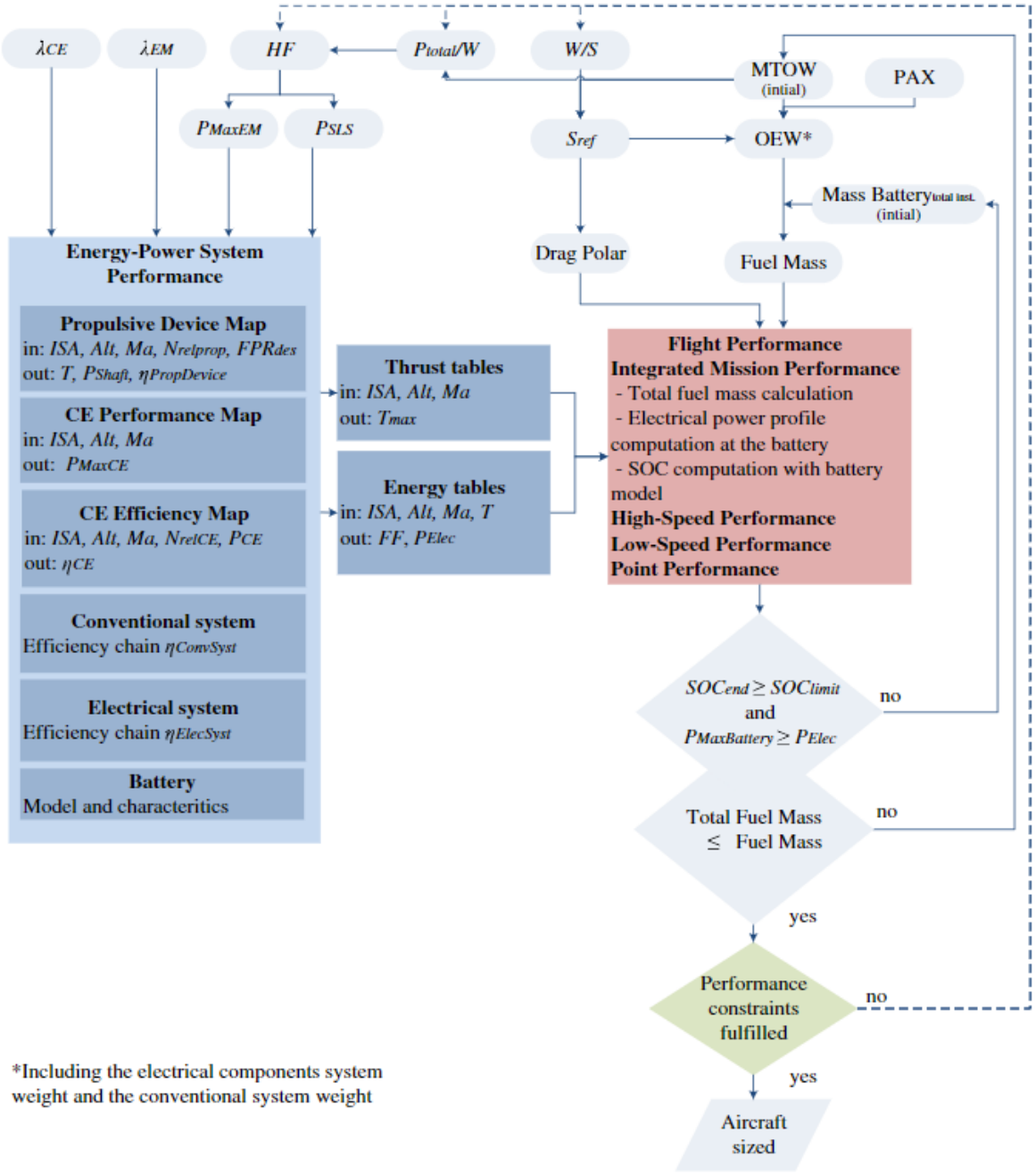

Figure 2.8: Flow chart illustrating the overall procedure for the conceptual design of a hybrid-electric aircraft according to the methodology proposed by Pornet et al.

Source: [4]

flight conditions (state variables here: the deviation from ISA temperature (ISA), flight altitude (Alt), and Mach number (Ma)). The methodology does, however, create multiple thrust tables, corresponding to various relevant thrust ratings, such as maximum takeoff (MTO), maximum climb (MCL), maximum cruise (MCR), maximum continuous (MCNT), and idle (IDL).

For parallel hybrid-electric aircraft, the main focus of this thesis and the only architecture discussed in the paper, the maximum total thrust produced by the propulsor (the only output of the thrust table) is defined in Equation (2.37), derived from the definition of the propulsive efficiency.

$$T_{max} = \eta_{PropDevice} \cdot \frac{P_{MaxConv} + P_{MaxElec}}{V} \tag{2.37}$$

The maximum power terms in Equation (2.37) refer to the maximum *allowed* power from these sources, as indicated by the presence of the power setting design variables λ_{CE} and λ_{EM} in Equations (2.38) and (2.39).

$$P_{MaxConv} = \eta_{ConvSyst} \cdot \lambda_{CE} \cdot P_{MaxCE} - P_{CEOffTake}, \qquad \text{with } \lambda_{CE} = \frac{P_{CE}}{P_{MaxCE}} \tag{2.38}$$

$$P_{MaxElec} = \min\left[\lambda_{EM} \cdot P_{MaxEM};\ \eta_{elecSyst} \cdot \left(P_{MaxBattery} - P_{ElecOffTake}\right)\right], \qquad \text{with} \lambda_{EM} = \frac{P_{EM}}{P_{MaxEM}} \tag{2.39}$$

It should be noted, that the maximum available electric motor power is restricted by two sources: the capability of the motor itself, and the maximum power the battery is capable of delivering. The maximum battery power, obtained via Equation (2.40), is itself dependent on the battery characteristics and the total installed battery mass. This methodology is peculiar in that most methods typically derive the required battery mass from the power demands, instead of limiting the power capabilities based on an assumed initial battery mass as is done here.

$$P_{Maxbattery} = p_{sp,\,battery} \cdot m_{battery,\,totalinst.} \tag{2.40}$$

Finally, the paper defines the electrical system efficiency $\eta_{ElecSyst}$ as the product of the component efficiencies of the PMAD and the electric motor. This implies, that the methodology does not account for the losses occurring in the cables connecting the electric components.

Energy tables: As HEPS equivalent to fuel-flow tables, the energy tables provide two outputs: the fuel flow (FF) of the conventional engine, and the amount of required electrical power P_{Elec}. Both parameters are returned for each combination of flight state (ISA, Alt, Ma) and the selected net engine thrust T. The methodology for the computations for the energy table relies on access to two outside performance maps: the "Propulsive Device Map", detailing the relation between the flight condition and the fan speed, and the corresponding thrust and shaft power; and the "CE Efficiency Map", providing the conventional engine's efficiency for the current flight condition and relative spool speed.
As the energy table data is defined by the flight condition and the total produced thrust, the procedure must first determine the fan speed (supposedly via an iteration to match the output thrust from the propulsive device map with the target thrust) before it can obtain the required shaft power P_{Shaft} directly from the propulsive device map. Using this required shaft power, the power required from the conventional engine is obtained according to Equation (2.41).

$$P_{CE} = \frac{P_{Shaft} - \lambda_{EM} \cdot P_{MaxEM}}{\eta_{ConvSyst}} \tag{2.41}$$

Obtaining the current efficiency of the conventional engine η_{CE} from the "CE Efficiency Map", the current fuel flow can be obtained via Equation (2.42). The required electrical power is simply determined according to Equation (2.43).

$$FF = \frac{P_{Fuel}}{FHV}, \qquad \text{with } P_{Fuel} = \frac{P_{CE}}{\eta_{CE}} \tag{2.42}$$

$$P_{Elec} = \frac{\lambda_{EM} \cdot P_{MaxEM}}{\eta_{ElecSyst}} \tag{2.43}$$

The overarching sizing methodology follows a different approach to the separation of performance prediction and mass estimation than most other methods. Whereas most methodologies begin with a prediction of the performance capabilities of the hybrid-electric powertrain and then use a numerical point mass mission simulation to determine the energy and power requirements for the battery mass estimation, Pornet et al. initiate the HEPS sizing process with an initial battery mass estimate, as illustrated in Figure 2.8. This assumed battery mass is then used in the performance prediction methodology when determining the maximum available electric system power (see Equations (2.39) and (2.40)). Following the mission analysis, the assumed battery mass is updated based on the determined power and energy demands for the next iteration.

Battery Sizing During each time-step of the mission performance analysis, the current flight condition and the corresponding thrust requirement are used to access the generated energy tables to interpolate the current values for the fuel flow and electric power demand. The fuel flow is then integrated over the simulated mission to obtain the total required fuel mass according to Equation (2.44).
The method used to update the battery mass is less clear, as a more detailed battery performance model is implemented, which models the variation in output voltage and efficiency due to battery discharge. Using this model, the battery state of charge SoC at each time-step is computed, which allows the mission simulation to provide the final state of charge SoC_{end} of the battery. Accounting for the difference between current and limit SoC, as well as the difference in maximum supplied and maximum required electric system power, the mass of the battery is updated, as indicated in Equation (2.45).

$$m_{Fuel} = \sum \dot{m}_{Fuel} \cdot \Delta t \tag{2.44}$$

$$m_{Battery} = f\left(SoC_{end},\, SoC_{limit},\, P_{MaxBattery},\, P_{MaxElec}\right) \tag{2.45}$$

Finally, to support the assessment of the HEPS performance, the corresponding amount of energy stored in the battery and fuel can be computed using Equations (2.46) and (2.47). These energy values can then be used to determine the system degree-of-hybridisation for energy according to Equation (2.48).

$$E_{Battery,\,inst.} = m_{Battery,\,totalinst.} \cdot e_{sp.,\,Battery} \tag{2.46}$$

$$E_{Fuel,\,inst.} = m_{Fuel,\,totalinst.} \cdot FHV \tag{2.47}$$

$$DoH_E = \frac{E_{battery,\,inst.}}{E_{Fuel,\,inst.} + E_{Battery,\,inst.}} \tag{2.48}$$

Propulsion System Component Sizing The methodology does not specify explicit methods to estimate either the overall propulsion system mass or the individual component masses. However, the paper presents an overview of the propulsion system component assumptions used in the study, which include the specific power and efficiency of an HTS motor, controllers and converters for the PMAD, and HTS cables. It can therefore be assumed, that the propulsion system mass is estimated by a summation of individual component masses, which in turn are estimated based on their assumed specific power and the maximum power requirements as obtained during the mission simulation.

2.5. Publication: Hecken, Zhao, Iwanizki, Arzberger, Silberhorn, Plohr, Kyprianidis, Sahoo, Valente, Sumsurooah, Sielemann, Coïc, Bordenhagen, Scheunemann, and Jacobs [5]

Another high-detail methodology proposed in two publications, one by Hecken et al. [5] and a previous study by the same team published by Iwanizki et al. [7], was subject to similar demands as the methodology devised in this thesis, particularly with respects to its integration into conceptual design workflows. Figure 2.9a depicts the structure of the design workflow used in the studies by the authors. The methodology combines the prediction of the HEPS engine performance and the estimation of the resulting mass of the propulsion system into a single module, a deviation from the approach taken by all other methods.
Although the methodology is very similar in that it also scales initial performance maps for the fan and engine core to generate a "cumulative" performance map, there are still important distinctions. Most notably, as shown in Figure 2.9b, the inclusion of wing-tip and BLI fans, as well as the combination of performance prediction and mass estimation into a single process. While the additional fans' sizing can easily be separated from the sizing of the main engine, the direct coupling of the convergence of the propulsion system performance prediction and mass estimation is a distinct difference. This coupling results in the electric components being sized for every step of the performance convergence, not just once for the final state. The methodology devised in this thesis instead enables a converged performance prediction to be used by the mission simulation tool. Additionally, the proposed methodology by Hecken et al. employs a sequential process flow for the individual performance map scaling operations, with the updated scaling of the fans occurring only once the entire propulsion system components were sized for the previous iteration state.

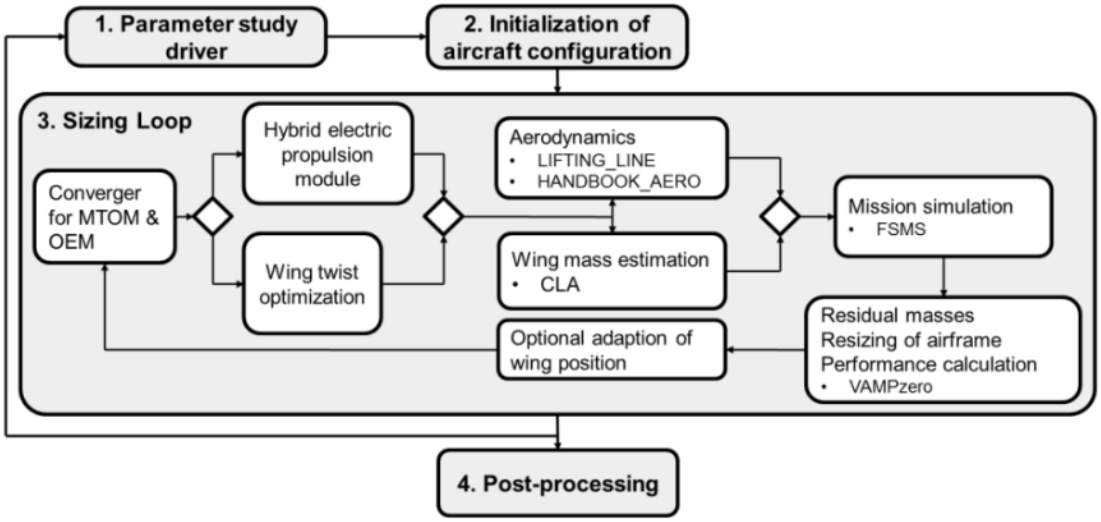

(a) Illustration of the structure of the workflow used by Hecken et al., showing how their HEPS sizing methodology is implemented into the conceptual design workflow.

Source: [5]

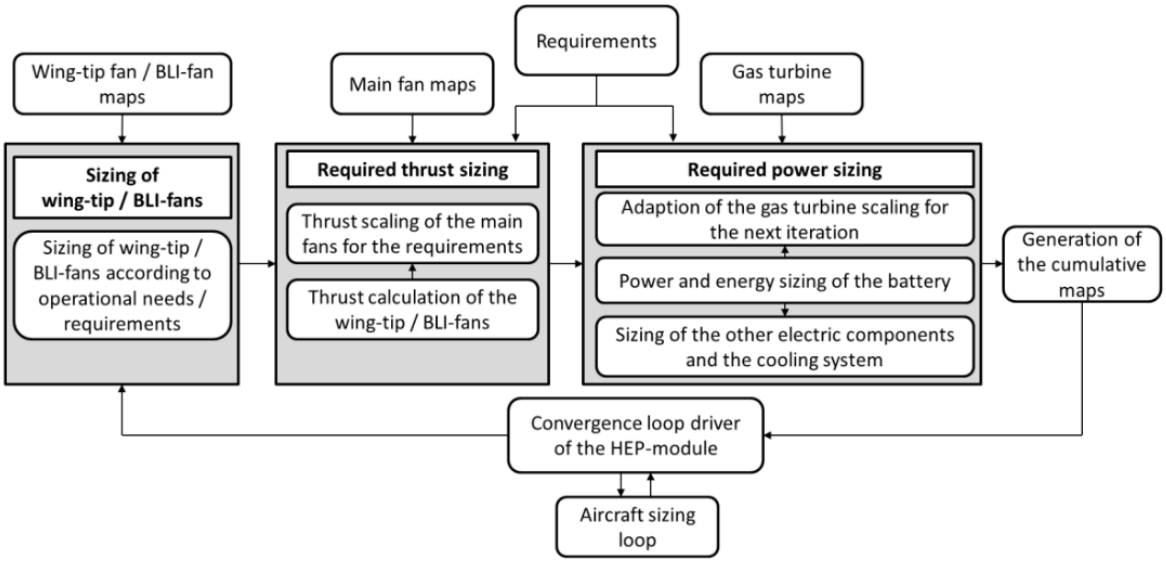

(b) Illustration of the process flow inside the "Hybrid electric propulsion module" from Figure 2.9a, depicting the HEPS sizing methodology (performance prediction *and* mass estimation).

Source: [5]

Figure 2.9: Illustrations of the process integration and the proposed methodology by Hecken et al.

A further similarity between this proposed methodology and the one devised in this thesis is the lack of concrete equations in the performance prediction. Both methodologies are based on the scaling of individual performance maps and the subsequent generation of a "combined performance map" detailing the final performance of the coherent HEPS engine. Thus, the methodologies are less about applying the correct equations but rather about following the correct logical procedure during the implementation into the design tool.

The order of operation for the performance sizing of the procedure shown in Figure 2.9b, excluding potential wing-tip or BLI fans, consists of two iterations performed within a single loop. In the first step, the engine fan's performance is scaled according to the thrust requirements. From this scaled performance map, the resulting shaft power requirements are used, in combination with the power capabilities of the current state of the gas turbine performance, to determine the amount of power that the battery must deliver. From the determined battery power P_{bat}, the current system DoH is determined according to Equation (2.49), which is

used in the first iteration to adapt the gas turbine scaling. The second part of the iteration is the adjustment of the fan thrust requirements to account for the change in gas turbine residual thrust due to the change in scaling.

$$DoH_{Hecken\ et\ al.} = \left(\frac{P_{bat}}{P_{gas\ turbines} + P_{bat}} \right) \tag{2.49}$$

It should be stressed, that the variable used to represent the electric propulsion system during the performance sizing is the electrical power provided by the battery P_{bat} instead of the mechanical power added onto the fan or engine shaft P_{EM} as used in most other methodologies. This choice requires the repeated sizing of each component in the electric powertrain to correctly relate the discrepancy between the required fan and available gas turbine *shaft powers* to the corresponding electrical power drawn from the battery. Choosing a DoH defined in terms of the electric motor instead of the battery power would allow a de-coupling of the performance prediction and mass estimation aspects.

The mass estimation of the HEPS powertrain components is, as apparent from Figure 2.9b, closely coupled to the performance prediction. Generally, it can be separated into a procedure to size the battery component, and another process to estimate the individual masses of all hybrid-electric powertrain components.

Battery Sizing While the power requirement for the battery sizing is supplied directly from the preceding scaling of the fan performance maps and the current gas turbine power capabilities, the energy demand is obtained from the simulation of the design mission during the previous evaluation in the main aircraft sizing iteration. Having established the current requirements for both power and energy, the battery can be sized according to the implemented model. The earlier publication by Iwanizki et al. [7] sizes the battery mass according to the simplified linear interdependency as shown in Figure 2.10. This first order approximation of a battery Ragone plot allows for an optimised mass estimate that "ideally" matches both power and energy demand.

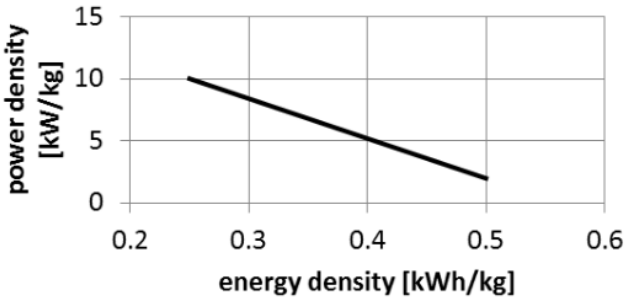

Figure 2.10: Visualisation of the simple battery model used in the sizing methodology of Hecken et al.

Source: [5]

The later publication by Hecken et al. [5], however, uses a more sophisticated battery model. This model, specific to Li-Ion batteries, sizes both the battery pack as well as the associated thermal subsystem required for the cooling of the battery. The battery pack mass, volume, and power losses are estimated based upon the power and energy demands from the propulsion system, the flight duration of the design mission, and the required minimum and reserve state of charge. For the sizing of the thermal subsystem, the model uses the computed power losses and the mass flow rate obtained from the sizing methodology of the on-board thermal management system to regulate the battery temperature range over the mission. It should be noted that while this approach is much more accurate than the one presented in the publication by Iwanizki et al., it not only requires more detailed input parameters about the expected battery performance characteristics, but also relies on the inclusion of a dedicated thermal management system sizing for the overall aircraft. Interestingly, the study by Hecken et al. also included a high-fidelity, component-based engine performance prediction tool to generate tailor-made engine performance maps for the scaling operations. The results discussed in the publication however were created using a fixed gas turbine, due to convergence difficulties.

Propulsion System Component Sizing Figure 2.11 presents an illustration of the general powertrain architecture considered in the methodology. It constitutes a series/parallel configuration, depending on the implementation of additional fans to supplement the parallel hybrid-electric turbofan engine. The schematic provided indicates the type of electrical components that were considered during the propulsion system component sizing of the methodology.

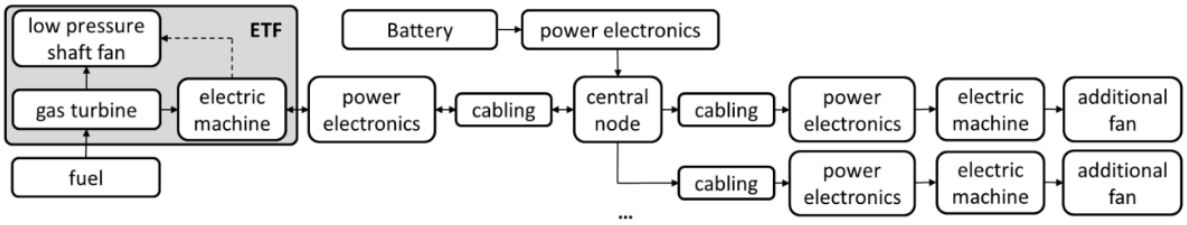

Figure 2.11: Illustration of the general powertrain architecture presented by Iwanizki et al. and used in a simplified "boosted turbofan" configuration in the sizing methodology by Hecken et al. Includes potential additional electrically driven fans for wing-tip propellers or BLI fans.

Source: [7]

The first publication by Iwanizki et al. only states that "[the] electric powertrain components are sized to transmit the maximum power required"[7], while accounting for the impact of preceding electric components. More detail is provided in the publication by Hecken et al. [5], although it is unclear if this constitutes a change between the studies or simply an omission during the first publication. The electric motor sizing selected a specific topology (Permanent Magnet Synchronous Machine PMSM) for which a design tool developed by the University of Nottingham is used. Besides modelling the electromagnetic, thermal and mechanical performance, this tool also calculates the machine's mass. Another detailed model has been implemented for the power electronic converters (PEC), which interfaces with other multidisciplinary subsystem models within the aircraft. This model sizes the performance of the electric power converter, however, the "mass and volume of the PEC, including the PEC modules, cooling system in addition to the controller and control cables, is generated as an output to the structural model of the aircraft"[5]. The exact sizing methods for the propulsion system components are thus not known.

2.6. Publication: Ang, Rao, Kanakis, and Lammen [6]

The final high-detail methodology presented in this overview was used in a study by Ang et al., which analysed the impact of "an assistive electrical system on the performance of a turbofan engine for an A320 class aircraft on a short-range mission"[6]. Opposed to all other publications presented here, this methodology was not devised to enable the conceptual design of generic hybrid-electric aircraft concepts of various levels of specialisation, but instead to retrofit a specific electric propulsions system limited to augment the conventional turbofan engine into an existing A320 class aircraft. Consequently, it focusses less on means to predict the engine performance based on limited inputs, but rather on a sophisticated modelling of the impact on the internal engine behaviour in the presence of electric boost power being provided to the LP spool.
A schematic of the assumed internal engine layout for the electrified turbofan engine is presented in Figure 2.12a. The shown layout is clearly a parallel HEPS architecture, and the restriction that the electric motor is merely intended to assist the engine further constraints this methodology to a "boosted turbofan" concept.
To assess the impact of the electrified propulsion system, the study performed a mission simulation of an A320 for a mission range of 1000 km, using a simulation model developed in MATLAB and Simulink that is based on the basic equations of motion. Access to the corresponding engine performance during the mission simulation is provided by means of sophisticated model of the CFM LEAP-1A engine in GSP, a component-based, 0D thermodynamic analysis tool for gas turbines developed by the NLR and TU Delft.
Figure 2.12b shows the created engine model as seen in the GSP environment, with the required power and current flight condition acting as model inputs. As the model is component-based, the methodology requires a detailed set of input design parameters to accurately represent the internal engine structure, in fact, the paper explicitly mentions scaling "turbomachinery maps [...] and [fine-tuning] using the methodology elaborated by Rademaker". To model the hybrid-electric operation of the engine, the GSP model is extended by adding the additional mechanical shaft power from the electric motor onto the LP shaft.
The impact of the hybrid-electric propulsion system on the overall aircraft weight is limited to the masses

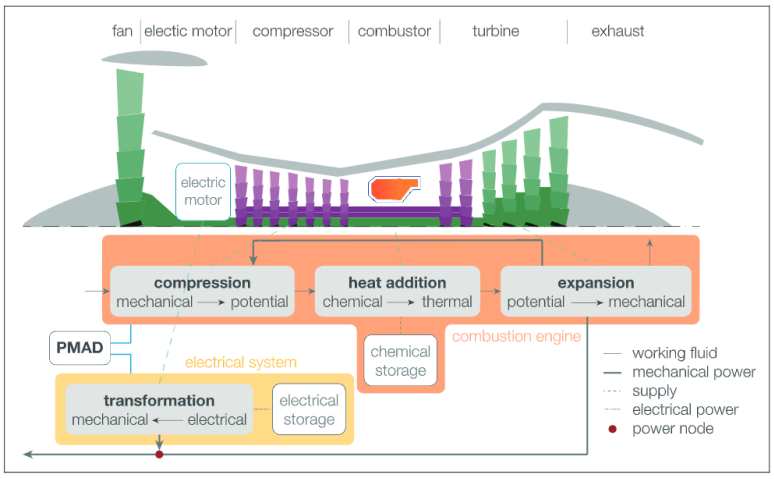

(a) Schematic illustration of the layout of the electrically assisted propulsion system (EAPS) from Ang et al.

Source: [6]

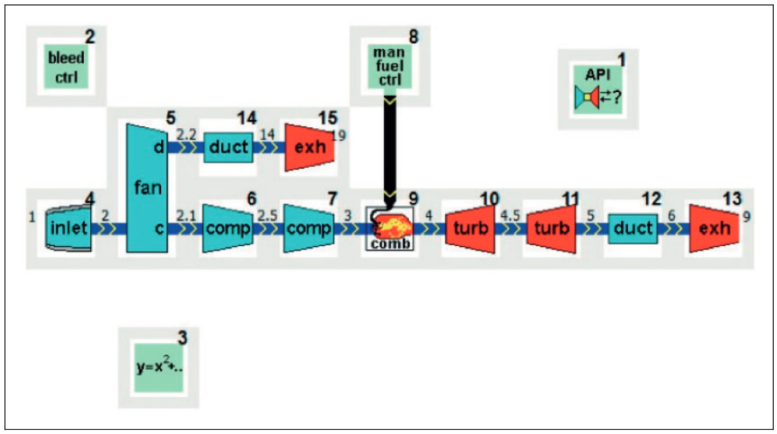

(b) The model of the conventional CFM LEAP-1A turbofan engine in GSP used by the methodology of Ang et al.

Source: [6]

Figure 2.12: Illustration of engine layout and GSP model from the methodology of Ang et al.

added by the battery, the inverter, and the electric motor. These three electrical components are defined by their specific power (and specific energy in case of the battery) and efficiency parameters. Their sizing is governed by the applied power management strategy and the corresponding results of the mission simulation in terms of required electrical energy and the encountered peak powers. No explicit relations are provided, but the supplied component performance characteristics indicates a simple sizing according to specific power and energy.

The estimation of the mass of the scaled turbofan engine is achieved via a statistical correlation to the sea-level static takeoff thrust $F_{SLS,\ TO,lbf}$. This relation is shown in Equation (2.50), where the provided thrust and the resulting mass are provided in pound force and pounds respectively.

$$m_{engine}[lb] = 2.7 \cdot F^{0.75}_{SLS,\ TO}[lbf] \tag{2.50}$$

2.7. Implications for Devised Sizing Methodology

The review of the already published hybrid-electric sizing methodologies has provided insight into both their similarities and differences. Using these insights, the novel methodology can be devised such, that it integrates into this set of methods as an expansion instead, without creating unnecessary redundancy. As apparent from the initial inspection, all considered methodologies address two main aspects: the prediction of the HEPS engine performance, and the estimation of the resulting mass increase due to adding the electric powertrain. While both aspects are equally important in the sizing of the hybrid-electric propulsion system,

they are largely independent from each other in terms of applicable methods. While both influence each other — the added mass of the HEPS powertrain impacting the required engine power, and the sized electric powertrain dictating the amount of electric energy, and thus battery mass, is required to be carried on-board — the underlying methods used for each aspect are mostly de-coupled, allowing an arbitrary combination of the various performance prediction and mass estimation methods.

The published engine performance prediction methodologies themselves can again be separated into two distinct categories: those following an abstract approach, wherein the electrification of the propulsion system is incorporated into the initial sizing via an adaptation of the constraint-diagram analysis; and the high-fidelity approach, which uses high-fidelity design tools, either to generate an initial performance prediction to be further manipulated, or by being used directly during each evaluation of the engine performance.
As mentioned, methodologies following the abstract approach implement the electrification of the propulsion system by adapting the equations used in the initial constraint analysis. This allows for the same methodology to be used to compare vastly different hybrid-electric configurations. This abstract nature however prevents the methodologies from accurately capturing small-scale effects of individual architectures, which reduces the accuracy when comparing similar concepts. The purpose of these methodologies is usually a broad investigation of the design space, providing an initial assessment of the potential of significantly different configurations.
The high-fidelity methodologies in contrast focus on providing a much more detailed representation of one specific hybrid-electric configuration. This is usually achieved by using a high-fidelity engine analysis tool to either create the initial prediction (typically in form of performance maps) which is then tailored to the exact specifications, or by creating a direct representation of the hybrid-electric powertrain within the high-fidelity tool. Creating a direct link to the tool enables a high-detail assessment of the HEPS engine architecture, often composed of component-based, 0D thermodynamic analyses. However, it requires a direct call to the tool every time the engine performance is accessed, which creates a significant demand in computational power. For this reason, the use of performance maps that are adapted to closely represent the desired HEPS engine configuration are often preferred, as this allows for a similar accuracy for a much lower computational power demand.
One aspect shared by both the abstract and high-fidelity approach methodologies is a close coupling between the engine performance prediction methods and the employed mission simulation and analysis methods. Due to the way they are defined, all presented engine performance prediction methodologies must be executed during each time-step of the mission simulation to enable the computation of the required fuel and electric energy demand. Not only does this prevent the use any existing mission simulation methodology/design tool, it also often fails to address how the impact of the engine operating outside it's optimal condition is accounted for. While one study (Pornet et al. [4]) addressed this via the use of a combustion engine efficiency map, most studies simply provide a relation between various component powers (or between a component power and corresponding energy) via a simple efficiency variable, without consideration on how to adapt these efficiencies to represent off-design conditions.
Finally, an interesting observation was made that the published methodologies appear to adhere to an *outside-in approach.* Following this approach, the employed methods determine the required propulsive power during each time-step of the mission simulation, and then translate this propulsive power inwards to compute individual component powers and finally the corresponding required fuel and electric energy. As such, these methods provide the *required engine performance* during each time-step.

In contrast to the engine performance prediction, the various published sizing methodologies provide little information on the mass estimation. All methodologies identify that, due to the nature of hybrid-electric propulsion, a mission simulation is required to determine the amount of electric energy required, and that a component-based estimation method is necessary to represent the entire hybrid-electric powertrain. There is however a difference between the methods on how many of the electric components of the powertrain need to be considered when estimating the final HEPS mass, with some studies considering only the battery and electric motor mass relevant.
Indeed, some of the above publications appear to consider the methods used for the electric component mass estimation to be secondary, simply stating that "Because a wide variety of different weight estimation methods can be used for this step, no models will be presented in this paper"[1]. Generally, the simplest — but also most versatile — component mass estimation methods are based on mass specific power characteristics, which allow a component mass estimation simply based on the maximum amount of electrical power they

encounter.
An exception to this general mass estimation method is the battery component, whose close-coupled dependency between energy and power characteristics require a more detailed component model. The models used to represent the battery component vary widely, from simply using specific energy and specific power values, to type-specific models that replicate a certain battery type down to the cell-voltage characteristics.

The insights gained from the analysis has guide the creation of the novel sizing methodology, both for the engine performance prediction and the electric component mass estimation methods.
For the performance prediction it was deemed important for the methodology to provide a higher level of detail than the abstract approach allows, as the intended use is the assessment of specific HEPS aircraft concepts and the impact of small changes in the design assumptions. However, the direct reliance on high-fidelity analysis tools is undesired due to the high computational costs. This lead to the decision to base the engine performance prediction methodology on the adaptation of original performance maps. Instead of using an engine analysis tool to generate a new performance map during each iteration step, the methodology uses two origin performance maps — obtained either from a single use of a high-fidelity design tool, or by using experimental data from real engines — which are scaled and combined according to the prescribed point performance requirements.
In this, the devised methodology follows an *inside-out approach*, rather than the typical outside-in. The prescribed point performance requirements are used to determine the critical propulsive power and thrust demand, which are then used to size the resulting coherent engine performance. During the mission simulation, each call to assess the current engine performance thus follows from this generated performance map. The methodology thus provides the *available engine performance* instead of creating a set of consecutive power requirements. A further benefit of this *inside-out approach* is that the engine performance prediction methods are de-coupled from the mission simulation. This allows the use of any existing mission simulation method or tool, provided it supports electric power usage.

In relation to the electric component mass estimation methods, the review of the published methodologies had a larger impact than for the performance prediction. While following the same approach of estimating the mass for each electric component separately, the methodology was explicitly designed to include a representation of all required components, not only the battery and electric motors.
Additionally, the methodology includes also an estimation of each electric components position within the aircraft's structure. This allows for the methodology to not only provide an estimate on how much mass is added, but also on how this added mass will impact the centre of gravity of the aircraft. As a large shift in aircraft CoG will impact the stability, and thus the positioning of the wing and tail, this aspect of the methodology allows a further impact to be analysed. The position of each individual component is determined according to formulated knowledge-rules, which account for variable placements due to previously assigned component positions.
Finally, the methodology was devised to incorporate a more detailed battery system sizing method. Instead of modelling the battery as a single large object, the methodology models individual battery packs. This not only allows an assessment of the impact of multiple packs, such as the corresponding CoG shift and the required additional transmission lines, but also better reflects the real world limitations of batteries.

3

HEPS Sizing Methodology

The methodology devised within this chapter is intended to be part of an overarching design process, it is not meant to be a standalone procedure that generates an aircraft concept from scratch. It should be understood as retrofitting a hybrid-electric propulsion system into an established conventional aircraft design, requiring an iterative process to converge the imposed changes on the aircraft concept's weight and balance due to the added electric components, as well as it's changed engine performance. In the formulation of the iterative workflow, it is left to the designer to decide if this involves updating the design for a new maximum takeoff weight (MTOW), or whether the MTOW is kept constant and other masses (e.g. the payload) are adapted. It is important to note, that while the methodology creates a hybrid-electric propulsion system that is retroactively inserted into a conventional design, it can still be internally implemented into any newly written design tool, as any conceptual design generation is in itself an iterative process.

A further focus was set on imposing as little restriction on the design freedom as possible, besides focussing on parallel configurations, and enable a wide variety of design space exploration studies. The methodologies presented in this chapter are thus valid for both normal- and super-conducting implementations of a hybrid-electric propulsion system. In the performance aspect of the sizing methodology the required performance of the propulsion system is determined purely based on the specified power split ratios, any necessary electricity to power the cryo-cooling system can simply be added to the required offtake power or be included during the battery sizing. The distinction between a normal- and super-conducting propulsion system would be introduced in the component sizing methodology. While this does not include any specialised models for super-conducting components, all selected methods are sufficiently generalised that they may represent both normal- and super-conducting components.

Within this chapter, the devised methodology will be explained, beginning with the required extensions to the established design process. For this purpose, the general requirements for the methodology, the gap in the existing methods, and a suggested integration of the new HEPS sizing methods into the existing design process will be discussed in Section 3.1. The subsequent Sections 3.2 and 3.3 contain the detailed explanation of the devised methods for the hybrid-electric engine performance prediction and the individual electrical component sizing respectively.

3.1. HEPS Sizing Process Extension

As stated in the chapter introduction, the aim of the new methodology is to extend the existing conceptual sizing process; to enable the use of the established methods to create hybrid-electric concepts. Most methods currently used are just as valid for HEPS concepts as they are for conventional designs, as the only difference lies in the propulsion chain.

To determine how the traditional conceptual design process can be extended to fulfil this function, it must be explicitly defined what the requirements for the new methodology are, which aspects of the sizing procedure is not yet provided by existing sizing methods, and how the newly devised methods can be integrated into the established design process.

3.1.1. Methodology Requirements

Before creating the actual methodology, it is important to properly formulate all the requirements it has to fulfil. While the scope of this thesis is limited to the creation of a methodology for *parallel* HEPS concepts (see Section 1.3), all requirements listed below are equally valid for any other realisation of a hybrid-electric concept. One of the requirements is included explicitly to facilitate the extension of the methodology for other HEPS configurations. The following five conditions have been identified as the main requirements. They guarantee that the devised methods are not only able to create a valid HEPS concept, but also fulfil other functionalities.

1. The devised methods must be based on physical characteristics, no statistical, regression-based equations may be used.
2. The devised methodology must be compatible with existing design processes.
3. The devised methodology must not be limited to one specific realisation of hybrid-electric propulsion (e.g. "boosted turbofan"); it must be applicable for a variety of HEPS concepts
4. The devised methods must be able to operate without direct interaction with the user.
5. All required input data must be of a low level of detail.

While all requirements are equally important and must be fulfilled, they may either be imposed by circumstances or be an active choice. The following paragraphs will elaborate on the reasoning behind each requirement, and indicate further implications.

1. The devised methods must be based on physical characteristics, no statistical, regression-based equations may be used.

This first requirement is imposed by the very purpose of this methodology: there simply are no actual HEPS aircraft concepts available that could be used to create a statistical basis for a regression. The few aircraft produced that use an electrified propulsion system belong to the general aviation category and are typically used as demonstrators of all-electric propulsion [23]. Furthermore, the use of regression-based equations is per its definition only capable of creating designs similar to what has been done before. The whole purpose of this methodology is to facilitate the generation of novel designs to investigate more of the available design space.

Even if actual aircraft were available as reference, this requirement would still be formulated, as it follows the general trend in conceptual aircraft design to employ more physics-based methods. These methods simply allow a more flexible approach to aircraft design, and are becoming more and more feasible with the increased computational power of modern computers.

2. The devised methodology must be compatible with existing design processes.

As stated in the chapter introduction, the new methodology is intended to be an extension of the established conceptual design methods, not a replacement. By requiring the new methodology to be compatible with existing design processes, it provides the means for researchers to simply apply it to their established design workflows, allowing more effort to be concentrated on the actual work of investigating the performance potential of their HEPS concepts.

The most significant consequence of this requirement is, that the methodology adopted the approach to retrofit the hybrid-electric propulsion system into an existing conventional design. By retroactively determining the required HEPS performance and using an iteration to converge to a cohesive hybrid-electric concept, the methodology is immediately compatible with any conceptual design tool that generates a complete conventional concept. This does not indicated that the methodology only works as a retrofit, as it can easily be implemented directly in the initial conceptual design iteration, but it is enforcing that it works on an established concept.

3. The devised methodology must not be limited to one specific realisation of hybrid-electric propulsion; it must be applicable for a variety of HEPS concepts.

To address this requirement, the new methodology was designed to facilitate a modular implementation. While the methodology as presented in the following sections cannot include the functionality to create all possible hybrid-electric configurations, it is devised in such a way that any required extension is easily integrated. This especially translates into the way it is implemented into a design tool, adopting a modular

approach that emphasises a separation of the functionality such that each module works independently and contains everything necessary for its execution.
A tool that was created to size the electric components for a parallel hybrid-electric powertrain could easily be extended to size a series HEPS concept by implementing a module that uses the same component models, but connects them in a series configuration. The only newly supplied knowledge is on the connection order; all methods containing information on the sizing methods of the components and their positioning can be reused.

4. The devised methods must be able to operate without direct interaction with the user.
It was decided to add a requirement which dictated that the new methodology had to be able to automate the design process based on supplied general inputs. To achieve this, it is necessary for the employed methods to contain a certain degree of design knowledge; all required input data that is specific to the current concept, has to be obtained from the design data itself. This is essentially a step into the Knowledge Based Engineering (KBE) paradigm, which is intrinsically closely compatible with a physics-based design approach.

5. All required input data must be of a low level of detail.
One major drawback of physics-based design methods is their oftentimes high level of detail of the required input data. Because they work on the actual physical relation of the various components, they require a much more detailed description of the current state than statistical regression based estimation methods. At the conceptual design stage, this high level of detail is often not yet available.
This requirement is formulated to guarantee that the devised methods are still suitable for a *conceptual* concept design, instead of requiring inputs of a level of detail more common later in the preliminary stage. For example, the models used to describe the electric components will mostly be limited to use the efficiency, as well as the specific power and specific energy, as design parameters. This is intended to ensure that the created methodology is simultaneously accurate and compatible with conceptual design

3.1.2. Gap in Existing Sizing Methods

Based on the analysis of the published literature, the gap in the existing hybrid-electric sizing methodologies has been identified. Reflecting the findings in Chapter 2, the novel methodology must address two aspects: the prediction of the resulting engine performance and the estimation of the mass added by the electric components.
For the first aspect, a need for a high-detail representation of the propulsion system performance at low computational costs was identified. This is intended to be achieved by creating a methodology based on the scaling and combining of individual origin performance maps. To account for different implementations of the electric propulsion system, different methods for how the scaled origin performance maps are combined can be created. Not only does this provide access to the available performance of a coherent engine design, but the de-coupling from the mission analysis — most methods in published methodologies require the solving of power-balances during each time-step of the mission simulation to compute the current required engine performance — reduces the computational load during these simulations.
The latter aspect must follow the universal approach of individually estimating the mass of each electric component within the powertrain, as no statistical relations exist, nor are these likely to appear due to the high degree of flexibility in the usage of the electric part of the propulsion system. Besides extending the sizing methodology to include all electric components, not just the battery and electric motors, a further need was identified to estimate not only the individual component masses but also their relative positions. The mass sizing of the individual components will be achieved via specific component models, which all provide a sufficiently abstract representation of their respective components to allow for the sizing of different variations of the same component type. For the determination of the respective component positions, specific knowledge-rule will be defined that dictate where each component type is to be located within the aircraft geometry. By providing a measure of both mass and location of each electric component, the impact of not only the added mass but also the implications by the corresponding potential shift in the aircraft's centre of gravity can be assessed. This allows an investigation of secondary effects of introducing an electric powertrain, such as a possible re-positioning of the main wing or a change in the empennage sizing.
The identified gap in the existing hybrid-electric sizing methodologies can thus be summarised as:

1. enable a high-detail estimation of the resulting HEPS engine performance
   - base the performance prediction methodology on the scaling and combining of individual origin performance maps
   - account for different implementations of the parallel electric system
2. provide methods for the sizing of the electrical components of the HEPS powertrain, including:
   - the estimation of individual electrical component masses
   - the estimation of the position of the centre of gravity of each electrical component

3.1.3. Integration into Established Design Process

Finally, it has to be discussed how the created HEPS sizing methods are intended to be integrated into the established conceptual design process. As stated in the chapter introduction, the new methodology is intended to be an extension of the existing design process, not a standalone procedure. It is therefore necessary to not only define the individual methods that enable the generation of the HEPS designs, but also to address how they are to be connected to the existing process.

The implementation into the sizing process differs slightly, depending on whether the methodology is applied to work in combination with an established conceptual design tool, or whether it is implemented directly into the conceptual design process. This is not due to a change in the underlying methods, but simply a matter of implementation and the available interfaces between all employed sizing methods.

Based on the defined project scope, and complying with the second formulated requirement, the discussion on the integration of the HEPS sizing methodology into the design process will focus on the implementation using an established design sizing tool, as the integration into a new design tool is heavily dependent on the internal layout of this new sizing tool.

An example implementation of the proposed hybrid-electric sizing methodology using an existing conventional design tool is illustrated in Figure 3.1, and a more detailed overview of the integration is provided in Section 6.1. In this approach, the existing conventional design tool is used to both supply the initial conventional design (as baseline for the HEPS concept and as a potential reference concept), and to act as a design convergence tool for the hybrid-electric concept. This assumes, that the chosen conventional design tool has the capability to include a generic, user-defined mass component in its internal weight and balance methods. An example of a conventional conceptual design tool with such a capability is the tool ‘openAD‘ of the DLR [a]. Within ‘openAD‘, a "miscellaneous" mass with corresponding position of its centre of gravity can be defined, which will be included in the overall concept’s weight and balance computations.

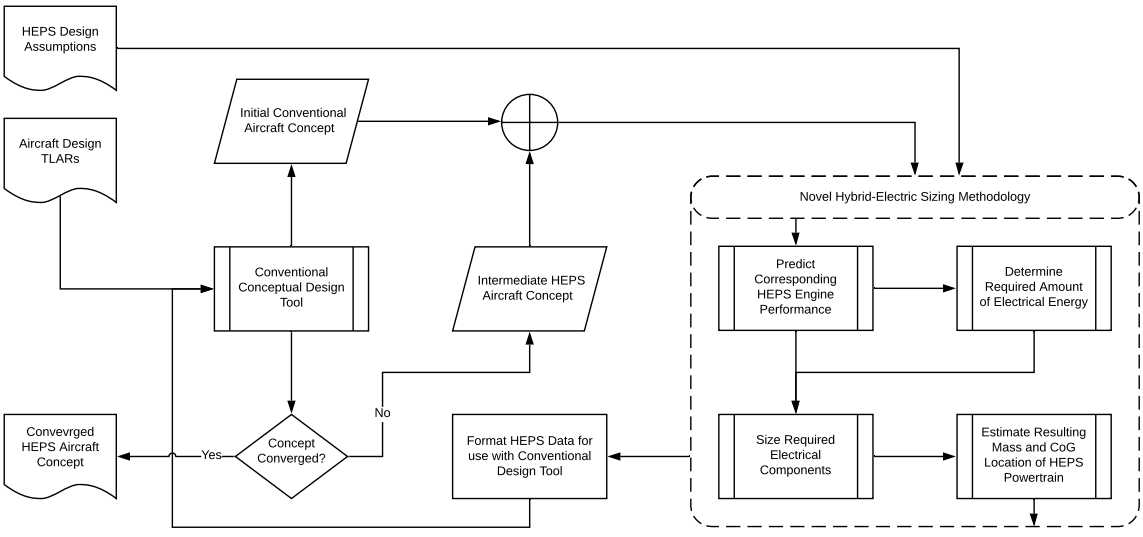

Figure 3.1: Example Illustration of a possible integration of the novel HEPS conceptual sizing methodology using an established conventional design tool.

[a] The tool ‘openAD‘ is currently in active development, and is not yet publicly available. For further information please contact openAD@dlr.de.

The integration of the hybrid-electric methodology introduces an additional convergence iteration, wherein the added mass due to the electric components, the changes in the required amount of conventional fuel, as well as the resulting shift in the aircraft's centre of gravity, are incorporated to form a cohesive HEPS aircraft concept. A simple realisation of this extension to the design process, as illustrated in Figure 3.1, begins with the established, conventional process. The desired Top Level Aircraft Requirements (TLAR) are formulated and the conventional design tool is executed to create a conventional turbofan aircraft concept. In addition to the conventional TLARs, the designer also defines the HEPS design assumptions: a set of design parameters that include the assumed electrical component technology levels, information on the HEPS configuration, the intended Degree-of-Hybridisation, and other specifications required for the sizing of the hybrid-electric system. Both the defined HEPS design assumptions and the created conventional concept, are then used as the starting point for the HEPS sizing methodology.

The hybrid-electric sizing procedure begins with the generation of a performance map that estimates the required HEPS engine performance corresponding to the conventional aircraft concept. A detailed description of the suggested process is given in Section 3.2, but essentially the process consists of combining a fan and engine core performance map such that the resulting hybrid performance map complies with a set of imposed point performances. Once the hybrid engine performance has been estimated, a simulation of the design mission is performed, using the new hybrid-electric engine performance map and the initial conventional aircraft concept. The results of this mission simulation will provide a new estimate of the required mass of conventional fuel, as well as the necessary amount electric energy to be stored on-board. The just determined amount of electrical energy and some data from the HEPS engine performance map (e.g. the maximum power added to the fan drive shaft by the electric motor) are then used to size the required electrical components (for a detailed description of the suggested methods for the sizing of the electrical components, see Section 3.3). Finally, the individual component mass and location data is combined into a single "HEPS powertrain" component, as most established design tools are incapable of representing individual electric propulsion components.

Depending on the tool used to govern the design convergence, the generated hybrid-electric design data is formatted to be compatible with the used design tool and then used as input for the next iteration. This process (create predicted HEPS engine performance, simulate design mission, size electrical components, update aircraft design for new mass & balance) is repeated, until the resulting aircraft design is considered converged, at which point the desired HEPS aircraft concept has been created.

It has to be stressed, when implementing the new methodology in combination with an existing conventional design tool, that it is crucial to conduct proper bookkeeping on the hybrid-electric propulsion system mass. Because a tool like 'openAD' will continue to size a conventional engine for the concept, simply adding the HEPS mass of the previous iteration will result in the concept featuring essentially two distinct propulsion systems. The tool internal engine mass has to be either set to zero (in this case the complete HEPS mass and CoG location are added as "miscellaneous"); or the mass corresponding to the engine components (i.e. the conventional engine core and the added electric motors) have to be considered the "hybrid engine mass", and the tool internal engine mass set to the corresponding value, while the mass of the remaining electrical components is added separately.

3.2. Engine Performance Prediction Methodology

A common approach for predicting the engine performance during conceptual design is via the use of performance maps. These maps typically represent the performance of a specific engine for a variety of operating conditions, usually using the altitude, Mach number, and produced total thrust as the state variables. The corresponding performance parameters are based either real engine data or a high-fidelity simulation using sophisticated engine design tools. When predicting the engine performance of the new aircraft concept, an appropriate engine performance map will be scaled to match the thrust performance at specific sizing points (e.g. take-off or climb requirements).

To comply with the compatibility with existing conceptual design processes, it was decided that the new HEPS methodology employs the same approach. Due to the novelty of the concept of hybrid-electric propulsion, the use of a performance map faced two obstacles: the lack of a standardised layout, and the lack of available reference data.

While the performance of conventional turbofan engines is controlled by a single parameter, the fuel flow, a hybrid-electric engine per definition requires multiple parameters (see Appendix A.1). The engine's perfor-

mance parameters can thus no longer be uniquely derived from the altitude, Mach number, and produced thrust alone. Consequently, the layout of a hybrid-electric engine performance map is no longer straight forward and may differ for different implementations. Section 3.2.1 offers an overview of the general layout of an engine performance map, as well as the suggested additions to represent the engine performance for a parallel hybrid-electric propulsion system.
To overcome the lack of available reference data, a procedure was developed that allows the generation of a hybrid-electric performance map estimation. This procedure is based on scaling origin fan and core performance maps to match the point-performance requirements at specified design sizing points. The hybrid-electric aspects of the propulsion system are introduced by specifying a desired power split ratio at each design sizing point. This procedure provides a good accuracy in the performance prediction for a limited number of necessary input variables; an in-depth explanation is presented in Section 3.2.2.
A big advantage of this approach in the methodology is the inherent compatibility with dedicated mission simulation design tools. Most performance prediction methodologies discussed in Chapter 2 required a new mission simulation methodology to be compatible with their performance prediction methods, with direct interaction during each time step. A created coherent performance map however, can simply be used as input for an established mission simulation tool.

3.2.1. Engine Performance Maps

The use of engine performance maps is widely spread in the field of conceptual aircraft design. It allows the prediction of the overall engine performance characteristics specific for the current aircraft design, without requiring expensive, in-depth computer simulations. The engine performance map for a conventional turbofan concept is straight forward, but the inclusion of a secondary energy and/or power source in a hybrid-electric concept requires an adaptation of the established performance map layout.

Conventional Engine Performance Map

For a conventional turbofan engine, a set of three state variables is sufficient to uniquely characterise the current operating conditions, allowing to determine the corresponding performance parameters (e.g. fuel flow, usable shaft power, produced emissions, etc.). The typically chosen state variables are the altitude, the Mach number, and the produced thrust per engine.
All vectors within an engine performance map are of equal length, meaning that each index corresponds to a unique operating condition. To reflect this in the state vectors, a specific hierarchy is imposed on the state variables. The hierarchy follows a logical breakdown, with the altitude serving as most top-level state. For each sample altitude, a specific range of Mach numbers is specified, reflecting that the aircraft can operate at different speeds for any given altitude. The chosen Mach number sample values correspond to the aircraft's flight envelope, and are thus covering a lower speed range at low altitudes, and faster speeds at higher altitudes. Finally, for each sample Mach number, the aircraft can produce different magnitudes of thrust, depending on the desired acceleration/deceleration. This is again reflected in the performance maps state vectors, by specifying a range of thrust values — from minimum to maximum available — at each Mach number at each altitude.
Figure 3.2 provides a visual representation of the state variable hierarchy as described. In the illustrated example, the altitude vector contains only the first altitude sample value ("Altitude 1"); the Mach number vector contains the first Mach number sample value from index[b] 0 to 9, and the next sample value from index 10 to 19; while the thrust vector contains a range of thrust values increasing from minimum to maximum available for each Mach number sample value. Furthermore, Figure 3.2 also illustrates how each entry in any performance parameter vector corresponds to the state described by the entries in the state vectors of the same index. The value of parameter 1 as displayed at index 9 in it's parameter vector corresponds to the state at index 9, which in the given example is [Altitude 1, Mach number 1, maximum thrust].
The standard layout of a conventional turbofan performance map conforming to the CPACS schema (using XML notation) is shown in Listing 3.1. The displayed performance map shows the same state variable hierarchy as presented in the illustrated example above: all visible entries in the altitude vector correspond to the first sample altitude; the first ten entries of the Mach number vector correspond to the first sample Mach number, before moving on to the second Mach number sample value; the thrust entries are continuously increasing from minimum to maximum available thrust for the given altitude & Mach number combination; each entry in the performance parameter vectors ("mDotFuel", "IPShaftNrel", and "P_Shaft") correspond to

[b] it should be noted that the provided example follows the index convention of vectors/arrays starting at index 0!

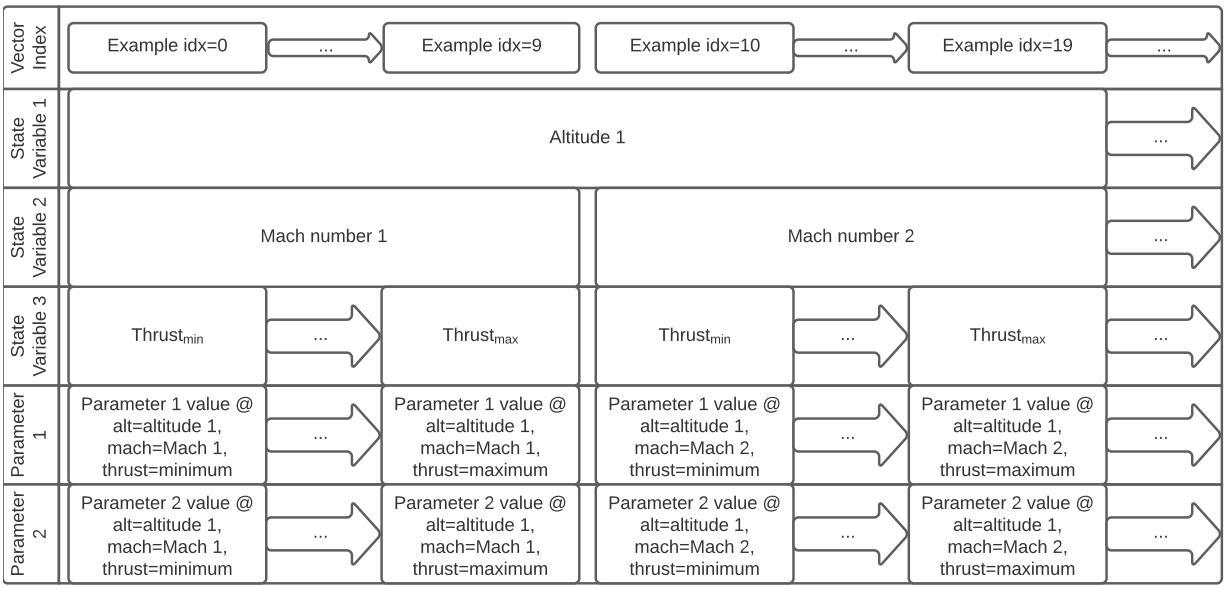

Figure 3.2: Illustration of the layout of an engine performance map, providing a visual representation of the hierarchy of the state variables and the breakdown of the performance parameter values. In the given example, each combination of altitude & Mach number contains a set of ten thrust sample values, as indicated by the displayed example indices.

the state defined by the entries at the same index, and are thus reflecting the continuous increase as shown in the thrust vector.
A major advantage of this style of performance map is that is facilitates easy interpolation. Because the information is stored in form of grid data, any available n-dimensional interpolator can directly use the performance map to interpolate the parameter value at any point within the data set. It should be noted, that in case of interpolation it is important to account for the difference in orders of magnitude in the values stored in the vectors, as this could potentially lead to inaccuracies.

```
<performanceMap>
    <name>standardMap</name>
    <flightLevel mapType="vector">0.0; 0.0; 0.0; 0.0; 0.0; 0.0; 0.0;...</flightLevel>
    <machNumber mapType="vector">0; 0; 0; 0; 0; 0; 0; 0; 0; 0; 0.1; ... </machNumber>
    <thrust mapType="vector">2354.; 3283.; 4669.; 6756.; 9171.; 11863.; ... </thrust>
    <mDotFuel mapType="vector">0.2094; 0.2789; 0.3719; 0.4965; 0.6326;... </mDotFuel>
    <IPShaftNrel mapType="vector">0.565; 0.631; 0.709; 0.798; 0.879;...</IPShaftNrel>
    <P_Shaft mapType="vector">-758882.; -2197252.; -4239029.; -7056309.;...</P_Shaft>
</performanceMap>
```

Listing 3.1: Example overview of the layout of a conventional engine performance map within an XML file, following the CPACS schema standard.

Hybrid-Electric Engine Performance Map

For a hybrid-electric aircraft concept, the state of the propulsion system can no longer be uniquely described by simply the altitude, Mach number and total produced thrust. Because of the duality of the propulsion system, the same state can be obtained via a variety of energy and/or power draw combinations from all available sources. To properly capture the state of a hybrid-electric system, the relative utilisation of each source has to be included in the performance map.
As per the scope limitations discussed in Section 1.3, this section will only discuss possible adaptations of engine performance maps for use for *parallel* hybrid-electric propulsion systems. It is also assumed, that the parallel HEPS configuration use battery-based storage for on-board electric energy. A series hybrid-electric propulsion system requires more fundamental adaptations of the conventional performance map, as the internal combustion engine is no longer coupled with the propulsion device, it is only used for electric power

generation. Indeed, it can be argued that, due to the decoupling of the ICE from the thrust production, the engine performance map for a series hybrid-electric propulsion system should no longer contain the data of the engine core. The conventional turbine engine will most likely operate at a constant operating condition, so as to maximise its efficiency, and has therefore no impact on the propulsion system dynamics.

A battery-based, pure parallel hybrid-electric propulsion system takes all electric power required to drive the electric motor from the on-board batteries. By adding a new parameter that describes the electric power's share of the total power, the state of the propulsion system can again be uniquely described. A engine performance map for a parallel HEPS concept thus requires the following four state variables: altitude, Mach number, total thrust per engine, active power split ratio.
The manner in which the new parameter has to be incorporated into the performance map is dependent on the implementation of the power management of the specific HEPS design. For any parallel HEPS configuration, the power management can either allow a direct control over the relative power draw, or enforce a specified power schedule, typically linked to the thrust setting. Prescribing the power schedule results in a less optimised utilisation of the hybrid-electric performance potential, but removes the power split ratio as a control variable, reducing the complexity and allowing the parallel HEPS engine performance map to be compatible with design and analysis tools that are limited to operate with the three conventional state variables. Allowing a direct control over the applied power split on the other hand, allows for maximum utilisation of the hybrid performance potential at the cost that design and analysis tools have to be capable of accounting for the additional state variable.

For the devised hybrid-electric sizing methodology, HEPS engine performance map structures for both approaches were devised. Performance maps describing a hybrid system that prescribed a strict power schedule are classified as "augmented", because the electric part of the system is typically used to augment the performance of the conventional turbofan instead of offering an optimised HEPS. For a hybrid system that allows independent control over the power split of the underlying propulsion systems, the resulting performance map is classified as "variable", because the user/designer can vary the desired power split ratio at each given operating condition.

"Augmented" Hybrid-Electric Engine Performance Map An augmented hybrid-electric engine performance map is characterised by limiting the control over the electric system. The philosophy is more in-line with the pilot's perspective, in that the thrust setting should be the only control parameter. It represents a HEPS engine concept as it would be installed on an aircraft, where the underlying algorithm of the flight computer would determine the one available power split ratio for the current operating condition.
For the discipline of aircraft design, an augmented performance map is obtained when prescribing either a rigid and parametrised, or a dynamic and adaptive power split schedule. The first option includes prescribing either a constant power split for all operating states (e.g. a constant power split of 15%) or a fixed parametrised power split (such as a linearly increasing electric power draw). To increase the effectiveness of the hybrid system, the shape of the increase in the electric power draw could be optimised for the typical mission profile. The second option — prescribing a dynamic and adaptive power split schedule — includes concepts that use primarily the ICE power and only add electric power once the ICE is operating at it's maximum power output. This approach is considered dynamic and adaptive, because it does not follow a rigid, prescribed schedule but the inherent characteristics of the ICE, and thus varies with the surrounding conditions (altitude & Mach number).
The layout of an augmented hybrid-electric engine performance map would not differ from the layout of a conventional one as illustrated in Figure 3.2, but the performance parameter vectors would now also contain a vector describing either the power split ratio active at that specific state, or directly the power provided by the electric part of the system. Any information on the electric aspect of the propulsion system would be stored in form of additional performance vectors, no further state vectors are added to the performance map. This is further illustrated in excerpt of an example "augmented" hybrid-electric engine performance map shown in Listing 3.2. The shown hybrid-electric performance map still uses the same state variables as the conventional example (altitude, Mach number, and total thrust), but added the relevant performance parameters for the electrical propulsion system. In this example the electrical system performance is represented by the mechanical power added to the fan shaft ('P_mech_EM') and the required amount of electrical power consumed by the electrical motor ('el_energy_flow').

```
<performanceMap>
    <name>standardMap</name>
    <flightLevel mapType="vector">0.0; 0.0; 0.0; 0.0; 0.0; 0.0; 0.0;...</flightLevel>
    <machNumber mapType="vector">0; 0; 0; 0; 0; 0; 0; 0; 0; 0; 0.1; ... </machNumber>
    <thrust mapType="vector">36286.; 59174.; 80976.; 100194. ;115201.; ... </thrust>
    <thrust_fan mapType="vector">33482.; 54420.; 73931.; 90686.; ... </thrust_fan>
    <power_fan mapType="vector">2541127; 5137432; 7935142; 10657457; ... </power_fan>
    <power_core mapType="vector">2541127; 5137432; 7935142; 10657457;...</power_core>
    <P_mech_EM mapType="vector">0; 0; 0; 0; 0; 0; 1155191.; 1666276.; ...</P_mech_EM>
    <el_energy_flow mapType="vector">0; 0; 0; 0; 0; 0; 1297968.; ...<\el_energy_flow>
    <mDotFuel mapType="vector">0.2235;0.3377;0.4638;0.606;0.7388;0.76;... </mDotFuel>
    <IPShaftNrel mapType="vector">0.593; 0.700; 0.794; 0.871; 0.924;...</IPShaftNrel>
</performanceMap>
```

Listing 3.2: Example overview of the layout of a HEPS engine performance map within an XML file, following the CPACS schema standard. The performance parameter vectors introduced by the electric part of the propulsion system are highlighted.

It should be noted, that it may appear that the vectors 'power_fan' and 'power_core' are identical, however this is caused by the limited space available to display the vector entries. Due to the large magnitude of the entries in the power vectors, only the first four entries can be displayed. Inspecting the vectors 'P_mech_EM' or 'el_energy_flow', it can be seen that the electric motor is only adding power starting at the seventh index, corresponding to the approach taken in the generation of the augmented HEPS performance map, that the ICE is used to its full potential before adding electric boost power.
A more obvious visual example of the difference between a conventional and an "augmented" hybrid-electric performance map is given in Figure 3.3. It compares the engine performance at sea-level for each available Mach number by plotting the engine fuel flow against the total produced thrust. Figure 3.3a clearly shows the expected continuous steady increase in fuel flow with increasing thrust production. The anomaly of increasing fuel flow for constant thrust seen for Mach numbers 0.0–0.2 is due to the engine flat rating, wherein the thrust was capped at the desired take-off thrust value of 120 kN. In contrast, the characteristics of the augmented HEPS engine performance map shown in Figure 3.3b exhibit a similar continuous stead increase in fuel flow until a certain point, after which the produced total thrust increases further but the fuel flow remains constant. The "plateaus" in the curves correspond to the operating condition, when the turbine engine is operating at its maximum capacity and the electric motor is providing additional power to the fan drive shaft. It should be noted, that the sizing criteria used for the generation of this example HEPS performance map specified a take-off thrust of 120 kN, same as shown in the conventional performance map. Due to the sizing procedure as detailed in Section 3.2.2, the total available thrust at sea-level static conditions exceeds this requirement, because a different sizing point was the active limitation. The shown HEPS engine performance thus corresponds to an engine that was not flat rated.

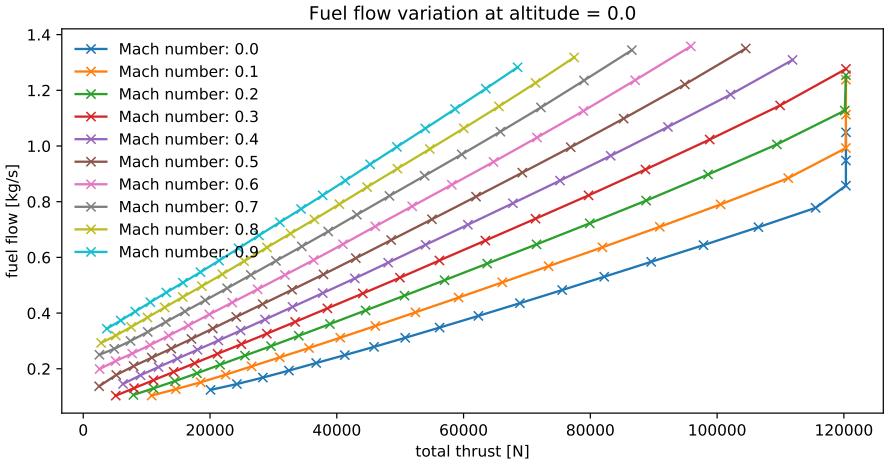

(a) Engine performance of the example conventional engine performance map, corresponding to Listing 3.1. Anomaly at total thrust = 120 kN for Mach number 0.0–0.2 due to engine flat rating.

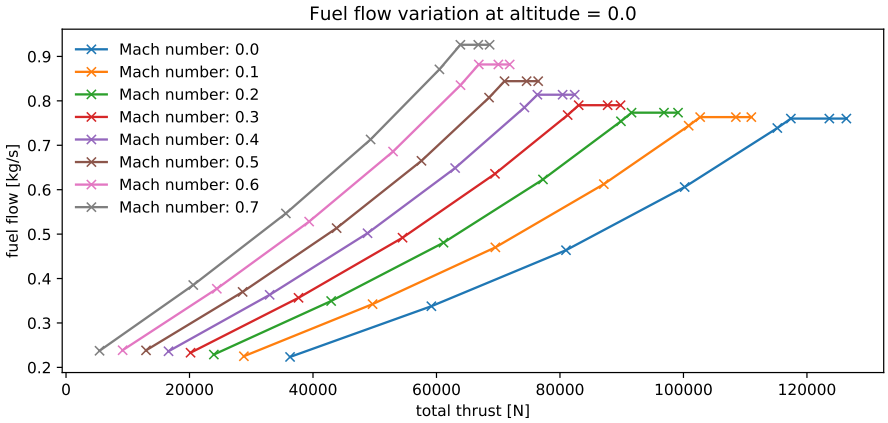

(b) Engine performance of example "augmented" hybrid-electric engine performance map, corresponding to Listing 3.2. Plateaus of constant fuel flow formed due to engine core operating at maximum capacity and additional shaft power added via electric motor. No engine flat rating applied.

Figure 3.3: Plots showing the dependency of the fuel flow vs. the total produced thrust at sea-level, for both conventional and "augmented" hybrid-electric engine performance map examples.

"Variable" Hybrid-Electric Engine Performance Map A variable hybrid-electric engine performance map covers the entire possible design space of the hybrid propulsion system. It includes all possible combinations of operating conditions and is thus ideally suited for analyses that include a thorough optimisation of the HEPS. Variable hybrid-electric engine performance maps include an extra state variable, therefore the standard layout as illustrated in Figure 3.2 is no longer valid and has to be adapted.

This adaptation can be realised in various ways, one of which is by generating a set of engine performance maps, each for a fixed constant value of the new state variable. The desired performance values are then obtained by interpolating this set of maps at the desired operating condition. A visualisation of this approach is displayed in Figure 3.4, in which the additional state variable is the power split ratio — denoting the electric system's share of the total power production — and using a set of four engine performance maps to cover the available design space. The main advantage of this approach is that the structure of each individual performance map conforms with the standard layout used for conventional performance maps.

An alternative approach is to integrate the additional state variable directly into the performance map by adding a fourth state vector. This simply extends the principle employed by the conventional engine performance map as discussed in Section 3.2.1. An example implementation of this alternative approach is illustrated in Figure 3.5, using again the power split ratio as fourth state variable. In this example, the extra state vector was inserted into the state variable hierarchy on the fourth level, but due to the nature of the variables, an implementation with the power split ratio at third level and the thrust values at fourth would also be possible. From the example it can immediately be seen, that the inclusion of an additional state variable will result in a significant increase in vector length. Assuming the variable hybrid engine performance map added N sample points of the power split ratio at each operating state, the length of each vector increased by the factor N.

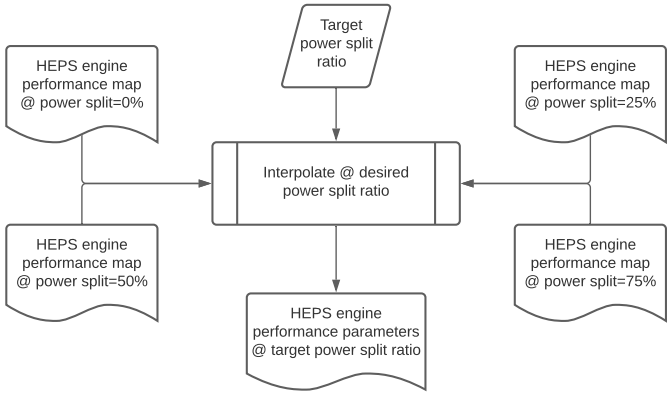

Figure 3.4: Visualisation of the "multiple map" approach for a "variable" hybrid-electric engine performance map.

Finally, it should be noted that while the new methodology includes these suggestions for "variable" hybrid-electric engine performance maps, no example procedure for their generations will be provided. To keep within the scope of this project, all devised procedures and methods formulated in Section 3.2.2 will be applicable for an "augmented" HEPS engine performance map.

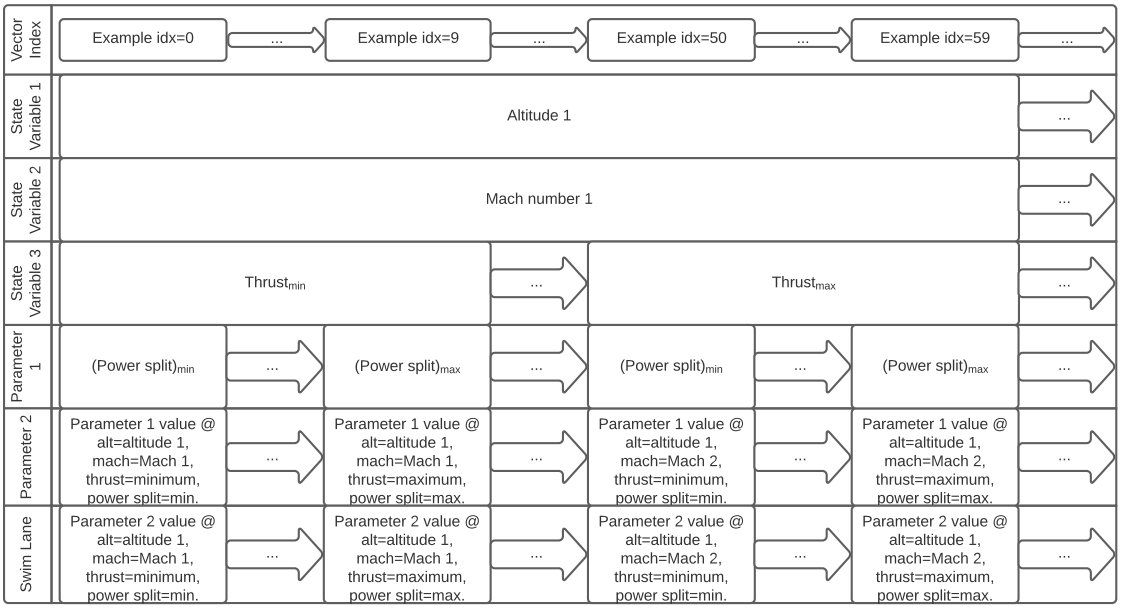

Figure 3.5: Illustration of the layout of a "variable" hybrid-electric engine performance map, providing a visual representation of the hierarchy of the state variables. In the given example, each combination of altitude, Mach number, and thrust contains a set of ten power split ratio sample values, as indicated by the displayed example indices.

3.2.2. HEPS Engine Performance Map Procedure

In Section 3.2.1 the potential layout and structure of different realisations of a hybrid-electric engine performance map were discussed. As stated, an engine performance map for a series HEPS architecture would fundamentally differ from the conventional layout, removing the turbine engine parameters and simply providing the required electric power at each sample point. While multiple variations of parallel hybrid-electric performance maps were discussed, it is not feasible within the scope of this thesis to devise an exact procedure on how to generate each of the mentioned variants.

The procedure as described here will detail the generation of an "augmented" HEPS engine performance map, wherein the internal combustion engine is used as the primary power source and the electric power is only added once the ICE is operating at its maximum capacity. Although the defined methods are explicit for this type of hybrid performance map, the methodology can easily be adapted to generate a different variant.

At a fundamental level, the methodology required to generate any type of hybrid-electric engine performance map for conceptual design purposes — for both parallel and series architectures — can be separated into three aspects:

1. Define HEPS performance requirements
2. Scale origin fan and engine core performance maps to match defined performance requirements
3. Generate HEPS engine performance map based on origin performance maps and electric propulsion requirements

These three fundamental aspects do not inherently impose any limitations on the hybrid architecture, it is the methods used during each step that introduce the restrictions. The type of performance requirements defined obviously vary between the two main architectures, but even the same architecture might require different specifications depending on the desired type of HEPS performance map. For a parallel hybrid-electric powertrain, the scaling of the fan and engine core performance maps is closely coupled, because the engine core produces a non-negligible thrust, which in turn reduces the required fan thrust for a given total

produced engine thrust. Conversely, a series hybrid-electric propulsion system has completely de-coupled the turbine engine from the thrust production. The fan and engine core performance maps will thus be scaled independently for their respective performance requirements. Finally, the generation of the intended HEPS engine performance map will by necessity be specific to the desired type of performance map.

The methodology devised in this thesis for the generation of an "augmented" parallel hybrid-electric engine performance map follows the same three fundamental aspects as discussed. As a short summation, the methodology aims to match the required fan and engine core performances at a set of defined design sizing points for the minimum possible performance. Matching for the lowest performance that still meets the requirements corresponds to the lowest possible mass of the propulsion system. Figure 3.6 shows a breakdown of the most important steps of the procedure, illustrating not only the individual steps to be taken, but also highlighting their place within the three main aspects. The following paragraphs will give a detailed explanation of the processes associated with each aspect.
The methodology makes a few assumptions on the integration of the electric components into the engine design. These assumptions are necessary to enable the engine performance prediction at a conceptual design level.

HEPS engine sizing assumptions:

- The used origin performance maps (fan and engine core) are representative of the final aircraft size category. A HEPS engine performance prediction for an aircraft of A320 size, should use origin maps intended for an A320 sized aircraft.
- The addition of mechanical power to the fan drive shaft via the electric motor does not impact the performance of the turbine engine. In essence, it is assumed that the electric motor does not increase the rotational speed of the shaft connected to the turbine engine, and thus does not introduce a mismatch of the velocity triangles in the turbomachinery of the engine core.
- The effect of the changed flow conditions entering the LPC (due to the added shaft power after the ICE operates at peak power) are not considered. It is assumed that the compressor is designed to operate according to the flow conditions corresponding to the maximum fan performance.
- The mechanical power output of the electric motor is determined based on the required shaft power to drive the fan and the available turbine shaft power (as dictated by the scaled engine core performance map). No consideration as to the feasibility of the computed output power according to current SoA was taken, it is assumed that the electric motor can be designed to provide the specified maximum mechanical output power.
- The resulting hybrid-electric engine performance prediction does not include flat rating. The resultant engine performance is obtained such, that the desired point performance at each design sizing point is assured. This can lead to an over-sizing at operating conditions corresponding to other design sizing points. If desired, the created HEPS engine performance map can be flat rated for a prescribed take-off thrust or similar in a post-process procedure, but this was not included in the devised methodology.

1. Define HEPS Performance Requirements The underlying principle of the devised procedure is based on scaling existing performance maps of the fan and engine core, assuming that the only impact of the electric part of the propulsion chain on the system performance is in the mechanical power added onto the drive shaft via the electric motor. To provide reference points for which the origin performance maps can be scaled, the designer has to specify the desired system performance at a set of design sizing points. Each of these design sizing points has to include data on the flight condition as well as the desired engine performance.

Necessary point performance parameters:

- Altitude & Mach number (current flight condition)
  ⇒ Required to identify the ambient conditions the engine is operating in
- Required total engine thrust
  ⇒ Dictates the *minimum* amount of thrust the HEPS engine has to be able to provide at this flight condition. Note: total engine thrust, not total aircraft thrust.

- Maximum allowed power split ratio
  ⇒ Implicitly defines the maximum mechanical output power of the electric motor — and correspondingly the minimum required shaft power of the ICE — by dictating the maximum power split ratio for the current operating condition (altitude, Mach number, and total produced thrust)
- Maximum available engine core power output
  ⇒ Optional, instead of power split ratio. Prescribes the maximum allowed amount of shaft power the engine core is capable of providing. The required mechanical output power of the electric motor and the corresponding power split ratio follow from the total power requirement (from fan shaft power and power offtakes).

Depending on the use case, the designer can either specify the desired maximum power split ratio or impose a constraint on the maximum size of the engine core. Typically, the power split ratio is used as control parameter for the electrification of the propulsion system, with studies investigating the effects of different power split ratio during various mission segments. Thus, specifying the power split ratio is considered the default for defining the design sizing points. The alternative option of specifying the maximum engine core shaft power allows the designer to directly address the engine core sizing, with the corresponding power split ratio being determined according to the required total power. This option is useful when the requirement directly constrains the gas turbine core and was used during the generation of the example "boosted turbofan" HEPS concepts (as elaborated in Section 4.1.2), where the engine core is sized to exactly match the steady cruise thrust requirements, but the engine fan was sized for the mid-cruise climb rate requirement.
It is possible to extend the methodology to include more performance requirements to be used for the scaling process, such as the necessary power offtakes to power other subsystems. Depending on whether these power offtakes are to be provided by the gas turbine engine or the battery, this would change either the final obtained scaled engine core performance map or increase the necessary battery mass. Either implementation does not impact the procedure illustrated in Figure 3.6, as all process steps are sufficiently abstract and do not dictate how exactly they are to be implemented.

2. Scale Origin Fan and Engine Core Performance Maps The origin performance map scaling procedure is a two-layered iteration process. The inner iteration loop deals with the computation of the required scaling factor for each individual design sizing point, while the outer iteration loop determines the applicable global scaling factor from the individual scaling factors and oversees the convergence of the actual scaling operation. In the top-left dashed block in Figure 3.6 the process flow of this two-layered iteration scheme is shown in more detail.
The inner iteration is executed for each loop of the outer scaling iteration, providing a set of potential scaling factors for each of the origin performance maps. Cycling through the defined design sizing points — and the corresponding point performance requirements — the iteration determines the scaling factor that would scale the current state of the origin performance map (the result of the previous outer iteration) such, that its performance at the current design sizing point matches the prescribed point performance exactly. For a parallel hybrid-electric architecture, this requires an interaction of the methods determining the fan and engine core scaling factor, because the defined total produced thrust is the result of the fan thrust and the residual core thrust. In fact, the determination of the individual scaling factors requires an additional, third iteration loop. Within this third iteration, the individual design sizing points current scaling factors are adjusted until the produced fan thrust and the corresponding added core thrust are matched to equal the desired total thrust.
Using the set of potential scaling factors obtained in the inner iteration loop, the outer iteration determines the appropriate global scaling factor to be applied to each origin map. Since each of the individual design point scaling factors is applied to the entire performance map, they can be considered as describing a limit case: to guarantee that the specified point performance is met by the performance map, the applied global scaling factor may not be smaller than the corresponding individual scaling factor. Therefore, to create a performance map that meets the point performance requirement of each design sizing point, the applied global scaling factor may not be smaller than the largest of the individual scaling factors. The final global scaling factor will be the result of the largest of the individual scaling factors and a chosen numerical updating scheme selected to enforce a smooth convergence.
Finally, the state of convergence of the origin performance map scaling process is assessed by comparing the current iterations global scaling factors to the previous iteration. Until the difference is deemed sufficiently small, the current state of the origin performance maps is used as the basis for the next iteration loop.

Figure 3.6: Process flowchart of the methodology devised for the generation of a parallel hybrid-electric engine performance map, using an origin fan and engine core performance map as basis.

3. Generate HEPS engine performance map In the last of the three main steps, the scaled origin performance maps are used to create a cohesive hybrid-electric engine performance map. At this point, the selection of the used methods determines the type of HEPS engine performance map that will be generated, as both "augmented" and "variable" HEPS performance maps are based on the same origin maps. In fact, the only difference in the generation procedure of the two types lies in the handling of the interpolated performance parameters. This difference will be explained in more detail later in this discussion.

As displayed in Figure 3.6, the process to generate the parallel HEPS engine performance map is separated into three generalised steps. The first two steps — "Determine compatible altitude & Mach number vectors" and "Determine thrust sample points" — address the discretisation of the three state variables and ensure that each defined sample point lies within the available set of the performance data. The third step — "Interpolate performance parameters at each sample point" — contains all operations in which the fan and engine core performance is assessed and adjusted to fit with the HEPS performance requirements.

The first step of the hybrid map generation procedure selects the parameter space of the altitude and Mach number state variables. Because the two origin performance maps may be obtained independently, it is not guaranteed that they use the same discretisation of the flight condition state. The computation of the engine performance parameters relies on the interpolation of the data in the origin performance maps, therefore it is vital that each sample point lies within the data set contain within the origin maps.
During the development of this sizing methodology, a select set of example fan and engine core performance maps provided by the DLR were used. These maps were created using the same sample point step size for the altitude vectors. They did, however, extend to different maximum altitudes and additionally differed in the presented Mach number range for each sample altitude. This is reflected in the sub-steps presented in Figure 3.6, where the altitude range is simply selected as the overlap of both performance maps, followed by determining the overlapping Mach number range for each altitude sample point.

In the second step of the map generation process, the thrust sample points for each combination of altitude & Mach number are defined. This process is non-trivial because the appropriate minimum and maximum thrust values at each flight condition are dependent on the underlying origin performance maps. As shown in the illustrated breakdown of this sub-process, an iteration which computes the thrust sample points for each flight condition individually is necessary. The iteration begins with the computation of five characteristic total thrust values:

1. total thrust @ minimum fan thrust
2. total thrust @ minimum engine core power
3. total thrust @ maximum fan thrust
4. total thrust @ maximum core power (only for "augmented" type performance map)
5. total thrust @ maximum total power

These thrust values are then used to determine the available thrust range of the current flight condition; the larger of the thrust values corresponding to the minimum fan thrust and minimum engine core power defines the lower limit of the current thrust range, while the smallest of the thrust values corresponding to the fan thrust, core power, and total power defines the upper limit. With the thrust range limits determined, the process then uses the user defined ‘thrust sample point settings‘ — containing the number of sample points per flight condition and the type of sample point distribution (uniform, cosine, etc.) — to compute the thrust sample points for the current flight condition. For a HEPS engine performance map of type "augmented", the total thrust value corresponding to the maximum engine core power is then inserted as an additional value into the thrust sample point array. This guarantees that the performance map captures the point where the electric motor power is added exactly, forming a perfectly straight plateau as shown in Figure 3.3b. Without this exact capture of the point, interpolating the performance would yield incorrect performance data due to the assumption of a direct linear connection between the two surrounding sample points.

The final step in the generation process is to obtain the actual predicted performance data of the hybrid-electric engine at each of the defined sample points. Analogous to the process used to determine the appropriate thrust value sample points, this again requires an iteration over the complete set of state variable sample points. For each combination of altitude, Mach number, and total thrust, the process interpolates to corresponding performance data from the origin performance maps. This interpolated data can then either be inserted directly into the HEPS performance map, or used as a basis for the computation of other desired performance parameters. For example, the required shaft power to drive the fan, the corresponding available engine core shaft power, and an assumption on the total HEPS powertrain efficiency, can be used to compute a new performance parameter that estimates the required electrical power drawn at this specific operating condition.

It is at this step where the performance data is interpolated, that the employed methods determine whether the resulting HEPS performance map will be of type "augmented" or "active" (constant active power-split ratio). An "augmented" type process will determine the current required core shaft power output directly from the required fan shaft power, and add electrical boost power only once it exceeds the maximum available core shaft power. By contrast, an "active" type process uses methods that determine the necessary core power based on the required fan power and the prescribed power split ratio instead.
Finally, it should be mentioned that any parameter derived from the performance parameters stored in the performance map — such as the electric power draw used as an example above — can also be determined in a post-processing procedure. It is not necessary to add any parameter that is intended to appear in the performance map directly into the initial interpolation iteration. This is relevant when working with an already established implementation of this methodology, instead of altering the existing code, it is possible to simply perform the process on the created performance map.

3.3. Electrical Component Sizing Methodology

The second of the two established gaps in the existing sizing methodology (see Section 3.1.2) was the lack of any conceptual sizing methods for an electric propulsion system. Most traditional conceptual component sizing methods are empirical in nature, derived from a regression analysis performed on an extensive set of reference components. In traditional conceptual design, the propulsion system of transport aircraft is sized using either a "fixed-engine" or a "rubber-engine" approach [18, p. 101]. As the name suggests, a "fixed-engine" approach uses an existing engine design and thus fixes the engine size and its performance, while a "rubber-engine" approach allows the engine design to be "stretched" to exactly match the desired thrust performance. Since no hybrid-electric engine design currently exists, the only option is to follow the "rubber-engine" approach.
Independent of the chosen approach, the conceptual aircraft design process typically considers the propulsion system as a single entity without considering its individual parts. The performance parameters deemed relevant for traditional aircraft concepts usually are:

- several characteristic thrust values
- the corresponding TSFC values
- the engine mass
- the outer dimensions (length and diameter)

Each of these parameters can be predicted via relatively simple empirical equations, using a limited number of input variables — a selection of the maximum SLS thrust, the assumed BPR, the maximum Mach number, and the ambient conditions at characteristic sizing points (take-off, cruise, etc.). Even at a later design stage, the methods used in aircraft design focus more on the integration of the engine into the airframe, particularly the design of the engine inlet and the minimisation of interference drag due to the engine nacelle. The actual design of the internal engine parts is typically left to a dedicated engine design project, although modern conceptual design processes often incorporate this aspect at least partially, by integrating a high-fidelity, often component-based engine analysis tool into the process-chain.

A hybrid-electric propulsion system can no longer be neatly separated from the aircraft design. To be able to model the most direct impact of the hybrid-electric system on the aircraft design, it is necessary to assess the mass added and the corresponding shift in the aircraft centre of gravity. Due to a lack of reference data, the only feasible approach is to estimate the mass and position of each electric component of the hybrid-electric propulsion system individually. The resulting mass and position estimates can then be combined with established weight estimation methods.
In the following subsections the methods devised for the sizing of the various electric components (both mass estimation and positioning) are discussed. All devised methods are based on individual component models, using simple, physical characteristics to estimate the component mass and other data specific to the physical component (outer dimensions, its maximum power capability, etc.). Additionally, the position of each component is based on established design knowledge: a parallel HEPS engine's electric motors are placed at the corresponding engine location; the batteries are staggered within the fuselage, alternating between the front and aft section; components of the distribution system are either placed with similar components (PMAD in the electronics bay), or their location is based the corresponding geometrical centroid (transmission lines).

Once every electric component required for the HEPS engine powertrain is sized according to the described methodology, the resulting overall efficiency of the electric powertrain can be computed via Equation (3.1). This computed overall efficiency can then be used in the next design iteration during the HEPS performance sizing process, allowing a more accurate estimation of the expected losses of the electric propulsion system. The computed overall efficiency only relates to the electric part of the propulsion system, the overall efficiency of the combined hybrid-electric engine is the combination of this and the conventional engine core efficiency.

$$\eta_{ov} = \eta_{EM,\,avg.} \cdot \eta_{PMAD} \cdot \eta_{circuit\ protection} \cdot \eta_{battery,\,avg.} \cdot \eta_{transmission\ line,\,avg.} \tag{3.1}$$

Finally, it has to be stated that the devised methods do not impose any restrictions as to the feasibility of the sized electrical components. It is possible to size electric components for the propulsion system, far beyond what is expected to be available within the next decades, simply by specifying overly ambitious performance parameters. This intentional choice removes the limitations imposed by current day predictions and enables the methodology to be used for any newly emerged technology.

3.3.1. General Component Sizing

The general component sizing methodology is applicable for all electric components whose mass sizing methods depend on a single performance characteristic: the component's *specific power*. These components — the Electric Motors (EM), the Power Management And Distribution (PMAD) system, the Circuit Protection (CP) system, and the Thermal Management System (TMS) — all share the same approach to the mass sizing, using the specific power from the desired component model and the power requirement obtained from the desired HEPS performance to estimate the necessary mass. A further similarity is that while abiding by different knowledge rules, their positioning methods are all independent from the remaining sizing operations, allowing for a de-coupling of the mass and position sizing. Figure 3.7 illustrates the general procedure for the sizing of these components.

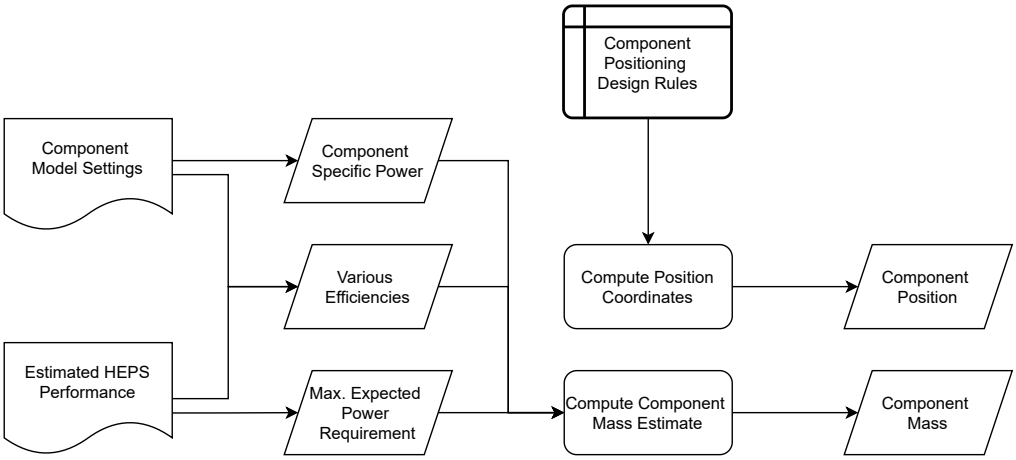

Figure 3.7: Illustration of the sizing procedure for a general component according to the devised methodology.

Electric Motor (EM) Component Sizing

The electric motors are represented by a simple, generalised model. By focusing on its most fundamental function — converting electric input power into mechanical output power — it is possible to achieve a sufficient level of accuracy without excluding any of the available electric motor configurations. The model represents the performance of the electric motor via two parameters: the *specific (mechanical) power*, denoting how much mechanical output power the electric motor can produce for every kilogram of mass; and the *component efficiency*, denoting how efficiently the electric motor can convert electric into mechanical power. By reducing the electric motor to these two parameters, it is possible to represent a large variety of possible electric motor types, including potential novel configurations emerging in the future. It is also compatible with superconducting electric motors, with the performance improvements reflected in the supplied input parameters and the necessary cooling equipment either modelled via the Thermal Management System (TMS, see Table 3.2) or by reducing the specific power accordingly.

The drawback of this simplified component model is that the electric motors are essentially considered as a point mass, without any indication of the corresponding outer dimensions, as these depend more heavily on the various motor types. It also assumes a constant specific power and efficiency, independent of the applied load. While this does not represent the real behaviour, it is sufficiently accurate for the conceptual design.

Sizing Methods The performance parameter of the *specific power* provides a simple relation between the maximum available mechanical output power and the associated component mass. Assuming the desired HEPS engine performance has been predicted according to the methodology presented in Section 3.2 (or an equivalent methodology), the maximum mechanical output power the electric motor must be able to deliver is readily available. Consequently, the component mass is simply obtained via Equation (3.2).

$$m_{EM} = \frac{P_{max.\ mech.\ EM}}{p_{sp.,\ EM}} \tag{3.2}$$

Analogous to the estimated electric motor mass, the maximum electric power that the component will demand of the hybrid-electric distribution system can be computed using the component efficiency, as shown in Equation (3.3).

$$P_{max.\ elec.\ EM} = \frac{P_{max.\ mech.\ EM}}{\eta_{EM}} \tag{3.3}$$

Component Positioning The positioning of the electric motors for a *parallel* hybrid-electric propulsion system is, per definition, determined by the location of the installed engine. Both the ICE and the electric motor are physically connected to the propulsor, the general position of the electric motors is thus clearly defined. The exact location within the internal geometry of the HEPS engine will highly depend on the individual engine design. For the conceptual design process however, using the C.o.G. location of the general engine for the electric motors is sufficiently accurate. The final position of the electric motor is thus obtained via a simple assignment of known coordinates as shown in Equation (3.4).

$$\begin{aligned} X_{EM} &= X_{C.o.G.,\ engine} \\ Y_{EM} &= Y_{C.o.G.,\ engine} \\ Z_{EM} &= Z_{C.o.G.,\ engine} \end{aligned} \tag{3.4}$$

Required Parameters Due to the simple nature of the underlying component model, a very limited number of parameters are required for the sizing and positioning of the electric motor. A brief overview is provided in Table 3.1.

Table 3.1: Overview of the required input parameter for the sizing and positioning of the electric motor component.

	Parameter	Unit	Description
Component Model	Specific Power	$\mathrm{W \cdot kg^{-1}}$	Specific mechanical output power, detailing the amount of mechanical output power the electric motor produces per unit mass.
	Efficiency	$[0,1]$	Electric motor efficiency, detailing the loss during the conversion process from electrical to mechanical power.
HEPS Performance Prediction	Max. Output Power	W	Maximum produced mechanical output power, detailing the amount of power the electric motor is capable of providing to boost the drive-shaft.
Aircraft Geometry	Engine C.o.G. coordinates	m	Engine C.o.G. position, the position coordinates of the HEPS engine's centre of gravity in the body axis system.

Power Management And Distribution (PMAD) Component Sizing

The Power Management And Distribution system is responsible for controlling the power flow in the entire hybrid-electric propulsion sub-system. Despite its importance, the actual physical component of the PMAD can also be represented by a simplified model and be sized according to the general procedure depicted in Figure 3.7. Similarly to the electric motor components, the only component parameters required for the sizing methods are the *specific power* and the *maximum power*, in this case the maximum electric power encountered by the PMAD. The model is again intentionally kept abstract, to not restrict the component to a specific type. As will be discussed in Table 3.2, the model includes additional performance parameters which will be required for the sizing of other electric components.

Sizing Methods The mass estimate is again obtained via the simple relation provided by the *specific power*. To estimate the maximum amount of electric power that will be distributed at any point in time, the maximum electric power required at the propulsors (summation of the maximum electric power draw of each installed electric motor) is adjusted for the predicted overall HEPS powertrain efficiency, as shown in Equation (3.5). The overall efficiency in the equation is typically taken from the data of the HEPS performance prediction, where it can be used in the post-processing to include the electric energy flow (i.e. power) vector in the engine performance map. Once all electric components are sized, it will be updated according to Equation (3.1). Using the estimate for the maximum distributed power, the PMAD mass is estimated according to Equation (3.6)

$$P_{max.\ distr.} = \frac{\sum_{i=1}^{N_{engine}} P_{max.\ elec.\ EM,\ i}}{\eta_{HEPS\ powertrain}} \tag{3.5}$$

$$m_{PMAD} = \frac{P_{max.\ distr.}}{p_{sp.,\ PMAD}} \tag{3.6}$$

Component Positioning The PMAD, as part of the electrical distribution system, should logically be located in the power electronics (PE) bay, which is typically positioned right behind the main landing gear bay. Considering that the components of an electric propulsion system would naturally operate at much larger orders of magnitude than the other electrical systems, their inclusion in the power electronics bay will increase the required space therein. To remain within the scope of conceptual design, the designer is able to supply an assumed length in x-direction for the power electronics bay. The final position of the PMAD component is then simply assumed as within the defined power electronics bay.

To determine the PMAD position, first the position of the most aft main landing gear (MLG) bay must be determined. As typically only the position of the extended main landing gear is defined during the conceptual design phase, the defined extended x-position, the bogie length, and the defined wheel radius are used to estimate the x-position of the end of the main landing gear bay according to Equation (3.7). The end position as determined by the equation below leaves a gap between the most aft wheel and the bay equal to one wheel radius.

$$X_{end,\ MLG\ bay} = X_{MLG,\ extended} + \frac{l_{bogie}}{2} + 2 \cdot R_{wheel} \tag{3.7}$$

Using the assumed length of the electronics bay, the x-position of the PMAD is easily estimated. The y-position falls on the fuselage centreline, and the z-position is assumed to coincide with the midpoint of the centre spars, as this is assumed to approximate the halfway point between the cabin floor and the bottom of the fuselage. The final PMAD coordinate definitions are shown in Equation (3.8).

$$\begin{aligned} X_{PMAD} &= X_{end,\ MLG} + \frac{l_{PE\ bay}}{2} \\ Y_{PMAD} &= 0 \\ Z_{PMAD} &= \frac{Z_{FS} + Z_{RS}}{2} \end{aligned} \tag{3.8}$$

Required Parameters The simplified PMAD model and the corresponding sizing methodology require numerous input parameters. Although not required for the sizing or positioning of the PMAD component itself, all performance characteristics presented in Table 3.2 are essential for the complete HEPS sizing methodology.

Table 3.2: Overview of the required input parameter for the sizing and positioning of the PMAD component. Includes input parameters required by the component model essential for the sizing of other HEPS components.

	Parameter	Unit	Description
Component Model	Specific Power	$W \cdot kg^{-1}$	Specific power, detailing the amount of electrical power distributed per unit mass.
	Efficiency	$[0,1]$	PMAD efficiency, detailing the efficiency at which the PMAD distributes electric power between different components.
	Voltage Type	-	System voltage type, detailing the type of voltage (AC or DC) used in the distribution system.
	Integrated Protection	-	Integrated circuit protection, declares if the PMAD contains integrated circuit protection measures or whether a dedicated system is required.
Design Choices	Voltage Level	V	System voltage level, detailing the desired voltage level used in the distribution system.
	PE bay length	m	Power Electronics bay length, detailing the assumed length of the space required within the fuselage for the power electronics bay.
HEPS Performance Prediction	Max. EM Output Power	W	Maximum mechanical output power, detailing the amount of power each installed electric motor is capable of providing to boost the connected drive-shaft.
Aircraft Geometry	MLG x-coordinate	m	Main Landing Gear x-position, detailing the x-coordinate of the extended main landing gear most aft, in the body axis system.
	MLG bogie length	m	Main Landing Gear bogie length, detailing the total length of the bogie of the most aft main landing gear.
	Wheel radius	m	Main wheel radius, detailing the radius of the wheel installed on the most aft main landing gear.
	Spars z-coordinate	m	Center wingbox spar z-position, detailing the z-coordinate of the front and rear spars forming the center wing box, in the body axis system.

Circuit Protection (CP) Component Sizing

Circuit protection (CP) is an essential component in any electric circuit, but becomes extra important on an aircraft due to its inherent vulnerable state. It not only protects the crew and passengers from potential dangers, but also prevents potential faults from propagating through the entire network. Typically power switches and circuit breakers are used for the protective measures, but at higher loads the disconnecting of transmission lines can lead to electric arcing, requiring alternative circuit protection devices. For the devised methodology, no assumption on the used type of circuit protection device is made. If a dedicated component

is required, the user is expected to provide the assumed specific power and efficiency performance parameters corresponding to the desired technology.

Sizing Methods Whether a circuit protection component has to be sized or not is determined by the inputs provided to the PMAD model, as the CP functionality may also be integrated into the PMAD. Should a dedicated circuit protection system be required, the sizing procedure is analogous to that for the PMAD: using the maximum encountered distributed electric power from Equation (3.5), the mass is computed using Equation (3.9). Due to the typically significant difference in order of magnitude for specific power, the impact of the dedicated circuit protection system on the overall mass prediction is expected to be small.

$$m_{CP} = \frac{P_{max.\,distr.}}{p_{sp.,\,CP}} \tag{3.9}$$

Component Positioning Considering the option to have the circuit protection system integrated into the PMADsystem, its positioning methodology closely follows the process defined for the PMAD. Just like the PMAD, the circuit protection is part of the electrical propulsion system. In case the PMAD requires a dedicated circuit protection system to be designed, its position is assumed to coincide with the position of the PMAD. The circuit protection system component coordinates are thus obtained from the PMAD according to Equation (3.10).

$$\begin{aligned} X_{CP} &= X_{PMAD} \\ Y_{CP} &= Y_{PMAD} \\ Z_{CP} &= Z_{PMAD} \end{aligned} \tag{3.10}$$

Required Parameters Similarly to the electric motors, the dedicated circuit protection system requires a very basic set of input parameters. Additionally, although already computed during the sizing of the PMAD component, the input parameters necessary to determine the maximum distributed electric power are also included in Table 3.3 for consistency.

Table 3.3: Overview of the required input parameter for the sizing and positioning of the dedicated circuit protection system component

	Parameter	Unit	Description
Component Model	Specific Power	$\mathrm{W \cdot kg^{-1}}$	Specific power, detailing the amount of electric power within the distribution system that can be protected per unit mass.
	Efficiency	$[0,1]$	Component efficiency, detailing the loss occurring due to the added components the distributed power has to pass through.
HEPS Performance Prediction	Max. EM Output Power	W	Maximum mechanical output power, detailing the amount of power each installed electric motor is capable of providing to boost the connected drive-shaft.
	HEPS powertrain efficiency	$[0,1]$	The assumed total powertrain efficiency, detailing the total losses throughout the hybrid-electric propulsion sub-system.
HEPS Sized Components	PMAD C.o.G. coordinates	m	PMAD C.o.G. position, the position coordinates of the previously sized PMAD's centre of gravity in the body axis system.

Thermal Management System (TMS) Component Sizing
The thermal management system (TMS) is another vital component of the hybrid-electric propulsion system. While mostly negligible for the propulsion system on conventional aircraft concepts, the much larger magnitude of electrical power handled by a HEPS powertrain necessitates a proper control of the electrical system temperature. Although it is possible to include a detailed sizing of the TMS for a hybrid-electric propulsion system during the conceptual design, as was done by Lents et al. [14], a much more simplified model is used as representation, which also allows for more flexibility. The methodology for sizing the TMS as discussed here is intended for a normal-conducting electric system, but due to its abstract nature it can be used to model a cryo-cooling systemused for super-conduction. It is however recommended to extend the presented sizing process in the future, to obtain a more accurate prediction.
The TMS component sized according to this methodology applies only to the electrical propulsion system. It is intended to estimate the additional mass introduced due to the cooling requirements of the hybrid-electric propulsion system, and is intended to be integrated into the TMS of the whole aircraft.

Sizing Methods At the current state of the methodology, the mass of the required thermal management system is simply determined via an input performance parameter that relates the electric power passing through the propulsion system to the corresponding TMS mass. Using the maximum occurring distribution power from Equation (3.5), the mass is estimated using Equation (3.11)

$$m_{TMS} = \frac{P_{max.\,distr.}}{p_{sp.,TMS}} \tag{3.11}$$

Initially it was planned to include a method that estimates the generated heat in each component methodology, and then base the TMS sizing methods on the total amount of generated heat. However, it was found that the performance of the thermal management system was not only dependent on the heat power to be removed, but also the actual temperature thereof. Implementing methods considering both the heat power as well as the individual component temperatures and how these are transferred to the TMS would require a much more detailed modelling of the propulsion system. To remain within the scope of this thesis — and conceptual design itself — it was decided to leave this more detailed sizing of the thermal management system to a later design stage, when the aircraft concept is already more clearly defined.

Component Positioning Considering the sizing methodology explicitly intends for the HEPS TMS to be integrated into the whole aircraft TMS, it logically follows that it is also located at the same position. Following this logic, the sized HEPS TMS is added to the Pressurisation and Air Conditioning Kit (PACK), which is typically located outside the fuselage in the wing-body fairing. To obtain an exact estimate of the resultant CoG location of the added mass, it is assumed to coincide with the intersection of the wing leading edge and the fuselage.
Devising a method for determining the exact coordinates is mostly a matter of design tool implementation. Assuming the design tool features a virtual geometry model of the aircraft, geometrical functions can be used to find the intersection point of the wing leading edge and the fuselage. This point can then be used as a substitute for the position of the TMS within the wing-body fairing. Due to symmetry, the y-coordinate of the TMS system will be assumed on the fuselage centreline (y=0.0), while the x- and z-coordinate are taken from the determined wing-fuselage intersection point, resulting in the coordinate definitions as shown in Equation (3.12).

$$\begin{aligned} X_{TMS} &= f\left(wing\ component,\ fuselage\ component\right) \\ Y_{TMS} &= 0.0 \\ Z_{TMS} &= f\left(wing\ component,\ fuselage\ component\right) \end{aligned} \tag{3.12}$$

All mass is is assigned to the location where the PACK is expected, meaning the impact of the required parts to transport the heat from its origin to the heat exchangers is ignored. Furthermore, it is assumed that the space available within the wing-body fairing is large enough to accommodate the heat exchangers necessary to remove all heat generated by the electric propulsion system. Depending on the Degree-of-Hybridisation of the hybrid-electric propulsion system, this may not be achievable. Additionally, while the sizing methodology is sufficiently abstract to allow the sizing of a cryogenic cooling system (provided the method is appropriately extended), the positioning methodology does not allow to account for the cooling system or the mass of the required cryogenic fluid.

Required Parameters Due to the generalised nature of the current TMS model, only the three parameters shown in Table 3.4 are necessary for the sizing process, assuming the usage of built-in geometric functions for the positioning. Extending or replacing the limited TMS model will naturally impact the number of inputs required.

Table 3.4: Overview of the required input parameter for the sizing and positioning of the thermal management system for the sized electric components.

	Parameter	Unit	Description
Component Model	Specific Power	$W \cdot kg^{-1}$	Specific power, detailing the amount of electric power within the distribution system whose generated heat can be managed by the thermal management system, per unit mass. Relates to input of electric power in distribution system, not the heat dissipated per unit mass!
HEPS Performance Prediction	Max. EM Output Power	W	Maximum mechanical output power, detailing the amount of power each installed electric motor is capable of providing to boost the connected drive-shaft.
	HEPS powertrain efficiency	[0, 1]	The assumed total powertrain efficiency, detailing the total losses throughout the hybrid-electric propulsion sub-system.
HEPS Sized Components	Wing-Fuselage intersection point	m	Intersection point of wing LE and fuselage, the position coordinates of the point of intersection between the main wing leading-edge and the fuselage, in the body axis system.

3.3.2. Battery Component Sizing

The batteries are the most important component for the HEPS component sizing, as not only do they impose a significant mass penalty, but depending on their position the shift in the aircraft's balance will cause a change in the overall aircraft concept. They are also the most complex to model, as it combines energy storage and power production functionalities. The chosen simplified model manages to provide an estimate of the most important characteristics, while limiting the required input data to those parameter typically presented for expected future developments.

Because the chosen battery model as described below includes a maximum achievable capacity for an individual battery pack, the devised methodology separates the sizing of the batteries for a hybrid-electric propulsion system into two separate aspects. The first, denoted the "Battery System Sizing" concerns the configuration and interaction of the various battery packs, while the "Battery Pack Sizing" addresses the performance and physical properties of the individual battery packs. Both will be described in detail below.

Battery Model

The model devised to represent the batteries of the hybrid-electric propulsion system was created to be compatible with the performance characteristics presented in the battery technology forecast from the EU commission [24]. A battery pack component can be sized based solely on the maximum pack capacity Q, the maximum C-rate C, the specific energy $e_{sp.}$, the maximum depth of discharge DoD, and the energy density $\rho energy$. While most battery sizing methods in literature define a relation between the specific power and the specific energy externally, using the maximum allowed C-rate and the specific energy instead, integrates a representation of the power-energy interdependency based on physical properties of the batteries into the model itself. Additionally, by specifying the maximum capacity for a single battery pack, the methodology is able to size individual battery packs, which results in a more accurate representation of the corresponding

mass penalty due to the required transmission lines (see Section 3.3.3). As the sizing of the battery component for the hybrid-electric propulsion system is governed by the energy and power characteristics, the battery capacity is expressed in the unit of watt-hour (W·h) or kilowatt-hour (kW·h), as is standard for conceptual HEPS design.
To restrict the level of detail of the required input parameters, the battery model is limited to simulate the battery performance on a pack level, ignoring the individual cell characteristics. As such, it assumed that the battery pack provides a constant voltage equal to the distribution system voltage defined in the PMAD, as indicated in Table 3.2. In the integration of the battery model into the component sizing design tool, the sizing methods were extended to allow the user to provide the specific power instead of, or in addition to, the maximum C-rate. The tool automatically checks the compatibility of the provided inputs and raises an error should the provided data be inconsistent.
Should the aircraft concept be intended to be equipped with two different types of batteries, the methodology can simply be applied twice, once for each type. In this case, the user has to separate the total amount of stored electric energy into the amount to be stored per battery type. In the current state of the methodology and its implementation in the design tool, it is assumed that one battery type will be used as a "main" battery, with the second type being an "auxiliary" battery. The main battery will be used until the power draw exceeds a threshold, at which point the hybrid-electric system switches to the auxiliary battery. This implies, that at any point in time only one type of battery will be active, the auxiliary battery will thus provide the electric power *instead of* the main battery, not *in addition to*. In this case, the user must also prescribe the maximum amount of power to be drawn from the "main" battery type, while the maximum amount of power to be drawn from the "auxiliary" battery is simply taken from the HEPS engine performance map. However, the methodology can easily be adapted such, that the "auxiliary" battery delivers power *in addition to* the "main" battery. In either case, the following "Battery System Sizing" and "Battery Pack Sizing" procedures described below are simple executed twice, with the respective input parameters for the two battery types. The most important aspect to consider is the implementation of the battery pack positioning in the used design tool. As the methodology sizes individual battery packs and positions them sequentially inside the fuselage, the design tool must use the same internal storage for the space already occupied by previously sized battery packs, as explained in the respective paragraph.

Battery System Sizing Methods

Having imposed a limit as to the maximum capacity for an individual battery pack, the methodology is required to automatically find the "ideal" combination of battery packs. This addressing both the total number of packs as well how these are to be connected, which will be referred to as the "Battery System Architecture". The battery system sizing methodology is distinguished by working with a *variable design C-rate*, which is synonymous with a variable specific power at a constant specific energy. While the absolute maximum power output of the individual battery packs will still correspond to a discharge at the *maximum model C-rate* $C_{max.}$, the sizing methods will operate under the assumption, that the batteries will be discharged at the *maximum design C-rate* $C_{max.,\,design}$ when providing the maximum system power. Ideally, this will be used during the aircraft concept iteration to continually adapt the prescribed battery model to achieve the best performance. Observing the prediction of future battery technology development presented by the European Commission [24], three battery type classifications ("energy", "power", and "high power") with different performance characteristics are expected. These differ not only in their presented discharge C-rates and corresponding achievable specific energy characteristics, but also their maximum pack capacities. A reduction in the maximum allowed discharge C-rate might thus result in a different battery type being better suited for the aircraft concept.
The critical battery properties for the sizing of the "ideal" battery system architecture are the *maximum pack capacity*, the *maximum C-rate*, and the *pack specific energy*, as well as the the power and energy requirements — to maximum required power draw and the total amount of stored electric energy for the design mission — from the HEPS performance prediction. It should be noted, that while the methodology is described as providing the "ideal" or "optimum" battery system architecture, this is not obtained via a detailed optimisation procedure. The methodology simply operates under the assumption, that the configuration that results in the smallest total number of required battery packs will correspond to the lowest possible system mass.
The battery system sizing process, as illustrated in Figure 3.8, begins by determining both the absolute minimum *total* number of battery packs ($N_{min.,\,energy}$), as well as the minimum number of battery packs connected in *parallel* ($N_{min.,\,power}$). These two numbers correspond to the requirements formulated by the HEPS performance prediction and the simulated design mission on the energy (total amount of stored elec-

tric energy) and on the power (total power provided equals the sum of the power drawn from each battery pack connected in parallel), for a discharge at the maximum possible C-rate. The numerical values are computed according to Equations (3.15) and (3.16) respectively. It should be noted that the shown equations produce integer values, exclusively rounded up to the next higher number, as indicated by the "ceiling brackets". The total power supplied by the combined battery packs is estimated via Equation (3.13) (currently identical to $P_{max.\ distr.}$ from PMAD sizing), and for both equations determining the number of packs, the *usable* maximum pack capacity, as computed according to Equation (3.14), is used.

$$P_{max,\ total} = \frac{\sum_{i=1}^{N_{engine}} P_{max.\ elec.\ EM,\ i}}{\eta_{HEPS\ powertrain}} = P_{max.\ distr.} \tag{3.13}$$

$$Q_{pack,\ max.\ usable} = DoD_{max.} \cdot Q_{pack,\ max.} \tag{3.14}$$

$$N_{pack,\ min.,\ energy} = \left\lceil \frac{Q_{total,\ req.}}{Q_{pack\ max.,usable}} \right\rceil \tag{3.15}$$

$$N_{pack,\ min.,\ power} = \left\lceil \frac{P_{max,\ total}}{C_{max} \cdot Q_{pack\ max.,\ usable}} \right\rceil \tag{3.16}$$

It is highly unlikely, that the computed number of packs for both requirements coincides. Should the power requirement by critical, the number of packs connected in parallel is larger than the minimum total number of packs required. In this case, the battery system architecture will contain exactly one set of $N_{pack,\ min.,\ power}$ battery packs, and store more than the necessary amount of electric energy. More likely, however, is that the energy requirement is critical, meaning that the battery system requires more than the minimum number of packs in parallel. Unfortunately, it is not valid to simply size for the exactly one set of $N_{pack,\ min.,\ energy}$ battery packs. While this would indeed fulfil the requirement on the stored electric energy, the batteries would no longer be discharged at the prescribed maximum C-rate, as this would provide more than the required electric power. Instead, the methodology will determine for which discharge C-rate the required number of battery packs in parallel is an exact multiple of the required total number of battery packs.

To limit the process to only valid potential C-rates, the investigation will be governed by the potential number of battery packs in parallel. The interval of potential alternative number of battery packs in parallel is restricted to any value from the minimum number $N_{pack,\ min.,\ power}$ determined via Equation (3.16) to one less than twice this number, as shown in Equation (3.17). This upper limit is imposed to prevent the generation of redundant combinations, as $2 \cdot N_{pack,\ min.,\ power}$ can be achieved by having twice as many battery packs connected in parallel at a severely reduced C-rate, or by simply installing two sets of $N_{pack,\ min.,\ power}$, to be used consecutively. Both options will result in the same total number of battery packs, therefore being considered equally "optimal" by the simplified assumptions that a low number of packs equals a low total mass. As the latter corresponds to the individual battery packs resembling the user prescribed battery model more closely, it was chosen as the more desirable option

$$\left[N_{pack,\ parallel},\ \ldots,\ 2 \cdot N_{pack,\ parallel} - 1\right] \tag{3.17}$$

As indicated in the process flow of Figure 3.8, the methodology computes the corresponding required maximum pack power and associated C-rate, as well as the resulting number of sets necessary to abide by the overall HEPS energy requirement, for each potential number of battery packs in parallel $N_{parallel,\ i}$. These computations are performed according to Equations (3.18) to (3.20), and the obtained results stored such, that they can be associated to the applicable $N_{parallel,\ i}$. The total number of battery packs will always be a multiple of the number of packs in parallel, because the hybrid-electric propulsion system must always be capable of delivering the maximum electric power, no matter at which point in the flight envelope or mission phase. As the maximum total HEPS power can only be supplied by discharging all battery pack in parallel at their maximum design C-rate, there must always be a set of exactly $N_{parallel}$ battery packs available.

$$C_{option,\,i} = \frac{P_{max,\,pack}}{Q_{pack\ max.,\,usable}} = \frac{P_{max,\,total}}{N_{parallel,\,i} \cdot Q_{pack\ max.,\,usable}} \tag{3.18}$$

$$F_{seq,\,option,\,i} = \left\lceil \frac{N_{pack,\,min.,\,energy}}{N_{parallel,\,i}} \right\rceil \tag{3.19}$$

$$N_{total,\,alternativ,\,i} = F_{seq,\,option,\,i} \cdot N_{parallel,\,i} \tag{3.20}$$

Ultimately, the combination that results in the lowest total number of battery packs is selected as the "optimum". In case of multiple options with the same number of total battery packs (see the potential values for an example case provided in Table 3.5), the option that most closely resembles the battery performance as prescribed by the provided component model is chosen — essentially the lowest number of packs in parallel, as this corresponds to a battery discharge at a higher C-rate. For the example case provided in Table 3.5, this corresponds to the option of $N_{parallel,\,option} = 6$ with the associated four sets of battery packs to be used in sequence.

Table 3.5: Total number of battery packs for the possible combinations of number of battery packs in parallel and the associated number of sets of battery packs in sequence, for an example case with $N_{pack,\,min.,\,power} = 5$ and $N_{pack,\,min.,\,energy} = 24$. For each potential number of packs in parallel $N_{parallel,\,option}$, the valid total number of battery packs that satisfies both the energy and power requirements of the overall HEPS sub-system are indicated.

$N_{parallel,\,option}$	Number of Sets in sequence F_{seq}			
	2	3	4	5
5	10	15	20	(25)
6	12	18	(24)	30
7	14	21	(28)	35
8	16	(24)	32	40
9	18	(27)	36	45

Finally, the battery system sizing methodology updates the performance requirements for the individual battery packs to match the determined battery system architecture. The underlying battery model parameters remain unchanged, but the "optimal" *design C-rate* is added, which will be used for the pack sizing methods. Additionally, the HEPS energy and power requirements (total amount of stored electric energy and maximum total power draw) are converted into the corresponding battery pack energy and power requirements according to Equations (3.21) and (3.22), denoting the amount of *usable* energy stored and the maximum electric power drawn per battery pack.

$$Q_{pack,\,usable,\,req.} = \frac{Q_{total,\,req.}}{N_{total,\,final}} \tag{3.21}$$

$$P_{max.,\,pack,\,req.} = \frac{P_{max,\,total}}{N_{parallel,\,final}} \tag{3.22}$$

At the time of this thesis report, the methodology implemented in the component design tool (see Section 6.4) differs from the above described methodology. It still corresponds to a previous iteration, wherein two battery system architectures are sized in parallel, one at the maximum model C-rate and one at the determined "optimum" C-rate (excluding the exact $N_{pack,\,min.,\,power} = 5$ from the investigated interval). Both sized battery systems are then compared as to their total mass and the option with a lower mass is selected for the aircraft concept, while the other is discarded. While it does impose a higher computational cost, the created results do not differ, as both options are included in the set of investigated potential number of packs in parallel in the methodology presented above.

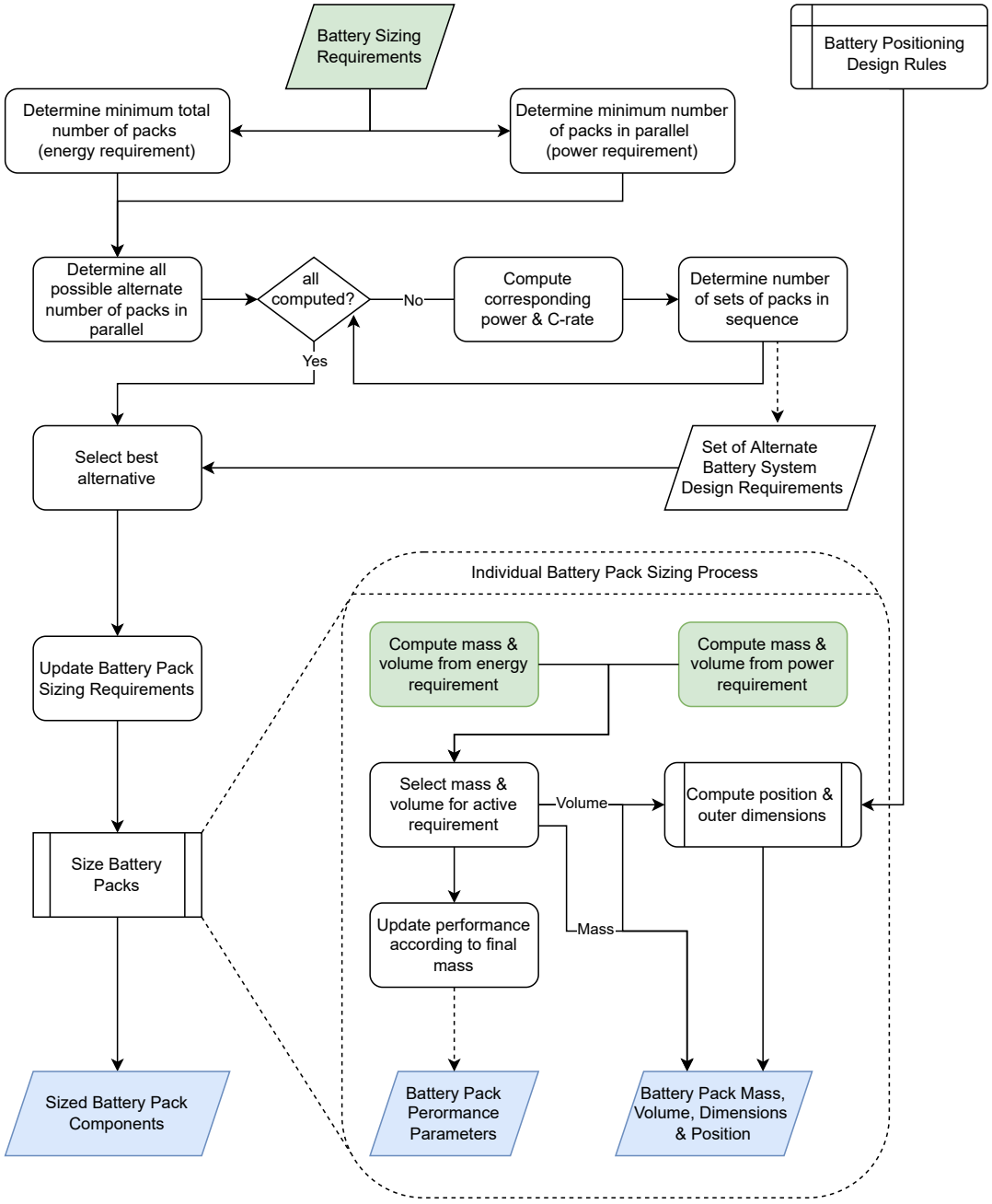

Figure 3.8: Illustration of the methodology workflow for the sizing of the battery components of a parallel hybrid-electric propulsion system. This process flow addresses the procedure on how to determine the "optimal" configuration of individual battery packs to abide by the system performance requirements, while also providing an overview of the sizing logic applied for each individual battery pack.

Battery Pack Sizing Methods

After determining the "optimum" battery system architecture and computing the resulting battery pack performance requirements, the individual battery packs can be sized. These performance requirements are the maximum amount of power that the battery pack must be able to provide (via Equation (3.22) and the total amount of *usable* electric energy stored in the pack (via Equation (3.21). Because the battery model performance parameters are defined relative to the *total* pack capacity, and since virtually every type of battery cannot be repeatedly fully discharged without a deterioration of it's performance, the sizing computations are performed using the total pack capacity, computed via Equation (3.23).

$$Q_{pack,\,total,\,req.} = \frac{Q_{pack,\,usable,\,req.}}{DoD_{max.,\,pack}} \tag{3.23}$$

Using the defined maximum possible power draw and total pack capacity requirements, the sizing of the individual battery pack component can be conducted as broadly outlined in Figure 3.8. Due to the inherent battery characteristic of simultaneously storing energy and providing electric power, the sizing method must determine whether the power or the energy performance requirement is constraining the design. Thus the methodology computes the potential battery pack masses for both requirements, before selecting the larger mass as sizing, as shown in Equations (3.24a) to (3.24c). Analogous to the mass, the corresponding battery pack volume is computed, following the same principle but replacing the specific energy with the energy density, as outlined in Equations (3.25a) to (3.25c).

$$m_{pack,\,energy} = \frac{Q_{pack,\,total,\,req.}}{e_{sp.,\,pack}} \tag{3.24a}$$

$$m_{pack,\,power} = \frac{P_{max.,\,pack,\,req.}}{p_{sp.,\,pack}} = \frac{P_{max.,\,pack,\,req.}}{DoD_{max.} \cdot e_{sp.,\,pack} \cdot C_{max.,\,design}} \tag{3.24b}$$

$$m_{pack} = max\big(m_{pack,\,energy},\, m_{pack,\,power}\big) \tag{3.24c}$$

$$V_{pack,\,energy} = \frac{Q_{pack,\,total,\,req.}}{\rho_{energy,\,pack}} \tag{3.25a}$$

$$V_{pack,\,power} = \frac{P_{max.,\,pack,\,req.}}{\rho_{power,\,pack}} = \frac{P_{max.,\,pack,\,req.}}{p_{sp.,\,pack} \cdot \underbrace{\frac{\rho_{energy,\,pack}}{e_{sp.,\,pack}}}_{=\rho_{battery}\,[\mathrm{kg \cdot m^{-3}}]}} \tag{3.25b}$$

$$V_{pack} = max\big(V_{pack,\,energy},\, V_{pack,\,power}\big) \tag{3.25c}$$

As the battery pack is sized for either the energy *or* the power requirement, the final performance of the battery pack no longer matches the required performance of the non-critical requirement, but exceed it. The final performance parameters of the sized battery pack are thus updated to properly reflect the determined final mass according to Equations (3.26) to (3.28).

$$Q_{pack,\,total} = e_{sp.,\,pack} \cdot m_{pack} \tag{3.26}$$

$$Q_{pack,\,usable} = DoD_{max.} \cdot Q_{pack,\,total} \tag{3.27}$$

$$P_{max.,\,pack} = \underbrace{DoD_{max.} \cdot e_{sp.,\,pack} \cdot C_{max.}}_{=p_{sp.,\,max.,\,pack}} \cdot m_{pack} \tag{3.28}$$

Note, that the maximum discharge C-rate used in Equation (3.28) is the *maximum model C-rate*, not the previously computed *maximum design C-rate*. While the battery pack was sized according to the desired maximum C-rate, the battery itself is still capable of being safely discharged at the maximum prescribed in the user-supplied model. The maximum possible power the battery pack is capable of providing is thus larger than the maximum power that is expected to be drawn according to the HEPS engine performance prediction. While this is a side-effect of the methodology determining an "ideal" design C-rate, it can be considered as an added layer of redundancy. Should a battery pack in the set fail, the remaining battery packs can be discharged at a C-rate above the design target, thus compensating for the failed component.
Finally, the computation of the outer dimensions of the battery pack are more complicated and usually coupled to the positioning methodology. While it is possible to manually prescribe the lengths in y- and z-direction as a constraint, the developed methodology to automatically determine the dimensions is limited due to the restricted amount of information available during conceptual design. This methodology, explained in detail in the next paragraph, operates by separating the outer dimensions into the cross-sectional area in the y-z-plane and the corresponding length along the body x-axis. The numeric value for the cross-section area is determined during the positioning operations and the resulting length of the battery pack is computed using Equation (3.29).

$$l_{x,\,pack} = \frac{V_{pack}}{A_{x-sec.,\,pack}} \tag{3.29}$$

Battery Pack Positioning
Devising the positioning methodology for the battery system was complicated by two aspects: the battery system is separated into individual battery packs; and opposed to the other "general" components, no equiv-

alent or corresponding component of the conventional concept can be used to prescribe the position. In its current state, the methodology positions all battery packs within the fuselage and does not support their placement in neither the wing-body fairing nor in dedicated externally mounted pods. To reduce the effect the placement of the various battery packs has on the aircraft balance, the packs are alternatively located in the forward and aft part of the fuselage, separated by the centre wing box and the main landing gear and/or electronics bay. Each subsequent battery pack is placed further away from the fuselage center, thus concentrating the added mass as close to the aircraft centre of gravity as possible. For example: battery pack 1 is stored in the aft fuselage, behind the electronics bay; battery pack 2 is stored in the forward fuselage, in front of the front spar; battery pack 3 is positioned behind battery pack 1; battery pack 4 is positioned in front of battery pack 2; and so on. While this method intrudes on the available cargo space, a placement inside the wing analogous to the fuel tanks was deemed infeasible, as hybrid-electric concept requires the battery packs *in addition* to the existing fuel tanks.

The devised battery pack positioning (and outer dimension sizing) methodology were inspired by the Unit Load Devices (ULD) containers used for cargo storage. Ideally, the individual battery packs can be integrated into the HEPS sub-system in such a way, that they can easily be removed and replaced. This not only improves the maintainability of the components, but also drastically reduces the aircraft turnaround times, as the batteries no longer have to be charged while inside the aircraft. This can also increase the battery packs life cycle, as on-ground charging is no longer exposed to a time constraint, allowing a slower, more efficient charging at vastly reduced C-rates.

Due to the underlying assumptions the y-position for each battery pack is fixed on the fuselage centreline (Equation (3.30)), and the z-coordinate coincides with the midpoint of the centre spars (Equation (3.31)), as this is assumed to approximate the halfway point between the cabin floor and the bottom of the fuselage. The presented methodology will thus only determine the individual positions along the x-axis.

$$Y_{pack} = 0 \tag{3.30}$$

$$Z_{pack} = \frac{Z_{FS} + Z_{RS}}{2} \tag{3.31}$$

Figure 3.9 provides an illustration of positioning logic, explicitly separated into individual process flows for the placement in the forward and aft fuselage. While the general processes as shown in the blocks are the same for both flows, the used methods, while symmetric, differ in their implementation.

The "Battery Pack Sizing Data" provided at the start of the process denotes the sized battery pack and represents a link to the sizing methods used above. The first operation in the sizingmethodology is to determine whether the current battery pack is to be placed in the forward or aft fuselage. At this point the choice to place the first battery pack in the forward or aft fuselage segment is arbitrary, as default it was decided to begin in the aft fuselage. For each fuselage segment, the general process is identical, with the implemented methods mirroring each others calculations — in the forward fuselage, the battery pack is placed as much aft as possible, while in the aft fuselage, the battery pack is placed as much forward as possible.

For each battery pack a unique position limit can be defined, constraining how far aft in the forward and how far forward in the aft fuselage the pack can be placed. These position limits depend either on the aircraft structure (front spar and power electronics bay) or the previously positioned battery packs, and can be computed according to Equations (3.32) and (3.33). In addition to providing the limit position in the computation of the offset later during the iteration, it is also used as an initial starting point for the position convergence iteration.

$$\begin{aligned} X_{limit,\,FS} &= X_{FS} \\ X_{limit,\,packs} &= min\left(\{X_{start}\}_{assign.\ battery\ pack\ space}\right) \\ X_{limit,\,current} &= min\left(X_{limit,\,FS},\, X_{limit,\,packs}\right) \\ &\quad + \Delta X_{battery\ spacing} \end{aligned} \tag{3.32}$$

$$\begin{aligned} X_{limit,\,PE\ bay} &= X_{end,\,PE\ bay} \text{ [c]} \\ X_{limit,\,packs} &= max\left(\{X_{end}\}_{assign.\ battery\ pack\ space}\right) \\ X_{limit,\,current} &= max\left(X_{limit,\,PE\ bay},\, X_{limit,\,packs}\right) \\ &\quad + \Delta X_{battery\ spacing} \end{aligned} \tag{3.33}$$

The methods above automatically account for any previously positioned battery packs and add a battery spacing offset ($\Delta X_{battery\ spacing}$), which can be set by the designer. It should be noted, that the notation $\{X_{start}\}$ and $\{X_{end}\}$ implies a set of values, corresponding to the start and end positions of all previously

[c] for the determination of the location of the power electronics bay, see the positioning methods of the PMAD in Equations (3.7) and (3.8)

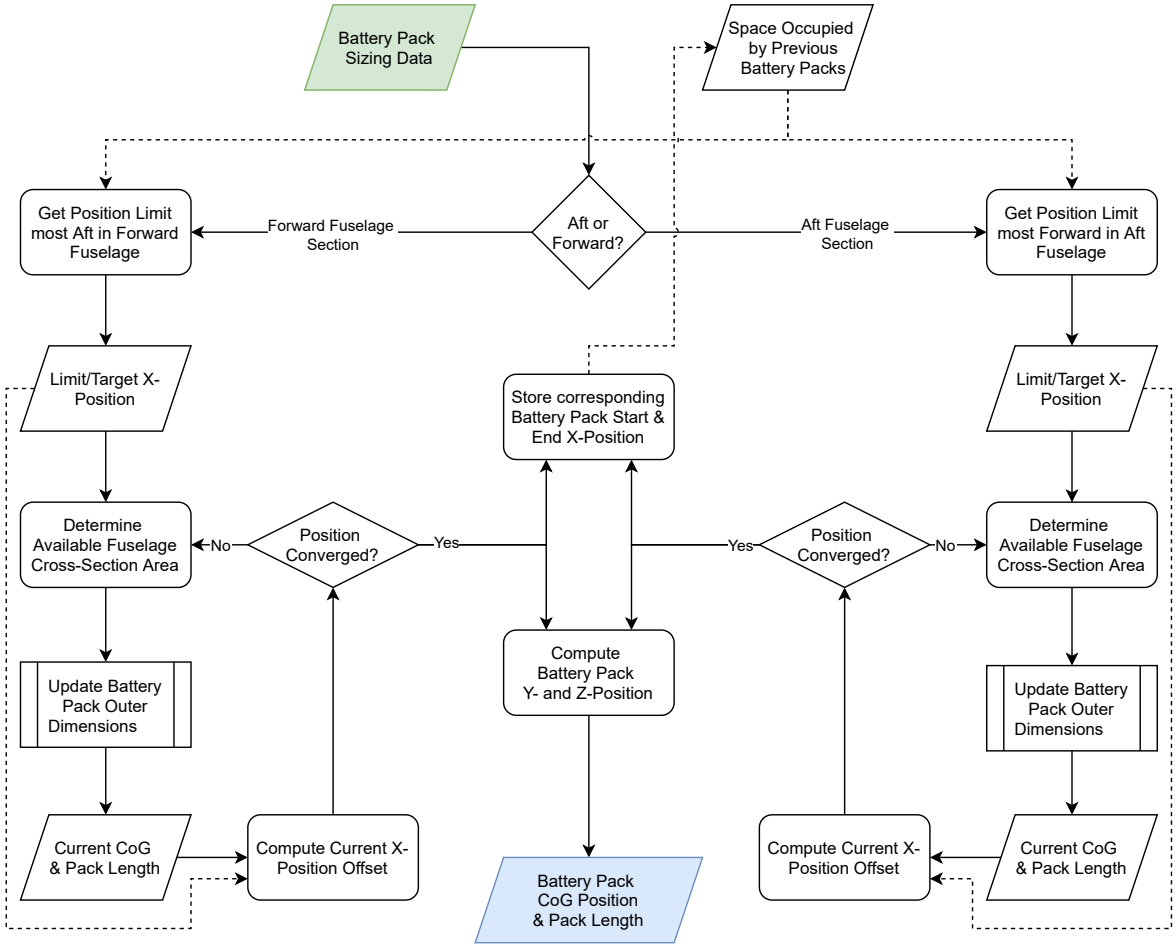

Figure 3.9: Illustration of the positioning methodology proposed for the placement of the individual battery packs. While symmetric, the process flow for the positioning in the forward and aft fuselage differ in their implementation into a design tool due to the opposite shifting of the battery pack during the placement iteration, which is emphasised by explicitly displaying both procedures. In case of multiple types of batteries being sized for the aircraft concept, the same process is to be used, with the "Space Occupied by Previous Battery Packs" containing all previously sized battery packs of all considered battery types.

placed battery packs. This starting point is also used during each step of the iteration to compute the required shift.

As the determination of the outer dimensions of a battery pack depends on the cross-section area available in the fuselage, an iteration is required to determine the converged position for each pack. This iteration begins with the determination of the cross-sectional area available for the battery pack at the current position. The actual method for this depends on the available functionality of the design tool, but modern design tools often include a virtual geometric model of the aircraft concept with supporting functions to compute the intersected area of various shapes. Using these modelling functions, the total fuselage cross-section area at the specified x-position can be computed. For conceptual design, it is easiest to then simply assume a certain percent-fraction of how much of the fuselage cross-section area can be used for battery storage, and calculate the fuselage cross-section area available for battery storage via Equation (3.34). Should a detailed modelling of the internal fuselage structure be implemented already (or the cabin floor position be defined), a more detailed method than presented here can be substituted.

$$\begin{aligned} A_{x-sec.,\,fuselage} &= f\left(X-position\right) \\ A_{x-sec.,\,avail.} &= \underbrace{\left(\frac{A_{x-sec.,\,battery}}{A_{x-sec.,\,fuselage}}\right)}_{\text{Design Assumption}} \cdot A_{x-sec.,\,fuselage} \end{aligned} \tag{3.34}$$

The computed available battery cross-section area is then used according to the sizing methodology in Equation (3.29) to update the battery's length along the x-axis, denoted in Figure 3.9 by the pre-defined process. Using the new length of the battery pack and the previously determined position limit, the offset of the battery pack border is computed and the current CoG position estimate updated, according to Equations (3.35a) and (3.35b) and Equations (3.36a) and (3.36b) for the placement in the forward and aft fuselage respectively.

$$\Delta X_{battery} = \left(X_{current} + \frac{l_{battery}}{2}\right) - X_{limit,\,current} \tag{3.35a}$$

$$X_{current,\,new} = X_{current,\,old} - \Delta X_{battery} \tag{3.35b}$$

$$\Delta X_{battery} = X_{limit,\,current} - \left(X_{current} - \frac{l_{battery}}{2}\right) \tag{3.36a}$$

$$X_{current,\,new} = X_{current,\,old} + \Delta X_{battery} \tag{3.36b}$$

Once the difference in the updated battery pack x-position is sufficiently small, the internal placement iteration is converged. The corresponding start and end x-position of the battery pack is computed via Equations (3.37) and (3.38) and added to the assigned battery space used in Equations (3.32) and (3.33).

$$X_{start,\,battery} = X_{CoG} - \frac{l_{battery}}{2} \tag{3.37}$$

$$X_{end,\,battery} = X_{CoG} + \frac{l_{battery}}{2} \tag{3.38}$$

Finally, the battery pack's Y- and Z-position is computed, either via Equations (3.30) and (3.31) or a different implemented method, thus defining the 3D coordinates of the battery pack.

Required Parameters

Due to the increased complexity of the battery system and pack component sizing methods, the total number of required inputs is larger than for any other electrical component. Table 3.6 provides an extensive overview of all parameters that are required for the sizing of both the battery system, as well as the individual battery packs. The various parameters are grouped according to their origin as one of the following: "Component Model" specific parameters, used to define the type of battery pack that is sized; "Design Inputs" specific parameters, being choices imposed by the user to govern the desired hybrid-electric system for the aircraft concept; "HEPS Performance Prediction" specific parameters, referring to data obtained from the prior performance prediction using the methodology from Section 3.2; and the "Aircraft Geometry" specific parameters, which contains data extracted from the current aircraft geometric model.

Table 3.6: Overview of the required input parameter for the sizing and positioning of the battery system and the battery pack components. If multiple battery types are used in combination, all design inputs and component model parameters must be defined per used battery type.

	Parameter	Unit	Description
Component Model	Max. Pack Capacity	$\mathrm{kW \cdot h}$	Maximum possible battery pack capacity, defining the maximum capacity that can be achieved for an individual battery pack.
	Max. C-rate	$\mathrm{h^{-1}}$	The maximum allowed discharge C-rate, defines the maximum C-rate at which the battery pack may be discharged according to specifications.
	Specific Energy	$\mathrm{W \cdot h \cdot kg^{-1}}$	Battery pack specific energy, detailing the amount of electrical energy that can be stored in the battery pack per unit mass.
	Energy Density	$\mathrm{W \cdot h \cdot m^{-3}}$	Battery pack energy density, detailing the amount of electrical energy that can be stored in the battery pack per unit volume.

Continued on next page

Table 3.6: (cont.) Overview of the required input parameter for the sizing and positioning of the battery system and the battery pack components. If multiple battery types are used in combination, all design inputs and component model parameters must be defined per used battery type.

	Parameter	Unit	Description
	Max. DoD	$[0,1]$	Maximum Depth of Discharge, detailing how much of the stored energy can be discharged without negatively effecting the battery pack health.
	Efficiency	-	Battery pack efficiency, detailing the efficiency at which the battery pack provides electric power.
Design Inputs	Number Battery Types	-	The total number of different battery types to be used during the battery sizing, allowing the user to size the battery system with different battery types in combination.
	Req. Electrical Energy	$W \cdot h$	Required electrical energy/total capacity, describing the total amount of *usable* electrical energy that must be stored on-board to enable the design mission.
	Max. Output Power	W	Maximum electrical output power of a battery system, defines the maximum electrical output power provided by a battery system of a specific battery type.
HEPS Performance Prediction	Max. EM Input Power	W	Maximum electrical power required by the electric motors, detailing the amount of electrical power each installed electric motor requires when providing their maximum boost power to the connected drive-shaft.
	HEPS powertrain efficiency	$[0,1]$	The assumed total HEPS powertrain efficiency.
	Battery Area Ratio	$[0,1]$	The available battery-fuselage area ratio, design parameter that describes how much of the fuselage cross-section area is available for battery storage.
	Battery Spacing	m	The required spacing between two adjacent battery packs, allows the user to define a desired offset between the sized battery pack components.
Aircraft Geometry	Fuselage Cross-section area	m^2	The fuselage cross-section area, the total fuselage cross-section area at the current x-position.
	Spars x- and z-coordinate	m	Front- and rear-spar x- and z-positions, detailing the coordinates of the front and rear spars forming the center wing box, in the body axis system.
	MLG x-coordinate	m	Main Landing Gear x-position, detailing the x-coordinate of the extended main landing gear most aft, in the body axis system.
	MLG bogie length	m	Main Landing Gear bogie length, detailing the total length of the bogie of the most aft main landing gear.
	Wheel radius	m	Main wheel radius, detailing the radius of the wheel installed on the most aft main landing gear.

3.3.3. Transmission Line (TL) Component Sizing

The transmission lines are the last remaining component to be sized for a *parallel* hybrid-electric propulsion sub-system. A clear distinction is made between a "transmission line" and a "cable". In the devised methodology, a "transmission line" is defined as the general connection between two electric propulsion components, through which the required electric power is transmitted, whereas a "cable" is defined as the physical cable inside of each transmission line, through which the electric current is flowing when power is transmitted through the corresponding transmission line. By introducing this distinction, it is possible to implement separate models for the sizing of the general transmission line and the physical cables used therein, which in turn enables the implementation of different cable models. The choice of cable model may also be dependent on the defined type of the distribution system voltage, as AC and DC system are subjected to different requirements and limitations. In the current methodology, only cable models for a DC power distribution system are implemented, due to their advantages in terms of conductor mass and electromagnetic compatibility [25, p. 66]. Additionally, the implementation into the design tools as described in Section 6.4.1 is limited to only one cable model for the entire distribution network. A more optimised network may be achievable by tailoring the cable models to the electric components being connected.
For the devised methodology, a unique transmission line is sized for each connection from a battery pack to the PMAD, and again from the PMAD to each electric motor. The dedicated circuit protection system requires no connection, as it is already assumed to coincide with the PMAD position, and the necessary infrastructure to transport the generated heat to the electrical components thermal management system is assumed included in either the TMS specific power parameter or the individual component model.

Cable Models

By decoupling the transmission line from the physical cables, the methodology is capable of implementing a variety of possible cable model, from a simple, normal-conducting cable to even super-critical cables. The models are unique for each underlying cable type, and interface with the transmission line sizing methods by providing the resulting mass and efficiency of the cables.

Simple Cable Model The default cable model for the component sizing methodology corresponds to a simple, normal-conducting cable, and was proposed by Sgueglia et al. [17]. This cable model, characterised by a maximum allowed current and a linear cable density, has been used for the generation of the example HEPS aircraft concepts used in Chapter 4.
Using the maximum electrical power that is to be transferred through the transmission line and the distribution system voltage as defined in the PMAD, the corresponding electrical current is computed via Equation (3.39). From the total current and the allowed maximum current per cable, the total number of cables within the transmission line is easily computed according to Equation (3.40). Note, that the total number of cables is an integer rounded up from the computed value.

$$I_{total} = \frac{P_{max.,\,TL}}{V_{distr.\,system}} \tag{3.39}$$

$$N_{cable} = \left\lceil \frac{I_{total}}{I_{max.,\,cable}} \right\rceil \tag{3.40}$$

From the total number of cables, the resulting cable mass can be computed using the provided cable linear density and the total length from the transmission line sizing methods, as shown in Equation (3.41). As indicated by Sgueglia et al., the final mass will be increased due to the installation and health monitoring systems, which will be accounted for by the application of two corresponding mass penalty factors. The numeric values of the factors are user-defined inputs and can be used to calibrate the cable system.

$$m_{cable} = N_{cable} \cdot \rho_{cable} \cdot l_{cable} \cdot (1 + F_{instal.} + F_{HMS}) \tag{3.41}$$

Finally, the determined number of cables can also be used to define a maximum possible transmission power through the transmission line, larger than the required maximum transmission power. This power could be used for a check on redundancy and failure safety in combination with discharging a battery pack at it's maximum C-rate instead of the design C-rate in case of a battery pack failure. This however, is not currently included in the methodology.

To estimate the efficiency of the cables in the transmission line, the simple model includes the parameter *specific losses*, relating the occurring losses to the cable length. From the total required cable lengths obtained in the transmission line sizing, the total losses in the cable, and the resulting efficiency, are computed according to Equations (3.42) and (3.43).

$$P_{loss,\,cable} = p_{sp.,\,loss,\,cable} \cdot l_{cable} \tag{3.42}$$

$$\eta_{cable} = \frac{P_{max.,\,TL} - P_{loss,\,cable}}{P_{max.,\,TL}} \tag{3.43}$$

Advanced Cable Models Two more advanced cable models are presented in the thesis of Stückl [25], one for normal-conduction and one for super-conduction. The normal-conducting cable model constructs the cable from the inside-out, according to the necessary transmission power and physical material properties of all components required in the cable layout. While not presented here in detail, the result of this cable model is a linear cable density and the specific cable losses, both as a function of the maximum transmission power and the distribution voltage.
The model proposed for superconducting cables, specifically high-temperature superconducting (HTS), focusses more on the estimation of the thermal losses of the cable rather than their mass. For both the cable mass as well as the losses of the cable itself, Stückl assumes a linear relation of 5 $\mathrm{kg \cdot m^{-1}}$ and 0.5 $\mathrm{W \cdot m^{-1}}$ respectively. The losses at the cable termination, the connection interface between the cable and the connected components, are estimated based on method proposed by Gouge et al. [26]. According to this method, each electrical connection causes a heat input into the cryogenic cooling fluid of 45 $\mathrm{W \cdot kA^{-1}}$, plus an additional heat load $Q_{env.}$ due to the ambient environment of up to 200 W. The resulting formula to estimate the heat load for an HTS cable termination is presented in Equation (3.44). Note, that the heat load is provided in watt, whilst the current passing through the electrical connection is provided in kilo-ampere.

$$Q_{term.} = 45 \cdot N_{elec.,\,connections} \cdot I_{elec.,\,connections} + Q_{env.} \tag{3.44}$$

As both cable models proposed by Stückl provide a linear cable density and a method to estimate the total losses, both models can easily be implemented to interface with the overall transmission line sizing methods via the total transmission line length.

Transmission Line Sizing Methods
The sizing method of the transmission line components does not directly involve the estimation of the component mass like it does for all other component sizing methods, as this functionality is delegated to the selected underlying cable model. Instead, it deals with the coordination of the input parameters — particularly the choice of cable model, the required transmission power, and the choice of redundancy — as well as the interpretation of the estimated line path.
For the transmission line mass estimation, the sizing methods determine the total length resulting from the estimated path and apply an integer redundancy factor. Should the line path estimation be implemented such, that multiple, redundant paths are defined, the mass sizing method will compute the total length as the sum of the individual paths instead of applying the redundancy factor.
It is assumed, that the path or paths of the transmission line are defined as a sequence of coordinate points, thus all following calculations are discrete. The total length of any discretely defined path can be computed using Equation (3.45), based on the standard definition of a vector length.

$$l_{path} = \sum_{i=1}^{N_{points}} \sqrt{\Delta X_i^2 + \Delta Y_i^2 + \Delta Z_i^2} \tag{3.45}$$

with:

$$\Delta X_i = X_{i+1} - X_i; \quad \Delta Y_i = Y_{i+1} - Y_i; \quad \Delta Z_i = Z_{i+1} - Z_i$$

Using the above definition to compute the length of any arbitrary path, the transmission line sizing methodology uses the mass estimation method of the underlying cable model to predict the final transmission line mass. Depending on how the user approaches the implementation of redundancy, the method either applies

a simple redundancy factor to the cable mass, or determines the corresponding cable masses for each defined path individually, as shown in Equation (3.46). This implementation not only complies with the requirement for modularity of the cable models, but is also compatible with any methodology to estimate the transmission line path, provided the path is defined as a sequence of discrete coordinates.

$$m_{TL} = \begin{cases} m_{cable}\left(@l_{path}\right) \cdot F_{redundancy}, & \text{if a single path \& redundancy factor are defined} \\ \sum_{i=0}^{N_{paths}} m_{cable}\left(@l_{path,\,i}\right), & \text{if multiple paths are defined} \end{cases} \tag{3.46}$$

Finally, the transmission line determines the applicable component efficiency. Because the cable efficiency is computed via the total losses, which in turn are dependent on the total cable length, and due to the possibly differing length of redundant transmission line paths, the component efficiency is determined for the *average* transmission line length. This lengths is computed according to Equation (3.47). The resulting component efficiency is then simply the cable efficiency for this average transmission line length, as displayed in Equation (3.48).

$$l_{TL,\,avg.} = \begin{cases} l_{TL}, & \text{if a single path is defined} \\ \dfrac{\sum_{i=0}^{N_{paths}} l_{TL,\,i}}{N_{paths}}, & \text{if multiple paths are defined} \end{cases} \tag{3.47}$$

$$\eta_{TL} = \eta_{cable}\left(@l_{TL,\,avg.}\right) \tag{3.48}$$

Transmission Line Positioning and Path Estimation

The position of each transmission line to be used for updating the aircraft concept's weight and balance calculations depends on the defined path between the two components it connects. As the final number and position of the required battery packs is variable and determined automatically during the sizing process, so is the required number of transmission lines and their path. While it is possible to implement a detailed, high-fidelity algorithm to optimise the exact path — including multiple redundant paths abiding by the required minimum spacial separation — the conceptual design phase is better served by means of simple estimation. This simple estimation, explained in detail below, is used by the methodology to create unique transmission line connection between each battery pack and the PMAD, as well as the PMAD and electric motors installed in the engines. The handling of which battery packs are connected in parallel and which in sequence (see Section 3.3.2) is assumed to be handled during the installation of the PMAD, and is thus irrelevant for the transmission line path estimation.

A good approximation of the total path length of a transmission line is obtained by modelling the path between the connected components as a series of steps connecting the component centres of gravity, with each step being taken along one of the body-system axes. While this does not account for a path moving twice along the same axis in opposite directions (e.g. from the battery CoG to the fuselage shell, and back from the fuselage shell to the PMAD CoG) or along a diagonal path (e.g. along a wing spar), the resulting accuracy is sufficient for conceptual design. Figure 3.10 illustrates an example implementation of the proposed path methodology. The paths of two transmission lines are depicted, connecting first a battery pack from the forward fuselage section with the PMAD in the power electronics bay, and secondly said PMAD with an electric motor mounted within the underwing engine. For each transmission line path, the required steps along each of the body axes are drawn.

The predicted path is created by first determining the distance between the components to be connected in each of the three dimensions, as shown in Equation (3.49) (and illustrated in Figure 3.10). Afterwards, the transmission line path is defined by a set of four coordinates, beginning at the start component and then taking a step according to the determined offsets along each of the body axes to stop at the end component, as shown in Equation (3.50).

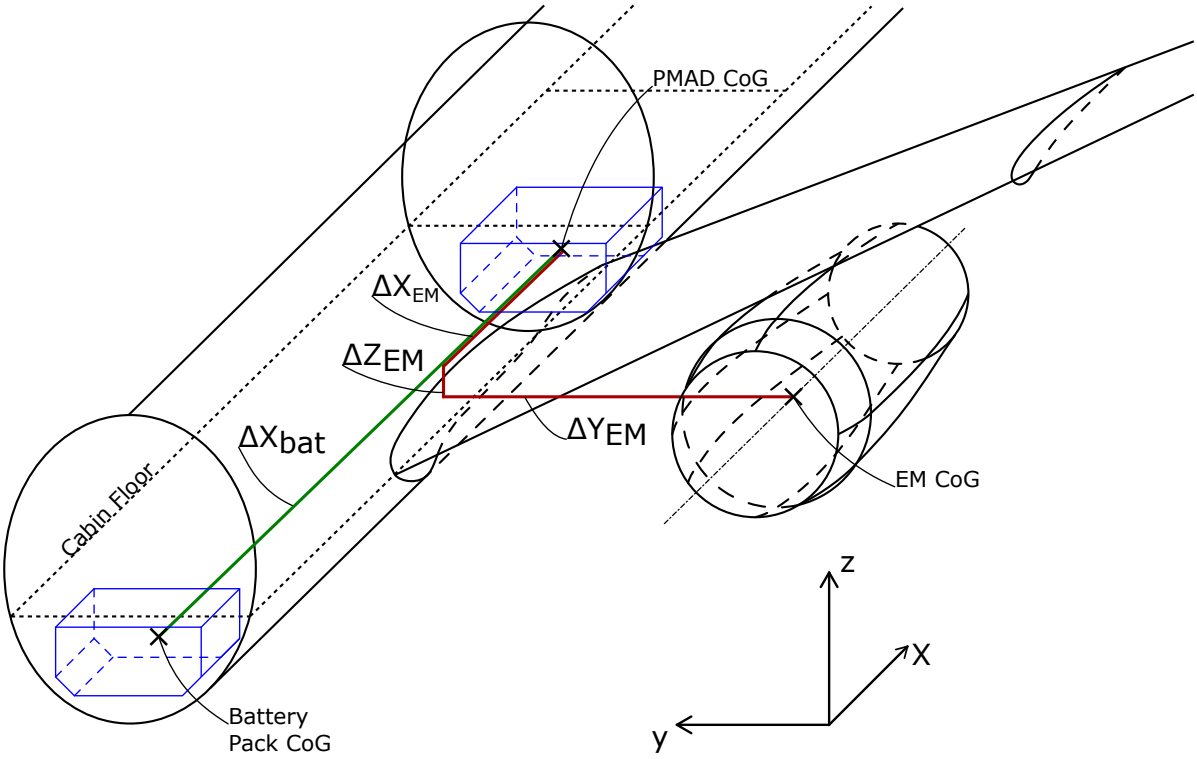

Figure 3.10: Schematic drawing to illustrate the logic behind the transmission line path estimation, the blue boxes indicate available space for electric propulsion components inside the fuselage. As prescribed by the path estimation knowledge rule, all battery packs are directly connected to the PMAD (green connection), and the PMAD is in turn connected to each electric motor (red connection). One example for each connection type is presented above, clearly displaying resulting transmission line paths. Note, that due to the definitions of the y- and z-positions of both the battery packs and PMAD, these components are only connected by a step along the x-axis, resulting in a slight under-estimation of the total path length.

$$\begin{aligned} \Delta X &= X_{end\ component} - X_{start\ component} \\ \Delta Y &= Y_{end\ component} - Y_{start\ component} \\ \Delta Z &= Z_{end\ component} - Z_{start\ component} \end{aligned} \tag{3.49}$$

$$\begin{aligned} Path = \Big[& (X_{start}, \quad Y_{start}, \quad Z_{start} \quad), \\ & (X_{start} + \Delta X, \ Y_{start}, \quad Z_{start} \quad), \\ & (X_{start} + \Delta X, \ Y_{start} + \Delta Y, \ Z_{start} \quad), \\ & \underbrace{(X_{start} + \Delta X, \ Y_{start} + \Delta Y, \ Z_{start} + \Delta Z)}_{(X_{end},\ Y_{end},\ Z_{end})} \Big] \end{aligned} \tag{3.50}$$

As the overall HEPS sizing procedure requires a combined mass and centre of gravity estimate to update the aircraft concept's balance calculations, the path of each transmission line has to be summarised into a single point, which represents it's centre of mass. Using the equations for calculating the centroid of a line, simplified for a sequence of straight line segments, the centre of gravity of any transmission line is determined via Equation (3.51). The symbols $\tilde{x}_i$, $\tilde{y}_i$, and $\tilde{z}_i$ correspond to the respective midpoint coordinate of the i^{th} line segment, easily determined as the average of the coordinate of two consecutive points in the defined line path.

$$CoG_{transmission\ line} = \begin{bmatrix} \overline{X} \\ \overline{Y} \\ \overline{Z} \end{bmatrix} = \begin{bmatrix} \frac{\sum \tilde{x}_i \Delta L_i}{\sum \Delta L_i} \\ \frac{\sum \tilde{y}_i \Delta L_i}{\sum \Delta L_i} \\ \frac{\sum \tilde{z}_i \Delta L_i}{\sum \Delta L_i} \end{bmatrix} \tag{3.51}$$

Required Parameters

The required parameters for the sizing of the transmission line components are highly dependent on the chosen cable model. An overview of all necessary input parameters for a transmission line sizing according to the simple cable model and path estimation method as presented above is given in Table 3.7. As can clearly be seen, the only required inputs related to the transmission line directly are the desired redundancy factor and cable model. The distribution system voltage, while having a great impact on the cable sizing, is considered a design choice of the PMAD sizing, and thus listed as obtained from another sized electric component.

Table 3.7: Overview of the required input parameter for the sizing of a Transmission Line component. Includes input parameters specific to the example cable model used in the generation of the example HEPS aircraft concepts in Chapter 4. Assumes transmission lines paths estimated according to above methodology.

	Parameter	Unit	Description
Cable Model	Max. Current	A	Maximum allowed current, detailing the maximum amount of electric current that can flow through a single cable.
	Cable Density	$kg \cdot m^{-1}$	Cable linear density, detailing the cable mass per unit length.
	Mass Penalty Factors	-	Various mass penalty factors, detailing the increase in final cable mass due to required additional sources, such as the installation or health monitoring systems.
	Specific Loss	$W \cdot m^{-1}$	Specific loss of the cable, detailing the amount of electric power lost per unit length.
Design Choices	Cable Model	-	The desired cable model to be used in the sizing, determines the required parameters for the cable sizing.
	Redundancy Factor	-	The desired level of redundancy for the transmission lines, detailing how many transmission lines are to be sized per electric component connection.
Other Electric Components	Voltage Level	V	System voltage level, detailing the desired voltage level used in the distribution system. Obtained from PMAD component.
	Max. Electric Power	W	Maximum electric power, detailing the maximum amount of electric power to be transmitted via the transmission line. Obtained via the battery system sizing of the battery components.
	Component Position	m	Position coordinates of other electric components, detailing the position coordinates of the centre of gravity of the components to be connected via the currently sized transmission line.

4

Verification Case Studies

To demonstrate the feasibility of the devised hybrid-electric sizing methodology, a series of verification case studies were performed. During each of these studies, example aircraft concepts were created and compared with either real-world aircraft, data from published research, or previous example concepts. All generated example concepts were only created to verify the methodology, and are not intended to be analysed with the aim of gaining insights into the potential benefits of a specific aircraft concept. The employed level of detail of the used concept generation workflow (see Chapter 7) are sufficient to assess the general accuracy of the implemented sizing methodology, but does not allow for an in-depth assessment of minute improvements.

Table 4.1 provides a quick overview over which aspects of the devised hybrid-electric sizing methodology are proven in the respective case studies. As can be seen, each consecutive case study builds upon the insights gained in the previous, beginning with an assessment of conventional turbofan concepts to provide the initial confidence that the underlying principle — individually scaling two separate fan and engine core performance maps to achieve all prescribed point performance requirements with the smallest possible engine, before combing these scaled origin performance maps into a cohesive overall engine performance map — is capable of producing an accurate prediction of the resulting engine performance.

Table 4.1: Overview illustrating which aspects of the devised hybrid-electric sizing methodology were proven in the respective case studies. Conducted analyses offered additional insights besides the proven aspects.

Proven Aspect	Case Study			
	Conventional (Section 4.2)	Boosted Turbofan "BTF" (Section 4.3)	Fixed Initial Cruise Altitude (Section 4.4)	Increased Battery E_{sp} (Section 4.5)
Performance Fundamental Principle	✓			
HEPS Engine Performance Prediction		✓	✓	
HEPS Mass Estimation		✓		
External Constraint Compatibility			✓	
Methodology Sensitivity				✓
Battery Pack Sizing Capability				✓

Following the proof of the underlying principle, Case Study 2 addresses the methodology's capability of sizing parallel hybrid-electric aircraft concepts. The chosen example HEPS concept is a "boosted turbofan" configuration, as this is not only the most likely to be realised in the near-to-mid future, but is also quite prevalent in published literature. Based on the interpretation of the obtained concept, Case Study 3 was initiated wherein a fixed initial cruise altitude was imposed on the concept design. This not only verified that the methodology can handle external constraints, but also allowed for an investigation on how the predicted HEPS engine performance varies for a different set of active design sizing points. Finally, Case Study 4 investigates the impact of a small increase in the assumed battery performance. This not only provided insight into the sensitivity of the design methodology in relation to the provided input data, but also illustrated the potential of the unique battery sizing method employed by the methodology, as detailed in Section 3.3.2.

4.1. Case Study Inputs and Design Choices

For a consistent comparison, all generated example aircraft concepts were sized using the same respective workflows and design requirements. A detailed breakdown of the structure of the conceptual design workflows for both the conventional and the hybrid-electric aircraft concepts is provided in Chapter 7. This section contains an overview of the choices made during the generation of the example concepts, including the Top-Level Aircraft Requirements (TLARs) and concept specific parameters (e.g. the fixed design parameters, the desired power-split ratios, or the limitation of the step-climb altitudes), the desired performance at each design sizing point, the exact definition of the mission for which the example concepts were designed, and the explanation on how the consumed fuel and electric energy during the ground segments were determined.

4.1.1. Top Level Aircraft Requirements and Relevant Concept Inputs

The TLARs used during the sizing of each example concept, as presented in Table 4.2, are primarily based on the A320neo, which is used as reference aircraft for the comparison in Case Study I (Section 4.2) to validate the underlying principle of the performance sizing methodology. To obtain concepts that enable a valid comparison between conventional and hybrid-electric aircraft, the chosen TLARs impose that all sized concepts are designed for the same purpose: a medium-range (much longer than typical for HEPS aircraft in contemporary literature), low-transonic cruise flight; and takeoff and landing performance compatible with the corresponding usual airports. Additionally, the payload and passenger capacity was selected to reflect a typical narrow-body airliner. Finally, TLARs pertaining to the reserve segment are formulated according to either the ICAO requirements or in-house design knowledge.

Table 4.2: Overview of the formulated Top-Level Aircraft Requirements (TLARs) imposed during the sizing of all example aircraft concepts, both conventional and hybrid-electric.

Parameter	Value	Rationale
Design Range	4630 km (2500 nmi)	Corresponds to the design range of the A320neo, according to payload-range diagram for 180 PAX @ 105 kg · PAX^{-1} [27].
Cruise Mach Number	0.78	Typical cruise Mach number for A320-size short-to-medium range airliners.[a]
Takeoff Distance	1950 m	Corresponds to runway length requirement for A320neo @ MTOW=79 t, for ISA conditions and airport pressure altitude of 0 ft [27].
Approach Speed	67.65 m · s^{-1} (131.5 kt)	Corresponds to final approach speed of A320neo @ MLW=67.4 t [27].

Continued on next page

Table 4.2: (cont.) Overview of the formulated Top-Level Aircraft Requirements (TLARs) imposed during the sizing of all example aircraft concepts, both conventional and hybrid-electric.

Parameter	Value	Rationale
Max. Payload Mass	20 t	Based on maximum payload of A320neo, slightly increased to obtain more concise value.
Number of Passengers	180 PAX	Corresponds to standard seating capacity of A320neo in Single-Class layout [27].
Passenger Mass	$105\,\mathrm{kg}\cdot\mathrm{PAX}^{-1}$	Recommended standard passenger mass (passenger + checked luggage), according to EASA [28].
Airport Altitude	0 m	Prescribes sea-level altitude of design airport, implying that all formulated takeoff and landing requirements apply at sea-level conditions.
Distance Alternate Airport	370.4 km	Assumed average distance to alternate airport following an aborted landing, based on DLR design knowledge.
Loiter Time	1800 s	Accounts for 30 min of loiter as required according to ICAO Annex 6, Part I, section 4.3.6 "Fuel Requirements" [29].
Fuel Contingency	5 %	Required contingency fuel reserve, according to ICAO Annex 6, Part I, section 4.3.6 "Fuel Requirements" (4.3.6.3c) [29].

[a] Value of 0.78 stated in "Aircraft Performance Database" of EUROCONTROL (`https://contentzone.eurocontrol.int/aircraftperformance/details.aspx?ICAO=A20N`) and corresponds to statement in an article about A320neo improvements on the Airbus website in 2016 (`https://web.archive.org/web/20160403132507/http://www.airbus.com/aircraftfamilies/passengeraircraft/a320family/technology-and-innovation/`)

The fixed design choices listed in Table 4.3 are mainly intended to compensate for the rudimentary nature of the used conceptual design workflow, addressing the lack of dedicated design tools for a more sophisticated analysis of, for example, the aerodynamic or structure performance of the concept. They also impose a limitation on the wing span to enforce a compliance with targeted airport capabilities. While this naturally exacerbates the performance penalties due to an increase in aircraft weight for the hybrid-electric concepts, it is considered more important to create aircraft concept that are equivalent in terms of their purpose, rather than their design.
Besides the supplied maximum achievable lift coefficient values for takeoff and landing configuration, these fixed design parameters focus mostly on prescribing the desired wing planform and the characteristic fuselage lengths. This facilitates a better comparison to the A320neo reference aircraft, even when the design masses increase significantly.

Table 4.3: Overview of the fixed design choices imposed during the sizing of all example aircraft concepts. These parameters constrict the available design space to enable a relevant comparison of the generated concepts.

Parameter	Value	Rationale
$C_{L,\,max}$ Takeoff	2.55	Assumed as reasonable value for current SoA high lift devices in takeoff configuration.
$C_{L,\,max}$ Landing	2.9	Assumed as reasonable value for current SoA high lift devices in landing configuration.
Min. Static Margin	0.18	Prescribed a fixed the minimum static margin to guarantee static stability.
Wing Span	35.9 m	Impose limit of less than 36 m wing span to comply with ICAO airport box limits (ICAO Code 4C, same as A320neo).
Wing Taper Ratio	0.224	Approximately equivalent to A320neo wing taper ratio; enforces comparable wing planform to reference aircraft.
Wing Dihedral	7°	Prescribed to obtain comparable wing dihedral to A320neo.
HTP Dihedral	7°	Prescribed to obtain comparable HTP dihedral to A320neo.
Inboard TE Sweep	0°	Prescribe 0° inboard trailing edge sweep angle to obtain A320neo-like wing planform.
Fuselage Length	37.57 m	Prescribe total aircraft fuselage length to coincide with A320neo for better comparison.
Fuselage Height	4.14 m	Prescribe fuselage height to coincide with A320neo for better comparison.
Fuselage Width	3.95 m	Prescribe fuselage width to coincide with A320neo for better comparison.
Number of Passengers per Row	6	Prescribe Single-Class passenger cabin layout.

Finally, Table 4.4 contains the fixed design choices required for the formulation of the desired point performance used in the definition of the design sizing points as detailed in Section 4.1.2. The increase in flight altitude during a cruise step-climb is fixed to 2000 ft to abide by the semicircular/hemispheric rule, which dictates the grouping of flights into either even or odd thousands flight level, depending on whether they are westbound or eastbound respectively. Additionally, it prescribes a minimum rate of climb that the aircraft must be able to achieve once it reached the increased altitude after the step climb, such that potential evasive manoeuvres are possible. Lastly, it prescribes the desired design power-split ratios for the respective design sizing points. Alternatively, a maximum engine core output power can be defined instead of design power-split ratios, as is done for the "mid-cruise_climb" design sizing point. In the case of this thesis however, the maximum allowed engine core power is calculated during each iteration step and not prescribed as a fixed input value.

Table 4.4: Overview of the design choices imposed on the desired aircraft and hybrid-electric engine performance, relevant for the definition of the individual design sizing point performance requirements.

Parameter	Value	Rationale
Step-Climb Altitude Increase	609.6 m (2000 ft)	Prescribes an increase in altitude during the step-climb procedure of 2000 ft to abide by the semicircular/hemispheric rule,[a] assuming Reduced Vertical Separation Minima (RVSM).
Minimum Cruise Rate of Climb	$300\,\mathrm{ft}\cdot\mathrm{min}^{-1}$	Prescribes the minimum rate of climb required at top of climb as well as the altitude after performing the step-climb. Example value of $300\,\mathrm{ft}\cdot\mathrm{min}^{-1}$ chosen to avoid over-sizing of engines.
Desired Power-Split Ratios	0.17 (Takeoff) 0.09 (Climb) 0.0 (Cruise, steady flight)	The chosen "desired" power-split ratios for the generation of the example "boosted turbofan" HEPS aircraft concepts.

[a] Semicircular/hemispheric rule (with RVSM) dictates that all eastbound flights are assigned an odd thousands Flight Level, while all westbound flights are assigned an even thousands Flight Level. In some countries, the separation is oriented north/south, instead of east/west (e.g. Italy, Portugal, New Zealand).

4.1.2. Design Sizing Point Definition

For the sizing of the example concepts, the point performance at four characteristic points within the flight envelope of the design mission are defined. These four points form the basis for the predicted engine performance, as explained in Section 3.2.2, and are called "design sizing points" throughout this thesis. For the example aircraft concepts generated, the following design sizing points were defined:

1. SLS Takeoff
2. Top of Climb
3. Mid-Cruise (2x, steady and step-climb)

These points were chosen because they indicate the aircraft's performance during the three main performance scenarios. A detailed description of the exact performance that was prescribed for each point is given in the following paragraphs.
It must be stressed that the prescribed values for the power-split ratio are indicating the *maximum allowed* value of the power-split ratio at each design sizing point. It is very likely that the power-split ratio actually active at the point is much lower in the predicted engine performance map, as the sizing of an "augmented" hybrid-electric performance map sizes the engine core according to the design sizing point that requires the largest relative shaft power output.

SLS Takeoff Design Sizing Point The sea-level static takeoff performance is the point in the flight envelope that is usually sizing for the engine performance of transport aircraft in traditional conceptual aircraft design. Based on the desired takeoff performance — typically in terms of a maximum balanced takeoff distance — and the certification requirements on climb performance with one engine inoperative, the minimum required thrust-to-weight ratio for ISA standard conditions is determined. This fixes the required thrust at takeoff, with the performance at all other points within the flight envelope following from the corresponding engine performance. Potential cruise thrust requirements are converted into equivalent SLS thrust-to-weight ratios via theoretical thrust-lapse models, and are usually non-sizing.
The values prescribed for the concept generation in this study are presented in Table 4.5. Note, the absence of a numerical value presented for the required takeoff thrust, as this value is directly dependent on the current MTOW of the aircraft concept due to the typical sizing methods computing the required thrust-to-weight ratio instead of the actual required thrust.

Table 4.5: The prescribed point performance required from the engine for SLS takeoff conditions.

Parameter	Value	Source
Altitude	0.0	Fixed at standard sea-level.
Mach Number	0.0	Fixed at 0.0 for static takeoff.
Total Thrust[a]	Variable	Taken from CPACS file, corresponding to openAD sizing computations for current state of A/C concept.
Power-Split Ratio	0.17[b,c]	Supplied by user, in case of boosted Turbofan concept kept constant at 17%.

[a] The required total thrust per engine, not of the entire aircraft.
[b] The chosen value of 17 % is based on a study by Tan [30].
[c] Value only valid for the example "boosted Turbofan" concept.

Top of Climb Design Sizing Point The Top of Climb design sizing point is of interest as it reflects both the climb and cruising performance. By specifying the available thrust and Mach number at the final point in the climb phase, this design sizing point indirectly prescribes the maximum thrust available throughout the entire climb phase. The more thrust available, the faster the aircraft is able to climb to cruising altitude, depending the definition of the climb segment of the design mission. Additionally, prescribing a very low value for the maximum allowed power-split ratio might restrict the reduction in engine core size (if the top of climb design sizing point should be actively sizing for the generated hybrid-electric engine performance map).
Besides the climb performance, the altitude assigned to this design sizing point corresponds to the initial cruise altitude determined during the mission simulation of the previous convergence iteration step. It is thus also prescribing the total thrust available to the aircraft at the immediate beginning of the cruise phase, possibly restricting the ability to accelerate from climb to cruise Mach number (depending on the Mach numbers defined for the respective segments in the mission definition).

Table 4.6: The prescribed point performance required from the engine for Top of Climb conditions.

Parameter	Value	Source
Altitude	Variable	Set to correspond to the ICA computed in the mission simulation of the previous design convergence iteration step.
Mach Number	0.76	Fixed at 0.76, corresponding to the target Mach number during climb as defined in the mission simulation (see Chapter 8).
Total Thrust[a]	Variable	Computed according to Equation (4.1) for the current state of the aircraft concept.
Power-Split Ratio	0.09[b,c]	Supplied by user, in case of boosted Turbofan concept kept constant at 9%.

[a] The required total thrust per engine, not of the entire aircraft.
[b] The chosen value of 9 % is based on a study by Tan [30].
[c] Value only valid for the example "boosted Turbofan" concept.

Although the mission simulation tool ‘AMC‘ includes the aircraft performance at the top of climb point in it’s <results> node in the CPACS file, the values for the thrust available therein cannot be used for the definition of the design sizing point. The available thrust values of the point performance from ‘AMC‘ are the actual thrust produced at that point during the simulated mission, as well as the maximum thrust available at that combination of altitude and Mach number, according to the engine performance map. Both values are unsuitable, as the design sizing point prescribes the *desired minimum thrust available*. Table 4.6 provides an

overview of the data prescribed for the top of climb design sizing point.
The actual thrust the engine is desired to be capable of producing at the top of climb point depends on three aspects: the aircraft drag to be compensated, the acceleration from climbing to cruising Mach, and the minimum achievable rate of climb. As the mission definition does not define a time for the acceleration from climbing to cruising Mach, the required total thrust at the design sizing point is computed based on only the aircraft drag and the minimum rate of climb.

$$T_{ToC} = \frac{1}{N_{engine}} \cdot \left(D_{total,\ ToC} + \frac{RoC_{min,\ ToC} \cdot W_{A/C,\ ToC}}{V_{TAS,\ ToC}} \right) \tag{4.1}$$

Equation (4.1) presents the formula used to compute the desired minimum available thrust per engine at the top of climb. As can be seen, the rate of climb component includes the momentary aircraft weight and the airspeed corresponding to the Mach number specified. As the aircraft will not have to simultaneously climb at the specified RoC and accelerate to cruising Mach, the excess thrust available from the rate of climb requirement is deemed sufficient to produce the desired acceleration during normal operation.

Mid-Cruise Design Sizing Point The last two points of interest for the sizing of the desired engine performance are at mid-cruise. At this point, depending on the intended design range, the aircraft is likely to perform a step-climb to optimise it's cruise performance. The engine performance available at the mid-cruise point — being the point that most consistently is nearest the point of the actual step climb and is thus used as a proxy — is critical in optimising the aircraft concepts cruise performance. Performing a step climb enables the aircraft to cruise at more efficient altitudes and thus reduce fuel consumption, however, should the mid-cruise point be active during the sizing of engine performance, it has to be guaranteed that the engine can provide sufficient thrust to comply with the required minimum rate of climb.

The mission simulation tool 'AMC' computes not only the optimum ICA, but also automatically determines the point during cruise at which to initiate the step climb. At each sample point during the cruise segment, the tool computes the specific air range (SAR) and the available rate of climb at the next higher flight level (AMC can account for directional limits of flight levels, by specifying a "stepClimbAltitudeDifference" in the cruise segment data of the defined mission). Should the climb to the next altitude be beneficial, and should the available rate of climb at the next higher altitude exceed the required minimum rate of climb, the mission simulation will perform a climb manoeuvre.
As 'AMC' checks for the rate of climb at the next possible cruise altitude, the mid-cruise design sizing points must also specify the point performance at the next higher flight level. This altitude is computed via Equation (4.2), where the increase in altitude Δh is specified by the user and corresponds to the value for the "stepClimbAltitudeDifference" in the cruise segment of the mission definition.

$$h_{mid} = h_{mid,\ AMC} + \Delta h_{mid} \tag{4.2}$$

For the increased altitude, the required thrust per engine can then be computed from the drag and rate of climb components, analogous to the Top of Climb design sizing point. At this point, the necessity for defining two design sizing points become apparent. To utilise the main principle of a "boosted turbofan" parallel HEPS concept — augmenting the engine with electric boost power such that the conventional engine core is operating optimally during cruise — it has to be enforced that the engine core alone is capable of providing all the required thrust for straight and steady flight. Simultaneously, the engine must be able to provide excess thrust to achieve a minimum rate of climb for events such as traffic avoidance. With the engine core already operating at maximum capacity, electric boost power must be added. As the amount of excess thrust, and thus electric boost power, varies with the total aircraft mass, those two requirements cannot be enforced be prescribing a fixed power split ratio. Thus, two design sizing points are defined, one to prescribed the required mid-cruise steady flight performance ("mid-cruise_steady"), and one to define the necessary performance to abide the mid-cruise climb requirements ("mid-cruise_climb").
The exact thrust values are computed based on the total aircraft drag at the specified altitude and Mach number (obtained from current aircraft's aerodynamic performance map), the required minimum rate of climb, the instantaneous aircraft weight, and the current true airspeed. Equations (4.3) and (4.4) provide the exact formulae used for the thrust value computations, indicating that the drag and airspeed values correspond to the increased altitude computed via Equation (4.2).

$$T_{mid,\,steady} = \frac{1}{N_{engine}} \cdot D_{total,\,mid} \Big|_{D = D(@h_{mid})} \tag{4.3}$$

$$T_{mid,\,climb} = \frac{1}{N_{engine}} \cdot \left(D_{total,\,mid} + \frac{RoC_{min,\,mid} \cdot W_{A/C,\,mid}}{V_{TAS,\,mid}} \right) \Big|_{\substack{D = D(@h_{mid}) \\ V = V(@h_{mid})}} \tag{4.4}$$

As shown in Table 4.7, the Mach number is fixed according to the design mission and TLARs. For the sizing of "boosted turbofan" HEPS engine, the power split ratio for the "mid-cruise_steady" design sizing point is set to 0.0, as this enforces the conventional engine core to be scaled to provide 100% of the steady cruise power. To size the HEPS engine for the "mid-cruise_climb" performance, the alternative definition mentioned in Section 3.2.2 is used. The maximum shaft power output of the conventional engine core as determined in the previous iteration step is prescribed as the current limit for the origin performance map scaling.

Table 4.7: The prescribed point performances required from the engine for the mid-cruise steady flight and climb conditions.

Parameter	Value	Source
Altitude	Variable	Set according the mid-cruise altitude computed in the mission simulation of the previous design convergence iteration step, updated using Equation (4.2).
Mach Number	0.78	Fixed at 0.78, corresponding to the cruise Mach number as defined in the design mission (see Table 8.1).
Total Thrust[a]	Variable	Computed according to Equation (4.3) or Equation (4.4) for the current state of the aircraft concept.
Power-Split Ratio[b]	0.00	Supplied by user, in case of boosted Turbofan concept kept constant at 0% to cruise at maximum engine core efficiency.
Max. GT shaft power[c]	Variable	Obtained from HEPS engine performance at design sizing point "mid-cruise_steady" during previous design convergence iteration step.

[a] The required total thrust per engine, not of the entire aircraft.
[b] Only defined for design sizing point "mid-cruise_steady" of "boosted turbofan" concept.
[c] Only defined for design sizing point "mid-cruise_climb" of "boosted torbofan" concept.

4.1.3. Case Studies Design Mission

Each of the case studies documented in the subsequent Sections 4.2 to 4.5 uses the same design mission during the example concept sizing. Similarly to the TLARs detailed in Section 4.1.1, the design mission also uses the A320neo as reference, as this corresponds to the typical mission current conventional short-to-medium range transport aircraft are designed for.

The design mission follows a typical civil air transport mission in that it consists of the actual main mission, and an aborted landing followed by a cruise to, and a loitering phase at, the alternate airport. The exact definition within CPACS used in the verification case studies was obtained from the DLR and is based on the design mission used in the studies conducted by Iwanizki et al. [7] and Hecken et al. [5]. It features a design range of 2500 nmi, based on the range of an A320neo at a payload corresponding to 180 PAX, and is presented in more detail in Chapter 8.

Figure 4.1 provides an overview of the used design mission, qualitatively illustrating the mission profile and indicating the segments each mission phase consists of. An alternative main mission could be defined according to the data provided under `https://contentzone.eurocontrol.int/aircraftperformance/details.aspx?ICAO=A320`, which features a more detailed breakdown of the climb and descent phases. For

the purpose of generation of example concepts as proof of concept of the sizing methodology however, the simpler representation used here is sufficient.

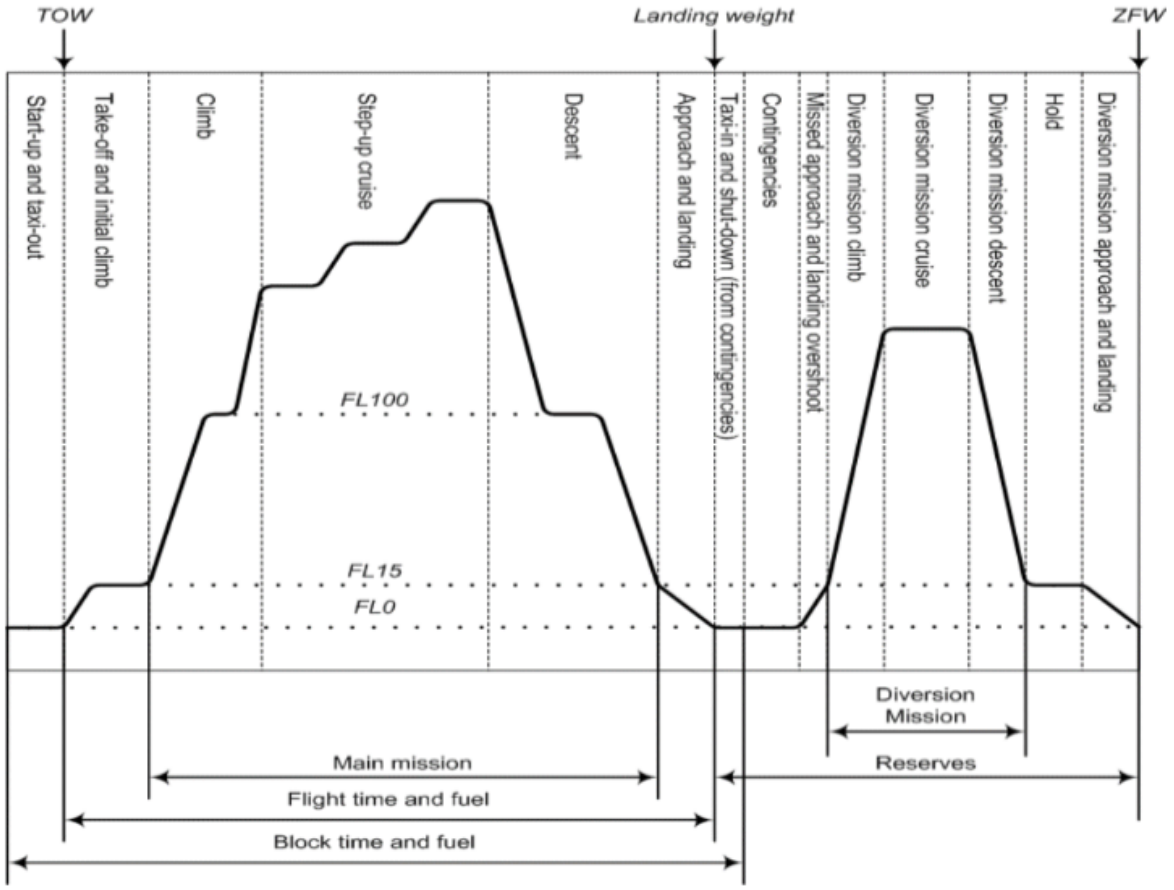

Figure 4.1: Illustration depicting the altitude-profile of the design mission, indicating relevant flight phases and mission segments.

Source: [5]

Due to limitations in the mission simulation tool, only segments in which the aircraft operates entirely airborne can be fully simulated. As such, a number of segments are considered "ground segments" ("taxi out" and "taxi in", "takeoff", and "approach/landing"), and their contribution to the total amount of required fuel and electric energy is prescribed rather than computed during the simulation. To properly reflect the updated prediction of the engine performance, the corresponding changes in consumed fuel/energy are computed during each design iteration step as explained in Section 4.1.4.

Following the "takeoff" ground segment, including the initial climb to 1500 ft, the simulation of the main mission begins with a 2-layered climb to the initial cruise altitude, which is either fixed or based on the optimum cruise altitude computed in the previous design iteration step. During the climb, the aircraft first climbs at a constant CAS to FL100, before it accelerates to the climb CAS prescribed for the second climb phase. In the beginning, the second climb phase is performed at constant CAS, until the change in altitude causes the CAS and Mach constraints to coincide. Afterwards, the climb is continued at constant Mach until cruise altitude. Because in the used mission definition the prescribed climb Mach number is lower than the desired cruise Mach, the final segment of the climb phase consists of an acceleration to the cruise Mach number.
The cruise phase is represented by a single segment, as the final cruise range is calculated based on the flight distance covered during climb and descent, and the total range requirement is defined for the overarching main mission. For the cruise of the main mission, the constraints dictate a maximum altitude, a desired Mach number, and the allowed altitude difference when performing a step-climb, which forces the cruise to be performed at exact flight levels.

Following the cruise, the descent is initiated by a deceleration to descent velocity (until both CAS and Mach are below the prescribed constraint), followed by a descent first at constant Mach, then at constant CAS, equivalent to the climb phase. Finally, the "approach/landing" ground segment covers the final descent from 1500 ft to mean sea-level and the touchdown deceleration. Similarly to the "takeoff" ground segment, the consumed fuel and electric energy is prescribed instead of computed and will be updated during each design iteration step.

The second part of the design mission is the diversion to an alternate airport following an aborted landing. Differing to the mission profile presented in Figure 4.1, the diversion mission was separated into two phases, an "alternate mission" for the flight from the target to the alternate airport, and an "alternate holding" which performed a loitering period at the alternate airport, as demanded by the ICAO Annex 6 [29].
The "alternate mission" is essentially a repeat of the "main mission", albeit with a cruise at a constant, lower altitude and at reduced Mach. Again, a 2-layered climb phase with intermediate acceleration, and a final altitude of only 7620 m (FL250) is prescribed. The cruise segment of the alternate mission is performed at constant altitude, as the small range required would not allow for a step-climb. To optimise the aircraft performance, the Mach number is reduced based on the assumption that the alternate cruise would be performed at the same dynamic pressure as the main mission cruise. The alternate descent is again a repeat of the main mission descent, consisting of a deceleration to descent velocity and a 2-step descent to 1500 ft.
Upon arriving at FL15, the second diversion phase begins with a deceleration to the loiter Mach number. The loiter/holding segment has a prescribed duration and continuously computes the Mach number for optimised performance. In the definition of the loiter segment in Section 8.2, an upper and lower bound for the Mach number can be set. Following the loiter segment, the approach and landing segment of the diversion mission is again a pre-defined amount of consumed fuel and electric energy.
Finally, the "taxi in" ground segment and a contingency fuel fraction are included in the design mission. The taxi ground segment is updated during each design iteration step as all ground segments and the contingency prescribes a percentage fuel fraction. Although included between the main and alternate mission in Figure 4.1, the mission simulation actually computed the taxi in after the completion of the diversion.

4.1.4. Ground Segments Performance Definition

As stated when discussing the design mission definition in Section 4.1.3, the used mission simulation tool AMC only simulates the aircraft performance for segments that are entirely airborne. All segments containing any operation performed on the ground, are included in the mission simulation via a prescribed "fuelConsumed" and "energyConsumed". As these values are still dependent on the engine performance, they naturally vary over the course of the design iteration. Here it will be explained how the consumed fuel and electric energy for each of the defined ground segments were updated, using the updated engine performance map from the preceding (HEPS) engine sizing tool.
Each of the ground segments includes a prescribed duration of the segment, indicating the time that passed between the start and end conditions. By defining a set of assumed values for the altitude, Mach number, and thrust setting at the start and end of each segment respectively, the corresponding amount of consumed fuel and electric energy can be computed from the engine performance map. The thrust setting is converted to engine thrust, and the corresponding entries for fuel flow and electric power are averaged between the start and end condition. Multiplication with the ground segment duration yields the total consumed fuel and electric energy, as shown in Equations (4.5) and (4.6).

$$m_{\text{fuel, ground seg.}} = \frac{\dot{m}_{\text{fuel, seg., start}} + \dot{m}_{\text{fuel, seg., end}}}{2} \cdot \Delta t_{\text{seg.}} \qquad \text{with } \dot{m} = f(h, M, T) \tag{4.5}$$

$$E_{\text{elec., groudn seg.}} = \frac{P_{\text{elec., seg., start}} + P_{\text{elec., seg., end}}}{2} \cdot \Delta t_{\text{seg.}} \qquad \text{with } P = f(h, M, T) \tag{4.6}$$

Taxi Ground Segment For both taxi ground segments the same assumptions summarised in Table 4.8 were made. According to the design mission definition the altitude of both airports is set to mean sea-level. The allowed speed of taxi operations is limited and thus essentially standstill when considering the full range of velocity of the engine performance map. Finally, the thrust is set to idle as detailed in the A320 Instructor Support manual [31, p. 16], which corresponds a thrust setting of 0.0 for the performance map. To prevent rounding inaccuracy in the simulation tool causing an error, the thrust setting is set to just slightly above 0.0.

Table 4.8: The assumed values for the state variables required to estimate the fuel and electric energy consumed during the taxi out and taxi in ground segments.

State Variable	Assumed Value	
	Start Condition	End Condition
Altitude	0.0 m	0.0 m
Mach number	0.0	0.0
Thrust setting	0.00001[a]	0.00001[a]

[a] Prescribing thrust setting slightly positive to avoid interpolation error due to accessing data outside data set of performance map caused by rounding error.

Takeoff (Main Mission) The takeoff ground segment of the main mission assumes a normal takeoff from standstill at a mean sea-level airport. This is reflected in the data provided in Table 4.9, with a starting condition at zero movement and a Mach number of 0.2 as end condition. The final speed is based on the minimum control speed in air during takeoff as specified in the A320 Instructor Support manual [31, p. 23]. A V_{mca} of 110.5–111.5 kt, depending on the installed engine of the A320ceo, corresponds to a Mach number of ≈ 0.17. Considering the initial climb is included in the takeoff ground segment, a Mach number of 0.2 is considered a reasonable assumption. The thrust setting is set to maximum thrust throughout the segment, as it is considered to begin with the application of takeoff thrust by the pilot.
An incorrect prescription of an altitude of 0.0 m for the end condition was found only after the generation of the example concepts was complete. The correct altitude at the end of the takeoff segment is 457.2 m, to reflect the initial climb to the starting altitude of the first climb segment (see Table 8.1). However, this error is considered minor and does not significantly impact the estimations of the consumed fuel and electric energy.

Table 4.9: The assumed values for the state variables required to estimate the fuel and electric energy consumed during the takeoff ground segment of the main mission.

State Variable	Assumed Value	
	Start Condition	End Condition
Altitude	0.0 m	0.0 m[a]
Mach number	0.0	0.2
Thrust setting	0.99999[b]	0.99999[b]

[a] Altitude at end of takeoff should be 457.2 m to include the initial climb, but this error is minor.
[b] Prescribing thrust setting slightly below maximum to avoid interpolation error due to accessing data outside data set of performance map caused by rounding error.

Approach/Landing (Main Mission) As the approach is included in the ground segment, the start condition altitude is taken from the end of the final descent segment as defined in Table 8.1. The Mach number assumptions in Table 4.10 are Mach 0.2, which matches the A320neo approach speed of 131.5 kt [27, p. 3-5-0], and the taxi speed of Mach 0.0.
The thrust profile used for this ground segment assumes the use of thrust reversers to shorten the breaking distance and reduce the wear on the tire breaks. According to the A320 Instructor Support manual, "it is recommended to smoothly bring the reverser thrust to Idle at around [60 kt IAS]"[31, p. 75]. It also states that "The Maximum reverser thrust is obtained at N1 between 70–85 %". Seeing as the reverser thrust is most effective at high speeds, it was decided to set the start condition as maximum thrust (to err on the conservative side for the fuel/energy use) and the end condition as idle thrust, which should reflect a use of thrust reverser during the first half of the deceleration run reasonably well.

Table 4.10: The assumed values for the state variables required to estimate the fuel and electric energy consumed during the approach/-landing ground segment of the main mission.

State Variable	Assumed Value	
	Start Condition	End Condition
Altitude	457.2 m	0.0 m
Mach number	0.2	0.0
Thrust setting	0.99999[a]	0.00001[a]

[a] Prescribing thrust setting slightly below maximum/above minimum to avoid interpolation error due to accessing data outside data set of performance map caused by rounding error.

Takeoff (Diversion Mission) Opposed to the main mission takeoff segment, the diversion mission's takeoff segment does not start from standstill, as it is a go-around following an aborted landing. As the approach part of the manoeuvre is already covered by the approach/landing segment of the main mission, the starting altitude is assumed at sea-level. Assuming a landing aborted at the last moment, the go-around takeoff is initiated at a velocity below approach speed and idle thrust, as shown in Table 4.11.

Table 4.11: The assumed values for the state variables required to estimate the fuel and electric energy consumed during the takeoff ground segment of the diversion mission.

State Variable	Assumed Value	
	Start Condition	End Condition
Altitude	0.0 m	0.0 m[a]
Mach number	0.1	0.2
Thrust setting	0.00001[b]	0.99999[b]

[a] Altitude at end of takeoff should be 457.2 m to include the initial climb, but this error is minor.
[b] Prescribing thrust setting slightly above minimum/below maximum to avoid interpolation error due to accessing data outside data set of performance map caused by rounding error.

Approach/Landing (Diversion Mission) Finally, the approach and landing segment conditions of the diversion mission in Table 4.12 are identical to the main mission's, as the only difference between the two is the landing mass of the aircraft following the additional diversion mission.
Both include the final descent from 457.2 m, a Mach number of 0.2 corresponding to the approach speed of 131.5 kt, and a starting condition of maximum thrust to reflect the use of reverser thrust.

Table 4.12: The assumed values for the state variables required to estimate the fuel and electric energy consumed during the approach/-landing ground segment of the diversion mission.

State Variable	Assumed Value	
	Start Condition	End Condition
Altitude	457.2 m	0.0 m
Mach number	0.2	0.0
Thrust setting	0.99999[a]	0.00001[a]

[a] Prescribing thrust setting slightly below maximum/above minimum to avoid interpolation error due to accessing data outside data set of performance map caused by rounding error.

4.2. Case Study 1: Conventional Turbofan Concept

The first case study aims to confirm the underlying principle of the engine performance prediction methodology; the fundamental assumption that a cohesive engine performance prediction can be obtained by combining individually scaled fan and engine core performance maps. To achieve this, the tool which implemented the devised engine performance prediction methodology was integrated into a rudimentary conceptual sizing workflow as presented in Chapter 7, using the TLARs and fixed design parameters as presented in Section 4.1.1.

4.2.1. Comparison A320neo vs. generated conventional turbofan concepts

For the assessment and comparison with the existing A320neo, two conventional turbofan concepts were generated. The first concept, denoted "Conventional I", was created using the functionality of the mission simulation tool AMC to determine the optimum cruise altitude. With this function active, AMC determines the most efficient cruise altitude for the provided design mission based on the supplied aircraft aerodynamic performance map and the engine performance map. For the set-up used in the conceptual sizing workflow, this results in a concept whose engine performance will be sized according to the takeoff requirements, with a lowered initial cruise altitude corresponding to the takeoff-sized engines operating at maximum output, as this is their most efficient operating condition.
While this approach is sensible for a clean-sheet concept design, the purpose of this case study is a comparison with the existing A320neo. Therefore, an aircraft concept that more closely resembles the A320neo is obtained by fixing the initial cruise altitude to 37,000 ft ("Conventional II"), which corresponds to the cruise altitude employed by these aircraft for missions of similar range. The closest active route found operated by an A320neo, is Spirit Airlines flight NK2152 (from Los Angeles LAX to New York LaGuardia LGA) with a great circle distance of 3974 km/2146 nmi. It features a constant cruise altitude of 37,000 ft without a step-climb.

Table 4.13: An overview of the main design parameters, comparing the existing A320neo against the generated reference conventional turbofan aircraft concepts, sized to conform to the same performance requirements.

Parameter	Unit	A320neo (WV052)	Conventional I (variable ICA)	Conventional II (fixed ICA)
Wing Span	m	35.8	35.9	35.9
Reference Area	m^2	122.4	117.15	120.4
Aspect Ratio	-	10.47	11.00	10.7
Sweep (LE)	°	27.0	30.9	31.0
Wing Loading (MTOW)	$kg \cdot m^{-2}$	629.08	628.12	629.17
Thrust-to-Weight (ISA)	-	0.32	0.297	0.302
Fan Diameter	m	1.98[a]	1.63	1.82
MTOW	kg	77000	73585	75765
OEM	kg	43500[b]	41675	43360
MZFW	kg	62800	61675	63360
Design Payload Mass	kg	18900[b]	18900	18900
Fuel Mass (Design)	kg	14600[b]	13075	13585
Engine Mass	kg	3000[a]	2308	2868
Excess Specific Power (ICA)	$ft \cdot min^{-1}$	-	415	481

Continued on next page

Table 4.13: (cont.) An overview of the main design parameters, comparing the existing A320neo against the generated reference conventional turbofan aircraft concepts, sized to conform to the same performance requirements.

Parameter	Unit	A320neo (WV052)	Conventional I (variable ICA)	Conventional II (fixed ICA)
Excess Specific Power (Mid-Cr)	$ft \cdot min^{-1}$	-	534[c]	644[c]
Time to Climb	min	26.3[d]	26.7	22.7
Altitude (ICA)	m	11277.6	10058.4	11277.6
	(ft)	(37000)[e]	(33000)	(37000)
Mach (Cruise)	-	0.78	0.78	0.78
C_L (Mid-CR)	-	-	0.51	0.62
L/D (Mid-CR)	-	-	18.3	18.5
TSFC (Start of Cruise)	$kg \cdot s^{-1} \cdot N^{-1}$	1.312×10^{-5}– 1.44×10^{-5} [f]	1.385e-5	1.356e-5
TSFC (Mid-Cr)[g]	$kg \cdot s^{-1} \cdot N^{-1}$	1.312×10^{-5}– 1.44×10^{-5} [f]	1.364e-5	1.336-5
TSFC (End of Cruise)	$kg \cdot s^{-1} \cdot N^{-1}$	1.312×10^{-5}– 1.44×10^{-5} [f]	1.347e-5	1.329-5
$Thrust_{TO,\,req.}$ (SLS)[h]	kN	-	106.65	109.99
$Thrust_{max,\,req.}$ (SLS)[h]	kN	120.64[i]	107.16	112.25
$Thrust_{max,\,avail.}$ (SLS)[h]	kN	120.64[i]	107.16	133.32
Fan Active Design Point	-	-	Mid-Cruise_Climb[k]	Mid-Cruise_Climb
Engine Core Active Design Point	-	-	Takeoff	Mid-Cruise_Climb

[a] Corresponds to CFM LEAP-1A engine option.
[b] OEM estimated using maximum payload mass of 19.3 tons, based on A320neo payload-range diagram [27]; Design Payload Mass based on 180 PAX at 105 kg; Fuel Mass based on MTOW, OEM, and Design Payload Mass.
[c] Corresponds to a minimum rate of climb of 300 ft/min at 2000 ft above cruise altitude, as per input requirement.
[d] Based on: `https://contentzone.eurocontrol.int/aircraftperformance/details.aspx?ICAO=A20N`
[e] Based on Spirit Airlines flight NK2152 (LAX to LGA), 3974 km great circle distance.
[f] Based on TSFC=1.544 × 10^{-5} kg/s/N of the CFM-56-5B4 [32, Table 3.1] and a 15% improvement in fuel efficiency (`https://www.cfmaeroengines.com/engines/leap`), and an article published by Aviation International News (`https://www.ainonline.com/aviation-news/air-transport/2019-08-19/aviadvigatel-mulls-higher-thrust-pd-14s-replace-ps-90a`).
[g] During steady, straight flight. Not during step-climb.
[h] $Thrust_{TO,req.}$ is the thrust required for the takeoff field length requirement; $Thrust_{max,req.}$ is the SLS thrust needed to conform to all thrust requirements; $Thrust_{max,avail.}$ is the maximum thrust the engine is capable of delivering.
[i] As the LEAP-1A is also installed on the A321neo, it is assumed flat-rated to 120.64 kN takeoff thrust for A320neo aircraft. A321neo takeoff thrust equals 143.05 kN.
[k] Although the fan is listed as being sized according to the "Mid-Cruise_Climb" instead of the "Takeoff" design point, the two design points actually overlap and require the exact same scaling. The tool simply picked the "Mid-Cruise_Climb" sizing point because it is listed before the "Takeoff" sizing point. This behaviour is due to the decision to allow any arbitrary design point from being defined, with no internal assessment as to the importance of individual design points.

Table 4.13 presents an overview of select concept design parameters, comparing the existing A320neo with the generated example concepts "Conventional I" and "Conventional II". Both generated conventional concepts exhibit a close resemblance to the A320neo, with both design masses and wing planform parameters (span, reference area, aspect ratio, and sweep angle) deviating by less than 5 %. Especially the fixed ICA concept bears a coincidence, with the both the MTOW and wing reference area varying by only 1.6 %. The exception being the fuel masses required for the design mission, which are determined to be 10.5 % and 7 %

lower than for the A320neo. The wing-loading is identical for all concepts, implying an accurate choice in the fixed landing lift-coefficient, as the wing-loading is sized for the prescribed approach speed. The small variation in the thrust-to-weight ratio is likely caused by the slight differences in the aspect ratio, as a more slender wing reduces the induced drag and thus improves the OEI climb performance, thereby allowing a smaller engine.

A notable difference between the reference A320neo and the generated conventional concepts is the consistently smaller sized engines. Although the "Conventional II" concept almost exactly coincides with the A320neo, it's engine is still 4.4 % lighter and the fan diameter 8.1 % smaller. The "Conventional I" concept allowing for a variable ICA presents an even larger difference of 23 % and 17.7 % respectively. This is likely caused by the CFM LEAP-1A engine installed on the A320neo being actually over-sized for the aircraft. To ensure pilot compatibility within the A320neo family, which includes the larger A321neo, all aircraft must be installed with the same engines, which are then simply flat rated for the specific type. As such, the CFM LEAP-1A engine is actually sized according to the A321neo requirements and flat rated to 120 kN SLS thrust for the A320neo.
This is further confirmed when inspecting the thrust performance of the predicted engines. While the "Conventional II" concept requires less thrust to comply with the takeoff and climb requirements (112.25 kN instead of 120.64 kN), the actually available thrust at sea-level static conditions without flat rating approaches the capabilities of the LEAP-1A engine as installed on the A321neo (133.32 kN of available thrust on the estimated engine compared to 147.3 kN of available takeoff thrust on the A321neo).
Finally, a comparison of the presented TSFC values confirms that the sized engines are not only of comparable size and capability, but also of comparable efficiency as the LEAP-1A. Both generated concept's engines are within the range estimated for the LEAP-1A based on published data, with "Conventional II" performing slightly better due to being sized for cruise performance. This indicates that not only the employed methodology, but also the provided origin fan and engine core performance maps, are valid.

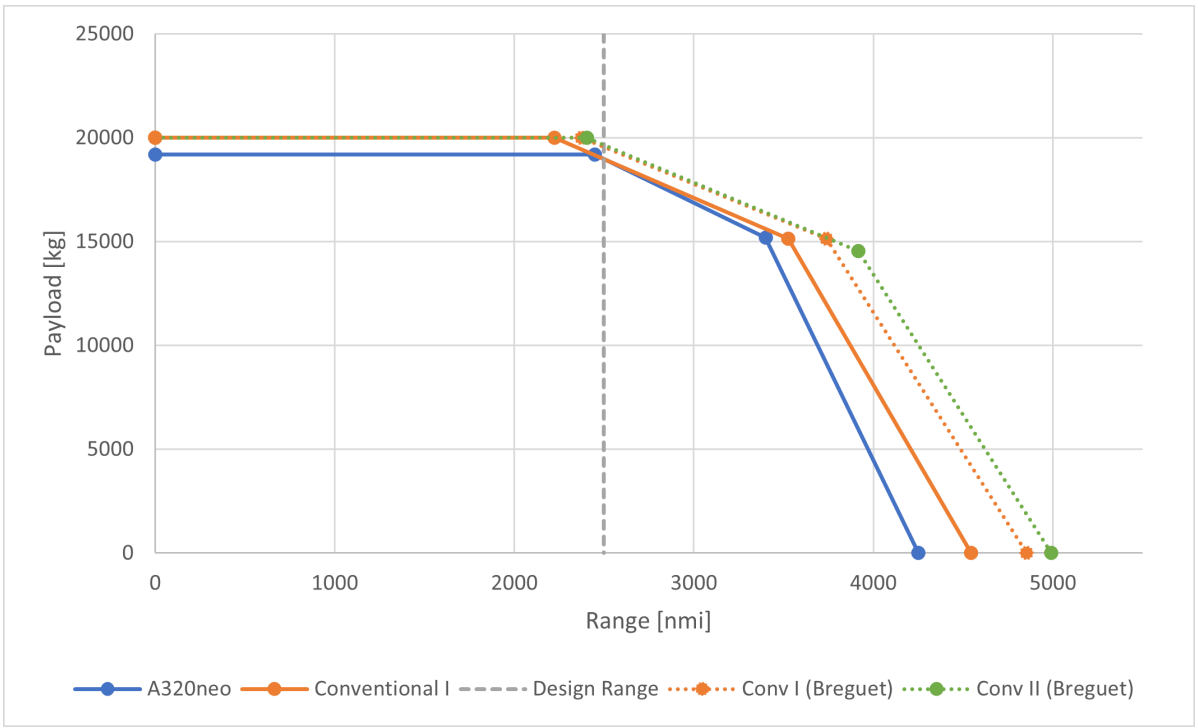

Figure 4.2: Comparison of the payload-range capabilities of the A320neo and the generated example conventional turbofan aircraft concepts. Due to complications during the computation of the payload-range diagram for the "Conventional II" concept in AMC, an estimation using the Braguet range-equation was included for both generated concepts.

Figure 4.2 presents the a comparison of the payload-range diagrams of the existing A320neo and the generated conventional concepts. Unfortunately, the workflow for the "Conventional II" concept encountered an error while computing the payload-range diagram, therefore an estimate using the Braguet range-equation from Equation (4.7) has been included for both example concepts. For the estimations, data from the design

mission simulation during the main conversion loop was used for the flight speed, the average TSFC and lift-to-drag ratio values, and the reserve fuel mass.

$$R_{Breguet} = \frac{V_{TAS}}{g} \cdot \frac{1}{TSFC_{CR,\,avg.}} \cdot \left(L/D\right)_{CR,\,avg.} \cdot ln\left(\frac{W_{initial}}{W_{final}}\right) \tag{4.7}$$

Comparing the plots representing the A320neo and the one generated by the mission simulation tool ("Conventional I" in the figure), a similar behaviour can be observed. An exact overlap at the selected design range of 2500 nmi can be identified, and the payload-fuel displacement allows for the same final payload at maximum fuel range. The stronger increase in range due to the payload-fuel displacement can be attributed to either a more efficient engine operating at a lower TSFC or a higher estimated lift-to-drag ratio due to the conceptual workflow not including a dedicated aerodynamic analysis tool, as implied by the Braguet range-equation in Equation (4.7).
Furthermore, the comparison of the two payload-range plots for the generated example concepts estimated via the range-equation shows an extremely similar behaviour. The increase in range for the "Conv II" concept is caused by the stronger payload-fuel displacement due to the larger wing size enabling a higher maximum fuel mass. Otherwise, the plots are identical with in excess range being caused by the Breguet estimation ignoring the climb and descent phases and assuming a cruise-only mission.
Overall, the payload-range plots of both the "Conventional I" and "Conventional II" concepts closely resemble the reference A320neo's capabilities, further confirming the accuracy and validity of the generated example conventional turbofan concepts.

4.2.2. Conventional Turbofan Engine Performance Prediction

Finally, Figure 4.3 illustrates the obtained conventional engine performance for the "Conventional II" example concept. The plots are obtained from the generated engine performance map, plotting the required engine shaft power for the corresponding produced total thrust. For each altitude within the engine performance envelope,here from 0–12,192 m (0–40,000 ft), the performance map provides the performance characteristics for a range of Mach numbers. Depending on the altitude, this range varies between a low-speed and a high-speed set of Mach numbers.

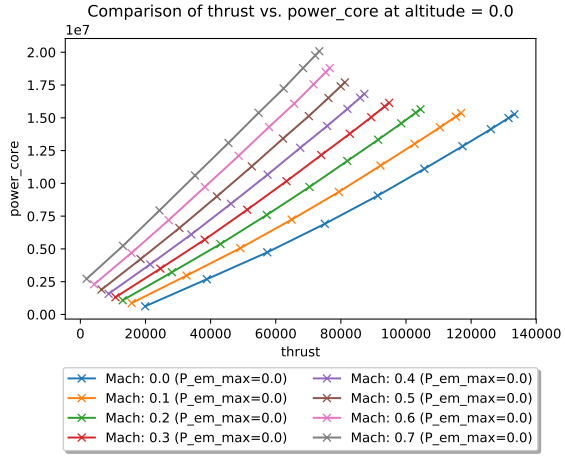

(a) Estimated performance map for the conventional turbofan engine operating at sea level.

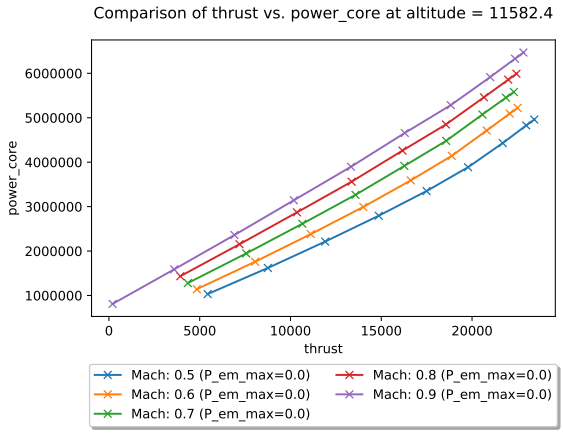

(b) Estimated performance map for the conventional turbofan engine operating at an altitude of 38,000 ft.

Figure 4.3: Plots showing the dependency of the engine core power vs. the total produced thrust for the conventional turbofan engine of the concept with fixed ICA ("Conventional II"), as predicted by the design sizing tool 'HEPSretro_Performance'.

As can be seen in Figure 4.3a, no flat-rating is applied to the generated engine performance prediction. The engine's performance behaviour is as expected of a conventional turbofan engine, with a slightly stronger increase in the required power compared to the increase in produced thrust. Also as expected, the maximum available total thrust decreases with increasing flight velocity, coupled with an increase in power draw to produce an set amount of thrust. Analogous to the sea-level performance, the engine performance at cruise altitude as shown in Figure 4.3b (here at 38,000 ft) is as expected. A significant reduction in the order of

magnitude in both produced thrust and shaft power, however the same behaviour with relation to increasing thrust demand and different Mach numbers.
The purpose of presenting these plots to visualise the performance map of the generated conventional turbofan engine is twofold: First, to demonstrate that not only the isolated values presented in Table 4.13, but also the overall behaviour and characteristics of the generated performance map are as expected; and second, to provide a visual understand of the performance behaviour of a conventional turbofan engine. This second aspect will be utilised in Section 4.3, when analysing the engine performance map for a "boosted turbofan" HEPS concept to emphasise that the generated HEPS engine is essentially a conventional turbofan in the low- to mid-thrust ranges.

4.2.3. Discussion

Ultimately, the case study achieved it's goal of confirming the viability of the chosen approach to predict the engine performance. Both generated conventional aircraft concepts exhibit a close resemblance to the reference A320neo aircraft, with the remaining small deviations being an accurate reflection of the difference in achieved performance due to external constraints such as the chosen cruise altitude or the installation of an intentionally over-sized engine for aircraft family compatibility. The close resemblance is further confirmed by the comparison of the payload-range capabilities, which present an exact match in design range point, a close match in maximum fuel range at an almost identical payload, and a small improvement in ferrying range due to a more efficient engine. An inspection of the predicted engine performance characteristics at different altitudes and the variation for increasing Mach number match the behaviour expected of a conventional turbofan engine. A slightly non-linear relation in required shaft power and produced total thrust, a reduction in maximum achievable thrust with increasing Mach number for a set altitude, and a significant reduction in both shaft power and total thrust capabilities with increasing altitude.
The proven close resemblance of the generated conventional aircraft concepts with the existing reference aircraft confirms that the employed engine performance prediction methodology generated an accurate representation of a conventional turbofan engine. It can thus be claimed that the underlying principle of individually scaling a provided fan and an engine core performance map according to a set of design sizing points, and combining those scaled origin performance maps into a cohesive engine performance map, is valid.

4.3. Case Study 2: "Boosted Turbofan" HEPS Concept

The main goal of the second case study is to provide proof that the devised methodology is indeed capable of producing usable hybrid-electric aircraft concepts. For this purpose, a hybrid-electric equivalent to the conventional concept generated in case study 1 is created using the exact same TLARs. The sizing methodology was implemented into two distinct design tools — accounting for the engine performance prediction and the electrical component mass estimation respectively — and integrated into a rudimentary conceptual sizing workflow as presented in Chapter 7.
Besides using the same TLARs as shown in Tables 4.2 to 4.4, the assumed performance characteristics of the various electrical components that comprise the electric powertrain are presented in Table 4.14. For most included components, the performance is simplified to only the specific power and the expected efficiency, as this provides an inclusive mechanism to estimate the resulting mass and the overall system efficiency. Exceptions to this are the battery packs, whose coupling of the energy-power-characteristics require a more sophisticated method, and the transmission lines, as this component includes the sizing of the actual cables used as conductors.
The chosen architecture of the example hybrid-electric concept is a so-called "boosted turbofan" parallel-HEPS configuration. The principle thought of this configuration is to install an electric propulsion system to provide boost power to the fan shaft during peak loads, thereby allowing the conventional engine core to be sized specifically for cruise condition. Due to this minimalist approach to the electrification of the propulsion system, a "boosted turbofan" concept suffers less from the incurred weight penalty caused by the added mass of the on-board batteries. It is therefore the most likely type of hybrid-electric propulsion system to be realised in the near-to-mid future.

Table 4.14: Overview of the assumed performance characteristics for the electrical components of the hybrid-electric powertrain.

Parameter	Value	Origin
		Electric Motor
Specific Power	9000 $W \cdot kg^{-1}$	Corresponds to the value assumed by the committee of the National Academies of Sciences (N.A.o.S.) [8] to be a realistic estimate for future technology (see Table A.6).
Capability	-	No assumption made as to the maximum power capability of the electric motor. It is assumed that the required power capability for a "boosted turbofan" electric motor falls within the range provided by the N.A.o.S. [8] in Table A.6.
Efficiency	0.97	Oriented on assumptions on electric motor efficiency by Welstead & Felder [16] and Jansen et al. [9] in Table A.4.
		Battery Pack
Max. Pack Capacity	160 kWh[a]	Based on target performance for future battery technology as formulated by the European Technology and Innovation Platform for power-batteries [24] (see Table A.3).
Specific Energy	382.5 $Wh \cdot kg^{-1}$	Based on performance presented in Table A.3. Corresponds to 450 $Wh \cdot kg^{-1}$ specific energy at cell level and a 85 % cell/pack weight ratio.
C-rate for Max. Power Draw	8 h^{-1}	Maximum allowed discharge rate to achieve the specific energy stated above.
Specific Power (derived)	2448 $W \cdot kg^{-1}$	Maximum achievable specific power when discharging the 382.5 $Wh \cdot kg^{-1}$ battery pack at 8C.
Energy Density	1206 $kWh \cdot m^{-3}$	The volumetric energy density was estimated via the average density for Li-Ion batteries of 2580 $kg \cdot m^{-3}$ and the specific energy. [b]
Efficiency	0.97	A value at the higher end of the range provided from the analysed literature in Table A.2 was selected.
Max. Depth of Discharge	80 %	Maximum depth of discharge corresponds to provided number of cycle life in Table A.3.
		PMAD
Operating Voltage	1000 V DC	Assumed high transmission voltage for electric power to lower the conductor mass. Value chosen is based on the VoltAir project [12] and the example voltages chosen by Stückl in the assessment of his cable model [25, p. 33].
Specific Power	16,000 $W \cdot kg^{-1}$	Large variation of predicted specific power in published literature (see Table A.9). Value chosen as realistic assumption for near-term, based on Brown [33].
Efficiency	0.988	Efficiency corresponding to the assumed specific power as stated by Brown [33].
		Circuit Protection

Continued on next page

Table 4.14: (cont.) Overview of the assumed performance characteristics for the electrical components of the hybrid-electric powertrain.

Parameter	Value	Origin
Specific Power	$200\,\mathrm{kW \cdot kg^{-1}}$	Dedicated circuit protection system specific power assumed based on publication by Jansen et al. [9].
Efficiency	0.995	Efficiency corresponding to assumed specific power.
		Transmission Line
Max. Current per Cable	360 A	Maximum allowed current per individual cable in transmission line, according to the simple cable model published by Sgueglia et al. [17].
Cable linear density	$1\,\mathrm{kg \cdot m^{-1}}$	The assumed linear density of the cable from the same published study by Sgueglia et al. [17].
Specific Loss	$80\,\mathrm{W \cdot m^{-1}}$	An assumption of how much energy is lost per unit length of the cable used within the transmission line.
Install. Mass Penalty Factor	0.3	Increase in mass of the transmission line due to the installation of the cables, according to the publication by Sgueglia et al. [17].
HMS Mass Penalty Factor	0.05	Increase in mass of the transmission line due to the health monitoring system, according to the publication by Sgueglia et al. [17].
		Thermal Management System
Specific Power	$36{,}600\,\mathrm{W \cdot kg^{-1}}$	Simplified performance parameter due to the inherent complexity of a thermal management system. Value based on the performance of the TMS sized by Lents et al. [14].

[a] The actual maximum battery pack capacity should be 15 kWh, however due to a convergence issue during the sizing iteration the capacity was increased for this specific concept.
[b] A mistake was made in the set-up of the workflow and a higher specific energy than assumed was used for the computation of the energy density. However, as the volumetric sizing of the battery packs was non-critical, this was deemed inconsequential.

4.3.1. Comparison "Conventional I" vs. "HEPS 160kWh" boosted turbofan concepts

A first impression on the accuracy of the devised sizing methodology is offered by assessing the feasibility of the generated example HEPS concept. While a feasible HEPS concept does not directly verifies the methodology, it is a clear indication that both the predicted engine performance and the amount of added mass were estimated correctly. Table 4.15 presents the comparison of the "Conventional I" and the boosted turbofan concept, denoted "HEPS 8C 160kWh" to reflect the choice of a battery model featuring a maximum discharge at a C-rate of 8.0 and the small in crease in maximum battery pack capacity. The table features the same design parameters as used in the comparison of the generated conventional concepts against the A320neo.

Inspecting the main planform parameters, it can be seen that the HEPS concept features a 12.69 % larger wing, corresponding exactly to the 12.71 % increase in MTOW as expected, due to the identical wing loading (determined by the supplied approach speed and assumed lift coefficient in landing configuration). Because the wing span was fixed to 35.9 m to comply with the same airport box limitation, this increase in wing area results in a smaller aspect ratio and higher leading edge sweep. It also causes the increase in thrust-to-weight ratio, as a lower aspect ratio increases the induced drag and thus increases the required thrust during OEI climb. The required thrust-to-weight ratio of the "Conventional I" concept for takeoff distance and the CS25.121b certification is identical, whereas the thrust-to-weight ratio of the "HEPS 8C 160kWh" remains at 0.297 for takeoff, but increases to 0.32 for the CS25.121b certification case.

Table 4.15: An overview of the main design parameters, comparing the generated example aircraft concepts using a conventional and a boosted hybrid-electric turbofan engine. Both concepts abide by the same TLARs and were sized with a variable ICA, allowing the sizing workflow to determine the individual "optimum" cruise altitude.

Parameter	Unit	Conventional I (variable ICA)	HEPS 8C 160kWh [a] (variable ICA)
Wing Span	m	35.9	35.9
Reference Area	m^2	117.15	132.02
Aspect Ratio	-	11.00	9.76
Sweep (LE)	°	30.9	31.55
Wing Loading (MTOW)	$kg \cdot m^{-2}$	628.12	628.20
Thrust-to-Weight (ISA)	-	0.297	0.32
Fan Diameter	m	1.63	1.8
MTOW	kg	73585	82935
OEM	kg	41675	49500
MZFW	kg	61675	69500
Design Payload Mass	kg	18900	18900
Fuel Mass (Design)	kg	13075	14695
Engine Mass[b]	kg	2308	3110
HEPS Mass[b]	kg	-	4250
Excess Specific Power (ICA)	$ft \cdot min^{-1}$	415	604
Excess Specific Power (Mid-Cr)[c]	$ft \cdot min^{-1}$	534	744 / 543 [d]
Time to Climb	min	26.7	22.1
Altitude (ICA)	m	10058.4	9144.0
	(ft)	(33000)	(30000)
Mach (Cruise)	-	0.78	0.78
C_L (Mid-CR)	-	0.51	0.448 / 0.489 [e]
L/D (Mid-CR)	-	18.3	18.0 / 18.3 [e]
TSFC (Start of Cruise)	$kg \cdot s^{-1} \cdot N^{-1}$	1.385e-5	1.370e-5
TSFC (Mid-Cr)[f]	$kg \cdot s^{-1} \cdot N^{-1}$	1.364e-5	1.361e-5 [d]
			1.363e-1 [d]
TSFC (End of Cruise)	$kg \cdot s^{-1} \cdot N^{-1}$	1.347e-5	1.351-5
Total Electric Energy	kWh	-	971.67
$P_{EM,\ max.\ avail.}$	kW	-	2725

Continued on next page

Table 4.15: (cont.) An overview of the main design parameters, comparing the generated example aircraft concepts using a conventional and a boosted hybrid-electric turbofan engine. Both concepts abide by the same TLARs and were sized with a variable ICA, allowing the sizing workflow to determine the individual "optimum" cruise altitude.

Parameter	Unit	Conventional I (variable ICA)	HEPS 8C 160kWh[a] (variable ICA)
$\text{Thrust}_{TO,\,req.}$ (SLS)[g]	kN	106.65	112.22
$\text{Thrust}_{max,\,req.}$ (SLS)[g]	kN	107.16	130.72
$\text{Thrust}_{max,\,avail.}$ (SLS)[g]	kN	107.16	130.98
Fan Active Design Point	-	Mid-Cruise_Climb[h]	Takeoff
Engine Core Active Design Point	-	Takeoff	Takeoff

[a] The max. capacity per battery pack had to be increased from 150 kWh to 160 kWh to achieve a proper convergence.
[b] The electric motor mass is considered part of engine mass and therefore excluded from the HEPS mass.
[c] Corresponds to a minimum rate of climb of 300 ft/min at 2000 ft above cruise altitude, as per input requirement.
[d] The mission simulation performed a step-climb during cruise, the provided values correspond to the RoC/TSFC during straight and steady flight, before and after the step climb respectively.
[e] C_L and L/D values during straight and steady flight before and after the step-climb respectively.
[f] During steady, straight flight. Not during step-climb.
[g] $\text{Thrust}_{TO,req.}$ is the thrust required for the takeoff field length requirement; $\text{Thrust}_{max,req.}$ is the SLS thrust needed to conform to all thrust requirements; $\text{Thrust}_{max,avail.}$ is the maximum thrust the engine is capable of delivering.
[h] Although the fan is listed as being sized according to the "Mid-Cruise_Climb" instead of the "Takeoff" design point, the two design points actually overlap and require the exact same scaling. The tool simply picked the "Mid-Cruise_Climb" sizing point because it is listed before the "Takeoff" sizing point. This behaviour is due to the decision to allow any arbitrary design point from being defined, with no internal assessment as to the importance of individual design points.

The increase in MTOW of almost 10 t is of an expected order of magnitude considering the design range of 2500 nmi. It is caused by the added mass of about 4.8 t for the electrical propulsion system (counting the mass of the electric motors which are included in the HEPS engine mass) and the corresponding snowball effect. Unfortunately, this increase in MTOW appears to negate any potential increase in engine efficiency, as the HEPS engine is neither lighter nor smaller than it's conventional equivalent, and the required mission block fuel has also increased by over 1.5 t (12.4 %).
As already implied by the matching of increase in MTOW and fuel mass, the generated boosted turbofan engine appears to not be able to realise the theoretical benefit of an increase in cruise efficiency. This is reflected in the presented values for the TSFC throughout the cruise phase. While the boosted turbofan manages to achieve a higher TSFC at the start of cruise, by mid-cruise both engines operate at the same efficiency, and towards the end of cruise the conventional engine has an even lower TSFC. Inspecting the design point for which the engine was sized, it becomes apparent that both concepts' engines are actually sized according to the takeoff requirements. This was caused by the design workflow being able to vary the cruise altitude. Instead of sizing the engine core for the cruise condition, the design iteration reduced the cruise altitude until the engine core corresponding to the takeoff performance requirement was capable of providing the necessary cruise thrust. It is a logical consequence for prescribing a fixed takeoff power-split ratio, this allows the smallest possible engine core. The initial cruise altitude ICA of the boosted turbofan was reduced by 3000 ft compared to the conventional concept. Seeing as both concepts are sized for the same takeoff requirements, albeit with some differences due to certification requirements, it is likely that this reduction in cruise altitude is directly proportional to the prescribed takeoff power-split ratio. Specifying a smaller power-split, will result in a smaller downscaling of the engine core and thus a less sever reduction in optimum ICA.

Overall, the created "boosted turbofan" HEPS concept is comparable to the reference conventional concept. The changes in the wing design are a logical conclusions of the added mass and the imposed constraints, and the failure to realise an increase in engine efficiency during cruise can be attributed to the lack of constraint on the cruise altitude. All differences can be explained, indicating that the underlying methodology used for the concept generation is providing reliable results corresponding to the provided inputs.
The inspection of the payload-range diagram comparison in Figure 4.4 closely mirrors the behaviour ob-

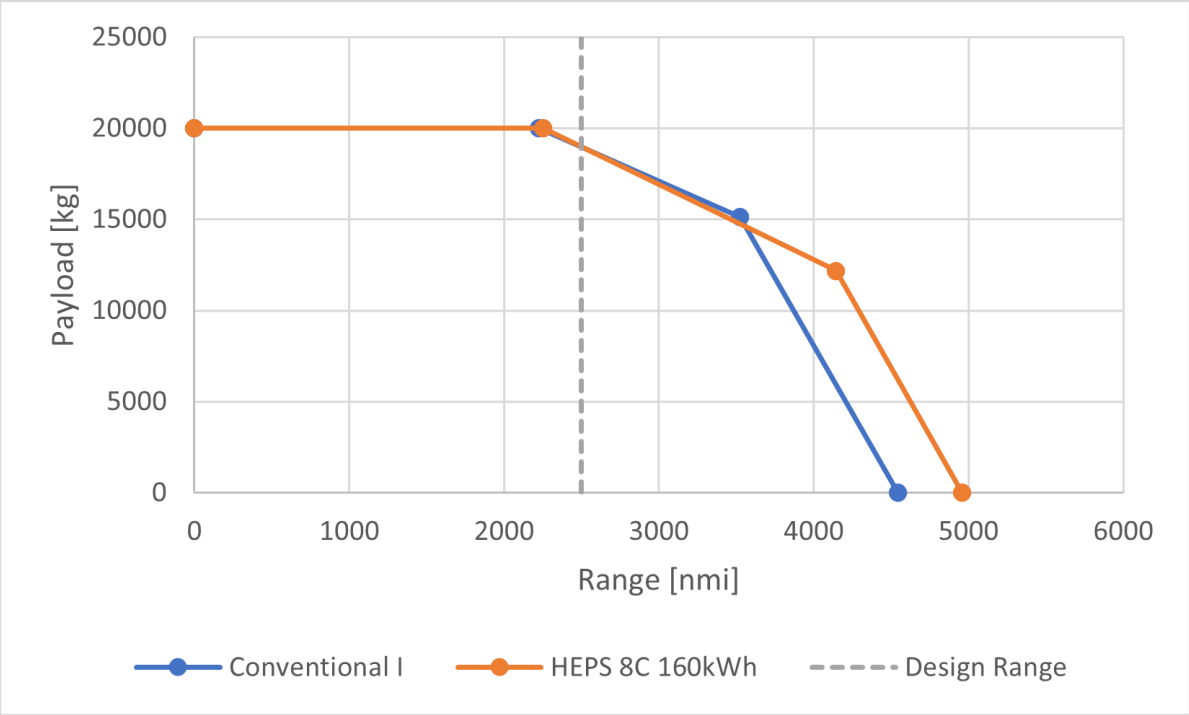

Figure 4.4: Comparison of the payload-range capabilities of the "Conventional I" and "HEPS 8C 160kWh" example concepts, both with variable ICA.

served in Figure 4.2 for the example conventional concepts, with an exact overlap of the design range payload. An increase in the maximum fuel mass for the "HEPS 8C 160kWh" concept due to the noticeably larger wing, however, results in a stronger range increase from the payload-fuel displacement, which also extends the maximum ferry range.

4.3.2. HEPS Engine Performance Prediction

To evaluate whether the predicted engine performance is indeed representative of a "boosted turbofan" hybrid-electric configuration, the relation between the produced total thrust and the corresponding engine core shaft power is analysed. Figure 4.5 presents four graphs, each corresponding to an increasing flight altitude. Within each graph, the produced thrust is plotted against the required engine core power for a range of Mach numbers.

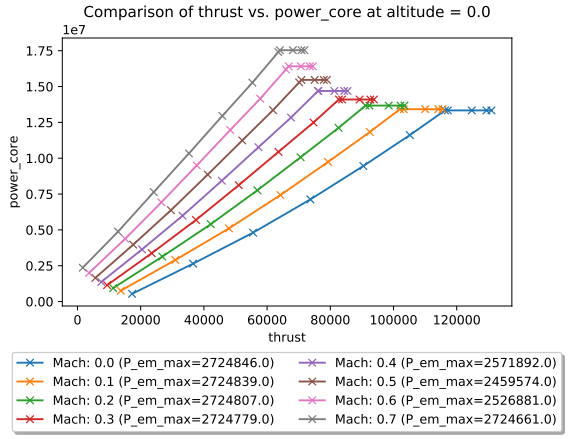

(a) Estimated performance map for the "HEPS 8C 160kWh" boosted turbofan engine operating at sea level.

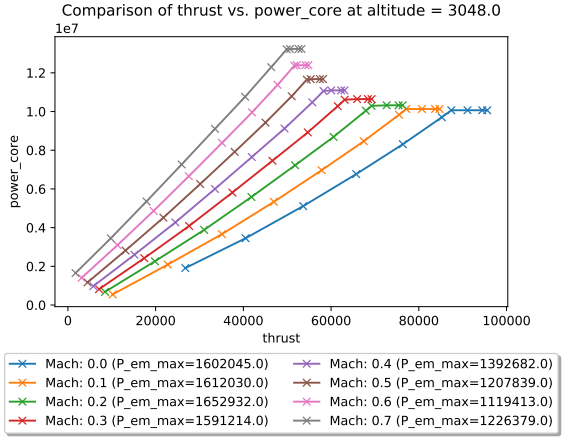

(b) Estimated performance map for the "HEPS 8C 160kWh" boosted turbofan engine operating at an altitude of 10,000 ft.

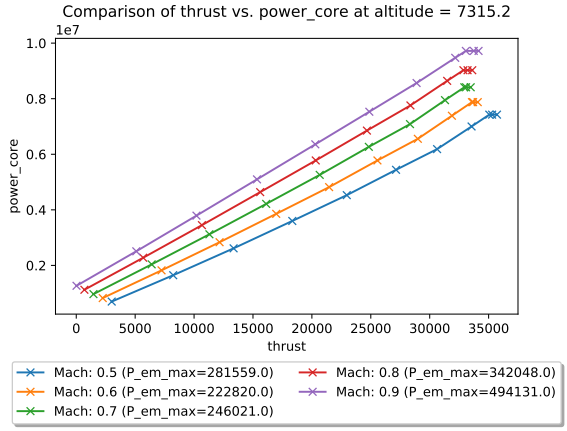

(c) Estimated performance map for the "HEPS 8C 160kWh" boosted turbofan engine operating at an altitude of 24,000 ft.

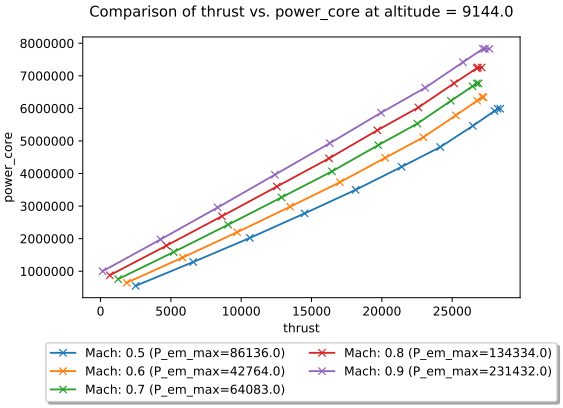

(d) Estimated performance map for the "HEPS 8C 160kWh" boosted turbofan engine operating at an altitude of 30,000 ft.

Figure 4.5: Plots showing the dependency of the engine core power vs. the total produced thrust for the conventional turbofan engine of the concept with fixed ICA, as predicted by the design sizing tool 'HEPSretro_Performance'.

In Figure 4.5a the thrust-power relation at sea-level is displayed. For the low-to-mid thrust ranges, the HEPS engine exhibits the same behaviour as the conventional engine in Figure 4.3a. This is exactly as expected, as a "boosted turbofan" behaves identical to a conventional turbofan until the engine core reaches it's maximum output power, after which the thrust can be further increased by adding electric power onto the fan shaft. In the thrust vs. core power plots, this is indicated by a plateau of constant core power.
These plateaus are clearly visible in both Figures 4.5a and 4.5b, and are still discernible in Figure 4.5c, but are essentially absent in Figure 4.5d. The reduction in the presence of the characteristic plateaus with increasing altitude implies that the engine core becomes more capable of providing the required power to drive the fan as the altitude increases. And this is indeed a realistic behaviour, because the lapse rate with increasing altitude is larger for the fan than it is for the engine core. A study conducted by Keith Jr. for NASA in 1975 found, that an increase in bypass ratio of a turbofan engine resulted in noticeably stronger reduction in cruise thrust. For a turbofan with a bypass ratio of about 4, the maximum cruise thrust was 27 % of the takeoff thrust, whereas a bypass ratio of 7.5 resulted in a maximum cruise thrust of only 22.5 % [34, Figure 2]. As the core the engines can be assumed equivalent and thus experiencing the same power lapse, this difference in available thrust implies a stronger sensitivity to altitude for the fan.
The absence of the characteristic plateaus in Figure 4.5d, which corresponds to the cruise altitude, also explains the lack of improved TSFC for the boosted turbofan. At this altitude, the engine is essentially a conventional turbofan with additional dead-weight from the electric motors added. The core is not operating at maximum capacity, as some thrust-potential must be kept available for further climbing.

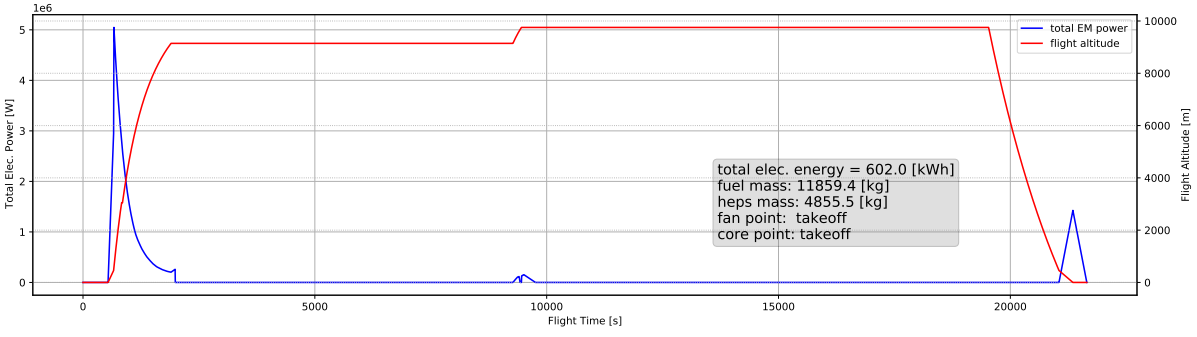

Figure 4.6: Visualisation of the electric power-usage profile of the "HEPS 8C 160kWh" concept during the design mission, excluding divergence to alternate airport. Plot presents the total electric power drawn by the electric motors, overlaid over the altitude profile of the mission.

A further proof that the generated engine performance prediction is an accurate representation of a "boosted turbofan" HEPS engine is provided by the power-usage profile of the design mission as displayed in Figure 4.6. This plots the total amount of electric power drawn by the propulsion system during the design mission, overlaid over the altitude profile. It clearly shows the peak in power draw at takeoff, followed by a consistent decrease in required electric boost power as the aircraft approaches cruise, where the engine core is capable of providing all required power. As the mission simulation performs a climb at maximum thrust, the shape of the reduction in electric boost power reflects the difference in lapse rate between the fan and engine core as well as the impact of the acceleration.
As expected, the steady cruise flight is performed without augmentation by the electric propulsion system, except for the step climb which encounters a negligible electric contribution. The peak in electric power draw during landing corresponds to the application of the thrust reversers at full throttle, although this might be omitted in real operation due to the reduction in landing distance being unlikely to worth the incurred mass penalty.

Overall, the performance predicted for the boosted turbofan HEPS engine of the "HEPS 8C 160kWh" example concept exhibits all the characteristics expected of a boosted turbofan. The engine behaves identical to a conventional turbofan in the low- and mid-thrust ranges, and presents the characteristic plateaus in the thrust-power plots. Although this behaviour diminishes with increasing altitude — caused by the engine core being sized for takeoff instead of cruise conditions due to sizing workflow allowing a variation in ICA — the generated engine performance map accurately represents the engine performance for the given set of design constraints. To obtain a boosted turbofan whose engine core is indeed sized for cruise instead of the cruise altitude being reduced to fit the engine, it might be necessary to prescribe a fixed ICA.

4.3.3. HEPS Mass Estimation

Providing proof of the accuracy of the mass estimation methodology is is complicated not only due to the absence of real-world data, but also by the inherent incompatibility of most published studies. The mass added by the hybrid-electric propulsion system not only depends on the assumptions about the technology level of each component, but also, due to the large impact of the battery mass, to a large degree on the design mission. A compatible study that can potentially be used for a comparison was conducted by Hecken et al. [5]. Although it includes "boosted turbofan" concepts sized for a design range of 2500 nmi, the study did not impose a span limit and the obtained results are thus for larger aspect ratios. Additionally, a different type of battery model was used, which prescribed a linear relationship between the specific energy and specific power. For the included range of specific energy (250–500 $\mathrm{Wh \cdot kg^{-1}}$) and the corresponding specific power values (10,000–2500 $\mathrm{W \cdot kg^{-1}}$), this results in a variation of the discharge C-rate between 40–5. This different battery model complicates the comparison of the applicable specific energy for the battery sizing, making it impossible to tell if the observed small difference in estimated mass increase is due to the methodology itself or the assumed battery performance.

Table 4.16: Comparison of the mass changes between the conventional reference and the sized "boosted turbofan" HEPS aircraft concepts for a study published by Hecken et al. [5] and this case study.

Parameter	Hecken et al. [5]	"HEPS 8C 160kWh"
MTOW Increase	+10 %	+13 %
OEM Increase	+15 %	+19 %
Fuel Mass Increase	+8–9 %	+12 %
HEPS Mass	≈4000 kg	4855 kg[a]

[a] Provided value for HEPS Mass includes the electric motor masses for a correct comparison to the value presented for the study by Hecken et al.

A comparison of the closest match in concepts between Hecken et al. and this case study is provided in Table 4.16. The table presents the relative increase in select design masses, measured between the "boosted turbofan" concepts and their respective equivalent conventional turbofan concept. Besides a difference in wing planform, and thus aerodynamic performance, the study by Hecken et al. also employed a different

battery sizing approach. Instead of prescribing a limit on the size of individual battery packs and determining the best possible C-rate for a fixed specific energy, the study only evaluates the impact of the specific energy and specific power, linked by a linear relation. Overall, as shown in the table, the two studies produce similar results, with the example concept created in this thesis estimating a slightly larger increase in mass. The MTOW, OEM, and fuel masses are consistently over-estimated by about 3 percent points, whereas the HEPS mass is estimated to be more than 20 % larger. Nevertheless, both studies exhibit mass increases of similar scale, given the differences in design constraints and modelling of the battery component.

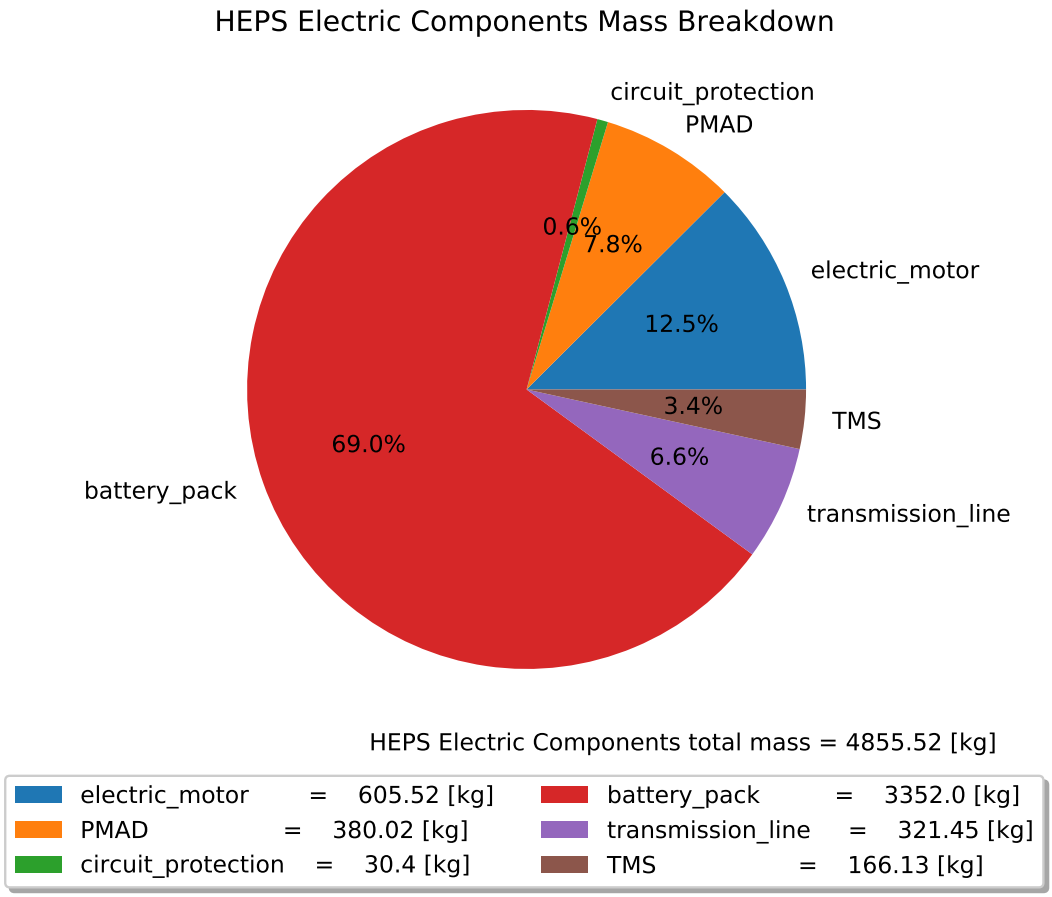

Figure 4.7: Electric component mass breakdown of concept "HEPS 8C 160kWh"

The exact mass breakdown of the computed electrical components of the hybrid-electric propulsion system for the "HEPS 8C 160kWh" example concept is given in Figure 4.7. It clearly shows the massive impact of the batteries, accounting for over two-thirds of the total HEPS mass. Interestingly, although omitted by many published studies, the PMAD and the transmission line components account for almost 15 % of the total mass. This indicates that, while indeed less important than the batteries, it is of a similar magnitude to the electric motors and should be included in all future studies.

To better understand how these individual component mass were determined, Table 4.17 provides an overview of the component characteristics and the corresponding powertrain requirements that were used to compute the respective component masses. For most components this is simply the specific power and the power encountered during the mission. The transmission line components differ depending on which components they connect, though most are connecting a battery pack to the PMAD and thus encounter the same maximum power. Those transmission lines require three cable per connection to abide by the current constraint, which results in a linear density of 4.05 kg per transmission line.
A more complex procedure was completed for the individual battery packs (see Section 3.3.2). Investigating for all combination of battery packs in parallel between $N_{parallel}$ = 6 and $N_{parallel}$ = 11, it was found that the minimum number of total packs was achieved for $N_{parallel}$ = 8. This corresponded with an active C-rate

of 5.93 h^{-1} instead of the maximum allowed 8.0 h^{-1}, and a power and capacity requirement of 760 kW and 152 kWh respectively. Using the larger of the two masses as final battery pack mass requires the updating of the battery pack performance, as either the power draw or energy storage capacity will now be larger than what was required. Additionally, sizing for a lower C-rate also technically allows for a larger power draw as the design C-rate specified in the component model is still valid. However, to utilise this potential the transmission lines must be sized accordingly, as with the current implementation they only allow for the design power draw.

Table 4.17: Overview of the sized electric components for concept "HEPS 8C 160kWh". Provides the assumed component performance characteristic(s), the related requirements set by the desired HEPS performance, and the resulting component mass.

Component Name	Component Characteristics	HEPS powertrain requirements	Component Mass
Electric Motor	$p_{sp} = 9\,\mathrm{kW \cdot kg^{-1}}$	$P_{EM,\,max.} = 2724.85\,\mathrm{kW}$	$\underline{m_{EM} = 302.76\,\mathrm{kg}}$ [a]
PMAD	$p_{sp} = 16\,\mathrm{kW \cdot kg^{-1}}$	$P_{distr.,\,max.} = 6080.34\,\mathrm{kW}$	$\underline{m_{PMAD} = 380.02\,\mathrm{kg}}$
Circuit Protection	$p_{sp} = 200\,\mathrm{kW \cdot kg^{-1}}$	$P_{distr.,\,max.} = 6080.34\,\mathrm{kW}$	$\underline{m_{CP} = 30.40\,\mathrm{kg}}$
TMS	$p_{sp} = 36.6\,\mathrm{kW \cdot kg^{-1}}$	$P_{distr.,\,max.} = 6080.34\,\mathrm{kW}$	$\underline{m_{TMS} = 166.13\,\mathrm{kg}}$
Transmission Line [b]	$I_{max.,\,cable} = 360\,\mathrm{A}$	$P_{max.} = 1025.7\,\mathrm{kW}$ [c]	$\underline{m_{TL} = 37.75\,\mathrm{kg}}$ [d]
	$\rho_{cable} = 1.0\,\mathrm{kg \cdot m^{-1}}$	$V_{distr.} = 1000\,\mathrm{V}$	
	$F_{instal.} = 0.3$	$l_{tot,\,TL} = 9.32\,\mathrm{m}$	
	$F_{HMS} = 0.05$		
Battery Pack [e]	$e_{sp.,\,pack} = 382.5\,\mathrm{Wh \cdot kg^{-1}}$	$N_{parallel} = 8$	$m_{bat.,\,energy} = 397.1\,\mathrm{kg}$
	$C_{active} = 5.93\,\mathrm{h^{-1}}$	$N_{total} = 8$	$m_{bat.,\,power} = 418.9\,\mathrm{kg}$
	$\mathrm{DoD}_{max.} = 80\,\%$	$P_{max.,\,tot} = 6080.34\,\mathrm{kW}$	$m_{battery,\,pack} = 419\,\mathrm{kg}$
	$p_{sp.,\,pack}$ [f] $= 1814.58\,\mathrm{kW \cdot kg^{-1}}$	$P_{max.,\,pack} = 760.04\,\mathrm{kW}$	$\underline{m_{battery,\,tot} = 3352\,\mathrm{kg}}$
		$Q_{use.,\,tot} = 972\,\mathrm{kWh}$	
		$Q_{abs.,\,pack,\,req.} = 151.875\,\mathrm{kWh}$	

[a] Mass of a single electric motor, not the combined mass of all sized electric motors.
[b] Using transmission line connecting battery pack 8 to the PMAD as example for the performed computations. Variations between individual transmission lines due to different total length and transmission power (e.g. connecting battery packs vs. electric motors).
[c] Maximum power the sized battery packs can provide, may exceed the max. power draw during normal operation.
[d] Total mass of example transmission line, combining all required cables and installation and HMS mass penalty factors. Individual transmission line mass varies based on battery pack position.
[e] Example calculations for a single battery pack; all sized battery packs have the same mass.
[f] Battery pack specific power was computed as the product of the max. DoD, the specific energy, and the active C-rate: $p_{sp.} = DoD_{max} \cdot e_{sp.} \cdot C_{discharge}$.

4.3.4. Discussion

The case study was conducted for the purpose of providing evidence that the devised sizing methodology is capable of producing usable outputs for hybrid-electric aircraft concepts. The "boosted turbofan" configuration was chosen as example for parallel HEPS concepts, as includes the architecture layout typical to all parallel hybrid-electric powertrains while minimising the incurred weight penalty due to no electric power being consumed during cruise. The assumed performance characteristics of the electrical components of the powertrain correspond to typical values found in literature, while the expected battery performance constitutes a conservative estimation.

Comparing the generated boosted turbofan concept against it's equivalent conventional turbofan concept

as presented in Section 4.2 shows a clear similarity. Although the addition of the electric propulsion system causes a significant increase in all design masses, the overall aircraft design and performance remain comparable. The lack of a constraint on the cruise altitude during the sizing iteration however, causes the hybrid-electric engine to also be sized for takeoff conditions. Instead of sizing the engine core for cruise flight and using the available electric boost power to achieve the required takeoff performance, the design reduced the initial cruise altitude until the required engine core performance during cruise coincides with the capabilities of the engine core sized for takeoff. This results in the engine not operating more efficiently during cruise, as evident by the comparable TSFC values. Consequently, the increase in aircraft mass is directly translated into an increase in required mission block fuel.

Although the generated "boosted turbofan" concept fails to utilise the potential of hybrid-electric propulsion, the underlying methodology — both for predicting the engine performance and for estimating the added mass due to the electric propulsion system — has been found to have produced accurate results. The generated engine performance map displays the exact behaviour expected of a "boosted turbofan" whose engine core was sized for takeoff conditions. In the low-to-mid thrust ranges, the engine behaves identical to a conventional turbofan, but exhibits the expected plateaus in the thrust–power plots where the engine core has reached it's maximum output power and the thrust is further increased via the electric boost power. It was found, however, that the engine fan is subjected to a stronger lapse rate with increasing altitude compared to the engine core, causing a reduction in the necessary power-split for maximum thrust.
The estimation of the masses added due to the electric propulsion system were compared to a compatible published study by Hecken et al. [5]. Both Hecken et al. and the concept of this study featured comparable increases in MTOW, OEM, and fuel mass. Although the "HEPS 8C 160kWh" featured a mass increase of about three percent-point more, it was inconclusive whether this was caused by a difference in the used methodologies or different assumptions on the component performance characteristics. The mass breakdown of the estimated HEPS masses displayed the expected distribution of mass over the individual components, with about two-thirds of the total mass being attributed to the battery. It also illustrated that although often omitted, the mass added by the PMAD and the transmission lines were or comparable magnitude to the electric motors and should be included. Finally, a presentation of the performed computations during the individual component mass estimations proves, that the presented values indeed correspond to the initial performance assumptions, verifying that the methodology was correctly implemented into the design tool.

This case study has successfully demonstrated that the devised methodology is capable of producing a "boosted turbofan" hybrid-electric aircraft concepts. The engine performance has been accurately predicted, correctly representing the impact on the overall engine performance due to the core being sized for takeoff conditions. Similarly, the mass estimation methodology captured the incurred weight penalty and demonstrated the capability of the battery sizing method to compute the most beneficial arrangement of dedicated battery packs.

4.4. Case Study 3: Fixed Initial Cruise Altitude

The third case study was initiated due to the observations made in Case Study 2; that the lack of a constraint on the cruise altitude caused the "boosted turbofan" engine core to be sized for takeoff instead of cruise conditions. Thus, this case study will generate a "boosted turbofan" example concept using identical design inputs to the "HEPS 8C 160kWh" concept, except the initial cruise altitude is fixed at 37,000 ft (and the maximum battery pack capacity was not increased but remained at the intended 150 kWh). This additionally provides further insight into how the devised methodology reacts to external constraints.

4.4.1. Comparison "HEPS 8C 160kWh" vs. "HEPS 8C ICA37"

The comparison of the main concept design parameters is presented in Table 4.18. Analogous to the comparison of Section 4.3, the wing loading of both boosted turbofan concept is essentially identical due to the same assumptions of approach speed and landing lift coefficient. However, due the large increase in MTOW, the constraint on the wing span has a much larger impact on the remaining aircraft sizing. The aspect ratio is reduced by 15 %, which causes a significant increase in the required thrust-to-weight ratio (12.2 %) due to OEI climb certification requirements (increase in induced drag due to less slender wing planform). Interestingly, despite this large increase in thrust requirement, the engine is entirely sized for mid-cruise conditions. The unexpectedly large increase in MTOW of almost 15 t (17.9 %), being seemingly caused entirely by increasing the required cruise altitude, is driven by the excessive increase in HEPS mass, about 80 % of which accounts

for the battery mass. Consequently, the remaining design masses feature similarly large increases.
Comparing the engine performance parameters of the two concepts, it can be concluded that prescribing a fixed ICA actually addressed the problems encountered in the previous case study. Both the fan and the engine core were sized for mid-cruise conditions: the fan according to the required thrust to obtain the prescribed minimum rate of climb 2000 ft above the current cruise altitude; and the engine core according to the prescribed output shaft power, which was taken from the previous iteration's assessment of the steady cruise flight condition.
The effect this has on the engine performance is most clearly apparent from the TSFC values. While both concepts operate at the same efficiency at start of cruise, the boosted turbofan of "HEPS 8C ICA37", which was actually sized for cruise performance, quickly overtakes the engine sized for takeoff conditions. At mid-cruise the TSFC is 1.25 %, and at the end of cruise even 2.5 % better. While this confirms that the difference in active sizing point for the engine performance prediction is correctly translated into a specific fuel consumption advantage, it fails to offset the massive increase in aircraft weight, resulting in a rise of required fuel mass of about 2.5 t.
From the amount of total electric energy required for the design mission, the cause for the massive increase in weight is apparent. The concept with fixed ICA required 212 % more electric energy than the variable ICA concept. This drastic increase cannot be simply due to up-scaling of the same engine performance as predicted for the "HEPS 8C 160kWh" concept and will be discussed in more detail in Section 4.4.3.

Table 4.18: Overview of the main design parameters, comparing the generated example boosted turbofan concepts "HEPS 8C 160kWh" against "HEPS 8C ICA37". Both concepts are sized according to the same TLARs and electrical component performance assumptions, the only difference is the constraint on the ICA for "HEPS 8C ICA37".

Parameter	Unit	HEPS 8C 160kWh [a] (variable ICA)	HEPS 8C ICA37 (fixed ICA)
Wing Span	m	35.9	35.9
Reference Area	m^2	132.02	155.42
Aspect Ratio	-	9.76	8.29
Sweep (LE)	°	31.55	32.57
Wing Loading (MTOW)	$kg \cdot m^{-2}$	628.20	629.20
Thrust-to-Weight (ISA)	-	0.32	0.359
Fan Diameter	m	1.8	2.09
MTOW	kg	82935	97785[b]
OEM	kg	49500	61775
MZFW	kg	69500	81775
Design Payload Mass	kg	18900	18900
Fuel Mass (Design)	kg	14695	17205
Engine Mass[c]	kg	3110	3944
HEPS Mass[c]	kg	4250	11771
Excess Specific Power (ICA)	$ft \cdot min^{-1}$	604	478
Excess Specific Power (Mid-Cr)[d]	$ft \cdot min^{-1}$	744 / 543 [e]	689

Continued on next page

Table 4.18: (cont.) Overview of the main design parameters, comparing the generated example boosted turbofan concepts "HEPS 8C 160kWh" against "HEPS 8C ICA37". Both concepts are sized according to the same TLARs and electrical component performance assumptions, the only difference is the constraint on the ICA for "HEPS 8C ICA37".

Parameter	Unit	HEPS 8C 160kWh [a] (variable ICA)	HEPS 8C ICA37 (fixed ICA)
Time to Climb	min	22.1	20.9
Altitude (ICA)	m	9144.0	11226.3
	(ft)	(30000)	(36832)
Mach (Cruise)	-	0.78	0.78
C_L (Mid-CR)	-	0.448 / 0.489 [f]	0.62
L/D (Mid-CR)	-	18.0 / 18.3 [f]	18.1
TSFC (Start of Cruise)	$kg \cdot s^{-1} \cdot N^{-1}$	1.370e-5	1.370e-5
TSFC (Mid-Cr)[g]	$kg \cdot s^{-1} \cdot N^{-1}$	1.361e-5 [e]	1.345e-5
		1.363e-1 [e]	
TSFC (End of Cruise)	$kg \cdot s^{-1} \cdot N^{-1}$	1.351-5	1.317e-5
Total Electric Energy	kWh	971.67	3030.2
$P_{EM,\ max.\ avail.}$	kW	2725	3361
$Thrust_{TO,\ req.}$ (SLS)[h]	kN	112.22	141.97
$Thrust_{max,\ req.}$ (SLS)[h]	kN	130.72	172.27
$Thrust_{max,\ avail.}$ (SLS)[h]	kN	130.98	176.02
Fan Active Design Point	-	Takeoff	Mid-Cruise_Climb
Engine Core Active Design Point	-	Takeoff	Mid-Cruise_Climb

[a] The max. capacity per battery pack had to be increased from 150 kWh to 160 kWh to achieve a proper convergence.
[b] Iteration converged to higher MTOW due to fluctuations in active design sizing points of engine performance prediction during early iteration steps (see Figure 4.8 and Table 4.19).
[c] The electric motor mass is considered part of engine mass and therefore excluded from the HEPS mass.
[d] Corresponds to a minimum rate of climb of 300 ft/min at 2000 ft above cruise altitude, as per input requirement.
[e] The mission simulation performed a step-climb during cruise, the provided values correspond to the RoC/TSFC during straight and steady flight, before and after the step climb respectively.
[f] C_L and L/D values during straight and steady flight before and after the step-climb respectively.
[g] During steady, straight flight. Not during step-climb.
[h] $Thrust_{TO,req.}$ is the thrust required for the takeoff field length requirement; $Thrust_{max,req.}$ is the SLS thrust needed to conform to all thrust requirements; $Thrust_{max,avail.}$ is the maximum thrust the engine is capable of delivering.

4.4.2. Drastic MTOW Increase Assessment

The observed increase in the aircraft MTOW is much larger than expected and unlikely to be caused entirely by the fixed initial cruise altitude. Figure 4.8 provides the aircraft concept's MTOW during each step of the design iteration. It is immediately clear, that the iteration initially converged to a much lower MTOW, quickly approaching 91 t before beginning to diverge until it stabilises around the final mass of 97.8 t.

Further investigation of the intermediate aircraft concepts reveals the design parameters responsible for the mass divergence. The variation in these parameters over the relevant design iteration steps are provided in Table 4.19. Essentially, the disruption to the mass convergence is caused by a repeated fluctuation in the active design sizing point for the engine core. From iteration 2 to 3, the engine performance prediction switches from "mid-cruise_climb" (low electric power utilisation) to "mid-cruise_steady" (high electric power utilisation"), which results in almost doubling the demand for electric energy and thus the required battery mass.

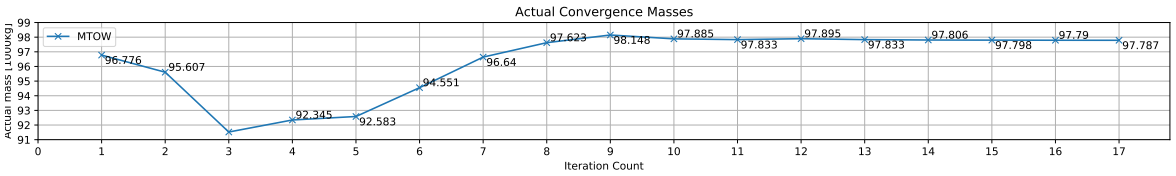

Figure 4.8: MTOW convergence behaviour of example concept "HEPS 8C ICA37" during the design iteration. Convergence to higher final mass illustrates generation of feasible, not optimal, design.

Between iteration 3 and 4, the engine core active design sizing point switches again, causing the engine performance prediction to produce a "low electric power utilisation" performance map. However, the increased MTOW during this iteration prevents this reduction in electric energy demand to return to the previous level, thereby negating much of the weight reduction. The is succeeded by another switch to the "high electric power utilisation" engine performance prediction from iteration 4 to 5, which again drastically increases the required battery mass. The cycle continues until the MTOW mass stabilises at a bit over twice the initial required battery mass.

Table 4.19: Summary of the variation in the design parameters responsible for the MTOW divergence over the relevant design iteration steps.

Iteration	Engine Core Active Sizing Point	Required Elec. Energy	Battery Mass
2	mid-cruise_climb	1395 kWh	4716 kg
3	mid-cruise_steady	2357 kWh	7812 kg
4	mid-cruise_climb	1974 kWh	7074 kg
5	mid-cruise_steady	2759 kWh	9432 kg
6	mid-cruise_climb	2962 kWh	10,218 kg
7	mid-cruise_steady	3160 kWh	10,611 kg
8	mid-cruise_steady	3135 kWh	10,611 kg

Figure 4.9 provides a visualisation to explain the difference in "low electric power utilisation" and "high electric power utilisation" engine performance. In Figure 4.9a, the electric power-usage profile for the design mission as used during iteration step 2 is shown. Because the engine core is sized for the mid-cruise step climb condition, this profile is similar to the one encountered in case study 2 (Figure 4.6), a sharp peak followed by a quick decrease approaching almost zero electric power at top of climb. Due to the rapid reduction in electric power draw during the climb phase, this profile has a low electric power utilisation. In contrast, Figure 4.9b features the electric power-usage profile from the design iteration step 3. Because the engine core is sized for the mid-cruise steady flight condition, relatively more electric boost power is required to obtain the maximum achievable thrust. For a design mission that performs the climb at maximum available thrust, this translates into a much larger utilisation of the electric power, as evidenced by the elongated peak and less rapid reduction in electric power draw.
It is important to note, that the reason for the low electric power usage in the performance prediction sized for "mid-cruise_climb" design point is caused by the specific definition of this design sizing point, and does not provide a general rule that all HEPS engines sized for this point will feature this profile. The "mid-cruise_climb" design sizing point prescribes a fixed minimum value for the shaft power available from the engine core, which is taken from the amount of shaft power required for the steady cruise flight during the previous iteration. During the early iteration steps, this value will be larger than what is required for steady cruise flight during the current iteration step. Thus, the engine core being sized for "mid-cruise_climb" does not mean that the engine core is sized to provide all power required for the climb manoeuvre, but instead that the imposed minimum engine core power is larger than what is required for steady flight.

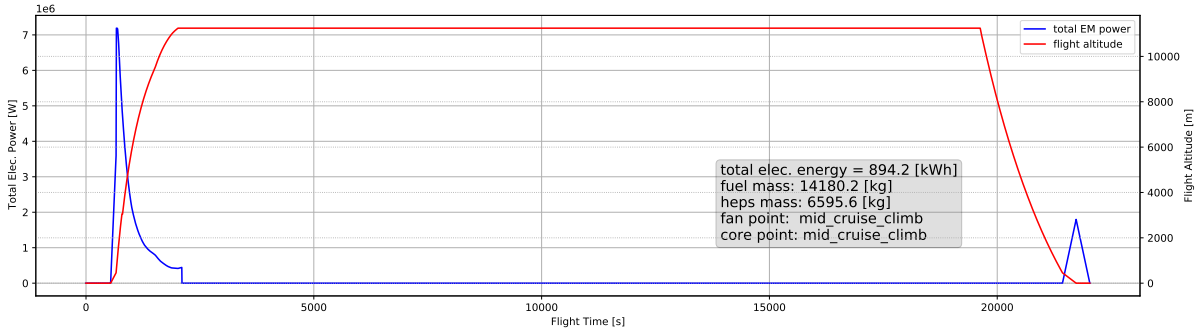

(a) power-usage profile of concept "HEPS 8C ICA37" during design iteration step 2.

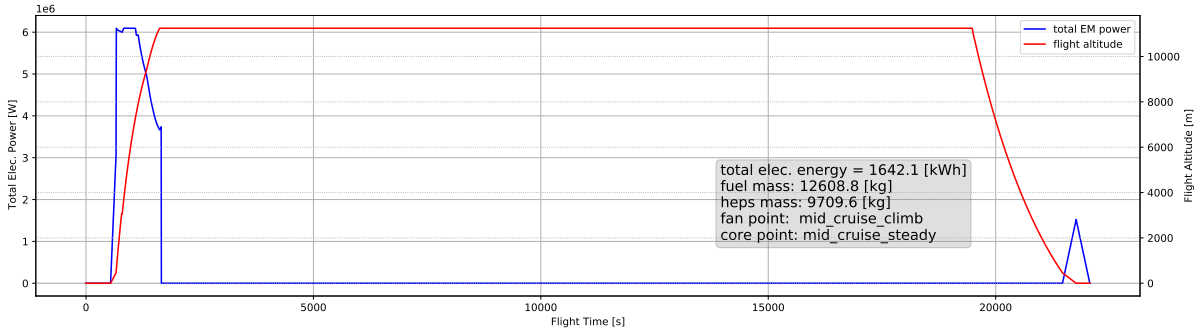

(b) power-usage profile of concept "HEPS 8C ICA37" during design iteration step 3.

Figure 4.9: Visualisation of the electric power usage during the main flight of the design mission, overlaid over the corresponding flight altitude, for the design iteration steps 2 and 3. Clearly illustrates the impact of engine core active design sizing point on resulting electric energy demand.

4.4.3. HEPS Engine Performance Prediction Comparison

A good visualisation of the cause for the excessive increase in electric energy demand for the "HEPS 8C ICA37" concept is obtained by comparing the electric power-usage profiles for the design mission, as shown in Figure 4.10. The "HEPS 8C 160kWh" concept features the low electric power utilisation profile shown in Figure 4.10a, due to the engine core being capable of providing all necessary power to achieve maximum thrust at cruise altitude. Having the engine core sized for takeoff requirements results in an engine performance that is less dependent on electric boost power to achieve maximum thrust as the altitude increases (see Figure 4.5). The "HEPS 8C ICA37" concept on the other hand, is sized such that the engine core is only capable of producing sufficient shaft power for straight and steady flight. It is dependent on electric boost power to achieve the maximum available thrust throught all flight altitudes. For a design mission featuring climb at maximum thrust, this results in the high electric power utilisation profile as shown in Figure 4.10b. As the total amount of electric energy consumed during the mission is simply the area under the electric power curve, Figure 4.10 clearly shows the cause of the rapid increase in the required electric energy for the "HEPS 8C ICA37" concept.

It should again be noted, that although the HEPS engine core of "HEPS 8C ICA37" is officially sized according to the "mid-cruise_climb" design sizing point, this does not mean the engine core is sized to provide the thrust necessary for cruise climb. It simply indicates, that the prescribed amount of shaft power provided by the engine core during climb (see Section 4.1.2) is larger than what is needed for straight and steady flight. Due to the definition of the design sizing points (taking the "mid-cruise_steady" core power output as the current requirement), it is likely that the prescribed core power is only marginally larger than then required steady flight power. Only during early iteration steps, when the steady flight core power reduces significantly between iteration steps, does this pose a potential problem.

Finally, Figure 4.11 provides a comparison of the predicted engine performance at sea-level and at cruise altitude for both the "HEPS 8C 160kWh" and "HEPS 8C ICA37" concepts. During takeoff, both engines exhibit the same behaviour, albeit at different magnitudes: a conventional turbofan engine in the low-to-mid thrust

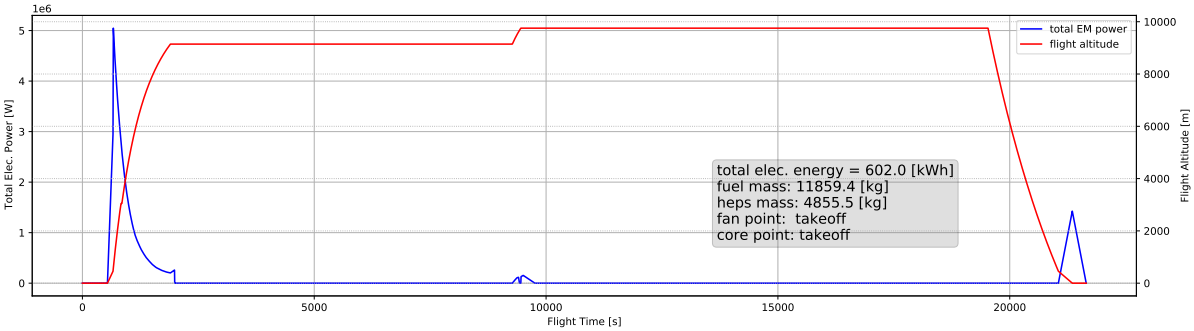

(a) The electric power-usage profile of the "HEPS 8C 160kWh" boosted turbofan concept, repeat of Figure 4.6 for direct comparison.

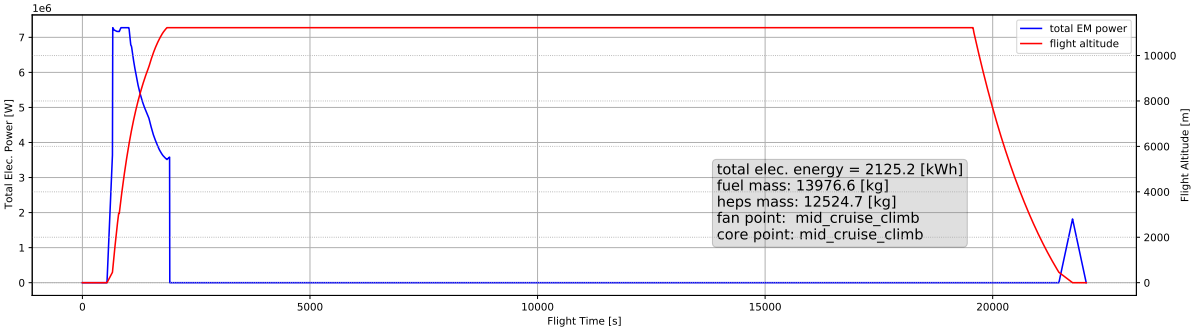

(b) Visualisation of the electric power-usage profile of the "HEPS 8C ICA37" concept during the design mission, illustrating impact of sizing the engine core for cruise conditions.

Figure 4.10: Visualisation of the electric power-usage profiles during the main flight of the design mission, overlaid over the corresponding flight altitude, for two different HEPS aircraft concepts. Additionally, the respective corresponding total fuel mass and required electric energy, the resulting mass of the entire hybrid-electric propulsion system, and the design points for which the engine was sized according to the devised engine performance methodology.

range, followed by a "plateau" of increasing thrust at constant engine core power when the electric boost is applied. The difference in the active sizing point becomes apparent at the cruise altitude performance, where the "HEPS 8C 160kWh" engine has essentially become a conventional turbofan engine over the entire thrust range, whereas the "HEPS 8C ICA37" engine retains the characteristic "plateaus" of a boosted turbofan.

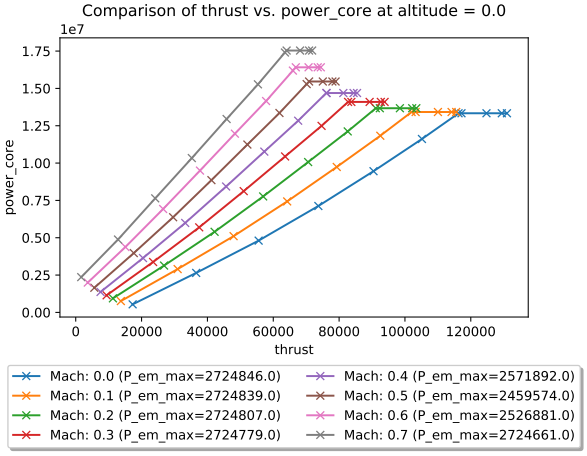

(a) Concept "HEPS 8C 160 kWh" at sea-level altitude.

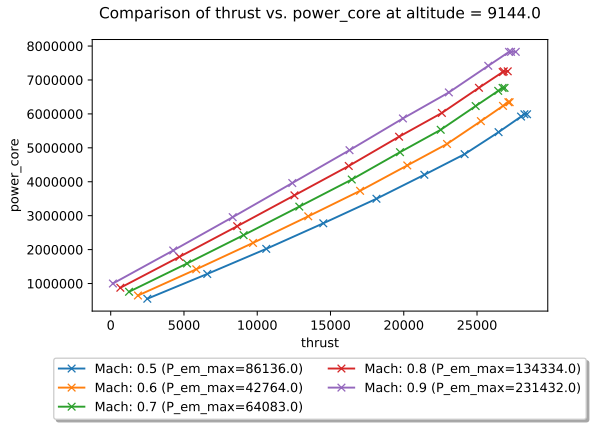

(b) Concept "HEPS 8C 160 kWh" at initial cruise altitude.

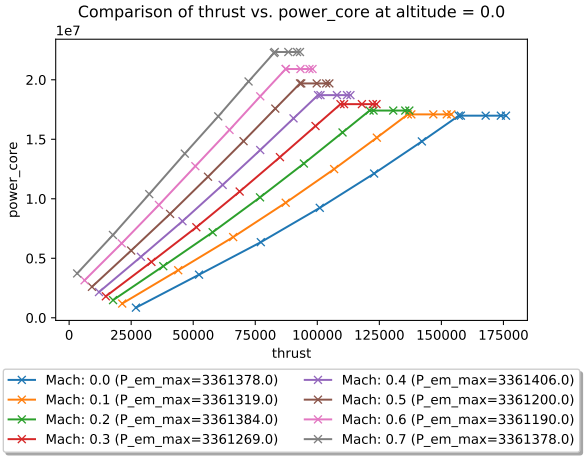

(c) Concept "HEPS 8C ICA37" at sea-level altitude.

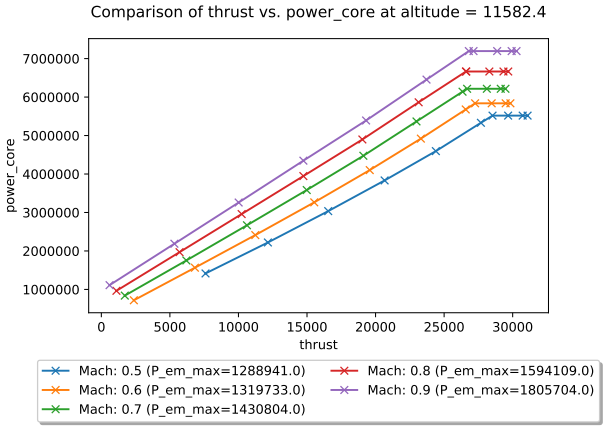

(d) Concept "HEPS 8C ICA37" close to initial cruise altitude.

Figure 4.11: Visualisation of the generated hybrid-electric engine performance maps comparing the engine turbine core power against the produced total thrust. "Plateaus" of constant core power and increasing thrust due to electric boost power.

The consistent presence of the plateaus over the entire performance envelope is the cause of the switch to a "high electric power utilisation" power-usage profile. This effect could be reduced by defining a different climb profile for the design mission, that does not perform a climb at maximum thrust. While the maximum thrust approach is employed by conventional turbofan aircraft to maximise fuel efficiency, it could be worthwhile to investigate if a more gradual climb profile would prove beneficial for "boosted turbofan" and other hybrid-electric aircraft concepts.

4.4.4. Discussion

The comparison of the new boosted turbofan concept with a fixed initial cruise altitude of 37,000 ft against the previous concept with a variable ICA revealed a larger difference than expected, due to the drastic increase in the converged MTOW. The 17.9 % increase in MTOW, caused by the tripling of the computed HEPS mass, resulted in a significant reduction in aspect ratio the corresponding increase in thrust-to-weight ratio (although this increase was not sizing, as the engine sized for cruise requirements was capable of providing the required takeoff thrust to exceed this thrust-to-weight ratio).
Despite the unexpected increase in aircraft weight and the associated design changes, the constraint on the cruise altitude managed to shift the active design sizing points of the engine performance prediction from takeoff to mid-cruise, as intended for a "boosted turbofan" HEPS aircraft. The engine sized for cruise condition exhibits the expected improvements in TSFC, starting comparable at start of cruise but achieving a 2.5 % benefit at end of cruise. This increased fuel efficiency was however unable to offset the penalty incurred by the increase in MTOW, resulting in an overall increase in block fuel requirement of about 2.5 t.

An assessment of the drastic increase in MTOW revealed that it was caused by a temporary divergence during the early design iteration, caused by the definition of the imposed design sizing points. For the "mid-cruise_climb" requirements, the design workflow imposed a minimum engine core power output equal to the amount of core power required for straight and steady flight during the previous iteration step. Due to the quick reduction in aircraft weight during the early iteration steps, this a cycling of active design sizing points for the engine core, alternating between the "mid-cruise_climb" and "mid-cruise_steady" requirements. Coupled with the large difference compared to the preceding iteration step, this caused an abrupt shift between a "low electric power utilisation" and a "high electric power utilisation" power-usage profile for the design mission, with the associated drastic increase in demand for on-board electric energy and thus battery mass.
This behaviour highlights that the devised methodology does not constitute an optimisation, it simply provides *a feasible design*. The responsibility to supervise, and potentially optimise, the convergence of the aircraft design concept remains with the user. A different definition of the "mid-cruise_climb" design sizing point — e.g. simply prescribing the minimum required engine core power during the cruise climb to be slightly smaller than the previous iterations steady flight core power — could potentially prevent such a dis-

turbance of the iteration convergence.
Although it resulted in a much higher demand for electric energy, the shift in active design sizing point from "takeoff" to "mid-cruise" resulted in the generation of proper "boosted turbofan" engine performance map. While the shape of the performance map was already correct during takeoff, the newly created engine exhibits the same characteristic "plateaus" at cruise altitude. The thrust required for straight and steady flight exactly matches the point of maximum engine core power, and additional thrust for climbing is available via electric boost power. A reduction of electric energy demand with the generated mid-cruise sized engine should be possible by adapting the definition of the climb phase in the design mission. While climbing at maximum thrust is ideal for conventional turbofan aircraft, a more gradual climb profile might prove beneficial for "boosted turbofan" and other hybrid-electric aircraft concepts.
Finally, the results of this case study confirm both the methodologies ability to generate an accurate "boosted turbofan" sized for mid-cruise requirements, as well as it's capability to adapt to changing external constraints. It correctly adjusts to the imposed altitude constraint, identifying it's impact on the critical design sizing point and generating the corresponding hybrid-electric engine performance map. The encountered drastic increase in aircraft MTOW is to be attributed to a non-optimised use by the designer, rather than a fault in the methodology itself.

4.5. Case Study 4: Increased Battery Specific Energy

The final case study performed the exact same design iteration as case study 3 in Section 4.4, with the exception that the assumed battery specific energy was increased by 30 % (from 382.5 $Wh \cdot kg^{-1}$ to 497.25 $Wh \cdot kg^{-1}$ at pack level). Analysing the obtained results will provide insight into two aspects: what the effect of a more powerful battery is on the encountered temporary mass divergence during the early iteration steps, and consequently how sensitive the methodology is to small variations in input data.
Although suggested in the previous case study, the definition of the "mid-cruise_climb" design sizing point was not changed, it is thus expected that the design iteration will encounter the exact same disturbance during the initial iteration steps. A change in the design sizing point definition will enable the generation of a better boosted turbofan concept, however, the purpose of these case studies is the verification of the methodology rather than the assessment of the potential of various "boosted turbofan" aircraft concepts.

4.5.1. Comparison "HEPS 8C ICA37" vs. "HEPS 8C 1.3E$_{sp}$"

Table 4.20 provides the familiar comparison of main design parameters between the two boosted turbofan concepts. As expected, the increase in MTOW is still significant compared to the variable "HEPS 8C 160kWh" concept, however, the improved battery specific energy has managed to reduce the weight penalty and the associated design changes significantly.
The wing reference area was reduced by 6.5 %, which caused an equivalent 6.5 % increase in the aspect ratio, improving the OEI climb performance and a correspondingly small reduction in the thrust-to-weight ratio. Due to the increase in specific energy, the amount of added HEPS mass was reduced by 26.6 %, resulting in a decrease in MTOW of over 6 t.

Table 4.20: Overview of the main design parameters, comparing the generated example boosted turbofan concepts "HEPS 8C ICA37" against "HEPS 8C 1.3E$_{sp}$". Both concepts are sized according to the same TLARs, electrical component performance assumptions, and ICA constraint, the only difference is the 30 % increase in battery specific energy for the "HEPS 8C 1.3E$_{sp}$" concept.

Parameter	Unit	HEPS 8C ICA37 (fixed ICA)	HEPS 8C 1.3E$_{sp}$ (fixed ICA)
Wing Span	m	35.9	35.9
Reference Area	m^2	155.42	145.88
Aspect Ratio	-	8.29	8.83
Sweep (LE)	°	32.57	32.14

Continued on next page

Table 4.20: (cont.) Overview of the main design parameters, comparing the generated example boosted turbofan concepts "HEPS 8C ICA37" against "HEPS 8C 1.3E$_{sp}$". Both concepts are sized according to the same TLARs, electrical component performance assumptions, and ICA constraint, the only difference is the 30 % increase in battery specific energy for the "HEPS 8C 1.3E$_{sp}$" concept.

Parameter	Unit	HEPS 8C ICA37 (fixed ICA)	HEPS 8C 1.3E$_{sp}$ (fixed ICA)
Wing Loading (MTOW)	$kg \cdot m^{-2}$	629.20	628.15
Thrust-to-Weight (ISA)	-	0.359	0.341
Fan Diameter	m	2.09	2.01
MTOW	kg	97785[a]	91635[a]
OEM	kg	61775	56800
MZFW	kg	81775	76800
Design Payload Mass	kg	18900	18900
Fuel Mass (Design)	kg	17205	16010
Engine Mass[b]	kg	3944	3642
HEPS Mass[b]	kg	11771	8640
Excess Specific Power (ICA)	$ft \cdot min^{-1}$	478	484
Excess Specific Power (Mid-Cr)[c]	$ft \cdot min^{-1}$	689	692
Time to Climb	min	20.9	21.0
Altitude (ICA)	m	11226.3	11277.6
	(ft)	(36832)	(37000)
Mach (Cruise)	-	0.78	0.78
C_L (Mid-CR)	-	0.62	0.62
L/D (Mid-CR)	-	18.1	18.3
TSFC (Start of Cruise)	$kg \cdot s^{-1} \cdot N^{-1}$	1.370e-5	1.369e-5
TSFC (Mid-Cr)[d]	$kg \cdot s^{-1} \cdot N^{-1}$	1.345e-5	1.345e-5
TSFC (End of Cruise)	$kg \cdot s^{-1} \cdot N^{-1}$	1.317e-5	1.317e-5
Total Electric Energy	kWh	3030.2	2754.04
$P_{EM,\ max.\ avail.}$	kW	3361	2925
$Thrust_{TO,\ req.}$ (SLS)[e]	kN	141.97	132.82
$Thrust_{max,\ req.}$ (SLS)[e]	kN	172.27	152.09
$Thrust_{max,\ avail.}$ (SLS)[e]	kN	176.02	163.61
Fan Active Design Point	-	Mid-Cruise_Climb	Mid-Cruise_Climb

Continued on next page

Table 4.20: (cont.) Overview of the main design parameters, comparing the generated example boosted turbofan concepts "HEPS 8C ICA37" against "HEPS 8C 1.3E$_{sp}$". Both concepts are sized according to the same TLARs, electrical component performance assumptions, and ICA constraint, the only difference is the 30 % increase in battery specific energy for the "HEPS 8C 1.3E$_{sp}$" concept.

Parameter	Unit	HEPS 8C ICA37 (fixed ICA)	HEPS 8C 1.3E$_{sp}$ (fixed ICA)
Engine Core Active Design Point	-	Mid-Cruise_Climb	Mid-Cruise_Steady

[a] Iteration converged to higher MTOW due to fluctuations in active design sizing points of engine performance prediction during early iteration steps (see Figure 4.8 and Table 4.19).
[b] The electric motor mass is considered part of engine mass and therefore excluded from the HEPS mass.
[c] Corresponds to a minimum rate of climb of 300 ft/min at 2000 ft above cruise altitude, as per input requirement.
[d] During steady, straight flight. Not during step-climb.
[e] Thrust$_{TO,req.}$ is the thrust required for the takeoff field length requirement; Thrust$_{max,req.}$ is the SLS thrust needed to conform to all thrust requirements; Thrust$_{max,avail.}$ is the maximum thrust the engine is capable of delivering.

Inspecting the predicted engine performance, it can be seen that while the overall size of the engine was reduced (less maximum thrust, lower mass, and smaller fan diameter), the cruise efficiency is identical. As both engines were sized according to the mid-cruise requirements using the same origin performance maps, it is logical that the TSFC values are identical for both engines. The smaller scale due to the lower aircraft mass however does impact the required block fuel. Due to the 30 % increase in battery specific energy, the required block fuel was reduced by 1.2 t, which accounts a reduction of about 7.5 %.

The direct impact of the improved battery performance is clearly visualised in Figure 4.12, which compares the MTOW convergence behaviour of the two fixed ICA boosted turbofan example concepts. While both concepts encounter the same disrupting event during the third iteration step, the larger specific energy of the battery in "HEPS 8C 1.3E$_{sp}$" prevents an immediate and drastic increase in MTOW. Instead, the MTOW remains relatively even until it converges to a slightly higher final value. Based on the presented behaviour, it can be extrapolated that an even higher increase in battery specific energy might prevent the disrupting event from causing a temporary increase in MTOW at all.

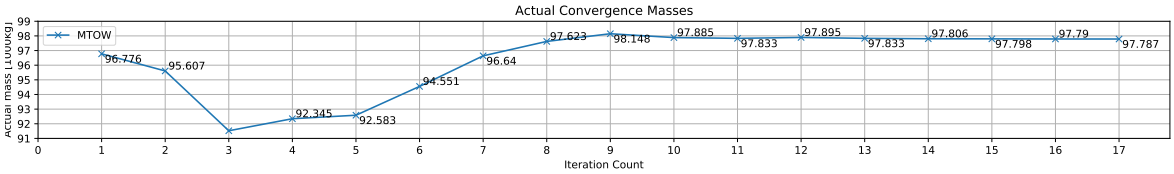

(a) "HEPS 8C ICA37" boosted turbofan concept with design ICA fixed at 37,000 ft.

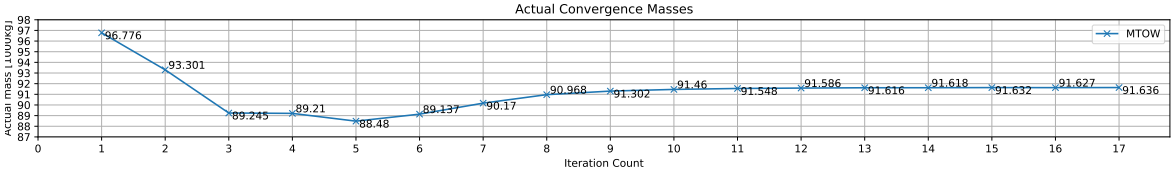

(b) "HEPS 8C 1.3E_{sp}" boosted turbofan concept with design ICA fixed at 37,000 ft and a 30 % increase in battery specific energy.

Figure 4.12: Comparison of the convergence behaviour of the concept MTOW during the design iteration of the two example hybrid-electric boosted turbofan concepts with a prescribed ICA.

It is important to note, that although an increase in the battery specific energy managed to negate most of the disruption in the MTOW convergence, this approach should not be considered a fix for the encountered problem. The underlying cause, as identified in Section 4.4.2, was the mismatch in the prescribed core power requirement for mid-cruise climb and steady flight. For future studies investigating the potential of hybrid-electric aircraft concepts, it is thus paramount to properly investigate what caused the disturbance, instead of simply increasing the performance assumptions.

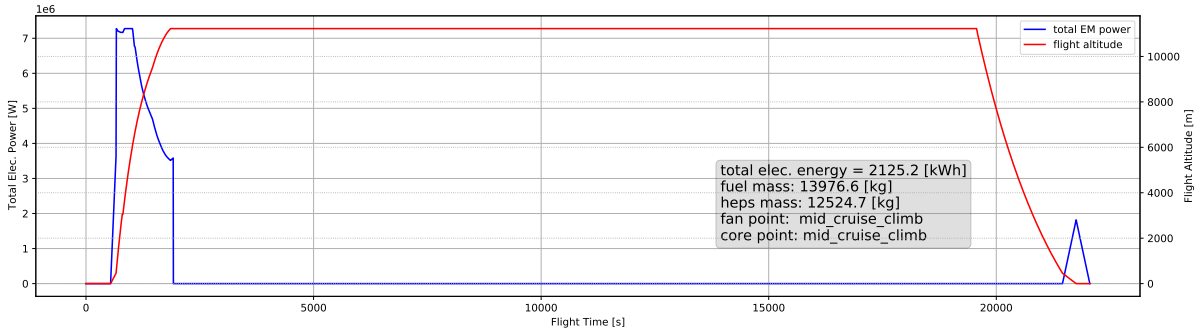

(a) Electric power-usage profile of the "HEPS 8C ICA37" concept during the design mission, engine core sized for mid-cruise requirements. Repeat of Figure 4.10b for direct comparison.

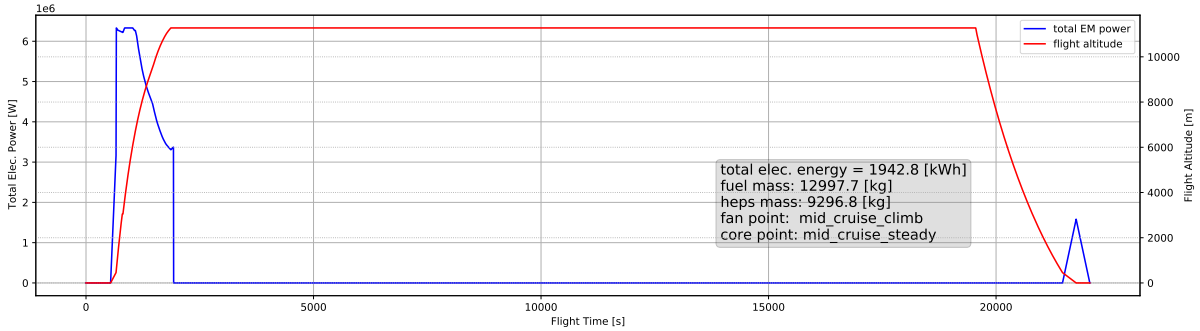

(b) Electric power-usage profile of the "HEPS 8C 1.3E$_{sp}$" concept during the design mission, engine core sized for mid-cruise requirements.

Figure 4.13: Visualisation of the electric power-usage profiles of the two boosted turbofan concepts sized for a fixed ICA of 37,000 ft. Identical "high electric power utilisation" of profile allows direct assessment of increased battery specific energy.

Finally, the comparison of the power-usage profiles of the two aircraft concepts in Figure 4.13 emphasises the similarity in the generated boosted turbofan engine performance predictions. Both feature the same "high electric power utilisation" profile corresponding to the performance maps with pronounced "plateaus" in their thrust-power relation at cruise altitude. The only difference is the magnitude of the consumed electric boost power, a direct result of the lowered MTOW and thus smaller engine.

4.5.2. Impact of the Unique Battery Pack Sizing Method

A more detailed look at the difference in the sized battery system of the two HEPS concepts is provided in Table 4.21. This table lists the requirements on the battery system in terms of total (usable) energy stored and the maximum total electric power draw and the layout of the resulting battery system, including the design discharge rate that was determined as optimal. To interpret the obtained results with relation to estimation methods from published literature, the equivalent mass for a battery system based purely on the specific energy and specific power is also provided.

From the table it becomes apparent that the 30 % increase in specific energy resulted in a 10 % reduction in required electric energy, both resulting in a 40 % reduction in total battery mass. The "HEPS 8C ICA37" concept features a battery architecture of 13 packs in parallel, with a sequence of two sets of packs to achieve the required amount of stored energy. The reduction of the design C-rate from the maximum value of 8.0 h^{-1} to 4.85 h^{-1} indicates a stronger emphasis on energy performance for the battery packs. In contrast, the "HEPS 8C 1.3E$_{sp}$" concept's battery system features a design C-rate of 6.87 h^{-1}, making use of the higher power performance of the individual battery packs to reduce the required number of packs in parallel.

An important observation can be found in the comparison of the sized battery system against an equivalent single pack system. When ignoring the limitations of a maximum capacity per battery pack, the resulting system achieves a mass about 300 kg lighter in both cases. While this implies that a single pack battery system performs better than a multi pack system, it must be noted that having a system consisting of multiple connected packs is more realistic. Using a multiple-pack system also affords an extra layer of failure protection,

as a single battery pack failure can easily be compensated by the other packs. Accounting for these advantages, an increase in estimated mass by 300 kg, an insignificant amount compared to the total system mass, can be considered negligible.

Table 4.21: Comparison of the sized battery systems for the boosted turbofan concepts with fixed ICA. Includes the total mass of an equivalent battery system that does not account for individual battery pack capacity limitations, as predominantly used in literature.

Concept	Total Energy / Max. Power	Battery Layout (N_{para} x F_{seq})	$N_{packs,\,total}$	Design C-rate	Total Battery Mass	Equiv. Mass Single Pack
"HEPS 8C ICA37"	3031 kWh / 7568.96 kW	13x2	26	4.85	10,218 kg	9905 kg[a]
"HEPS 8C 1.3E_{sp}"	2755 kWh / 6600.46 kW	8x3	24	6.87	7248 kg	6925.6 kg[b]

[a] Equivalent single pack battery sized for specific energy of 382.5 $Wh \cdot kg^{-1}$ and specific power of 2448 $W \cdot kg^{-1}$ (corresponds to discharge at 8C, accounting for maximum DoD of 80 %). Energy requirement critical.
[b] Equivalent single pack battery sized for specific energy of 497.25 $Wh \cdot kg^{-1}$ and specific power of 2732.9 $W \cdot kg^{-1}$ (corresponds to discharge at 8C, accounting for maximum DoD of 80 %). Energy requirement critical.

Finally, a breakdown of the computations performed during the battery system sizing process will demonstrate the advantage to the devised variable C-rate sizing method (see Section 3.3.2). The devised methodology sizes the battery system according to two different conditions before selecting the lighter option. Initially, the system is sized for the maximum allowed discharge C-rate as prescribed by the battery model, before investigating the optional C-rates for all realistic alternative number of packs in parallel. Using the assumed battery performance characteristics as shown in Table 4.14, the minimum total number of battery packs, as well as the minimum number of packs in parallel, are computed according to Equations (4.8a) and (4.8b) respectively.

$$N_{min.,\,energy} = \left\lceil \frac{Q_{usable,\,tot}}{Q_{usable,\,pack}} \right\rceil = \left\lceil \frac{2755\,\text{kWh}}{120\,\text{kWh}} \right\rceil = 23 \tag{4.8a}$$

$$N_{min.,\,power} = \left\lceil \frac{P_{max.,\,tot}}{C_{max.} \cdot Q_{usable,\,pack}} \right\rceil = \left\lceil \frac{6600.46\,\text{kW}}{8.0\,\text{h}^{-1} \cdot 120\,\text{kWh}} \right\rceil = 7 \tag{4.8b}$$

Subsequently, the battery packs are sized once for discharge at the maximum C-rate for an emphasis on power-performance, and once for a reduced C-rate for an emphasis on energy-performance. Following the computations, the variable C-rate option resulted in the lighter total battery mass.

Designing the batteries for discharging at the maximum C-rate, results in a configuration of individual battery packs according to Equation (4.9).

Compute for each potential $N_{parallel}$ in $\left[N_{min.,\,power}+1,\ ...,\ 2 \cdot N_{min.,\,power}-1\right]$:

$$N_{parallel} = N_{min.,\,power} \tag{4.9a}$$

$$F_{seq} = \left\lceil \frac{N_{min.,\,energy}}{N_{parallel}} \right\rceil = \left\lceil \frac{23}{7} \right\rceil = 4 \tag{4.9b}$$

$$N_{tot} = N_{min.,\,power} \cdot F_{seq} = 28 \tag{4.9c}$$

$$P_{max.,\,pack} = \frac{P_{max.,\,tot}}{N_{parallel}} \tag{4.10a}$$

$$C_{active} = \frac{P_{max.,\,pack}}{Q_{usable,\,pack}} \tag{4.10b}$$

$$F_{seq} = \left\lceil \frac{N_{min.,\,energy}}{N_{parallel}} \right\rceil \tag{4.10c}$$

$$N_{tot} = N_{parallel} \cdot F_{seq} \tag{4.10d}$$

For the battery pack configuration as established above, the individual battery pack performance requirements are formulated according to Equation (4.11).

$$P_{max.,\,pack} = \frac{P_{max.,\,tot}}{N_{parallel}} = \frac{6600.46\,\mathrm{kW}}{7} = 942.92\,\mathrm{kW} \quad (4.11a)$$

$$Q_{usable,\,pack,\,req.} = \frac{Q_{usable,\,tot}}{N_{tot}} = \frac{2755\,\mathrm{kWh}}{28} = 98.4\,\mathrm{kWh} \quad (4.11b)$$

$$Q_{abs.,\,pack,\,req.} = \frac{Q_{usable,\,pack,\,req.}}{DoD_{max}} = \frac{98.4\,\mathrm{kWh}}{0.8} = 123\,\mathrm{kWh} \quad (4.11c)$$

$$\begin{aligned} p_{sp,\,max.} &= DoD_{max} \cdot e_{sp,\,pack} \cdot C_{max.} \\ &= 0.8 \cdot 497.25\,\mathrm{Wh \cdot kg^{-1}} \cdot 8.0\,\mathrm{h^{-1}} \\ &= 3182.4\,\mathrm{W \cdot kg^{-1}} \end{aligned} \quad (4.11d)$$

The method determines the "optimum" configuration as the combination that results in the lowest N_{tot}, in the case of the example corresponding to "HEPS 8C 1.3E$_{sp}$" this occurs for $N_{tot} = 24$. This results in $N_{parallel} = 8$, $C_{active} = 6.87$, and $F_{seq} = 3$.

$$P_{max.,\,pack} = \frac{P_{max.,\,tot}}{N_{parallel}} = \frac{6600.46\,\mathrm{kW}}{8} = 825.06\,\mathrm{kW} \quad (4.12a)$$

$$Q_{usable,\,pack,\,req.} = \frac{Q_{usable,\,tot}}{N_{tot}} = \frac{2755\,\mathrm{kWh}}{24} = 114.8\,\mathrm{kWh} \quad (4.12b)$$

$$Q_{abs.,\,pack,\,req.} = \frac{Q_{usable,\,pack,\,req.}}{DoD_{max}} = \frac{114.8\,\mathrm{kWh}}{0.8} = 143.5\,\mathrm{kWh} \quad (4.12c)$$

$$\begin{aligned} p_{sp,\,active} &= DoD_{max} \cdot e_{sp,\,pack} \cdot C_{active} \\ &= 0.8 \cdot 497.25\,\mathrm{Wh \cdot kg^{-1}} \cdot 6.87\,\mathrm{h^{-1}} \\ &= 2732.9\,\mathrm{W \cdot kg^{-1}} \end{aligned} \quad (4.12d)$$

Finally, the the individual battery pack mass — and the corresponding total HEPS battery mass — is computed according to Equation (4.13). Of course, the final battery pack performance has to be updated for the sized mass, as a battery pack sized for the power requirement will be capable of storing more energy than stipulated by the energy requirement.

$$m_{bat.,\,energy} = \frac{Q_{abs.,\,pack,\,req.}}{e_{sp}} = \frac{123\,\mathrm{kWh}}{497.25\,\mathrm{Wh \cdot kg^{-1}}} = 247.4\,\mathrm{kg} \quad (4.13a)$$

$$m_{bat.,\,power} = \frac{P_{max.,\,pack}}{p_{sp,\,max.}} = \frac{942.92\,\mathrm{kW}}{3182.4\,\mathrm{W \cdot kg^{-1}}} = 296.3\,\mathrm{kg} \quad (4.13b)$$

$$\begin{aligned} m_{battery\,pack} &= max\left(m_{bat.,\,energy},\, m_{bat.,\,power}\right) \\ &= 296.3\,\mathrm{kg} \end{aligned} \quad (4.13c)$$

$$\begin{aligned} m_{battery,\,tot} &= N_{tot} \cdot m_{battery\,pack} \\ &= 28 \cdot 296.3\,\mathrm{kg} = \boxed{8296.4\,\mathrm{kg}} \end{aligned} \quad (4.13d)$$

Using the battery pack performance requirements from Equation (4.12) allows the mass computations of Equation (4.14), with the battery pack performance again being updated. Again, the final battery pack performance will be updated for the sized mass.

$$m_{bat.,\,energy} = \frac{Q_{abs.,\,pack,\,req.}}{e_{sp}} = \frac{143.5\,\mathrm{kWh}}{497.25\,\mathrm{Wh \cdot kg^{-1}}} = 288.6\,\mathrm{kg} \quad (4.14a)$$

$$m_{bat.,\,power} = \frac{P_{max.,\,pack}}{p_{sp,\,max.}} = \frac{825.06\,\mathrm{kW}}{2732.9\,\mathrm{Wh \cdot kg^{-1}}} = 302.0\,\mathrm{kg} \quad (4.14b)$$

$$\begin{aligned} m_{battery\,pack} &= max\left(m_{bat.,\,energy},\, m_{bat.,\,power}\right) \\ &= 302\,\mathrm{kg} \end{aligned} \quad (4.14c)$$

$$\begin{aligned} m_{battery,\,tot} &= N_{tot} \cdot m_{battery\,pack} \\ &= 24 \cdot 302\,\mathrm{kg} = \boxed{7248\,\mathrm{kg}} \end{aligned} \quad (4.14d)$$

The breakdown of the computations clearly shows the advantage of including the investigation of alternate discharge C-rates. Due to the devised methodology, ideal C-rate for the given situation was determined and the resulting battery system mass reduced by a little over 1.0 t.

4.5.3. Discussion

The increase in the battery specific energy assumption by 30 % resulted in an example concept much less affected by the disturbance in the MTOW convergence due to the cycling of active engine core design sizing points. The concept "HEPS 8C 1.3E$_{sp}$" converged to a final MTOW close to the aircraft mass when encountering the disturbance, producing a reduction in MTOW of over 6 t, which ultimately reduced the required block fuel by abotu 1.2 t. Being sized according to the same design sizing point, both concept's engines feature the same performance characteristics, although the "HEPS 8C 1.3E$_{sp}$" is noticeably smaller.

A comparison of the two concept's sized battery system highlights the underlying sizing method, which distinguishes individual battery packs instead of treating the battery as a single entity. This method not only splits the battery according to individual constraints on maximum pack capacity, but also investigates the optimal discharge C-rate to minimise the weight penalty. The breakdown of the performed computations during the sizing of the battery system for the "HEPS 8C 1.3E$_{sp}$ concept revealed, that this saved a little over 1.0 t.

Finally, the case study demonstrates that the methodology is sufficiently sensitive to the provided input parameters to accurately estimate the effect of small changes on the overall aircraft design. The clear representation of the impact of the increase in battery specific energy on the aircraft concept indicates, that the methodology can be used in future research studies investigating the potential of hybrid-electric aircraft concepts for various assumed electric component technology levels.

4.6. Case Studies: Discussion

Four case studies have been performed to assess the devised hybrid-electric sizing methodology, each intended to prove a specific aspect either via comparison to existing data or by interpreting the generated results. The conducted case studies were: Case Study 1, a comparison of two generated conventional turbofan aircraft concepts against the A320neo, providing a proof-of-concept for the underlying engine performance prediction methodology; Case Study 2, a comparison of the variable ICA conventional turbofan against an equivalent "boosted turbofan" concept, proving the engine prediction methodology's ability to represent a hybrid-electric powertrain and the accuracy of the component-based HEPS mass estimation methodology; Case Study 3, a comparison of two "boosted turbofan" concepts sized for a variable and a fixed ICA respectively, assessing the sizing methodology's flexibility relating to external constraints; and Case Study 4, a comparison of two "boosted turbofan" concepts sized for the exact input requirements except a 30 % increase in the assumed battery specific energy, assessing the sizing methodology's sensitivity and it's capability to be used for investigating the impact of small changes in input data.

The comparison with the A320neo in Case Study 1 showed a close resemblance between the generated example concepts and the real aircraft. While very similar in most parameters, both example concepts feature a noticeably smaller sized engine than the A320neo, with the variable ICA concept's engine being significantly smaller. Due to the A320neo featuring the exact same engine as the A321neo however, it likely that the A320neo's LEAP-1A engine is actually over-sized for the aircraft. This is further implied by the closer resemblance to the concepts for which the ICA was fixed to coincide with the known A320neo ICA. A comparison of the payload-range diagram for the aircraft yields a very similar mission performance and an exact match of the design point.

An inspection of the generated engine performance map for the conventional concept with a fixed ICA, visualised by plotting the generated thrust against the required engine core power, presents a behaviour consistent with the expectations of a turbofan engine. For a given altitude, the maximum achievable thrust reduces with increasing flight speed, while the amount of core power required to generate a given amount of thrust increases as well. Additionally, the lower air density with increasing altitude causes a reduction in both the thrust and power capabilities of the engine. While the overall relation remains similar, the magnitude of the achievable thrust and the corresponding required core power is significantly lower.

Due to both the similarity of the generated conventional concepts and the A320neo (particularly for the fixed ICA concept) and the accurate prediction of the engine performance over the entire envelope, the underlying principle of the engine performance prediction methodology is considered validated. It was shown that an engine performance map generated from two individually scaled origin fan and engine core performance maps indeed produced a coherent engine performance map that both matches the desired point performances and abides by the expected behaviour.

The generation of the first "boosted turbofan" concept in Case Study 2, featuring a variable initial cruise altitude optimised by the mission simulation tool, revealed a significant increase in aircraft weight compared to the equivalent conventional concept. An increase of almost 10 t in MOTW and over 1.5 t in block fuel for the same design mission illustrate the limitations in hybrid-electric aviation due to current battery technology. Despite a slight improvement in early cruise TSFC, the sized "boosted turbofan" HEPS engine did not manage to significantly improve the engine efficiency during cruise flight, largely due to the active design sizing point being the takeoff point performance. The principle thought behind the "boosted turbofan" is to improve the cruise TSFC by sizing the engine core for the cruise requirement, however allowing the design iteration to vary the initial cruise altitude resulted in an engine again sized for takeoff, albeit with a smaller core due to the prescribed electric boost power.
Nonetheless, the inspection of the generated engine performance map confirmed the methodology's ability to accurately predict the performance of a "boosted turbofan" engine. In the low-to-mid thrust ranges, the engine is essentially a conventional turbofan, however once the engine core operates at maximum capacity the produced thrust can be further increased by use of electric boost power. This effect is visible in the illustrations of the HEPS engine performance map as "plateaus" in the thrust vs. core power plots. Interestingly, due to the engine being sized for takeoff requirements, these characteristic plateaus disappear with increasing altitude. This is due to the engine fan experiencing a stronger lapse rate than the engine core, as confirmed by existing research into the effect of turbofan bypass ratio on the thrust lapse rate with increasing altitude.
In terms of the estimated mass increase due to the added hybrid-electric powertrain, a comparison with a published study revealed a close match. While this reference study sized their "boosted turbofan" concept for the same longer design range of 2500 nmi instead of the typical 900 nmi often found in HEPS literature, no restriction on the wing span was imposed, which resulted in a better aerodynamic performance. Nevertheless, the estimated increase in relevant design masses between the "boosted turbofan" and the corresponding equivalent conventional concept were comparable, with the concept using the methodology of this thesis featuring a consistently large estimation.

Based on the conducted assessment, both the engine performance prediction and the electric component mass estimation methodology were confirmed to provide accurate results. The predicted engine performance exhibits the exact behaviour as expected of a "boosted turbofan" engine, and accurately captures the effect of different altitude lapse rates for the fan and engine core due to the specific active design sizing point of this concept. Besides being compatible with published data, the estimation of the individual electronic components of the HEPS powertrain were also verified to be correct, given prescribed component performance assumptions.

To investigate the impact of the active design sizing point on the final generated engine performance map, as well as assess the methodology's compatibility with external constraints, the third case study generated a second "boosted turbofan" aircraft concept. This concept was sized for the same TLARs and design constraints as the one in Case Study 2, except that the initial cruise altitude was again fixed at 37,000 ft. The comparison of both "boosted turbofan" concepts revealed an increase in aircraft MTOW much beyond what was expected from a simple increase in cruise altitude. Upon investigation it was found that the cause for the drastic increase in MTOW was a temporary divergence during the early steps of the design iteration, caused by a repeated switch in which of the two mid-cruise design sizing points was active. This switch caused a fluctuation in the engine performance prediction between a "low electric power utilisation" and a "high electric power utilisation" profile, resulting a sudden doubling of the required on-board energy and the corresponding incurred mass penalty. The main cause for this event was introduced in the definition of the design sizing point for the mid-cruise climb performance, by using the previous iterations steady flight engine core power. Fixing this definition should prevent this disrupting event from occurring.
Despite the unexpected drastic increase in aircraft mass, the obtained results can be used to further verify the engine performance prediction methodology. Due to the fixed ICA, the final active design sizing points for the engine were the mid-cruise requirement as expected for a "boosted turbofan". Correspondingly, the TSFC during cruise improved by 1.25 % and 2.5 % during mid-cruise and end of cruise respectively. The difference in the active design sizing points can also be seen in the shape of the engine performance plots. While the engine performance behaves identically at takeoff, this concepts "boosted turbofan" engine does not reduce it's reliance on the electric boost power at higher altitudes. The characteristic "plateaus" are present even at cruise altitude, indicating that the engine core is indeed sized exactly for steady flight cruise thrust, requiring

electric boost power to achieve maximum thrust at cruise altitude.
This case study confirmed, that the devised sizing methodology responded correctly to the enforced initial cruise altitude by changing the critical design sizing points to mid-cruise. The corresponding change in the "boosted turbofan" engine performance prediction correctly captures the impact of this switch, requiring more consistent electric boost power and thus featuring a higher demand for on-board electric energy, given a design mission that performs a maximum trust climb.

Finally, the fourth case study investigated the impact when increasing the battery specific energy by 30 %. For the exact same design requirements as the concept from Case Study 3, this not only resulted in the expected reduction in battery mass, and thus MTOW, but also a much reduced reaction to the disruptive event encountered during the early iteration steps. While still halting the steady decrease, the mass now converged close the current MTOW value instead of increasing. The predicted engine performance featured the exact same behaviour as the previous concept, which was expected as both concepts' engines were sized for the mid-cruise requirements. However, the impact of the higher battery specific energy was correctly captured, as the lighter aircraft required less total thrust and thus featured a lower demand for on-board electric power. Another aspect verified using this case study was the unique battery pack sizing method. Contrary to most published HEPS mass estimation methods, the devised methodology does not size the battery a single component, but accounts for the limitation in individual battery pack capacity. A comparison between the estimated battery mass using this multiple pack layout against an equivalent single pack battery system revealed that the accounting for the capacity limitation only caused an increase in mass by about 300 kg. Considering the total battery system mass estimates were about 7 t and 10 t for the considered HEPS concepts, this is negligible. A further comparison between the options considered during the sizing of the multiple pack battery system provided proof that the implemented "optimisation" of the active battery C-rate managed to significantly reduce the multi-pack battery system mass.

Overall, the case studies have shown that the devised hybrid-electric conceptual sizing methodology is capable of producing accurate and reliable outputs for both the expected engine performance and the estimated additional mass. While only demonstrated for a "boosted turbofan" configuration, the performance prediction methodology can be adapted to other parallel HEPS architectures, such as those featuring a constant power-split ratio. The component-based HEPS mass estimation method has been proven to be reliable in it's calculations, including the unique battery system sizing method.
Both methodology's are sufficiently sensitive to changes in the input data that they can be used for future research studies. Recommended future studies for which the devised methodology could be used include an investigation of the required battery performance (specific energy and max. discharge C-rate/specific power) such that the improvement in cruise TSFC is sufficient to offset the increase in required thrust due to a larger aircraft mass, or an assessment of the change in aircraft emissions during cruise due to the engine core operating at higher capacity.

5

Conclusions and Recommendations

The formulated research objective objective encompassed three aspects, the development of a novel hybrid-electric conceptual sizing methodology, the implementation of this methodology into design tools for the incorporation into conceptual design workflows, and the verification of the subsequently produced results. All three aspects were achieved, as elaborated in more detail in Section 5.1. The insights gained throughout the thesis lead to many recommendations for future projects, both for the continued development of the methodology and it's application, which are discussed in Section 5.2.

5.1. Conclusions

An analysis of the published literature has revealed that the conceptual design of hybrid-electric aircraft concepts differs in three major aspects to that of conventional turbofan aircraft. Two of those aspects are a direct deviation from the established methodologies, while the third is a change imposed by those changes.
To account for the duality in the energy source and/or power conversion device of a hybrid-electric propulsion system (HEPS), the methods used to predict the required or available engine performance have to be severely adapted. In the literature, two approaches to this were presented, one more abstract, where the constraint diagram analysis of the initial sizing is adapted to account for the electric powertrain, often requiring various component-based power relations to be solved during each time-step of the subsequent mission simulation; or a more high-detail implementation, which either manipulates various created performance maps to represent the hybrid-electric propulsion system, or directly links the mission simulation to a sophisticated and high-fidelity engine analysis tool.
The second major aspect concerns the estimation of the mass added due to the introduced electric powertrain. As hybrid-electric propulsion is a novel concept and highly dependent on the specific implementation, no statistical, regression-based sizing methods exist. Thus, an electrical component-based mass estimation is required to supplement existing methods.
Finally, the third change is also imposed by the duality in the energy source. As the specific utilisation of the electric energy over the mission is significant in the sizing of the on-board energy source, a numeric mission simulation is necessary during the conceptual design.

A novel design methodology was devised to provide the means for a high-detail, inside-out engine performance prediction without prohibitive computational costs, as well as a detailed electric component mass and position estimation, which not only addresses the incurred weight panalty but also the corresponding impact on the aircraft's balance.
To enable the high-detail engine performance prediction, the methodology makes use of pre-computed (or measured) performance maps. These user-supplied maps represent the available performance of a fan and engine core design that reflects the technology level desired for the intended HEPS engine. The first step is the individual scaling of the provided "origin" performance maps according to a set of user-defined point performance requirements, which specify the ambient conditions, the thrust requirements, and the maximum desired power-split ratio or the maximum available engine core output shaft power. The scaling operation determines the most critical of the supplied point performances — it is possible for each origin performance map to be scaled according to a different active design sizing point — such that the resulting engine meets

the required performance of all points. Subsequently, the two origin maps are combined into a single, coherent engine performance map. For this, a set of sample points is defined to encompass the entire operational envelope, typically in terms of the flight altitude, the Mach number, and a set of total thrust values covering the range from idle to maximum available thrust. At each sample point, the scaled origin performance maps are interpolated to obtain the corresponding performance parameters. Depending on the specific methods used during the interpolation, different types of resulting engine performance maps can be produced. For the scope of this thesis, only the generation of conventional and two hybrid-electric types is supported: an "augmented" type, which corresponds to a "boosted turbofan" concept, and an "active" type, which prescribes a constant power-split ratio throughout the entire operative envelope.
The electric component sizing aspect of the design methodology follows the literature and estimates the mass and position of each component in the electric powertrain individually. Opposed to some of the published methods, it includes all electric components instead of focussing on only the battery and electric motors. It also extends the battery sizing methods to account for individual battery pack capacity limitations, separating the sizing into two procedures. The first determines the optimal number and combination of the individual battery packs and their corresponding performance requirements, and the second to size the actual battery pack components.
Each component is represented by a simplified component model and a respective knowledge-rule that defines it's positioning. The electric motors, PMAD, circuit protection device, and thermal management system use a simple model restricted to a specific power and a component efficiency. For the battery packs, the model accounts for the maximum capacity, specific energy, and various discharge parameters such as the maximum allowed C-rate. The transmission line sizing requires a model for the desired conductor/cable and further constraints obtained from the relative position of the connected components. Considering the knowledge-rules for the positioning, for again the electric motors, PMAD and circuit protection device, and thermal management system a simple fixed position is prescribed, the engine centre of gravity, the power electronics bay, and the wing-fuselage intersection respectively. The individual battery packs are positioned within the available cargo space inside the fuselage, alternating aft of the power electrics bay and forward of the centre wing box, accounting for any previously placed packs. Finally, the individual transmission line positions are computed as the centroid of the line path connecting the respective components, assuming a simple three-step path along the principle aircraft body axes.

An easy implementation of the devised methodology into established modern conceptual design workflows is achieved by creating two dedicated design tools. Each tool implemented one of the design methodology's aspects, the engine performance prediction and the electric component sizing. A modular approach was taken during the creation of the tools to allow for an easy adaptation and potential extension of the methods. Both tools were created using the CPACS standard as data interface for both input and output, which created an inherent compatibility with any other tools that supports CPACS.

Due to the lack of real-world data, a proper validation of the devised methodology is impossible, thus a verification build around a qualitative analysis and comparison to published concepts has to suffice.
The first step in the verification process was the creation of rudimentary conceptual design workflows for the generation of example aircraft concepts to be used in the verification case studies. Two separate workflows were required, one to size conventional turbofan aircraft, and one to generate example parallel HEPS aircraft concepts. They consist of an overall aircraft design tool ("openAD") for the concept synthesis; an engine performance tool (implementing the devised engine performance prediction methodology); a mission simulation tool ("AMC"); and, in case of the HEPS concepts, an electric component sizing tool (implementing the component sizing methodology).
Using these design workflows, four case studies were performed to assess the methodology's capabilities. The first case study confirmed the validity of the underlying principle of the engine performance prediction methodology by comparing two generated conventional turbofan concepts to the reference A320neo. In the second case study, the methodology's capability to size realistic hybrid-electric aircraft concepts was confirmed by generating an example "boosted turbofan" aircraft, whose predicted engine performance exhibited the expected behaviour, and the estimated change in design masses due to the electric components coincided with a published study. The third case study found that the methodology correctly handled the external constraint of a fixed initial cruise altitude, with both engine performance prediction and the corresponding change in component mass estimation correctly reacted to the shift in the active design sizing point. Finally, the fourth case study illustrated the sensitivity in relation to small changes in the input data

and demonstrated the unique battery sizing method.
Overall, the various case studies provided good evidence that the devised conceptual design methodology is capable of producing accurate estimations for the sizing of hybrid-electric propulsion system aircraft concepts. The engine performance of a parallel HEPS configuration can be correctly prediction, accounting for an extensive set of required point performances, and the sizing of the individual electric powertrain components provides a good estimate for the added mass, while accounting for component specific performance limitations.

5.2. Future Recommendations

Due to the large scope, numerous future recommendations were recorded throughout the thesis project. These recommendations relate to both the envisioned future development of devised methodology and its usage, as well as recommendations for future research projects. As such, the future recommendations are separated, with Section 5.2.1 presenting the former, and Section 5.2.2 the latter recommendations.

5.2.1. Methodology Development and Usage Recommendations

The first recommendation on the future development of the sizing methodology is in the implementation of further types of parallel hybrid-electric engine performance maps. While the current implemented types provide a good match for "boosted turbofan" configurations, they do not allow for the power-split ratio to be treated as an active control parameter. A potential performance map type to remedy this, could be to use the same scaled origin fan and engine core performance maps to generate a set of final engine performance maps with a different constant power-split ratio each. By interpolating between these performance maps, which cover a specified range of power-split ratios, the exact engine performance for the currently desired power-split ratio could be obtained.

A further two recommendations are made as to the development of the component sizing aspect of the design methodology. The first details an extension to the battery pack positioning method. It should be relatively straight forward to adapt the existing methods to allow a placement of individual battery packs inside externally mounted pods, either installed under the wing or inside the body fairing. The overall method would remain the same, using the existing CAD representation of the aircraft geometry to determine the available space within, such that a simple change in the definition of the initial position should suffice. Of course, the manner in which the subsequent placements are alternated would have to be adjusted to cycle through the available pods instead of switching between the forward and aft fuselage.

The second recommendation for the component sizing methodology pertains the sizing of the thermal management system. Due to the inherent complexity of this component, the currently implemented model is the only occurrence where a statistical relation was used. This direct relation between the electric power in the distribution network and the corresponding mass of the TMS does not align with the philosophy of the other component models, therefore a more detailed model based on actual physical properties would be preferred. Such a model could, for example, make use of the individual component efficiencies to compute the corresponding power losses, which can be directly converted into heat loads which the TMS would have to remove. Unfortunately, the accuracy of such a model might be limited, as the effectiveness of a TMS depends not only on the heat load, but also the relative temperature differences.

As the sizing methodology follows a high-detail approach for the engine performance prediction aspect, it's definition of the required point performances requires the user to specify the respective desired power-split ratios. It could prove beneficial to implement an "abstract" initial sizing methodology, such as the one described by Finger et al. in Section 2.1, to automate the determination of optimum power-split ratio values. The suggested initial sizing methodology allows the determination of the required power-split ratios for various design constraints such as the cruise speed or rate of climb limits, which can be directly translated into various design sizing points.

Finally, a last recommendation about the usage of the methodology must be stated. It is important to be aware that the methodology only generates *feasible*, not *optimal*, aircraft concepts. During the verification process, it was found that a generated design exhibited far larger design masses than expect, which could be traced to a slight error in the definition of the used design sizing points. It is thus recommended that the user

always takes care in how the methodology is integrated into the design workflows and critically reflect the generated design.

5.2.2. Future Research Recommendations

In terms of future research, the first recommendation is based on insights gained from the example concepts generated for the verification process. While many published studies focus on exclusively on the impact of the mass added by the battery and electric motors, it was found that for the evaluated concepts the PMAD and transmission line masses of a comparable importance to the electric motors. Indeed, for both concepts with a fixed ICA, the combined mass of the transmission line components exceeded the mass of the electric motors. It is thus recommended, that all future research studies investigating parallel hybrid-electric propulsion system include a mass estimation for the PMAD and transmission lines.

The final two recommendations relate to potential research studies for which the devised sizing methodology could be used. Firstly, an study to directly assess the variation and change in the produced emissions for various propulsion systems could easily be performed using the devised methodology. The engine performance prediction via user-provided origin performance maps allows an extremely easy implementation of an estimation of the resulting engine emissions. Simply provide an engine core origin performance map that details the emissions as a performance parameter, analogous to other performance parameters such as the fuel flow or the relative shaft speed, and the final coherent engine performance map will contain the emissions data scaled for the new engine.

Secondly, a potential research study investigating not the fuel saving potential of a concept for a given assumed technology level in a specific year, but rather finding the required performance of the electric components such that the resulting concept would equal the block fuel of an equivalent concept using current conventional engines. Instead of anticipating what technological advancement will be available in the future, the study would reverse the question and address what technological advancements would be required. This way, the obtained results are independent on how accurate the prediction on the future development of the electric components is. The required performance of the components would remain constant and the corresponding timeframe could be updated regularly to reflect the most recent prognoses. In fact, the methodology was devised with exactly such a study in mind, but the limitation of the project scope did not allow for it.

II

Supplementary Information

6

Design Process Integration

Having formulated the methodology for the conceptual sizing of a hybrid-electric aircraft concept in Chapter 3, this chapter will address how it can be integrated into the existing conventional design process in more detail. This integration is an essential part of the thesis project, as one of the fundamental requirements for the methodology was its compatibility with existing conceptual design workflows. By establishing a standard interface, the hybrid-electric sizing methods can easily be implemented into conceptual design studies, allowing an investigation of a much larger design space.

Section 6.1 will discuss the placement of the HEPS methodology in the overall design process workflow. It will use an stylised example of a modern design process to illustrate its integration into the overall workflow structure and address the dependencies on other parts of the workflow.

A logical solution to seamlessly integrate the sizing methodology into a conceptual design workflow is by creating dedicated sizing tools, using a standardised interface to facilitate easy compatibility with other design tools. Section 6.2 will address the underlying philosophy of the created design tools, commenting on the chosen interface, the internal tools structure, and the provided outputs.

Finally, Sections 6.3 and 6.4 will provide a detailed description of the created design tools for the HEPS performance prediction and component sizing estimation respectively. For each design tool, this includes an explanation of the implementation of the new methodology from Chapter 3, as well as an overview of all settings parameters available to the user and the generated output.

6.1. Design Process Chain Placement

A modern conceptual design process covers multiple levels of sophistication, typically separated into at least Level 0 and Level 1. Level 0 provides the initial sizing, general geometry layout and an empirical mass estimation, while Level 1 uses higher fidelity tools to analyse and optimise the current design. These processes are typically executed iteratively to obtain a converged, coherent concept design.

As discussed before, the devised conceptual HEPS design methodology covers two aspects: the estimation of the resulting HEPS engine performance; and the sizing of the required electrical components, estimating their masses and centre of gravity locations. These two methodologies are largely decoupled, only the component sizing methods require some input parameters taken from the estimated hybrid-electric engine performance. Thus, two dedicated design tool were created, the tool 'HEPSretro_Performance' to implement the procedure to predict the engine performance, and the tool 'HEPSretro_Components' to implement the methodology proposed for the sizing and positioning of the electric components. Each of these tools will be explained in detail in Sections 6.3 and 6.4 respectively.

Despite both tools requiring a relatively low level of fidelity in their input parameters, the underlying methodologies still fall within the Level 1 category of design methods. The HEPS performance prediction is dependent on detailed origin performance maps, and the component sizing is using physical characteristics instead of empirical methods. However, although both methodologies should be considered part of the engine/propulsion system sizing process, the dependency of the component sizing methods on the preceding computation of the necessary amount of on-board electric energy storage may require a different placement within the L1 chain of the design process.

To better visualise the placement of each HEPS design tool within the overall aircraft design process, an visualisation of a conceptual design workflow is shown in Figure 6.1. The figure illustrates the various processes that are executed during the workflow, clearly showing the separation into Level 0 and Level 1 processes. A conventional OAD tool creates an extensive initial concept design, which is then analysed and optimised using the more sophisticated, discipline specific design tools. The created, higher fidelity design concept is then used to improve the accuracy of the next iteration until the final aircraft design concept is obtained.

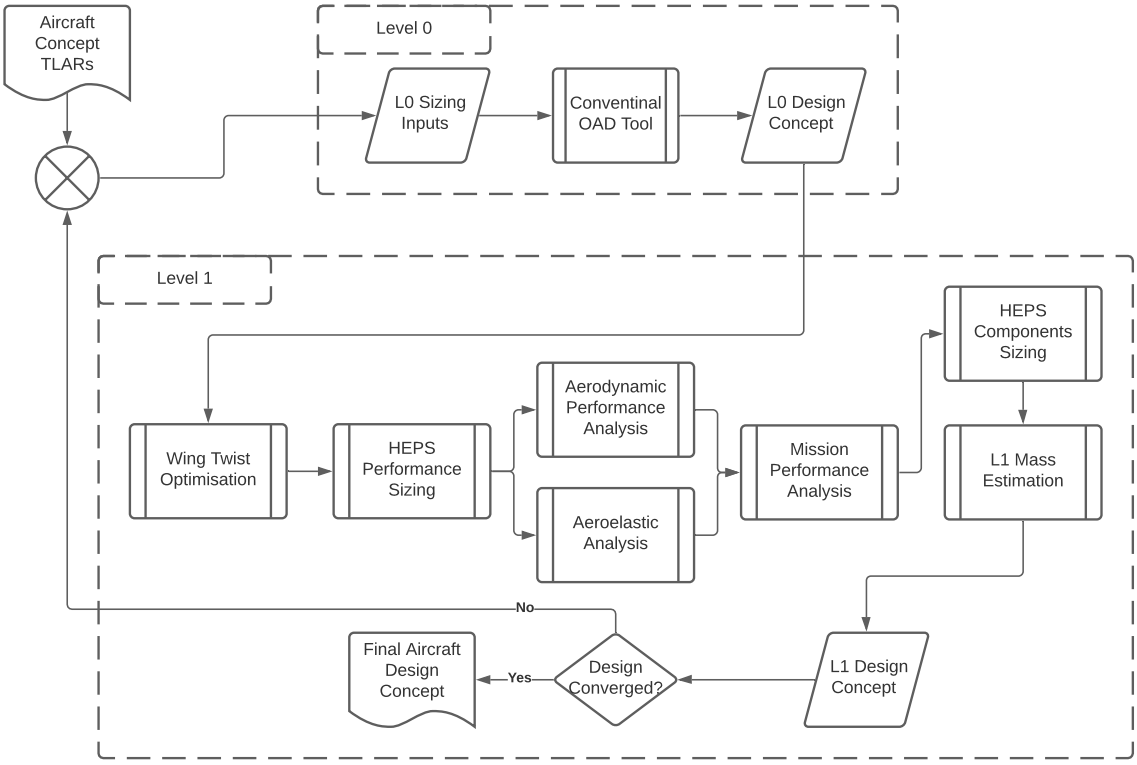

Figure 6.1: Simplified illustration of an example conceptual design workflow after the integration of the HEPS design tools, showing the distinction of the two levels of sophistication of the used design tools.

Although the example workflow in Figure 6.1 includes a specific HEPS performance sizing tool, a design workflow for a conventional turbofan would contain an equivalent dedicated tool to predict the conventional engine performance. In this way, the created engine performance design tool simply replaces the previous tool within the process chain. The major difference is introduced with the inclusion of the HEPS component sizing tool following the mission performance analysis. As stated when presenting the devised sizing methodology in Section 3.3, only the electric components of the hybrid-electric powertrain are sized. It is thus still necessary to perform the typical L1 mass estimation to obtain an accurate understanding of the various subsystem design masses. In this process chain layout, it is assumed that the implemented mission analysis tool is capable of handling a hybrid-electric engine performance map and can thus compute the total amount of necessary on-board electric energy required by the component sizing methodology.
Ultimately, the exact order of the two HEPS design tools is irrelevant, as long as the initial design includes the required input parameters. Due to the iterative nature of the overall aircraft design process, the output of both HEPS design tools will converge to a cohesive design, where the performance of the hybrid-electric propulsion system and its estimated mass and centre of gravity location correspond perfectly within the anticipated accuracy for conceptual design

6.2. Design Tool Philosophy

This section provides a brief overview of the general philosophy that was adhered to during the creation of the two HEPS aircraft design tools. The philosophy mostly determined the internal layout and structure of the tools, but also considered the interface of the tools and how to facilitate their integration into an overall

aircraft design workflow as described in Section 6.1. In the following, the three main aspects of the employed tool design philosophy are explained, concerning 1) the tools interface, 2) the internal layout, and 3) the structure and extend of the provided results export.

Using CPACS Data Format The CPACS data format is an Open Source data definition schema used to describe an aircraft concept. It was created by the DLR explicitly to facilitate the exchange of information between tools in multi-disciplinary and multi-fidelity design processes. All tools designed according to the CPACS data structure are compatible and can be connected according to their required input and provided output data.
This inherent compatibility with other tools is the reason that both HEPS design tools were created fully compliant to the CPACS standard. Both the input and the output data was structured according to the current release version of the Schema (CPACS 3.2).

Modular Internal Structure This aspect of the design philosophy had the largest impact on the tool design process. While the other two aspects deal with the external communication, how to interface and what data to exchange, this aspect directly impacts the internal working of the tools.
By enforcing a modular internal structure and taking an object-oriented programming approach, the tool is made significantly more flexible. Each sub-process is contained within a specific class, with the tool process flow being determined primarily by how these classes are implemented and connected. The main benefit of this flexibility of the design tool is twofold, relating to the maintenance and progression of the tool.

Firstly, the modular implementation of the sub-processes allows an easy replacement of the implemented methods, as long as the provided parameters remain compatible. Taking the sizing of the power transmission line components as example, the sizing methodology of the power transmission lines allows for the use of different underlying cable models (as explained in Section 3.3.3). While the employed simple normal-conducting cable model is sufficiently accurate for conceptual design, an alternate model wherein the cable is build from the inside-out can yield much more accurate results. Following the modular design philosophy, the design tool will contain a dedicated module/class for each cable model, which is used within the power transmission line module/class. To switch to the alternate cable model is easily achieved by changing which of the available cable modules is called within the transmission line class.

Secondly, besides replacing existing methods, new methodologies can be implemented just as easily. To extend the tool functionality to include the sizing of super-conducting components is as easy as the example above. Simply create a new module/class for super-conducting cables and replace the call for the cable model within the transmission line class. The same principle applies for the other components: create a new module for a super-conducting electric motor and replace the call within the main sizing coordination class; create another module for a TMS component that properly covers the requirements of cryogenic cooling and change the call within the sizing coordination class. A limitation to this is of course, that the required inputs for the newly created modules have to be available from the existing methods. In case additional inputs are required, a more extensive adaptation of the implemented modules may be necessary.
Even a more drastic extension to the design tool functionality, such as introducing new HEPS architectures to the component sizing, are facilitated by this modular approach. While such an extensive extension requires more work than simply adding a few modules, all existing modules are readily available to be used in the new methodology. Introducing a new architecture to the sizing process requires changes at a fundamental level, as the connection between the individual components differs substantially. In a procedural, script-based design tool, this would result in the duplication of many methods, but the modular approach allows the same component models to be used for all supported HEPS architectures.

The decision to enforce a modular internal structure was imposed mostly with the component sizing tool in mind. Allowing an easy implementation and changing of the underlying component models would guarantee that the tool can easily be extended for changes in the available components, or adapted for different desired level of fidelity. However, it is similarly applicable to the engine performance prediction tool, as different realisations of the hybrid performance map (see Section 3.2.1) still use many of the same processes.

Extensive Results Export The last aspect of the tool design philosophy concerned the produced output of the tools. While the necessary output was clearly defined in the requirements for each tool, the processes

that were executed to obtain those results create a multitude of additional data. This information may not be directly relevant for the main purpose of the design tool, but is nevertheless part of the created results, and may be useful for other design tools. For example, the creation of the hybrid-electric engine performance map according to a set of design sizing points is ultimately determined by the point performance at one of the provided points. While the information of exactly which one of these design sizing points is active is not relevant to the produced performance map, it can still give the designer further insight into how to optimise the design. Another example from the HEPS component sizing tool would be the overall powertrain efficiency. The stated purpose of the component sizing tool is to estimate the HEPS component masses and their corresponding CoG positions, but the implemented models also predict the component efficiencies. Using these individual efficiencies, a more accurate prediction of the overall powertrain efficiency can be determined, which can in turn improve the estimations in the secondary performance parameters of the hybrid-engine performance map.

Unfortunately, the current iteration of the official CPACS schema does not include any definitions for electrical components, or other design related information. An established workaround for this recurring problem is the <toolspecific> node available in CPACS, even though the original purpose for this node is to provide input data for specific tools, such as settings for specific aerodynamic solvers, desired numerical precision, or other control parameters. Due to the absence of any rigid layout for the content stored within the <toolspecific> node, besides imposing a dedicated <tool> sub-node for each individual tool, it has become a common practice to include a <results> node to export all relevant data produced within the tool.
Similarly, the newly created HEPS sizing tools follow this philosophy and will export all relevant produced data into a dedicated <results> node within the <toolspecific> node. The internal structuring of these <results> node will differ depending on what is deemed most logical for the specific tools.

6.3. The ‘HEPSretro_Performance‘ Tool

This chapter discusses the created design tool for the prediction of the hybrid-electric engine performance, whose underlying theory was presented in Section 3.2.2. It will discuss the expected level of fidelity; the internal structure of the tool, including a detailed breakdown of the various process flows; the available input parameters; as well as the generated output and additional results.

The purpose of this design tool was to create a dedicated building block for the conceptual design workflow that provides an estimation of the performance of a hybrid-electric propulsion system. While only the engine performance for a parallel architecture is currently implemented, the modular layout provides the option to easily extend the functionality.
Predicting the resulting hybrid-electric engine performance is a vital aspect of the HEPS sizing process, as it is necessary for the simulation of the design mission, during which the required amount of fuel and electric energy are determined. Furthermore, some performance parameters necessary for the sizing of the HEPS propulsion system components are taken directly from the predicted engine performance, such as the maximum mechanical output power of the installed electric motors, or the maximum amount of electrical power that has to be transported via the distribution system.
The created design tool to predict the engine performance is called ‘HEPSretro_Performance‘, because the tool retrofits the hybrid-electric propulsion system into an existing aircraft concept. It was written in python 2.7 and utilises the Tixi library [a] for interaction with the input and output CPACS files. Besides the DLR developed Tixi package, the tool requires the typical python packages ‘Numpy‘, ‘Scipy‘, and ‘Matplotlib‘.

6.3.1. Tool Level of Fidelity

To qualify the resulting level of fidelity of the produced output, the simplifications employed in the underlying methodology have to be considered. For the HEPS engine performance prediction tool, two distinct aspects introduce a simplification on the engine performance: the use of engine performance maps, and the scaling of the origin performance maps based on a single parameter.

First, the use of origin performance maps to represent the performance of the engine fan and the engine core

[a] The Tixi library is in active development by the DLR and offers a simple interface to the CPACS XML file. They also provide a wrapper around they C-based library to enable the easy use with different programming languages (currently supporting MATLAB, Fortran, and Python). For more information, see `https://github.com/DLR-SC/tixi/wiki`.

are by definition a simplification. A performance map simply provides a set of data points corresponding to the performance as measured (rarely) or predicted (most often) by established analysis tools. Accessing a performance map at any point other than exactly those sample points, yields simply the performance interpolated between the surrounding sample points. Depending on the spread of the sample points and the chosen method of interpolation, different predicted performance parameters may be obtained.
Secondly, the employed performance prediction methodology is based on scaling the supplied origin performance maps to correspond to the desired overall performance. A dedicated performance map for the engine fan and the engine gas turbine core are scaled individually and their performances matched such, that the combined produced thrust equals the desired overall engine thrust. In particular, the fan performance map is scaled according to the required fan thrust at each specified design sizing point, while the engine core map is scaled according to the power requirement associated with this fan thrust. Using this approach enforces the simplifying assumption that the performance behaviour of engine fans and engine cores do not change with their size. While this is not inherently true, the user is expected to provide origin performance maps that correspond to the scale of aircraft that is designed. This results in relatively small scaling operations for which the initial assumption of similar performance behaviour is valid.

Ultimately, the HEPS engine performance prediction tool is a low-fidelity process, which is typical for a conceptual design process. A too high level of fidelity is actually undesirable for the intended use-case of this tool, as the level of fidelity is proportional to the required run time.
The tool does not evaluate any actual engine performance, it only captures the aircraft vehicle level performance based on the provided data set of sample points. As such, the accuracy of the produced, low-fidelity output is entirely dependent on the quality of the provided input origin fan and engine core performance maps.

6.3.2. Engine Performance Prediction Methodology Implementation

While the methodology explained in Section 3.2.2 illustrates the logical procedure to generate an engine performance map for a parallel hybrid-electric propulsion system, the process flow within the design tool will differ. This is mostly due to the methodology providing a procedure using abstract tasks, whereas the process flow of the program explicitly defines the individual processes and their connections.
In the following figures, the individual processes are grouped by functionality, without indicating to which specific class they belong. This was done because the tool was build using an OOP approach, with methods and procedures defined in function specific classes and called when required. It is thus not possible to dictated the sequence in which classes and their methods are active.

Figure 6.2 displays the process flow used by the main file of the design tool. As shown, the only external inputs are the ’CPACS Input File’ and the ’Supplied Origin Performance Maps’, also provided as CPACS files. All settings on how the tool should operate are contained within the specific <tool> node inside the <toolspecific>, following standard CPACS notation.
Currently, only the estimation of the engine performance for a specific parallel HEPS architecture is implemented, which consists of an augmented parallel hybrid-electric architecture, wherein the conventional gas turbine engine core is used as primary power source, and the electric motors are used to provide additional shaft power once the ICE is operating at maximum capacity. Due to the limited utilisation of the electric propulsion system to merely boost the shaft power output of the conventional engine core, this concept is often called a "boosted turbofan". It should be noted, that while this concept is typically associated with a relatively low degree-of-hybridisation, this limitation is not imposed by the concept itself. Indeed, a "boosted turbofan" can be designed with a significant share of electric propulsive power.
The functionality to predict the performance of a HEPS engine that allows for a manual variation of the active power split ratio can be included, by implementing the methodology to create an "active" HEPS engine performance map (see Section 3.2.1). Without any adaptation of the performance sizing procedure, the determination of the performance of the gas turbine engine core would follow the same process as described in Section 3.2.2, based upon the supplied design sizing points.
Upon initialisation, the tool processes all relevant data provided in the ‘CPACS Input File‘. This includes the settings for specific processes, such as acceptable convergence tolerances, and general tool settings, the recording of the desired point performances at each design sizing points, as well as instantiating the interface to translate the relevant design information from the CPACS data structure to the tool internal format.
The first process executed by the tool is to pre-scale the supplied origin performance maps. This process

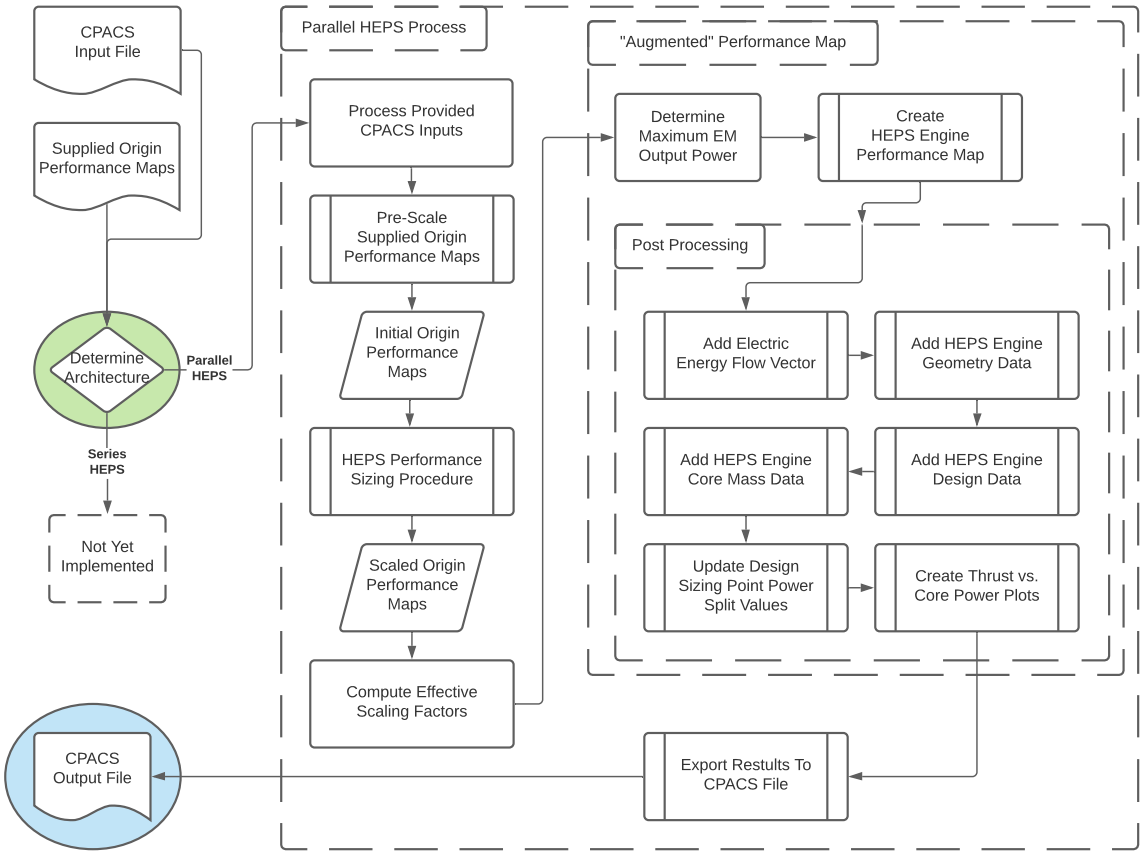

Figure 6.2: Overview of the main process flow within the ‘HEPSretro_Performance‘ tool used to predict the HEPS engine performance map. Each dashed group represents a specific aspect of the overall process, signifying the sizing of the origin fan & core performance maps, the creation of the HEPS performance map, and any desired post-processing procedures. Blocks with a double vertical border represent sub-processes with a complex underlying process flow, some of which are illustrated in the following figures. While displaying a clear separation of the series and parallel HEPS prediction processes, many of the procedures used within the ‘Parallel HEPS Process‘ can be reused in the ‘Series HEPS Process‘, particularly the CPACS performance map models, and the some underlying methods with in the ‘Create HEPS Engine Performance Map‘ process.

evaluates the fan and engine core performance maps supplied by the user and scales them such, that their data set is guaranteed to include each specified design sizing point. In the current implementation, the origin fan performance map is scaled to provide fan thrust values equal to at least 110% of the required total thrust at each design sizing point, while the engine core map is scaled to provide a shaft power output equal to at least 110% of the corresponding power necessary to drive the fan shaft at each design sizing point. The resulting fan and engine core performance maps are then used as the ‘Initial Origin Performance Maps‘ throughout the tool.

Following the pre-scaling of the origin performance maps, the actual performance sizing procedure of the parallel HEPS engine is performed. This is itself a complex process, which is shown in more detail in Figure 6.3 and will be discussed in the paragraph ‘HEPS Performance Sizing Procedure‘. Once the scaled origin performance maps are obtained, the corresponding ’effective scaling factors’ are computed. These parameters represent the scaling factor that, when applied to the ’Supplied Origin Performance Map’ (as supplied by the user, before the pre-scaling operation), will directly result in the determined ’Scaled Origin Performance Maps’. It is a measure of the extend to which the performance map originally supplied by the user has been scaled, and should be used as a check that the chosen input origin performance maps are appropriate for the aircraft concept.

At this stage, the process flow enters the procedure to generate the HEPS engine performance map. In the implemented methodology to create an "augmented" performance map, the determination of the required mechanical output power of the electric motor is based on the available ICE output power and the required shaft power associated with the corresponding fan thrust, as well as any potential power offtakes. To guarantee

consistency, the maximum power the electric motors supply at any of the design sizing points is determined and enforced as a hard limit during the HEPS map generation procedure. Analogous to the ‘HEPS Performance Sizing Procedure‘, the process to generate the hybrid-electric engine performance map is complex and thus described in more detail in the paragraph ‘Create HEPS Engine Performance Map‘ and Figure 6.6.
Finally, the generated HEPS engine performance map is used for, and subjected to, a series of post-processing operations. The processes shown in Figure 6.2 constitute all currently implemented post-processing procedures, the most important being ‘Add Electric Energy Flow Vector‘, ‘Add HEPS Engine Core Mass Data‘, and ‘Add HEPS Engine Geometry Data‘. The former adds the HEPS equivalent to the fuel flow to the performance map; the middle performs an estimation of the mass of the engine core of the HEPS engine; and the latter is currently limited to providing the outer fan diameter, scaled to correspond to the fan performance map via the disc loading. This engine core mass prediction can then be used for an updated estimation of the overall HEPS engine mass, using results obtained in the component sizing via the tool ‘HEPSretro_Components‘, which is explained in Section 6.4.
The final process block represents the interface with the CPACS standard. It translates the internal output data into the corresponding CPACS notation and creates the CPACS output file which can be used by other CPACS compatible design tools.

‘HEPS Performance Sizing Procedure‘ As stated above, the procedure followed to scale the origin performance maps is complex and requires a more detailed explanation. Figure 6.3 presents the process flow contained within the ‘HEPS Performance Sizing Procedure‘ block shown in Figure 6.2.

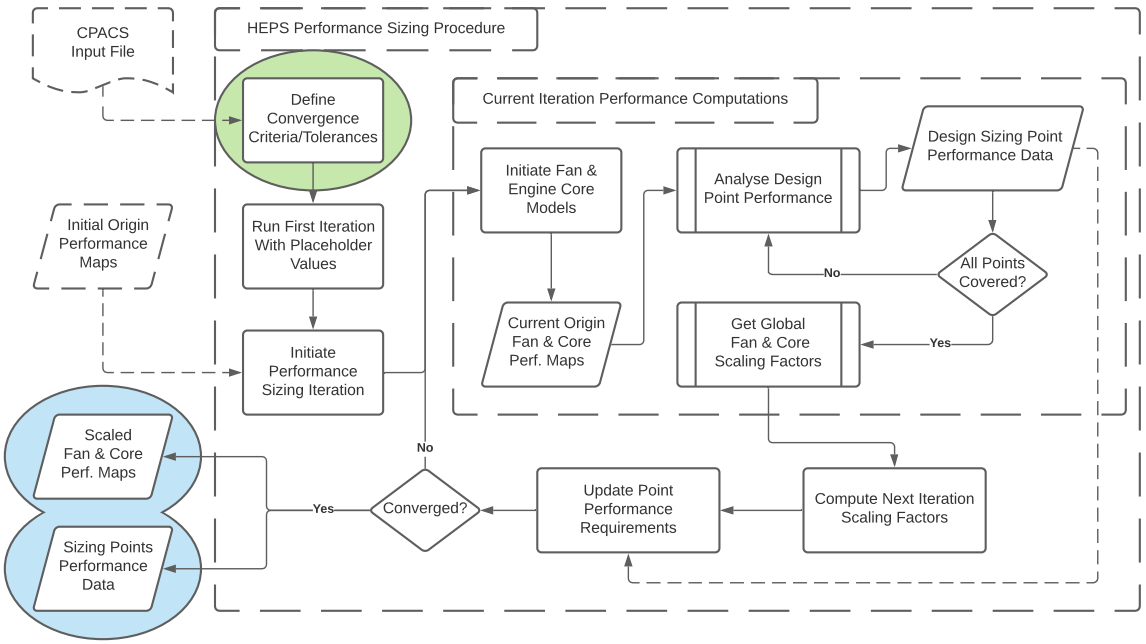

Figure 6.3: Process flow corresponding to the block ‘HEPS Performance Sizing Procedure‘ from Figure 6.2. It illustrates the required procedure to scale the provided origin fan & engine core performance maps to correspond to the intended HEPS engine performance. Dashed blocks outside the main dashed group represent forwarded input data, while dashed connections signify a secondary data flow.

The forwarded input data contained within the ‘CPACS Input File‘ includes the specified design sizing point performance requirements and the allowed convergence tolerances; the pre-scaled ’Initial Origin Performance Maps’ are forwarded using the tool internal format. Based on the required minimum tolerances, the convergence criteria for the scaling operation are defined, and the first iteration is performed using placeholder values. During this first iteration, the process determines the first value of the required *fan* thrust, as the design sizing points specify the desired *total* thrust. All following processes are governed by the current state of the ‘required fan thrust‘; the defined required total thrust will only be used as a convergence condition. Each consecutive iteration loop follows the same procedure until the change in the determined scaling factors fall below the defined tolerances.

Using the scaling factors computed in the previous iteration, the fan & engine core models are instantiated, supplying the current state of the origin performance maps, as well as relevant class methods to access the data therein. During each iteration loop, these current versions of the origin performance maps are evaluated at each design sizing point in an inner iteration. The actual process used to assess the point performance, visualised in Figure 6.4, is presented in more detail in the next paragraph. Briefly summarised, the inner iteration executes the point performance analysis for each design sizing point and stores the obtained performance data. This set of point performance data is then used in another process, visualised in Figure 6.4, to determine which factor would scale the current origin performance maps such, that they match the required point performances exactly.
For the purpose of a smooth and consistent convergence behaviour, the scaling factors to be used in the next iteration loop are then computed based on the just determined, and the previous iteration's, scaling factors. This prevents the current iteration loop from applying a too large scaling factor, resulting in an origin performance map whose data set does no longer include the values required during the next iteration. In the current implementation, the user can specify a weight (N_{fan} and N_{core}) to adjust how close to the computed scaling factor ($F_{fan,\,comp.}$ and $F_{core,\,comp.}$) the next iteration scaling factor shall be, which will determine how fast the scaling operation will converge. The actual scaling factors used in the next iteration loop are computed via Equation (6.1).

$$\begin{aligned} F_{fan} &= \frac{1.0 + N_{fan} \cdot F_{fan,\,comp.}}{N_{fan} + 1} \\ F_{core} &= \frac{1.0 + N_{core} \cdot F_{core,\,comp.}}{N_{core} + 1} \end{aligned} \tag{6.1}$$

Once the newly computed scaling factors deviate less than the specified tolerance, the scaling iteration is considered converged and the scaled origin performance maps, as well as the performance data for each design sizing point obtained during the last iteration, are forwarded to the next process.

'Analyse Design Point Performance' The process flow of the performance sizing procedure shown in Figure 6.3 contained two blocks which represented more complex processes, the first being the 'Analyse Design Point Performance' block, whose underlying process flow is shown in Figure 6.4. As explained before, this process is executed separately for each design sizing point during each loop of the performance map scaling iteration.
The data forwarded to this process consists of the tolerances for the thrust convergence, the point performance requirements of the design sizing point according to the current scaling iteration loop, and the current state of the origin performance maps. Correspondingly, the first steps of the design point performance analysis process are the definition of the convergence criteria, the definition of the current point performance requirements (current altitude, Mach number, required *total* thrust, the desired power split ratio or the *maximum available* gas turbine shaft power, and the required *fan* thrust of the previous performance map scaling iteration loop), and the instantiation of the fan and engine core models using the current state of the origin performance maps.
Once the fan and engine core models using the current iteration of the origin performance maps are instantiated, the design point performance analysis process enters a convergence loop, wherein the performance of the fan and engine core are matched. The total produced thrust of the engine is the result of the thrust produced by the fan, and the residual thrust produced due to the remaining pressure and velocity difference between the engine core exhaust and the ambient air flow. Since the conditions of the exhaust flow are dependent on the produced shaft power, a change in required fan thrust — and thus a change in required shaft power — will create a change in the produced residual core thrust. The employed thrust convergence will iterate the required fan thrust value, until the corresponding produced total thrust matches with the value specified in the supplied design sizing point requirements.

During the thrust iteration, the desired amount of produced fan thrust is specified, either from the initial point performance requirement (which is the fan thrust corresponding to the converged state of the previous performance map scaling iteration loop) or from the previous iteration loop. Using the altitude, Mach number, and the current value of required fan thrust, the processes determines the corresponding value of the required fan shaft power, as well as the maximum and minimum values of fan and engine core shaft power. While the required fan shaft power is necessary for the determination of the core thrust value, the maximum and minimum values are simply established as a measure of the limits of the origin performance map data

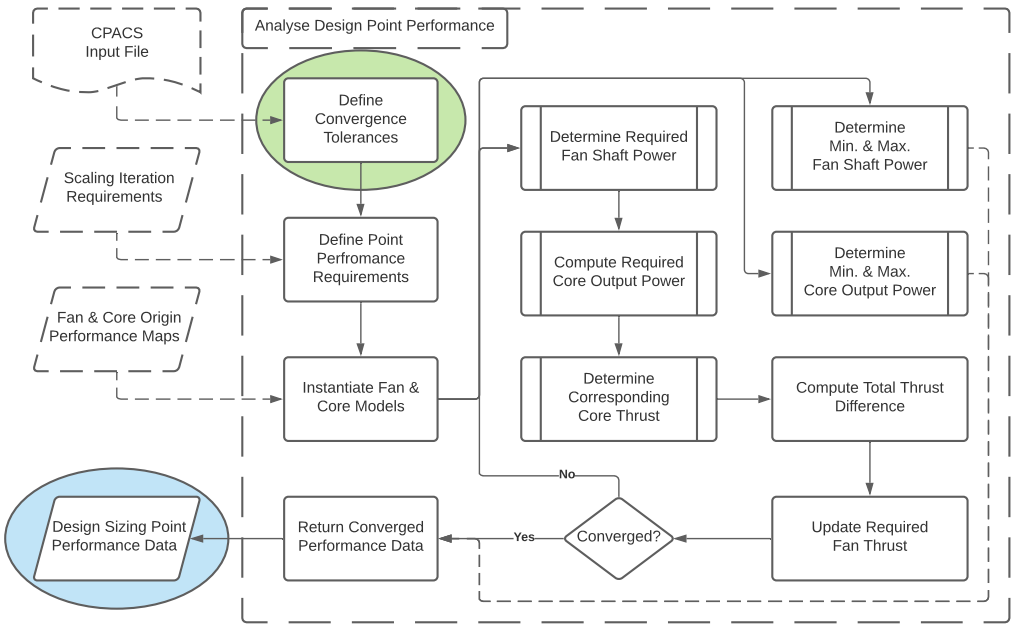

Figure 6.4: Process flow corresponding to the block ‘Analyse Design Point Performance‘ in Figure 6.3. It describes how the point performance for each of the design sizing points is assessed for the current iteration of the origin fan & engine core performance maps. The shown procedure is valid for a single design sizing point is is thus executed for each individual point.

sets. The required fan shaft power yields the required engine core output shaft power, and the corresponding residual engine core thrust.
The current value of the fan and engine core thrusts are used to compute the currently produced total thrust and the corresponding difference to the previous iteration loop. Subtracting the current value of the engine core thrust from the specified required total thrust (defined in the design sizing point requirements within the ‘CPACS Input File‘) provides the required fan thrust for the next iteration loop. Once the difference in the currently produced total thrust is less than the specified tolerance, the determined point performance data is collected and returned to the origin performance map scaling iteration from Figure 6.3.

‘Get Global Fan & Core Scaling Factors‘ The second block, shown in Figure 6.5, represented a more complex procedure within Figure 6.3 is ‘Get Global Fan & Core Scaling Factors‘. During this sub-process, the scaling factor is computed, which, when applied, would result in an origin performance map that matches the point performance of the most critical design sizing point exactly. For obvious reasons, each design sizing point requires a different scaling factor to exactly match the required with the available point performance. As the resulting performance map must be able to provide the required performance at all design sizing points, the largest absolute scaling factor (meaning the smallest reduction or largest increase) corresponds to the smallest possible maximum performance. This scaling factor is considered the "global" scaling factor of the current scaling iteration.
As both origin performance maps require separate global scaling factors, two distinct sub-processes are implemented in the tool: one to perform the computation for the fan origin performance map, the second one to perform the computations for the core origin performance map. Both processes follow the same procedure but differ in the governing parameter used to compute the individual point scaling factors. For the fan performance, the required fan thrust is compared to the maximum available fan thrust, while the core performance process considers the required output shaft power in relation to the maximum available output shaft power. Since both processes are identical except for the used performance parameter, the process flow illustrated in Figure 6.4 applies to both procedures.

First, the applicable performance model is instantiated using the current state of the origin performance map. The method to determine the global scaling factor is then iterating over each design sizing point to compute the respective point scaling factors. This is a simple operation of determining the maximum fan thrust/shaft

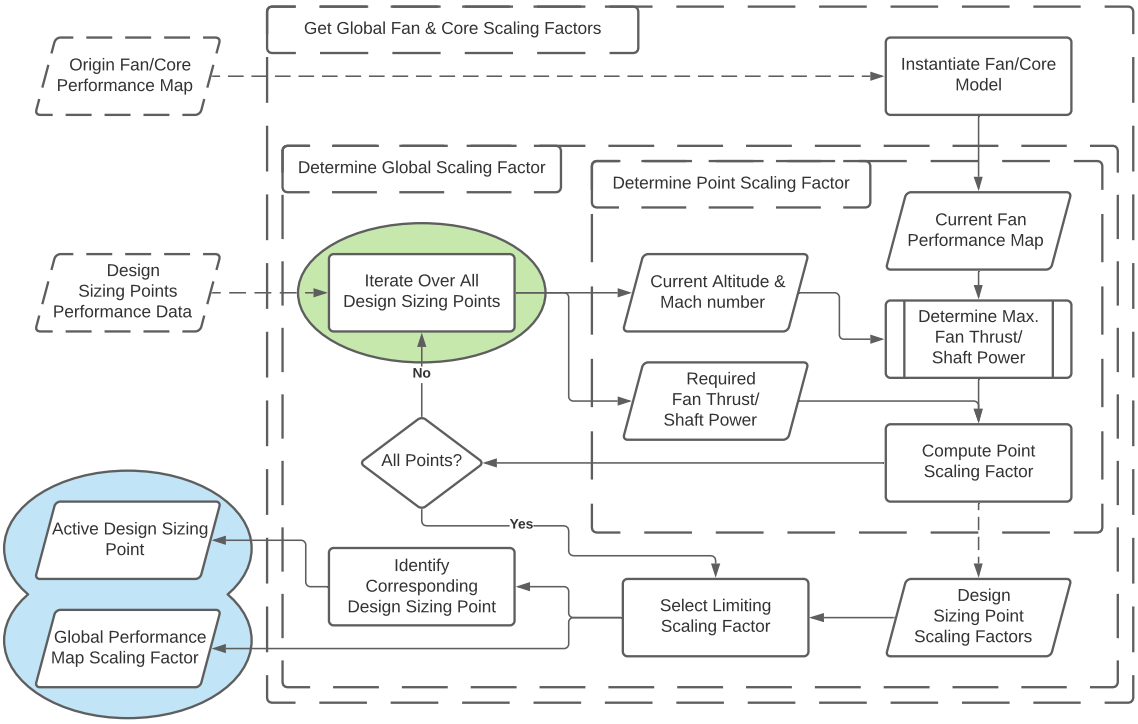

Figure 6.5: Process flow corresponding to the block 'Get Global Fan & Core Scaling Factors' in Figure 6.4. The general process used to determine the global scaling factor for the fan and engine core performance follows the same principle, differing only in using either the required fan thrust or the required output shaft power for the computations.

power available in the origin performance map at the current altitude & Mach number. Dividing the required fan thrust/shaft power by the maximum available value yields the corresponding point scaling factor.
The determine point scaling factor of each design sizing point is stored and once all points are evaluated, the global scaling factor is selected, by checking which point factor is limiting. Finally, the design sizing point corresponding to the selected global scaling factor is determined, and both are returned to the origin performance map scaling iteration. It should be noted that the determination of the active design sizing point is not necessary for the performance sizing procedure, it is simply intended as an additional output provided to the user to better interpret the produced results.

'Create HEPS Engine Performance Map' After discussing all relevant sub-process flows of the 'HEPS Performance Sizing Procedure' in the previous paragraphs, the implementation of the methodology to create the HEPS engine performance map from the scaled origin fan and engine core performance maps will be explained. In Figure 6.6 all operations executed during this procedure are displayed, corresponding to the single block 'Create HEPS Engine Performance Map' in Figure 6.2.

The data imported from the 'CPACS Input File' is limited to settings that govern the creation process. These include information on which performance parameters to include, as well as the number and distribution of thrust sample points for each altitude & Mach number combination. Besides the scaled origin performance maps, only the maximum output shaft power of the electric motor is required as additional input. Upon instantiation of the class which contains the methods to create the HEPS engine performance map, the settings for the creation process are defined, and the fan and engine core models are instantiated using the forwarded 'Scaled Origin Fan & Core Performance Maps'.
At this point, the process flow will differ depending on the choice of HEPS engine performance map that is to be created. As explained in Section 3.2.2, both "augmented" and "active" use the same origin performance maps, the difference lies in the manner in which they are combined. The current implementation of the design tool supports only the generation of "augmented" HEPS engine performance maps, hence the process flow discussed here will be limited correspondingly.

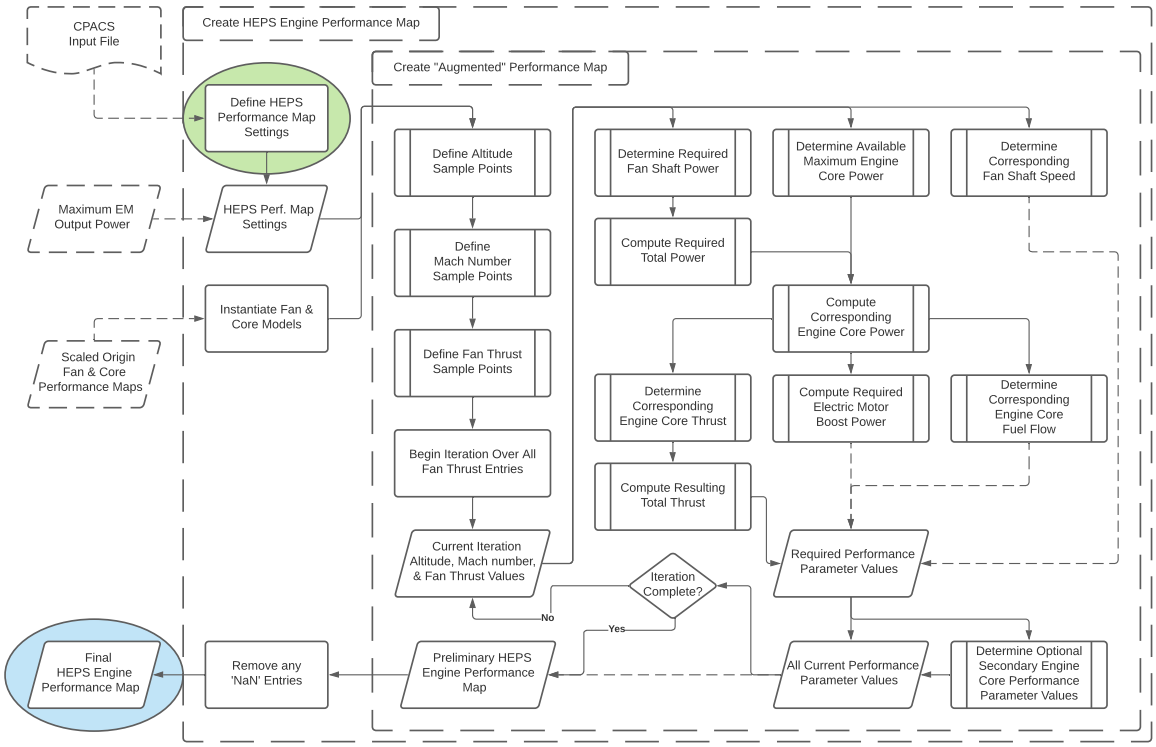

Figure 6.6: Process flow corresponding to the block ‘Create HEPS Engin Performance Map‘ in Figure 6.2. It presents the complete procedure followed to create a hybrid-electric engine performance map of type "augmented". The process iterates over the determined sample points (using the fan thrust values as iteration index) and determines the corresponding HEPS engine performance at each point. Dashed connections again illustrate secondary data flows; especially the assignment of the ‘All Current Performance Parameter Vales‘ to the ‘Preliminary HEPS Engine Performance Map‘ is essential.

The underlying principle on how the HEPS engine performance maps are generated from the scaled origin performance maps is the same for "augmented" and "active" type maps, as outlined in Figure 3.6. It begins with determining the combinations of altitude and Mach number sample points that are compatible with both origin performance maps, followed by a more complex procedure to define the thrust sample points for each combination of ambient conditions. Once the thrust sample points are defined, the process begins an iteration over all selected sample points (altitude, Mach number, and thrust), interpolates the corresponding performance parameters and stores the results in the new HEPS engine performance map. The major difference between the two types of performance maps for parallel HEPS engines lies in whether the power split ratio is considered a control or performance parameter. Treating it as a control parameter ("active" performance map) requires either the definition of an additional set of sample points, or the generation of multiple performance maps, each one for a set value of the power split ratio.

Although displayed as belonging to the process to create the "augmented" style HEPS engine performance map in Figure 6.6, many of the sub-processes are similarly used in the process flow of an "active" style performance map. However,, for the remainder of the discussion, the description will be limited to the process flow as shown.
The first step in combining the origin performance maps is the determination of the sample points to be used in the HEPS engine performance map. This is done in a staged procedure, corresponding to the hierarchy of the state variables of the performance maps, as explained in Section 3.2.1. First, the altitude sample points compatible with both origin performance maps are determined. This is a simple matter of making sure the selected altitude sample points fall within the data set of both origin performance maps, indicated by the simple constraints given in Equation (6.2).

$$\begin{aligned} h_{min.,\,HEPS} &\geq max\left(h_{min.,\,fan},\, h_{min.,\,core}\right) \\ h_{max.,\,HEPS} &\leq min\left(h_{max.,\,fan},\, h_{max.,\,core}\right) \end{aligned} \tag{6.2}$$

Next, the Mach number sample points corresponding to the previously defined altitude sample points are determined. This process follows the same approach as for the altitude sample points, however it has to be repeated for each altitude within the defined sample points, accordingly the constraints are defined as in Equation (6.3), where the index 'i' indicates the current value of the altitude.

$$\begin{aligned} M_{min.,\,HEPS}(h_i) &\geq max\big(M_{min.,\,fan}(h_i),\, M_{min.,\,core}(h_i)\big) \\ M_{max.,\,HEPS}(h_i) &\leq min\big(M_{max.,\,fan}(h_i),\, M_{max.,\,core}(h_i)\big) \end{aligned} \tag{6.3}$$

For both the altitude and Mach number sample point definitions, the current implementation defaults to a standard distribution of the sample points. The altitude sample points are modelled after either of the origin performance maps, simply checking that they do not exceed the available data set, while the procedure for the Mach number sample points determines the available maximum and minimum compatible Mach number values at each altitude and creates a set of sample points using a 0.1 step size.
Afterwards, the set of thrust sample points can be defined. This process is much more complex than for the altitude or Mach number sample points, and is discussed in detail in the next paragraph, and is illustrated by Figure 6.7. The final product of this process chain is a defined set of altitude, Mach number, and thrust sample points. In the implementation described here, the thrust sample points are defined for the fan thrust values, as the total produced thrust is a result of the available fan thrust and the corresponding residual engine core thrust.

Once all sample points for the HEPS engine performance map have been defined, the process begins an iteration. In current implementation of the tool, the iteration is performed using a three-layered nested for loop, iterating over the altitude, Mach number, and fan thrust values respectively. At the end of each iteration loop, the obtained parameter values, both control and performance, are simply appended to a list, creating the resulting vectors of the performance map.
During each loop of the iteration, the current state of the control variables are used as input to the fan and engine core model methods to interpolate the desired performance parameters. As shown in the visualisation of the iteration loop in Figure 6.6, three performance parameters can be obtained directly from the control variables: the currently required fan shaft power, the currently available maximum engine core output shaft power, and the fan shaft speed corresponding to the currently produced fan thrust. Using the determined required fan shaft power, and optionally the necessary offtake power, the currently required total output shaft power is computed. Combined with the previously determined maximum available engine core output power, this yields the current value of the engine core output shaft power. In the current implementation, this is a simple check whether the required total power is larger than the available maximum core power. Should the required total power exceed the available engine power, additional boost power is assumed to be added via the electric motor, as illustrated by the block 'Compute Required Electric Motor Boost Power'. Simultaneously, the current engine core output power allows the determination of the corresponding residual engine core thrust and the fuel flow. Finally, the fan thrust and the just determined residual core thrust are used to compute the produced total thrust.
These performance parameters are considered necessary for the HEPS performance to accurately model the performance of the parallel HEPS engine. The tool does offer the possibility to include further performance parameters in the generated HEPS performance map, as indicated by the block 'Determine Optional Secondary Engine Core Performance Parameter Values'. This is currently limited to performance parameters stored in the origin engine core performance map, as it is mainly aimed at parameters describing the produced emissions.

As already mentioned, at the end of each iteration loop the determined current values of the performance parameters are appended to a list storing the values of all previous iteration loops. These list expand with each iteration, until all sample points were evaluated, at which point any immediate post-processing operations are performed. Currently, this post-processing is limited to the removal of any 'NaN' entries within the generated performance map. Afterwards, the generation of the HEPS engine performance map is completed.

'Define Fan Thrust Sample Points' As with the 'HEPS Performance Sizing Procedure', the process flow explaining the procedure to create the HEPS engine performance map in Figure 6.6 contained a sub-process too complex to be directly included in the illustration. The actual process flow contained within the block 'Define Fan Thrust Sample Points' is instead visualised in Figure 6.7

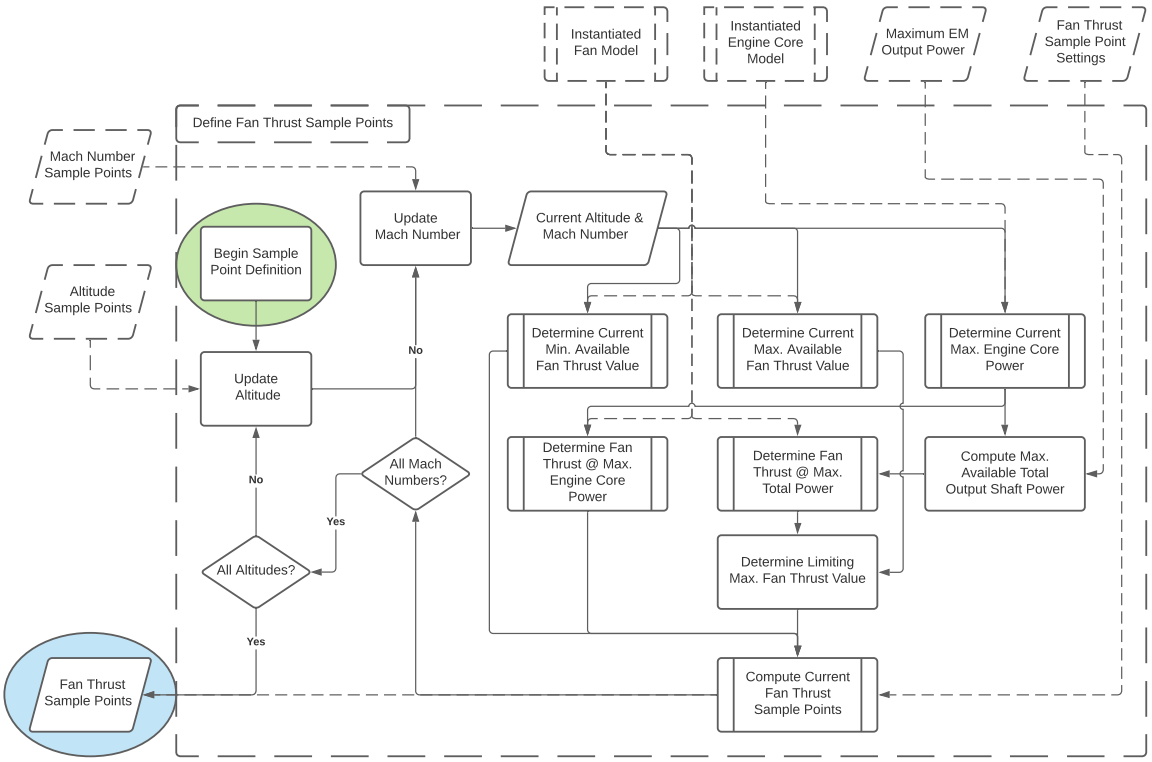

Figure 6.7: Process flow corresponding to the block ‘Define Fan Thrust Sample Points‘ in Figure 6.6. It determines the optimal range of fan thrust values for each altitude & Mach number combination, and creates sample points based on the desired distribution and number of points from the input CPACS file.

The process requires as input both the fan and engine core scaled origin performance maps, the maximum allowed output shaft power of the electric motors, the already defined altitude and Mach number sample points, and of course the settings for the thrust sample point distributions. It is specifically tailored to be used in the generation of "augmented" type HEPS engine performance maps, as it not only determines the applicable minimum and maximum fan thrust values, but ensures that characteristically important values are also included. Particularly, it includes the fan thrust values corresponding to the point, where the engine core operates at its maximum power output. Additionally, it automatically picks the appropriate limiting case, between the restrictions imposed by the fan performance data set, the engine core performance data set, and the enforced maximum electric motor boost power.

From the illustrated process flow it can be seen that the procedure to define the fan thrust sample points consists of a two-layered iteration, first over the altitude sample points, then for each altitude value over the corresponding Mach number sample points. Using the current altitude and Mach number, the process determines the current values for the minimum and maximum available fan thrust, as well as the maximum available engine core output power. The maximum core output power is used to determine the corresponding fan thrust, as well as — combined with the external information on the maximum allowed electric motor boost power — to compute the maximum available total power. This in turn is used to compute the fan thrust corresponding to the maximum available total output power. In total, four values of the fan thrust are determined, the minimum and maximum available values in the origin fan performance map, and the fan thrusts corresponding to the maximum available engine core and total shaft powers. The maximum fan thrust value to be used in the range corresponding to the current altitude & Mach number combination is then determined from the maximum available fan thrust, and the value corresponding to the maximum available total power (the lower of the two being limiting).

The remaining three fan thrust values — minimum, maximum, and corresponding to maximum available engine core power — are forwarded to a process dedicated to generate a corresponding set of sample points. This dedicated process evaluates the user defined settings for the thrust sample points, which declares the

desired number of points (excluding the sample point corresponding to the max. engine core power) as well as the intended distribution. In the current implementation, the thrust sample points support a uniform, a sine, and a cosine distribution.
Similarly to the creation of the HEPS engine performance map, the determined fan thrust sample points are continuously appended to a list, thereby expanding the fan thrust sample points at the end of each iteration loop. Once all altitude and Mach number combinations are evaluated, the complete set of fan thrust sample points is returned to the HEPS performance map creation process.

6.3.3. Available Tool Settings Parameters

The 'HEPSretro_Performance' tool was designed with many settings available to the user. Every parameter that could be changed was implemented such, that it can be set by the user simply by specifying it in the <toolspecific> node of the input CPACS file. The structure of the <toolspecific> node follows the CPACS 3.2 standard, with the general tool settings stored directly, and all other parameters stored within a sub-node corresponding to their purpose. Subsequently, the available input parameters of each group of settings is briefly discussed and presented in the corresponding Tables 6.1 to 6.8.

General Settings:
The general settings contain the most important parameters that the user has to adapt to his personal use-case. Here it is defined what type of architecture the tool shall create a performance map for, what type of performance map the tool shall generate, and which fan and engine core performance map (stored within the input CPACS file) shall be used in the sizing process. At the current stage of the tool, only parallel HEPS architectures and "augmented" or "active" HEPS performance maps are available, but once these procedures are implemented they can be easily selected. If the user does not have specific fan and engine core performance maps, leaving the respective fields blank will cause the tool to use the stored default maps (currently corresponding to an A320 sized aircraft).
Table 6.1 lists all parameters that are considered 'general settings', which are set directly within the <HEPSretro_Performance> node in the CPACS file. The table provides an example entry that can be provided to the tool, as well as a description of what the purpose of each specific parameter is.

Table 6.1: Overview of available general tool settings parameters for the performance prediction tool 'HEPSretro_Performance', defined directly in the <HEPSretro_Performance> node.

Parameter Name	Example Entry	Description
hybrid_architecture	parallel	Parameter to set what type of HEPS architecture the generated hybrid performance map shall correspond to.
hybrid_map_type	augmented	Parameter to set the type of HEPS engine performance map to be generated.
fan_map_CPACS_path [1]	/cpacs/originMaps/fanMap [2]	XPath within the input CPACS file to the origin map that contains the fan performance.
core_map_CPACS_path [1]	/cpacs/originMaps/coreMap[2]	XPath within the input CPACS file to the origin map that contains the engine core performance.
offtakes_map_CPACS_path[1]	/cpacs/originMaps/offMap [2]	XPath within the input CPACS file to the performance map that contains the data on the required power offtakes.

[1] Optional input parameter, uses default origin performance maps if not supplied.
[2] The example XPath provided here is a simple placeholder and does not abide by the CPACS standard.

Design Sizing Points Parameters:
Besides adapting the general settings, the design sizing points are the only parameters that the user absolutely has to specify for the tool to produce a proper HEPS engine performance map. In the design sizing points,

the user prescribes the desired performance at specific points in the flight envelope, which are used to match the scaled fan and engine core performance maps during the performance sizing process. While at least one design sizing point has to be provided, the user is not limited in how many design sizing point are defined, but each additional point is increasing the required computational effort and thus the runtime of the tool.
Table 6.2 lists all parameters that can be defined per design sizing point. Most parameter's purpose is self-explanatory, but it has to be noted that the assigned 'name' is used beyond giving the user a reference. The tool uses the defined 'name' entries as internal unique identifiers for the various sizing points, it is thus essential that each design sizing point is given a unique name. Finally, the generated performance map is representing a specific engine, and is thus presenting the estimated performance *per engine*. This is clearly mirrored in the defined design sizing points, where the parameter 'required_total_thrust' refers to the total thrust each engine shall be able to provide.

Table 6.2: Overview of available parameters specifying the design sizing points for the performance prediction tool 'HEPSretro_Performance'. These parameters are governing the actual performance of the sizing process, they are not settings to specify how the tool shall work, and are defined under the <sizing_points><sizing_point> node.

Parameter Name	Example Entry	Description
name	mid-climb	Defines the name of the specified design sizing point. This name will be used as an internal reference for each sizing point, and must thus be unique!
altitude	7000.0 m	The altitude at which the design sizing point specifies the desired point performance, given in meters above sea-level.
mach_number	0.7	The Mach number for which the design sizing point specifies the desired point performance.
required_total_thrust	35,000.0 N	The total thrust per engine(!) that is required for the desired performance at the specified design sizing point.
power_split	0.09	The desired maximum power split ratio with which the desired point performance shall be achieved, given as a percent-fraction.
GT_shaft_power_max	5,402,000.0 W	The maximum amount of shaft power the engine core is allowed to produce at the specified design sizing point. Alternative to prescribing a power-split ratio.
offtake_power	0.0	The amount of offtake power expected/necessary at the specified design sizing point, influences the scaling of the engine core.

Iteration Behaviour Settings:
The settings parameters presented in this paragraph govern the behaviour of the various iteration operations. They are separated depending on whether they specify parameters for the performance map scaling iteration — defined under the node <performanceProcess_toolSpecific> — or for the assessment of the point performance — defined under the node <designPoint_toolSettings>.
In Table 6.3 the available parameters are listed, separated according to their respective parent-nodes. The performance process parameters define the acceptable tolerance on the determined scaling factors, an upper limit on the performed iteration loops, and the weight applied in the process to determine the next scaling factor for both the fan and the engine core origin performance maps respectively. For the point performance assessment, the parameters define the acceptable tolerance of the determined total thrust and the limit for the thrust convergence iteration.
These parameters enable the user to fine-tune the convergence criteria of the various iteration procedures. Depending on the required accuracy of the produced output, the convergence tolerances can be adjusted to yield the optimum combination of accuracy and tool runtime.

Table 6.3: Overview of all available parameters to govern the convergence behaviour of the performance prediction tool 'HEP-Sretro_Performance' processes. The parameters are separated into two categories, distinguishing the origin performance map scaling iteration, and the total thrust iteration executed during each assessment of the design sizing point performance. They are defined under the <performanceProcess_toolSettings> and <designPoint_toolSettings> nodes respectively.

	Parameter Name	Example Entry	Description
performanceProcess_toolSettings[1]	fan_map_scaling_tolerance	0.01	Parameter to set the acceptable tolerance for the consecutive scaling factors in the fan performance map scaling iteration, given as a percent-fraction.
	fan_map_scaling_iter_limit	50	Parameter to set the maximum number of allowed iterations for the fan performance map scaling iteration.
	fan_scaling_factor_weight	4.0	Parameter to set how close the used scaling factor is to the previously computed scaling factor.
	core_map_scaling_tolerance	0.01	Parameter to set the acceptable tolerance for the consecutive scaling factors in the engine core performance map scaling iteration, given as a percent-fraction.
	core_map_scaling_iter_limit	50	Parameter to set the maximum number of allowed iterations for the engine core performance map scaling iteration.
	core_scaling_factor_weight	2.0	Parameter to set how close the used scaling factor is to the previously computed scaling factor.
designPoint _toolSettings[1]	thrust_tolerance	0.02	Parameter to set the acceptable tolerance for the thrust convergence iteration conducted during the design sizing point performance assessment.
	thrust_iter_limit	50	Parameter to set the maximum number of allowed iterations for the thrust convergence during the design sizing point performance assessment iterations.

[1] Name of the parent node under which the presented parameters are defined.

More interesting for a user however are the 'fan_scaling_factor_weight' and the 'core_scaling_factor_weight' parameters. These setting allow a tuning of how aggressive the origin performance map scaling iteration applies the computed scaling factors. The larger the prescribed weights, the closer to the computed scaling factor will be applied in the next iteration (see the described scheme in Equation (6.1)), which results in a faster convergence. This faster convergence however increases the risk of the origin performance maps being 'over-scaled', resulting in a performance map whose data set no longer includes the values required during the next iteration loop.

HEPS Engine Performance Map Settings:
The parameters in Table 6.4 influence the generated performance map for the HEPS engine. Here the user can specify a specific sample point distribution pattern, in case a certain region is more critical for their study. They can also dictate, how many sample points for each combination of altitude & Mach number the HEPS performance map shall contain. Additionally, it allows the user to specify to include either all, or only some specific, vectors from the origin core performance map that are not included in the standard layout. This option was originally included to allow information on the produced emissions of the engine core to be included in the hybrid-electric performance map.

Table 6.4: Overview of available settings parameters to adjust the generated HEPS engine performance map for the performance prediction tool ‘HEPSretro_Performance‘, defined under the <hybrid_map_toolSettings> node.

Parameter Name	Example Entry	Description
thrust_point_distribution	sine_end	Parameter to set the type of distribution of the thrust sample points. Distinguishes between "uniform" (equal spacing), "cosine" (more points at both ends), "sine_end" (more points at high thrust end), and "sine_front" (more points at low thrust end).
number_thrust_points	9	Sets how many thrust sample point shall be created for each combination of altitude & Mach number.
include_secondary_core_vectors [1]	true [2]	Boolean switch, determines if secondary (i.e. other than altitude, Mach number, shaft power, core thrust, and fuel flow) shall be included in the generated HEPS performance map.
additional_hybrid_vector_names [1]	emissions_CO2; emissions_NOX [1]	Parameter to define specific secondary vector names from the engine core performance map to be included in the generated HEPS engine performance map. This parameter allows to include only a select number of secondary vectors, instead of all as is done using ‘include_secondary_core_vectors‘.

[1] Parameter is one continuous string, but was separated to fit within the available space in the table. The proper spelling of the parameters is ‘include_secondary_core_vectors‘ and ‘additional_hybrid_vector_names‘; the correct formatting for the example entry is ‘emissions_CO2;emissions_NOX‘.

[2] Note that while python uses the capitalised boolean (True vs. False), the tixi library which is used to interact with the CPACS files uses lower-case boolean (true vs. false)!

While the parameters presented in Table 6.4 are generally applicable for any type of hybrid-electric engine performance map, they were created according to the required settings of an "augmented" performance map for a parallel HEPS engine. With future implementations of different types of performance maps or even alternate HEPS architectures, these parameters are likely to be extended depending on newly introduced settings variables.

Output Settings:
The parameters contained with the <output_toolSettings> node of the CPACS file allow the user to directly influence how the created HEPS engine performance map is exported into the output CPACS file. Conforming to the standard behaviour of already established CPACS compatible design tools, ‘HEPSretro_Performance‘ exports it’s produced results to the received input file, either altering the stored information or adding new data. The first two parameters listed in Table 6.5 enable the user to specify the name of the output CPACS file and into which directory it shall be saved. This allows for an easy tracking of which created output file belonged to which study.
The further parameters dictate how the generated HEPS performance map is stored within the CPACS file, while still being compliant to the CPACS standards. The user can manually dictate the desired decimal precision of both the entries in the HEPS performance map, as well as the parameters exported into the <results> node (for more information on the additional output, see Section 6.3.4). It also allows the user to specify a custom CPACS uID and name for both the engine node into which the HEPS performance map is stored, as well as the HEPS performance map itself. Finally, the user can specify that the scaled origin performance maps, which were used as the basis for the generated HEPS performance map, shall be exported into the engine node as well.

Table 6.5: Overview of the available parameters to adjust the produced output of the performance prediction tool 'HEP-Sretro_Performance', defined under the <output_toolSettings> node.

Parameter Name	Example Entry	Description
output_CPACS_filename	example_toolOutput	The name given to the generated output CPACS file. Allows for easy generation of multiple HEPS performance maps without manual renaming of the output file. If integrated into RCE, this functionality is limited by the tool integration settings of RCE.
output_CPACS_directory	C:\User\Username... ...\CPACSfiles [1]	Path to the directory into which the generated output CPACS file shall be saved. Must be an absolute path!
output_decimal_precision	3	Parameter to set the decimal precision of the exported results.
hybrid_map_decimal _precision[2]	4	Parameter to set the decimal precision of the values in the created HEPS engine performance map. Allows adjustments in case the user wants to include custom secondary vectors with small significant entries.
engine_uID	HEPS_engine	Specifies the uID that will be associated with the engine node that contains the generated HEPS performance map.
engine_name	conceptual_HEPS_engine	Specifies the name that will be associated with the engine node that contains the generated HEPS performance map.
hybrid_map_uID	hybridPerformanceMap	Specifies the uID that will be associated with the generated HEPS performance map within the engine node.
hybrid_map_name	augmentedHybridMap	Specifies the name that will be associated with the generated HEPS performance map.
include_origin_maps	true [2]	Boolean switch to set whether the generated output CPACS file shall include the (scaled) origin performance maps which were used to create the HEPS performance map.

[1] Example directory does not correspond to a suggested directory. It was chosen to illustrate that an absolute path has to be specified!
[2] Note that while python uses the capitalised boolean (True vs. False), the tixi library which is used to interact with the CPACS files uses lower-case boolean (true vs. false)!

Especially the parameters to specify the desired CPACS uIDs ('engine_uID' and 'hybrid_map_uID') are vitally important. While leaving these parameters blank in the provided <output_toolSettings> node of the input CPACS file simply causes the tool to assign a default value instead, assigning a uID that is already in use is more dangerous. If the user inadvertently assigns an 'engine_uID' for the HEPS engine that is already used for a different engine within the CPACS file, the tool will delete all data stored in the initial engine node. All information pertaining to the original engine will be lost. It should thus always be checked, that the prescribed uIDs are indeed unique.

Post-Processing Settings:
As shown in Figure 6.2, the tool's process flow includes numerous post-processing operations, during which the generated HEPS performance map is adapted or additional output parameters are determined. The pa-

rameters presented in Table 6.6 include not only settings for how these processes shall operate, but also input parameters that shall be used instead of the default values, if the user has access to more accurate estimates. One such input parameter is the ‘HEPS_powertrain_efficiency‘, which is used by the tool to add the vector ‘el_energy_flow‘ to the HEPS performance map (an electric equivalent to the fuel flow). If the tool is used in combination with the HEPS component sizing tool (‘HEPSretro_Components‘, detailed in Section 6.4), a more accurate estimation of the overall efficiency of the HEPS propulsion chain is available. Similarly, the user may want to specify a specific power of the engine core, to reflect a certain technology level of turbomachinery.
The parameters ‘OPR_CPACS_path‘, ‘FPR_CPACS_path‘, and ‘fan_outerRadius_CPACS_path‘ are necessary if the user specified origin performance maps for which these parameters are stored under a different XPath than used in the default performance maps.

Table 6.6: Overview of the available parameters to adjust the post-processing operations of the performance prediction tool ‘HEPSretro_Performance‘, defined under the <post_processing_toolSettings> node.

Parameter Name	Example Entry	Description
HEPS_powertrain _efficiency[a]	0.89	Sets the current assumption of the overall efficiency of the hybrid-electric propulsive chain. This is used to add a vector that denotes the electric power consumptions, denoted 'el_energy_flow', as an electric equivalent to the fuel flow vector.
OPR_CPACS_path	/output/engines/engine /analysis/opr00[a]	The XPath to the node in the origin engine core performance map, under which the Overall Pressure Ratio is stored. This value is assumed an accurate assumption for the OPR of the HEPS engine core.
FPR_CPACS_path	/output/engines/engine /analysis/fpr00[a]	The XPath to the node in the origin fan performance map, under which the Fan Pressure Ratio is stored. This value is assumed to be an accurate assumption for the FPR of the HEPS fan.
fan_outerRadius _CPACS_path[a]	/output/engines/engine /geometry/fan /outerRadius[a]	The XPath to the node under which the outer radius of the fan, corresponding to the supplied origin fan performance map, was stored. This fan radius will be scaled using the same ‘effective‘ scaling factor as the supplied performance map, to provide an estimate on the fan radius for the HEPS engine.
engine_core _specific_power[a]	14000.0	Parameter for the user to prescribe a specific power for the engine core, which will be used in the mass estimation of the engine core of the HEPS engine. If not supplied, the tool computes the specific power from the default engine core performance map.
create_altitude_plots	true [b]	Boolean to switch whether or not the tool creates the performance plots for various altitudes.
plot_altitudes	0.0;7000.0;11000.0	A CPACS vector (requires CPACS attribute ‘mapType="vector"‘ assigned to node) that provides for which altitudes the tool shall create the performance plots. If no altitudes are supplied and the parameter ‘create_altitude_plots‘ is set to ‘true‘, the tool will create a performance plot for each unique altitude value in the HEPS performance map.

Continued on next page

Table 6.6: (cont.) Overview of the available parameters to adjust the post-processing operations of the performance prediction tool 'HEPSretro_Performance', defined under the <post_processing_toolSettings> node.

Parameter Name	Example Entry	Description
plot_file_type	pdf	Parameter to allow the user to specify the desired file type of the generated performance plots.
x_vec_name	thrust	Parameter to set which of the vectors in the HEPS performance map shall be used as x-axis variable.
y_vec_name	power_core	Parameter to set which of the vectors in the HEPS performance map shall be used as y-axis variable.
no_title	false [b]	Switch to create performance plots without a title.

[a] Parameter is one word, but was separated to fit within the available space in table. The proper spelling is 'HEPS_powertrain_efficiency', 'fan_outerRadius_CPACS_path', and 'engine_core_specific_power'; and the spelling of the example entries is '/output/engines/engine/analysis/opr00', '/output/engines/engine/analysis/fpr00', and '/output/engines/engine/geometry/fan/outerRadius'.
[b] Note that while python uses the capitalised boolean (True vs. False), the tixi library which is used to interact with the CPACS files uses lower-case boolean (true vs. false)!

Finally, the tool can create performance plots, which show the relation between the data of two vectors. The remaining parameters listed in Table 6.6 allow the user to enable their creation and to dictate what plots are created.

Core & Fan Model Settings:
Finally, the last aspect of the tool for which the user can specify the toolSettings are the underlying fan and engine core models. The respective settings parameters are shown in Tables 6.7 and 6.8, and are mostly equivalent, with the core toolSettings including a few additional parameters.

Table 6.7: Overview of the available parameters to adjust the tool settings of the underlying fan model for the performance prediction tool 'HEPSretro_Performance', defined under the <fan_toolSettings> node.

Parameter Name	Example Entry	Description
fan_CPACS_filepath	C:\Users\Username... \originPerfMaps\fan.xml[1]	Absolute path to the file that contains the performance map that shall be used as origin fan performance map.
fan_CPACS_path	/output/engines/engine /analysis/performance Maps/performanceMap[2]	XPath to the performance map within the CPACS file specified under 'fan_CPASC_filepath'.
vector_names	flightLevel;machNumber ;thrust;Shaft_PW;Shaft_nrel[2]	A list of all vector names within the performance map, that the tool is supposed to import. Allows to exclude specific vectors.
normalised_vector _names [2]	Shaft_nrel	A list in the same format as 'vector_names', that specifies which of the vectors in the fan performance map are meant to be normalised, such that they remain normalised after the scaling operation.
altitude_vector_name	flightLevel	Specifies which of the vector names in the performance map correspond to the altitude sample points.

Continued on next page

Table 6.7: (cont.) Overview of the available parameters to adjust the tool settings of the underlying fan model for the performance prediction tool ‘HEPSretro_Performance‘, defined under the <fan_toolSettings> node.

Parameter Name	Example Entry	Description
mach_vector_name	machNumber	Specifies which of the vector names in the performance map corresponds to the Mach number sample points.
thrust_vector_name	thrust	Specifies which of the vector names in the performance map corresponds to the thrust sample points.
power_vector_name	mDotFuel	Specifies which of the vector names in the performance map corresponds to the fan shaft power.

[1] Example directory does not correspond to a suggested directory. It was chosen to illustrate that an absolute path has to be specified!
[2] Parameter is one word, but was separated to fit within the available space in table. The proper spelling of the parameters is ‘normalised_vector_names‘; while the correct spelling of the example entries is ‘/output/engines/engine/analysis/performanceMaps/performanceMap‘, and ‘flightLevel;machNumber;thrust;Shaft_PW;Shaft_nrel‘.

The parameters that are present for both models, are the settings on the path to the CPACS file that contains the origin performance map, and the correspond defined XPath to the performance map within this file. It is important to note here, that while these parameters can be prescribed here, these parameters are only used when the models are instantiated outside of the general tool’s process flow. When executing the tool as intended, the fan and engine core models are instantiated multiple times at different states of the process, and each time the origin performance map they use has been directly provided by the tool’s internal logic. Setting these two parameters in the input file will not change the origin performance maps used by the models throughout the tool’s execution, they are merely stated here to provide a complete overview.

Table 6.8: Overview of the available parameters to adjust the tool settings of the underlying engine core model for the performance prediction tool ‘HEPSretro_Performance‘, defined under the <core_toolSettings> node.

Parameter Name	Example Entry	Description
core_CPACS_filepath	C:\Users\Username... \originPerfMaps\core.xml[1]	Absolute path to the file that contains the performance map that shall be used as origin engine core performance map.
core_CPACS_path	/output/engines/engine /analysis/performance Maps/performanceMap[2]	XPath to the performance map within the CPACS file specified under ‘core_CPASC_filepath‘.
vector_names	flightLevel;machNumber ;thrust;mDotFuel;IPShaft _nrel;P_Shaft;P_elctr [2]	A list of all vector names within the performance map, that the tool is supposed to import. Allows to exclude specific vectors.
normalised_vector _names [2]	IPShaft_nrel	A list in the same format as ‘vector_names‘, that specifies which of the vectors in the core performance map are meant to be normalised, such that they remain normalised after the scaling operation.

Continued on next page

Table 6.8: (cont.) Overview of the available parameters to adjust the tool settings of the underlying engine core model for the performance prediction tool 'HEPSretro_Performance', defined under the <core_toolSettings> node.

Parameter Name	Example Entry	Description
altitude_vector_name	flightLevel	Specifies which of the vector names in the performance map correspond to the altitude sample points.
mach_vector_name	machNumber	Specifies which of the vector names in the performance map corresponds to the Mach number sample points.
power_vector_name	P_Shaft	Specifies which of the vector names in the performance map corresponds to the provided shaft power.
thrust_vector_name	thrust	Specifies which of the vector names in the performance map corresponds to the thrust sample points.
fuel_flow_vector_name	mDotFuel	Specifies name of vector in the performance map that corresponds to the fuel flow.
shaft_power_sign _negative [2]	true	Boolean switch to tell the tool whether the provided core performance map follows the convention of assigning negative values to the shaft power to signify that it is provided instead of consumed.

[1] Example directory does not correspond to a suggested directory. It was chosen to illustrate that an absolute path has to be specified!
[2] Parameter is one word, but was separated to fit within the available space in table. The proper spelling of the parameters is 'normalised_vector_names' and 'shaft_power_sign_negative'; while the correct spelling of the example entries is '/output/engines/engine/analysis/performanceMaps/performanceMap', and 'flightLevel;machNumber;thrust;mDotFuel;IPShaft_nrel;P_Shaft;P_elctr'.

Additional parameters shared between both models are the definition of the 'vector_names' and the 'normalised_vector_names', as well as the declaration of which vectors names in the origin performance maps correspond to the altitude, Mach number, shaft power (required or provided for the fan and engine core respectively), and the produced thrust. Opposed to the filepath and XPath variables described above, these parameters are actually important during the execution of the tool, and should accurately reflect the provided origin performance maps. The tool does include a default setting for each of the shared parameters, which complies to the current CPACS 3.2 naming convention where available.
Finally, the toolSettings for the engine core model include two additional input parameters, that set the 'fuel_flow_vector_name' and the 'shaft_power_sign_negative'. The former is self-explanatory, while the second parameter informs the tool of the sign convention applied to the shaft power vector in the supplied engine core origin performance map, as sometimes a negative sign is used to denote that the specified power is supplied instead of consumed.

6.3.4. Generated Output and Results

Finally, this subsection provides a brief overview of the provided output and any additional results that are exported to the output CPACS file. Listing 6.1 displays an excerpt from an example CPACS file created by the 'HEPSretro_Performance' design tool, presenting the <engine> node corresponding to the sized hybrid-electric propulsion system. In the CPACS standard, this node defines all data pertaining to the physical engine as an isolated object, de-coupled from the aircraft design on which it will be used.
As discussed, the main purpose of the design tool is to generate a performance map that provides an estimate on the resultant performance of the HEPS engine throughout the flight envelope. In the listing all vectors included in the hybrid-electric performance map are listed, but for improved visibility their entries are excluded. In addition to the generated HEPS performance map, the excerpt also includes the used origin

fan & engine core performance maps (see Table 6.5). Including the performance maps upon which the HEPS performance map is based allows the user to better interpret the expected performance of both the fan and the engine core.

```
<?xml version="1.0" encoding="utf-8"?>
<cpacs>
  <vehicles>
    <engines>
      <engine uID="HEPS_engine">
        <name>conceptual_HEPS_engine</name>
        <analysis>
          <assumed_HEPS_powertrain_efficiency>0.890
              </assumed_HEPS_powertrain_efficiency>
          <fpr00>1.376</fpr00>
          <opr00>38.860</opr00>
          <thrust00>126384.173</thrust00>
          <performanceMaps>
            <performanceMap uID="hybridPerformanceMap">
              <name>augmentedHybridPerformanceMap</name>
              <flightLevel mapType="vector">.....</flightLevel>
              <machNumber mapType="vector">.....</machNumber>
              <thrust mapType="vector">.....</thrust>
              <thrust_fan mapType="vector">.....</thrust_fan>
              <thrust_core mapType="vector">.....</thrust_core>
              <power_fan mapType="vector">.....</power_fan>
              <power_core mapType="vector">.....</power_core>
              <P_mech_EM mapType="vector">.....</P_mech_EM>
              <mDotFuel mapType="vector">.....</mDotFuel>
              <power_offtakes mapType="vector">.....</power_offtakes>
              <IPShaft_nrel mapType="vector">.....</IPShaft_nrel>
              <el_energy_flow mapType="vector">.....</el_energy_flow>
              <fan_shaft_nrel mapType="vector">.....</fan_shaft_nrel>
              <P_electr mapType="vector">.....</P_electr>
            </performanceMap>
            <performanceMap uID="originFanMap">
              ...
            </performanceMap>
            <performanceMap uID="originCoremap">
              ...
            </performanceMap>
          </performanceMaps>
        </analysis>
      </engine>
    </engines>
  <vehicles>
</cpacs>
```

Listing 6.1: Overview of the example output <engine> node created for a parallel hybrid-electric propulsion system.

Furthermore, the <engine> node contains additional design data on the HEPS engine. Besides the typical parameters of FPR, OPR, and SLS-thrust, it also includes a parameter specific to hybrid-electric propulsion, the ‘assumed_HEPS_powertrain_efficiency‘. This new parameter declares which overall efficiency was used when the performance vector ‘el_energy_flow‘, the electrical equivalent to the fuel flow, was created.
Finally, it should be noted that the engine mass is not included in the exported <engine> node. This decision was deliberate, as the total mass of the HEPS engine does depend on the sizing of the electrical components. The predicted mass of the engine core is thus exported as part of the additional results, in the <results> node within the <toolspecific> node.
During the execution of the process to generate the hybrid-electric performance map, the tool produces

many more potentially useful parameters that do not have a defined location within the CPACS standard. Those parameters, as shown in Listing 6.2, include for example the assumed engine core specific power, which was used to estimate the engine core mass; or the effective scaling factors for the fan and engine core origin maps, relating how much the provided origin performance maps were scaled to provide the desired combined performance. Many of these additional parameters are not explicitly requested, but still provide important information that may be useful for a different design tool — as mentioned earlier, the predicted engine core mass is not exported in the <engine> node, but here in the <results> to be used in the component sizing design tool.
Another useful set of parameters included in the <results> node is the final performance at the originally specified design sizing points. These parameters provide the user with an overview, of how exactly the specified requirements are met, and additionally provides a clear outlook of the maximum available performance according to the generated HEPS performance map. The user can use this to, for example, compare the desired and maximum available performance at each design sizing point, and adjust the desired performance to achieve an overall optimised engine.

```
<?xml version="1.0" encoding="utf-8"?>
<cpacs>
  <toolspecific>
    <tool>
      <name>HEPSretro_Performance</name>
      <toolversion>0.9.1-dev</toolversion>
      <HEPSretro_Performance>
          ...
          ...
          ...
          <results>
            <timestamp>2020-10-28 13:31:25</timestamp>
            <Tool_version>0.9.1.1</Tool_version>
            <tool_runtime>00:08:07 +144ms</tool_runtime>
            <sizing_process_runtime>00:00:17 +878ms</sizing_process_runtime>
            <map_creation_process_runtime>00:07:45 +194ms
                                                  </map_creation_process_runtime>
            <electric_motor_max_shaft_power>1666277.463
                                                  </electric_motor_max_shaft_power>
            <engine_core_mass>1240.592</engine_core_mass>
            <engine_core_specific_power>14000.000</engine_core_specific_power>
            <effective_fan_scaling_factor>0.7554</effective_fan_scaling_factor>
            <effective_core_scaling_factor>0.6024</effective_core_scaling_factor>
            <fan_map_final_scaling_difference>0.002</fan_map_final_scaling_difference>
            <core_map_final_scaling_difference>0.001
                                                  </core_map_final_scaling_difference>
            <active_design_sizing_points>
              <fan_sizing_active_point>mid_climb</fan_sizing_active_point>
              <core_sizing_active_point>mid_climb</core_sizing_active_point>
            </active_design_sizing_points>
            <final_design_sizing_points>
              <design_sizing_point>
                <name>mid_climb</name>
                <altitude>7315.000</altitude>
                <mach_number>0.700</mach_number>
                <total_thrust>35000.000</total_thrust>
                <fan_thrust>29534.795</fan_thrust>
                <power_split>0.090</power_split>
                <design_point_power_split>0.088</design_point_power_split>
                <max_possible_power_split>0.092</max_possible_power_split>
                <gas_turbine_shaft_power>8320426.543</gas_turbine_shaft_power>
                <EM_shaft_power>822899.328</EM_shaft_power>
```

```
            <fan_shaft_power>9143325.872</fan_shaft_power>
            <offtake_power>0.000</offtake_power>
            <max_engine_shaft_power>8330814.891</max_engine_shaft_power>
            <min_engine_shaft_power>1610768.136</min_engine_shaft_power>
            <core_thrust>5471.114</core_thrust>
            <final_iteration_thrust_tolerance>0.0000
                                              </final_iteration_thrust_tolerance>
            <max_core_thrust>5484.991</max_core_thrust>
            <max_fan_shaft_power>9172331.011</max_fan_shaft_power>
            <max_fan_thrust>29603.763</max_fan_thrust>
            <max_total_thrust>35088.755</max_total_thrust>
            <min_fan_shaft_power>1541648.794</min_fan_shaft_power>
          </design_sizing_point>
          <design_sizing_point>
            <name>mid_cruise</name>
            ...
          </design_sizing_point>
            <name>takeoff</name>
            ...
          </design_sizing_point>
        </final_design_sizing_points>
      </results>
    </HEPSretro_Performance>
  </tool>
 </toolspecific>
</cpacs>
```

Listing 6.2: Overview of the example additional output stored in the <results> node, created for a parallel hybrid-electric propulsion system.

6.4. The ‘HEPSretro_Components‘ Tool

A second design tool was created to implement the component sizing methodology into an easily integrated design workflow block. It operates based on a supplied initial aircraft concept design (either conventional or a previous iteration of a HEPS concept); the corresponding prediction of the HEPS engine performance, ideally obtained from the ‘HEPSretro_Performance‘ tool; and the results of the simulation of a specified design mission. The simulation of the design mission is necessary to obtain a realistic estimate of the required amount of electric energy stored on-board in batteries, a characteristic that has a significant impact on the mass penalty incurred from the hybrid-electric propulsion system.
During execution, the tool will size every electric component required for a parallel hybrid-electric propulsion system, using physical characteristics as explained in Section 3.3. Each component will be considered as an individual entity, not combined per component type. This is most clearly reflected when observing the components’ implemented positioning methodology, especially the methods for the battery and transmission line components.
Due to the modular approach of using a dedicated class with unique underlying component models, the level of fidelity of the produced results is highly dependent on the specific implemented model. However, in the current state of the tool, all implemented component models are of a conceptual design level of detail. Most components are simply prescribed a specific power and efficiency performance parameter, which are then used to provide a simple point-mass representation of the component. It is however possible to refine the fidelity by integrating more sophisticated component models, although this will negatively influence the computation times and may prohibit the use as a conceptual design tool.
Analogous to the created HEPS engine performance prediction tool, the HEPS component sizing tool is called ‘HEPSretro_Components‘. It was written in Python 3.7 and uses two packages developed by the DLR: the TIXI library for the direct interaction with the CPACS file, and the TiGL geometry library [b] for any aircraft geometry

[b] The TiGL geometry library is in active development by the DLR and offers a complete 3-dimensional geometric representation of the aircraft concept based on the parametric descriptions stored in a CPACS file. It uses the OpenCASCADE CAD kernel to model the geometry with NURBS surfaces, and offers functions to export the generated geometry to common CAD formats and to perform geometric

dependent computations. Besides the DLR developed Tixi and TiGL packages, the tool requires the typical python packages 'numpy' and 'matplotlib'.

6.4.1. Component Sizing Methodology Implementation

Even more than the performance prediction tool, the 'HEPSretro_Components' design tool employs an OOP approach for the tool to size the individual propulsion components. Each electrical component is represented by a dedicated class, containing at least one model which determines the component characteristics. The currently implemented models follow the methodology described in Section 3.3, but depending on the specific needs, these models can be adapted, extended, and/or replaced as desired.

Besides the individual component classes, to tool contains classes for each relevant aspect of the sizing process: a dedicated class each to define the instance (relating to a specific physical object) and model (relating to the underlying component model) parameters; another class that contains the knowledge-rules used to determine the position of each component; a class that coordinates the sizing of the individual propulsion components; a class to represent the design data of the used reference aircraft design; and finally a specific class to contain all post-processing procedures. Additionally, the interface with input and output CPACS files is handled by another dedicated class respectively.

Overall Tool Process Flow

Figure 6.8 illustrates the overall process flow of the components sizing design tool. The procedure begins with the instantiation of the 'CPACS Import Object', which contains the interface with the input CPACS file. As stated in the figure's caption, the doubled-arrow connections indicate the progression through the process flow, conveying which process is to be executed next. Should the denoted output of a process block itself contain a process flow, this secondary procedure will be completed before the initial process flow progresses to the next block. The single-arrow connections represent the produced results/output of the corresponding process, in this case the process 'Instantiate CPACS Import Object' produces an instantiated object, before the overall procedure moves on to 'Instantiate Component Sizing Coordinator'. The dashed-arrow connecting the 'CPACS Import Object' and the 'Component Sizing Coordinator' object indicates that the import object is forwarded to the instantiated component sizing coordinator, such that the coordinator can call on the methods defined within the import object.

The instantiated 'Component Sizing Coordinator' object contains and executes all processes required to size the individual electrical components, as indicated by the dashed block on the right-hand side. After it's execution, it provides a set of 'Sized Electric Components'. Following the doubled-arrow connection, the tool instantiates the 'Post-Processing Object', which also obtains the current state of the sized electric components. During the post-processing, the electric components are finalised, and the resulting overall 'HEPS powertrain efficiency' is computed.

Again, the doubled-arrow connection proceeds to create the mass-breakdown plots, which are exported into a dedicated 'ReturnDirectory' within the tool's directory, illustrated in Figure 6.8 by surrounding the 'Mass Breakdown Plots' with a blue field. Finally, the overall process flow instantiates the 'CPACS Export Object', analogous to the 'CPACS Import Object'. This object obtains the previously produced results and, using the stored information on the CPACS standard, produces the 'CPACS Output File'.

As mentioned before, the dashed block on the right-hand side of Figure 6.8 depicts the process flow followed within the 'Component Sizing Coordinator'. Similarly to the general tool process flow, it contains a overarching progression of different processes, each producing dedicated outputs/objects that are forwarded internally. Following the secondary double-arrow progress, the sizing procedure begins with the instantiation of an object to allow access to the stored default settings, to be used where the user did not provide necessary input settings. In the next step, the coordinator instantiates the objects that contain the methods to define the instance and model settings for the various component classes. These two objects are forwarded the previously created 'Default Settings Interface' object, and the 'DefineInstanceSettings' object additionally instantiates an 'Component Positioning Object', from the class that contains the knowledge-rules of the individual component positioning. The final auxiliary object to be created relates to the 'Reference Aircraft Data', and contains methods to extract information on the overall aircraft concept, such as engine positions and fuselage cross-sectional area.

computations. Furthermore, it provides interfaces to many common programming languages as well as the TiGL Viewer, which enables the visualisation of the generated geometry. For more information, see `https://dlr-sc.github.io/tigl/`.

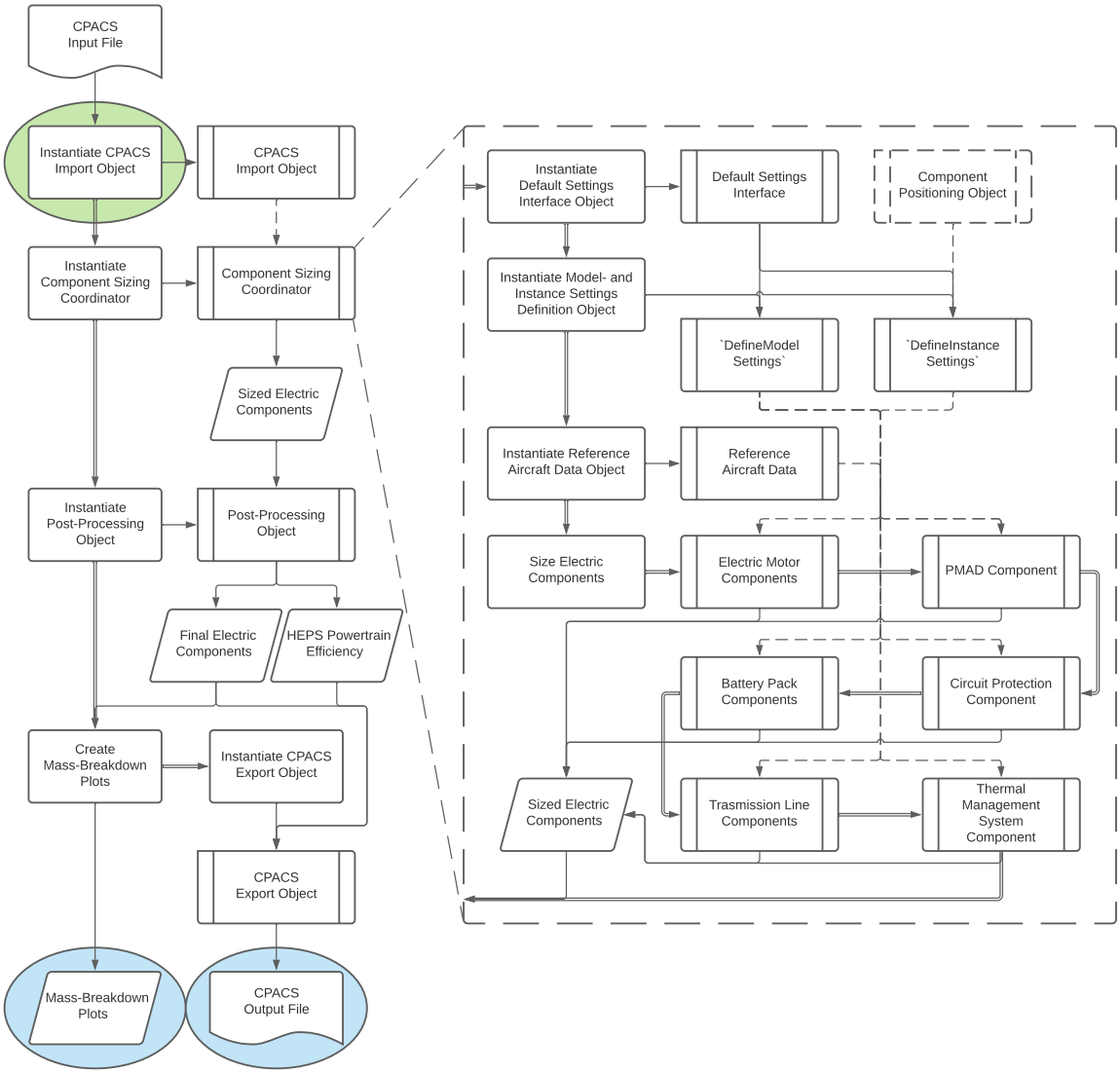

Figure 6.8: Overview of the main process flow within the ‘HEPSretro_Components‘ design tool used to size the electrical components of the hybrid-electric propulsion system. The main process flow is illustrated on the left-hand side, with the green background ellipse indicating the starting point and the blue background underlay denoting the final produced output/result. A doubled-arrow connections signifies a procession within the main procedure; a simple-arrow connection relates to a result/output produced by a process block; and a dashed-arrow connection refers to the internal forwarding of an instantiated object, allowing the process to call the methods defined within the specific object. Finally, the dashed block on the right-hand side illustrates the process flow contained within the ‘Component Sizing Coordinator‘ block.

With all auxiliary objects available, the sizing of the individual electric components begins, following the order as indicated by the double-arrow connections. For each component type, a specific process flow required for the sizing process, as illustrated in Figures 6.9 to 6.11. The procedure shown in these figures is executed for each individual component of the shown component types, as indicated by the process starting with a unique component identifier. The individual components are represented by a dedicated object, which are stored stored together and provide the final output of the ‘Component Sizing Coordinator‘.

Individual Component Sizing Process Flows

The process flow for the typical sizing procedure of electric components is illustrated in Figure 6.9. This procedure is used in the sizing of the electric motor, PMAD, circuit protection, and thermal management system components. It begins with the ‘Component Sizing Coordinator‘ defining the ‘Component uID‘, a unique identifier used both within the design tool and the created output CPACS file. For all sizing cases, the procedure distinguishes three specific aspects: the definition of the ‘Component Model Settings‘, the determi-

nation of the ‘Component Position Coordinates‘, and the subsequent definition of the ‘Component Instance Settings‘. While particular component types, such as the battery packs and transmission lines, may deviate from the clear separation of these three aspects as shown in Figure 6.9, they can still be clearly distinguished. Additionally, every component sizing process flow contains a link to the CPACS interface object. This necessary connection enables the sizing procedure to access the user inputs defined in the input file, used to determine the applicable component models, as well as specific performance parameters.

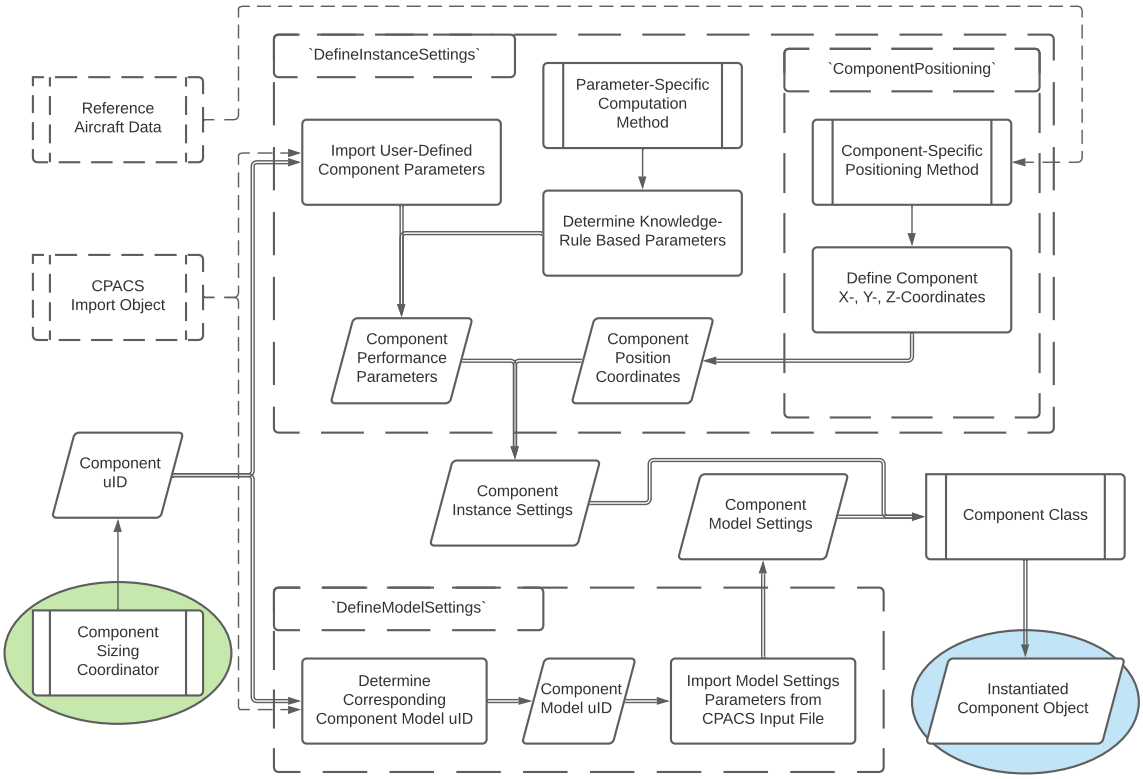

Figure 6.9: The general process flow used for the sizing of the electric components, corresponding to the individual component blocks shown in the right-hand side process flow of Figure 6.8, applicable to the sizing of the electric motors, the PMAD, the circuit protection system, and the Thermal Management System. Each dashed block represents a dedicated class which contains the shown processes, with the ‘ComponentPositioning‘ class being called from within the ‘DefineInstanceSettings‘ class. The green and blue background ellipses again signify the starting point and produced output respectively.

The inputs provided to each component class are separated into parameters containing information for the component model, and those containing data for the physical object, represented by a dedicated object — or ‘Instance‘ — within the tool. Model specific parameters are mostly shared between all objects of the same component type (e.g. the specific output power of the electric motors, the efficiency of the transmission lines, etc.), but it is possible to specify different models for individual component objects. For example, it is possible to assign different values to the specific power and energy density parameters of the battery model, allowing the sizing of specific battery components that store large amounts of electric energy for cruise, while simultaneously sizing battery components with high specific power outputs for the large power requirements during takeoff. Parameters specific to the physical object can be seen as the input parameters for the component models, creating the connection between the components and the aircraft concept. They contain information on the desired/required performance of the component, as well as the intended position on the aircraft.

As is shown in Figure 6.9, the defining of the model settings is typically a simple matter of determining the appropriate component model identifier and then importing the corresponding model parameters from the input CPACS file. The instance settings on the other hand are less direct, and are simultaneously obtained from three sources: supplied by the user in the input CPACS file, performance parameters determined via knowledge-based rules from other components, and the position coordinates determined via another set of knowledge-based rules. This is indicated in the figure via three double-arrow connections merging into a

single ‘Component Instance Settings‘ data set.
For the sizing layout of a typical electrical propulsion component, the methods used to determine the component’s position is entirely de-coupled from the overall sizing procedure. The position coordinates are determined relative to the reference aircraft data, usually coinciding with existing components such as the installed engines or the power electronics bay.
Upon obtaining the instance and model setting parameters, both are simply supplied to the component class, which is then creating an ‘Instantiated Component Object‘. This instantiated object contains all the information of the electric component that will be exported to the output CPACS file.

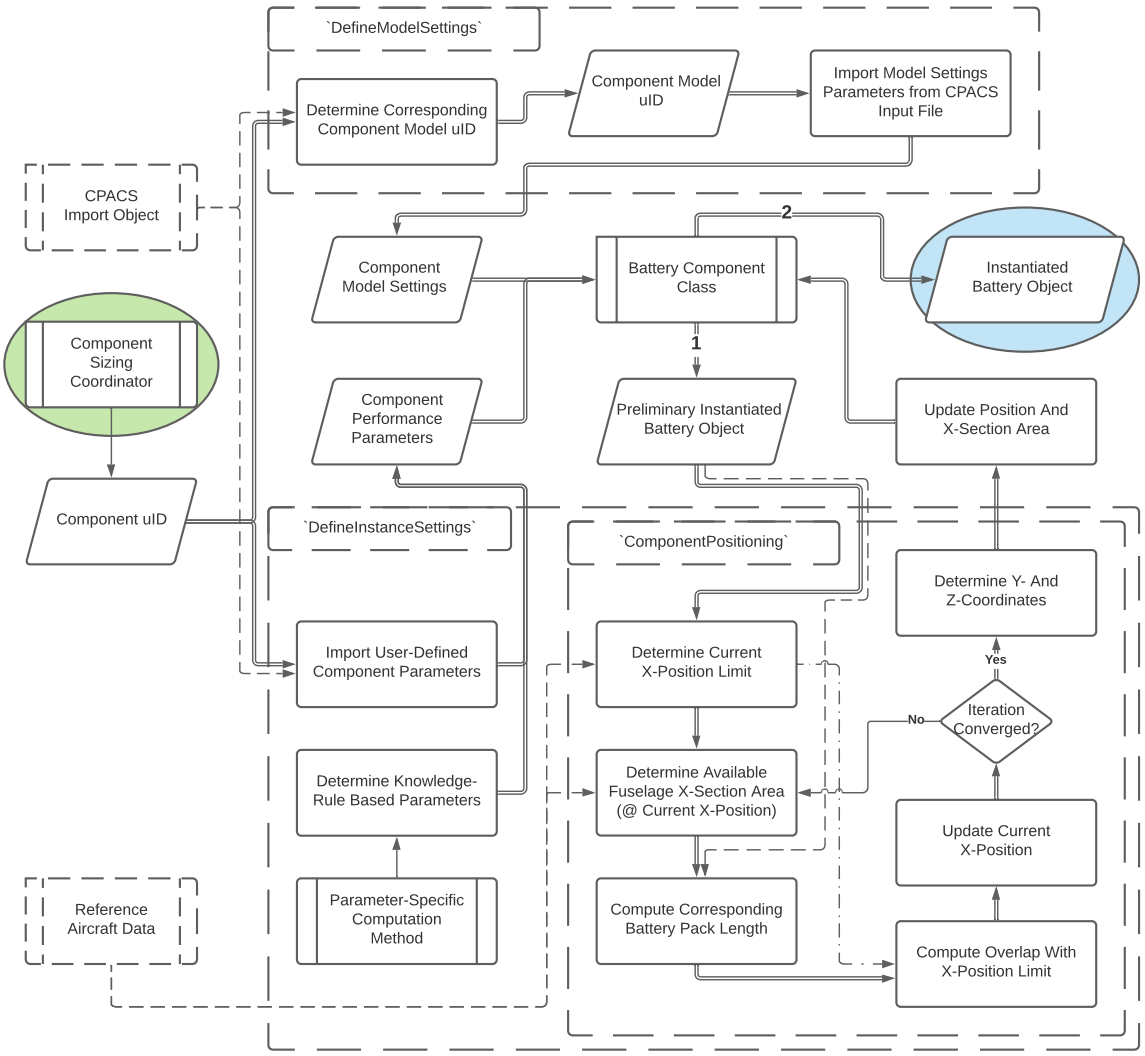

Figure 6.10: The process flow used to size each battery component, illustrating the significant deviation from the general procedure shown in Figure 6.9 and using the same means to indicate starting point and produced output. This component required a special implementation because the sizing and the positioning are coupled, with the assigned position limiting the available outer dimensions. The component class is thus instantiating two objects per component, a preliminary object to be used for the positioning calculations, and a final object to be exported.

The electric propulsion component whose sizing procedure deviates most drastically from the general process as explained above is the battery pack. As shown in Figure 6.10, the determination of the position coordinates is no longer de-coupled, but rather closely integrated in to component object creation. The definition of the model and performance parameters follows the same routine as for the typical components, but due to the implemented positioning methodology a preliminary battery object has to be instantiated to be used in the position coordinate determination process.

The process flow presented within the ‘Component Positioning‘ class method is a direct implementation of the methodology devised in Section 3.3.2. It begins with the determination of the current x-position limit for the battery pack, dependent on the relative location of the battery — forward or aft within the fuselage — and any previously sized battery components. The actual computation of the CoG coordinates are governed by the available cross-sectional area available for the battery pack at the current x-position and the corresponding required length along the x-axis of the battery pack. The procedure is than positioning the next iteration of the CoG x-position such, that the outer border of the battery pack coincides with the determined position limit, accounting for any user-defined offset between individual battery packs. Once the position iteration is converged, the updated coordinate data is forwarded to the battery component class and the final battery object is instantiated.

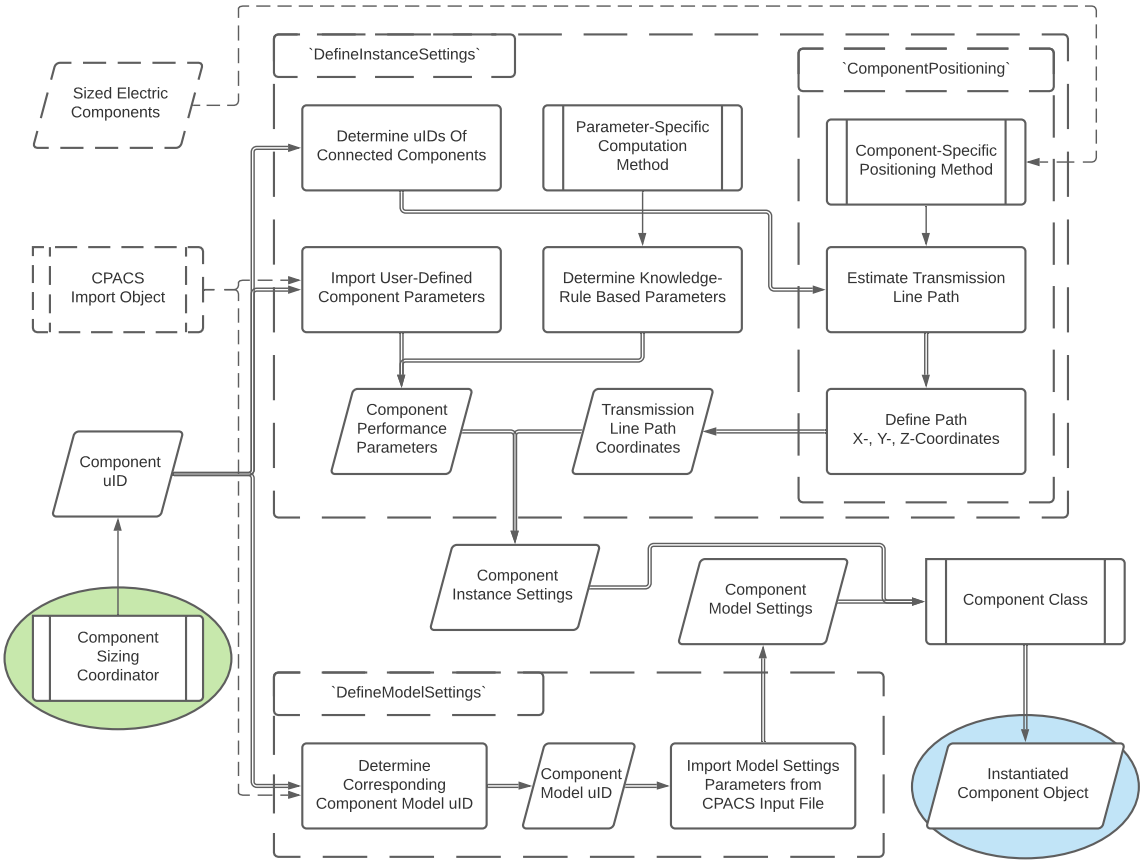

Figure 6.11: Process flow used to size the individual power transmission line components, illustrating the difference to general process shown in Figure 6.9 due to the transmission lines not being sized as a point mass. Again, the green and blue background underlays indicate the starting point and produced output of the procedure.

In contrast, the sizing procedure of the power transmission line components differs only marginally from the standard case. As depicted in Figure 6.11, the only difference to the sizing process is the addition of determining the unique identifiers of the components the specific transmission line is connecting. These component uIDs are required by the positioning method, as contrary to all other components, it determines an estimation of the path instead of the coordinates of a point mass.

It should be stressed, that the created component object of each transmission line still features an equivalent mass and CoG position coordinates, to be used to account for the mass and balance impact on the overall aircraft design. However, the methods used to compute these parameters are part of the transmission line component class. Indeed, the method implemented to compute the mass of the transmission line object requires the estimated path as input. The coordinates corresponding to the equivalent point mass are computed within the component class as discussed in Section 3.3.3.

6.4.2. Available Tool Settings Parameters

Analogous to the performance sizing tool, the component sizing tool ‘HEPS_Components‘ was designed with a substantial set of user settings. Once again, every parameter was implemented such, that it can be set by the user via the <toolspecific> node of the input CPACS file. The structure of the <toolspecific> node again follows the CPACS 3.2 standard, with all parameters stored in a sub-node corresponding to one of the three settings groups: "general_settings", "automatic_settings", or "model_settings". Subsequently, the available input parameters of each group of settings is briefly discussed and presented in the corresponding Tables 6.9 to 6.11.

General Settings:

The general settings contain the parameters to control the execution of the tool. This includes direct changes to the running of the tool, such as a definition of the input and output CPACS files, the desired decimal precision in the generated outputs, as well as switches for the automatic sizing and the generation of mass breakdown plots. Also included are the options to set the unit used for the energy requirements in the input CPACS file (supporting the official SI unit of J or the otherwise common unit of Wh) and to declare the assumed length in x-direction of the power electronics bay. Due to the underlying assumptions used for the positioning of the aft battery packs, the length of the power electronics bay influences the position of the first aft battery pack. All other parameters within the <general_settings> node relate to the CPACS internal identifiers of aircraft elements used during sizing computations. An overview of all parameters, including a brief description is provided in Table 6.9.

Table 6.9: Overview of available general settings parameters for the component sizing tool ‘HEPSretro_Components‘, governing tool execution and access to defined aircraft elements in the CPACS file.

Parameter Name	Example Entry	Description
input_filename	toolInput	Name of the CPACS file that contains the input data.
output_filename	example_toolOutput	Name that will be given to the created output CPACS file (contains all information from the input CPCAS file).
output_decimal_precision	3	Desired decimal precision for the vales added in the output CPACS file.
create_mass_breakdown _plots [a]	true	Boolean switch; triggers generation of mass breakdown plots.
mass_breakdown_file_type	png	File type of the generated mass breakdown plots.
automatic_component _sizing [a]	true	Boolean switch; toggles whether the tool automatically sizes the components or uses the information provided in the <components> node.
input_energy_unit	Joule	the unit for energy used in the input CPACS file (currently distinguishes "Joule"/"J" and "Watt-hour"/"Wh").
power_electronics_bay _x_length [a]	2.0	Sets the length in x-direction in meters inside the fuselage that is reserved for the power electronics bay.

Continued on next page

Table 6.9: (cont.) Overview of available general settings parameters for the component sizing tool 'HEPSretro_Components', governing tool execution and access to defined aircraft elements in the CPACS file.

Parameter Name	Example Entry	Description
aircraft_model_uID	AircraftModel[b]	The uID of the aircraft model under '/cpacs/vehicles/aircraft/model'. Must be given, otherwise TiGL will raise an error and be unable to open the CPACS file!
fuselage_uID	fuselage[b]	The uID of the part within the <fuselages><fuselage> node that refers to the actual aircraft fuselage.
main_wing _componentSegment_uID[a]	wing_Cseg[b]	The uID of the 'componentSegment' of the main wing.
spars _componentSegment_uID[a]	wing_Cseg[b]	The uID of the 'componentSegment' that contains the information of the spars inside the fuselage.
front_sparSegment_uID	wing_Spar_FS[b]	The uID of the 'sparSegment' that corresponds to the front spar.
rear_sparSegment_uID	wing_Spar_RS[b]	The uID of the 'sparSegment' that corresponds to the rear spar.

[a] Parameter is one continuous string, but was separated to fit within the available space in the table.
[b] Assigned uID depends on the settings/programming of other design tools in the conceptual design workflow.

Automatic Settings:
The automatic settings shown in Table 6.10 contain all parameters relevant for the automated sizing of the electric components. These parameters differ for the various components but can generally be separated into parameters describing performance of the electric component as a physical object and parameters that denote which underlying component model shall be used during the process.

Table 6.10: Overview of available parameter in the component sizing tool 'HEPSretro_Components' for the automatic sizing procedure. Includes individual component performance requirements and assigns desired underlying models.

Parameter Name	Example Entry	Description
engine_uIDs	engine12;engine34	Semi-colon separated list of engine uIDs for all engines to be fitted with an electric motor. In case of using symmetry conditions, it is assumed that the provided 'engine_uIDs' are in order from inboard → outboard.
engine_is_symmetric	true;true	Semi-colon separated list corresponding to the order of <engine_uIDs>. States which of the specified engine_uIDs uses the 'symmetry' attribute to represent engines on each side of the aircraft.

Continued on next page

Table 6.10: (cont.) Overview of available parameter in the component sizing tool ‘HEPSretro_Components‘ for the automatic sizing procedure. Includes individual component performance requirements and assigns desired underlying models.

Parameter Name	Example Entry	Description
engine_EM_model_uIDs	EM_model_main; EM_model_main[a]	Semi-colon separated list declaring which electric motor model shall be used during the sizing, corresponding to each engine defined in ‘engine_uIDs‘.
system_voltage_level	1000.0 V	Defines the voltage level used by the system for power transmission (defaults to using the breakdown voltage of 327 V DC according to Paschen's law).
PMAD_model_uID	PMAD_model	Declares which PMAD model defined under <model_settings> shall be used for the sizing.
CircuitProtection _model_uID [a]	circuit_protection_model	Declares which circuit protection model defined under <model_settings> shall be used for the sizing.
TMS_model_uID	TMS_model	Declares which TMS model defined under <model_settings> shall be used for the sizing.
TransmissionLine _model_uID [a]	TL_model_simple _normalconducting [a]	Declares which transmission line model defined under <model_settings> shall be used for the sizing.
TransmissionLine _redundancy [a]	1	Defines the desired redundancy factor (integer) for the sizing of the transmission lines.
MainBattery_model_uID	battery_model_energy	Declares which battery model defined under <model_settings> shall be used for the sizing of the main battery packs.
SecondaryBattery _model_uID [a]	battery_model_power	Declares which battery model defined under <model_settings> shall be used for the sizing of the secondary (high power) battery packs.
MainBatteries _available_energy [a]	9,599,999,760 J	Declares the required amount of electrical energy made available to the electric propulsion system from the main battery packs.
MainBatteries _max_output_power [a]	3,500,000 W	Declares the intended maximum total electric output power drawn from the main batteries.
SecondaryBatteries _available_energy [a]	1,800,000,000 J	Optional, only when using secondary battery packs. Declares the required amount of electrical energy made available to the propulsion system from the secondary battery packs.

Continued on next page

Table 6.10: (cont.) Overview of available parameter in the component sizing tool 'HEPSretro_Components' for the automatic sizing procedure. Includes individual component performance requirements and assigns desired underlying models.

Parameter Name	Example Entry	Description
battery_fuselage_area_ratio	0.24	Defines the ratio of how much of the cross-sectional area of the fuselage is available for battery pack storage.
mass_scaling_factors		
electric_motor	1.1 [b]	Desired mass scaling factor for estimated electric motor mass.
PMAD	0.95 [b]	Desired mass scaling factor for estimated PMAD mass.
circuit_protection	1.0 [b]	Desired mass scaling factor for estimated circuit protection mass.
battery_pack	1.0 [b]	Desired mass scaling factor for estimated battery pack mass.
transmission_line	1.2 [b]	Desired mass scaling factor for estimated transmission line mass.
TMS	0.85 [b]	Desired mass scaling factor for estimated TMS mass.

[a] Parameter is one continuous string, but was separated to fit within the available space in the table.
[b] Example entries for mass scaling factors do not constitute suggested values. They were chosen to illustrate that a calibration of individual component types is possible.

The performance specific parameters include the maximum encountered voltage or power values, or how much electric power has to be made available. Also included are parameters for specific sizing methods such as the transmission line redundancy factor, the fraction of the fuselage area available for battery storage, as well as any potentially desired mass scaling factors.
In relation to the underlying models, for each component type a parameter dictating the desired model identifier is declared, relating to the models as defined according to Table 6.11, allowing for different models to be used during the sizing of individual battery packs and electric motors. In case of the electric motors, a dedicated parameter provides a list of all engines to be fitted with an electric motor, allowing for aircraft concepts to be designed with both conventional and hybrid-electric engines installed simultaneously. Subsequently, the parameter defining the electric motor models to be used provides another list of electric motor model identifiers, corresponding to the previous list of engines to be fitted with an electric motor. This allows the tool to size each engine with a different type of electric motor installed. For the batteries, two parameters allow a definition of the desired component model to be used for the main and secondary batteries respectively.

Model Settings:
The node of the model settings contain all the information about the various underlying electric component models. For each model type, a sub-node of the <model_settings> node gathers an arbitrary number of component models. Depending on the implementation and any potential future changes or additions, the various models for the same component type can contain different parameters. Should, for example, a more detailed cable model be implemented for the transmission line sizing process, two transmission line models could be defined, containing the parameters required for their respective cable models.
Any model defined within the <model_settings> node will only be used, should its unique identifier (uID) be assigned to an electric component type in the <automatic_settings>. Due to tool limitations, only the electric motor sizing allows the use of different component models for the same component type. A comprehensive overview of all available model settings for the currently implemented component models is supplied in Table 6.11.

Table 6.11: Overview of all parameters available in the component sizing tool ‘HEPSretro_Components‘ to define the individual component models. For each component type, an arbitrary number of possible model settings can be define in that types sub-node. Only models whose uID has been assigned to a component in the <automatic_settings> will be used.

Parameter Name	Example Entry	Description
	battery_model uID="battery_model_energy"[a]	
name	battery_model_energy	The name given to the model by the user (not used for identification).
model_energy_unit	joule	Specifies the energy unit used within this specific battery model, distinguishes between J and Wh.
max_pack _capacity_total[b]	1,800,000,000 J	Declares the maximum capacity of a single battery pack according to this battery model. Provided in unit according to ‘model_energy_unit‘ (equiv. 500 kWh).
C_rate_max_power	2	Declares the C-rate for which the provided specific energy and specific power are achieved, essentially maximum allowed C-rate.
specific_energy	$1{,}683{,}000\,\mathrm{J\cdot kg^{-1}}$	Declares the specific energy of the battery at pack level (equiv. $467.5\,\mathrm{Wh\cdot kg^{-1}}$).
specific_power	$748.0\,\mathrm{W\cdot kg^{-1}}$	Optional input, internally computed from C-rate, specific power, and maximum DoD; Specifies the specific power of the battery at pack level.
energy_density	$4{,}342{,}140{,}000\,\mathrm{J\cdot m^{-3}}$	Declares the volumetric energy density of the battery pack. Provided according to energy unit as defined by ‘model_energy_unit‘.
max_discharge	0.8	Declares the maximum depth of discharge allowed for optimal cycle life. A factor of 0.8 corresponds to discharging up to 80% of capacity.
efficiency	0.97	Declares the assumed constant efficiency of the battery pack.
	electric_motor_model uID="EM_model_main"[a]	
name	EM_model_main	The name given to the model by the user (not used for identification).
efficiency	0.97	Declares the overall (assumed constant) efficiency of the motor.
specific_power	$9000.0\,\mathrm{W\cdot kg^{-1}}$	Declares the overall specific mechanical output power. Used as main design variable to allow representation of any type of electric motor.

Continued on next page

Table 6.11: (cont.) Overview of all parameters available in the component sizing tool 'HEPSretro_Components' to define the individual component models. For each component type, an arbitrary number of possible model settings can be define in that types sub-node. Only models whose uID has been assigned to a component in the <automatic_settings> will be used.

Parameter Name	Example Entry	Description
transmission_line_model uID="TL_model_simple_normalconducting"[a]		
name	TL_model_simple_normalconducting[b]	The name given to the model by the user (not used for identification).
installation_mass_penalty_factor[b]	0.3	Defines the mass penalty (fraction of total transmission line mass) for installation of the transmission line. Applied to the cable mass determined by the underlying cable model.
HMS_mass_penalty_factor[b]	0.05	Defines the mass penalty (fraction of total transmission line mass) for the health monitoring system of the transmission line. Applied to the cable mass determined by the underlying cable model.
cable_model	simple_normal_conducting[b]	Specifies the cable model to be used when sizing the transmission lines.
max_allowed_cable_current[b]	360.0 A	Required input parameter of the 'simple_normal_conducting' model: Declares the maximum current allowed per cable.
cable_linear_density	1.0 $kg \cdot m^{-1}$	Required input parameter of the 'simple_normal_conducting' model: Declares the linear density of each cable.
specific_losses	80.0 $W \cdot m^{-1}$	Defines the amount of power loss per length of cable.
PMAD_model uID="PMAD_model"[a]		
name	power_management_and_distribution_model[b]	The name given to the model by the user (not used for identification).
system_voltage_type	DC	Defines the desired voltage type as set by user. Sets the sized distribution network operates on AC or DC electricity.
specific_power	16,000.0 $W \cdot kg^{-1}$	Declares the effective specific power of the PMAD component.
efficiency	0.988	Declares the overall PMAD efficiency.
integrated_circuit_protection[b]	false	Boolean switch; toggles whether the defined PMAD component includes an integrated circuit protection system in the declared specific power and efficiency.
circuit_protection_model uID="circuit_protection_model"[a]		

Continued on next page

Table 6.11: (cont.) Overview of all parameters available in the component sizing tool ‘HEPSretro_Components‘ to define the individual component models. For each component type, an arbitrary number of possible model settings can be define in that types sub-node. Only models whose uID has been assigned to a component in the <automatic_settings> will be used.

Parameter Name	Example Entry	Description
name	default_circuit _protection_model[b]	The name given to the model by the user (not used for identification).
efficiency	0.995	Declares the efficiency of the circuit protection component.
specific_power	200,000.0 $W \cdot kg^{-1}$	Declares the effective specific electrical power of the circuit protection component.
	TMS_model uID="TMS_model"[a]	
name	thermal_management _system_model[b]	The name given to the model by the user (not used for identification).
specific_power	36,600.0 $W \cdot kg^{-1}$	Due to complexity and dependence on detailed analysis of other components, the TMS sizing is strongly limited. Only an effective specific power, relating the amount of propulsion system electric power that can be handled per unit mass of TMS.

[a] The uID used for identification in CPACS is stored as an attribute of the respective node, not as a field within the node itself.
[b] Parameter is one continuous string, but was separated to fit within the available space in the table.

6.4.3. Provided Default Parameters

Included in the sizing tool are a set of default parameters, which the tool will load in case the user has not provided the required input data. These default parameters include design decisions such as the electrical powertrain efficiency assumed in the previous engine performance prediction, assumptions for the placement of the battery packs, and default component models for the implemented electrical components. All data relating to component model parameters reflects typical values chosen in literature for the design of a parallel hybrid-electric aircraft concept. A full overview of all provided default parameters is given in Table 6.12.

Table 6.12: Overview of all default parameters provided by the ‘HEPSretro_Components‘ sizing tool.

Parameter Name	Default Value	Description/Origin
	default automatic settings	
HEPS_powertrain_efficiency[a]	0.85	Estimated overall efficiency of electric powertrain used in preceding performance prediction, used for estimation of maximum distribution power in PMAD and circuit protection sizing.

Continued on next page

Table 6.12: (cont.) Overview of all default parameters provided by the 'HEPSretro_Components' sizing tool.

Parameter Name	Default Value	Description/Origin
battery_fuselage _area_ratio[a]	0.238	User input; estimation of available cargo space inside fuselage due to lack of detailed cabin modelling during conceptual design phase.
power_electronics_bay _x_length[a]	2.0 m	User input; accounts for increase in size of power electronics compared to current transport aircraft due to significant increase in electric power levels from propulsion system.
battery_spacing	0.1 m	User input; defines distance between individual battery packs for safety and other installations.
	default electric motor model settings	
efficiency	0.95	Electric motor efficiency assumed to represent chosen electric motor design.
specific_power	9000.0 $W \cdot kg^{-1}$	Electric motor specific power assumed to represent chosen electric motor design.
	default battery pack model settings[b]	
energy_density	600,000.0 $Wh \cdot m^{-3}$	Energy density at pack level assumed to represent chosen battery design.
specific_energy	800.0 $Wh \cdot kg^{-1}$	Specific energy at pack level assumed to represent chosen battery design.
specific_power	2000.0 $W \cdot kg^{-1}$	Specific power at pack level assumed to represent chosen battery design.
max_discharge	0.8	Maximum allowed depth of discharge of battery to prevent life cycle degradation for chosen design.
efficiency	0.95	Battery efficiency assumed to represent chosen battery design.
	default PMAD model settings[c]	
efficiency	0.988	PMAD efficiency assumed to represent resultant efficiency of electric components regulating the power distribution.
specific_power	16,000.0 $W \cdot kg^{-1}$	Specific power assumed to represent the resultant power performance of electric components regulating the power distribution.

Continued on next page

Table 6.12: (cont.) Overview of all default parameters provided by the ‘HEPSretro_Components‘ sizing tool.

Parameter Name	Default Value	Description/Origin
distribution _voltage_type[a]	"DC"	Assumed type of power distribution chosen for aircraft concept.
	default circuit protection model settings	
efficiency	0.995	Circuit protection component efficiency assumed to represent chosen component design.
specific_power	200,000.0 $W \cdot kg^{-1}$	Specific power assumed to represent the performance of the chosen circuit protection design.
	default transmission line model settings	
cable_model	"simple_normal_conducting"	Defaults the sizing of the transmission lines to use the simple normal-conducting cables.
installation_mass _penalty_factor[a]	0.3	Mass factor assumed to represent the percentage of the final mass due to installation.
HMS_mass _penalty_factor[a]	0.05	Mass factor assumed to represent the percent of the final mass due to health monitoring system.
max_allowed _cable_current[a]	360.0 A	The maximum amount of current allowed per cable.
cable_linear_density	1.0 $kg \cdot m^{-1}$	The assumed linear density of the cable.
specific_losses	80.0 $W \cdot m^{-1}$	The assumed amount of power loss in the cables.
	default TMS model settings	
specific_power	36,600.0 $W \cdot kg^{-1}$	The assumed specific power, relating distributed electric power to the TMS mass, assumed to represent the thermal management system *for the electric propulsion system components only*.

[a] Parameter is one continuous string, but was separated to fit within the available space in the table.
[b] Default battery model settings correspond to previous implementation using explicit specific energy *and* specific power, instead of specific energy and max. C-rate. The max. C-rate is derived from the supplied specific energy and specific power.
[c] Parameter ‘integrated_circuit_protection‘ is optional and set to false per default.

6.4.4. Generated Output and Results

Finally, this subsection provides a discussion of the generated results and the structure of the tool’s output. Due to the official CPACS 3.2 definition not including a standard notation for electric components, the produced outputs of the ‘HEPSretro_Components‘ sizing tool are gathered into a unified <results> node within the tool’s node in the <toolspecific> node of the CPACS file. A stylised representation of the structure within the CPACS file is presented in Listing 6.3. The <results> node is appended within the tool’s <toolspecific> node following the settings nodes supplied in the CPACS input file, and the provided results can be separated into three groups. The first group contains the timestamp (providing the date as well as the time) to record when the output was produced, the final efficiency, and total mass of the entire electric propulsion system as

a single unit. The second group contains information about the sized battery architectures, the connection of individual battery packs and their resulting combined performance. In the provided example, only one type of battery was used during sizing. Lastly, the third group contains the information for each sized electric component. The individual components are grouped by component type, with the power management system, circuit protection system, and thermal management system being currently limited to only one component.

```
<?xml version="1.0" encoding="utf-8"?>
<cpacs>
  <toolspecific>
    <tool>
      <HEPSretro_Components>
        <general_settings>
        <automatic_settings>
        <model_settings>
        <results>
          <timestamp>XXXX-XX-XX XX:XX:XX</timestamp>
          <overall_powertrain_efficiency>X.XXX</overall_powertrain_efficiency>
          <HEPS_components_combined_mass>XXXX.X</HEPS_components_combined_mass>
          <mainBatteryArchitecture>
            <num_packs_parallel>X</num_packs_parallel>
            ...
            <total_usable_energy_available_Wh>XXXXXXX.X</total_usable_energy_available_Wh>
          </mainBatteryArchitecture>
          <power_management_systems>
            <PMAD> ..... </PMAD>
          <circuit_protection_systems>
            <circuit_protection_system> ..... </circuit_protection_system>
          <thermal_management_systems>
            <thermal_management_system> ..... </thermal_management_system>
          <electric_motors>
            <electric_motor> ..... </electric_motor>
            <electric_motor> ..... </electric_motor>
          <battery_packs>
            <battery> ..... </battery>
            ...
            <battery> ..... </battery>
          <transmission_lines>
            <transmission_line> ..... </transmission_line>
            ...
            <transmission_line> ..... </transmission_line>
        </results>
      </HEPSretro_Components>
    </tool>
  </toolspecific>
<cpacs>
```

Listing 6.3: Stylised overview of the layout of the <results> node in the produced output of the 'HEPSretro_Components' sizing tool.

While Listing 6.3 provides a good overview of the layout of the <results> node, the actual parameters included in the output are presented in Table 6.13. For the individual components, the parameters are sorted by component type, with parameters shared by all components summarised together. Each individual component node will contain a node about that component's <dimensions>, <mass_data>, <transformation>, and <design_data>. In most cases, the <dimensions> node will be empty, as the current state of the sizing methodology does not include methods to estimate the size of any components other than the battery packs and transmission lines. The <mass_data> node contains both the estimated mass of the component as well as the applied scaling factor. This factor is applied to the mass obtained from the implemented estimation method and can be used for calibration. Due to the standard notation of CPACS, the position of each component has to be defined as a translation from a fixed point of origin. Witin CPACS, each translation is considered

a transformation operation, thus the position of each component’s centre of gravity is defined in the <transformation> node as illustrated in Listing 6.4. Finally, the <design_data> node contains all the information pertaining to design choices or the derived performance characteristics of the component. This output is included to provide the user with a quick overview of performance capabilities, as it is possible that the sized component exceeds the requirement supplied by the user.

```
<?xml version="1.0" encoding="utf-8"?>
<cpacs>
  ...
  ...
  ...
  <results>
    <component_type>
      <component>
        ...
        <transformation>
          <translation refType="absGlobal">
            <x>computed x-position</x>
            <y>computed y-position</y>
            <z>computed z-position</z>
          </translation>
        </transformation>
      </component>
    </component_type>
    ...
  </results>
  ...
</cpacs>
```

Listing 6.4: Stylised overview of how a sized electric component’s centre of gravity position is stored in the output CPACS file.

It should be noted that, as apparent from the example values supplied in Table 6.13, the sizing tool performs it’s calculations using exact values. While it would make sense from a design perspective to, for example, round the occurring power levels to full thousands (i.e. use Kilowatt instead of Watt) in the output file, it was decided to provide the output as close to the actually used value to prevent the incorrect assumption that the computations were done on the rounded values.

Table 6.13: Overview of the example results output generated by the ‘HEPSretro_Components‘ sizing tool.

Output Parameter Name	Determined Value	Description
timestamp	2021-12-05 14:54:18	The timestamp showing when the tool was executed.
overall_powertrain _efficiency[a]	0.924	The newly computed overall efficiency of the electrical propulsion system, product of relevant component efficiencies.
HEPS_components _combined_mass[a]	6694.0	The combined total mass of the electrical propulsion system, sum of all sized electrical components, in kg.
mainBatteryArchitecture		

Continued on next page

Table 6.13: (cont.) Overview of the example results output generated by the 'HEPSretro_Components' sizing tool.

Output Parameter Name	Determined Value	Description
num_packs_parallel	7	The number of battery packs connected in parallel to abide the required max. power demand.
num_sets_sequence	2	The number of sets of battery packs in parallel, such that sufficient energy is stored while being able to provide the max. power at any point.
C_rate_max_power	4.34	The determined maximum C-rate to discharge the batteries when the max. power is drawn.
max_power_draw _design[a]	3,653,808.8	The maximum amount of total electric power drawn from all packs in parallel when discharging at the determined optimum max. C-rate (corresponds to max. power demand of HEPS), in W.
max_power_draw _available[a]	6,734,448.0	The maximum amount of total electrical power available if all battery packs are discharged at the maximum C-rate according to the underlying model, in W. Can be used to check choice of model.
total_usable_energy _required_Wh[a]	1,497,000.0	The total amount of usable energy required according to the input file, in Wh.
total_usable_energy _available_Wh[a]	1,683,612.0	The total amount of usable energy available according to the sized battery packs, in Wh.
	All Sized Electric Components	
parentUID	[*uID of parent*]	The CPACS uID of the parent of the sized component.
mass_data		
mass	[*computed component mass*]	The mass of the respective component as determined according to the implemented sizing methods, provided in kg.
applied_scaling_factor	[*applied factor*]	The user supplied mass scaling factor applied to the mass estimated via the implemented methodology.
transformation/translation[b]		
x	[*component x-coordinate*]	The x-position (relative to the global CPACS coordinate system) of the centre of gravity of the respective component.
y	[*component y-coordinate*]	The y-position (relative to the global CPACS coordinate system) of the centre of gravity of the respective component.

Continued on next page

Table 6.13: (cont.) Overview of the example results output generated by the 'HEPSretro_Components' sizing tool.

Output Parameter Name	Determined Value	Description
z	[*component z-coordinate*]	The z-position (relative to the global CPACS coordinate system) of the centre of gravity of the respective component.
The following content is specific to individual component types.		
PMAD Component		
design_data		
max_distribution _power	3,653,808.8	The maximum amount of electric power distributed by the PMAD component as determined by the tool, in W.
system_voltage_type	DC	The selected type of the electric distribution network.
system_voltage_level	1000.0	The selected level of voltage in the distribution network, in V.
efficiency	0.988	The effective efficiency of the PMAD component used during sizing.
specific_power	16,000.0	The specific power of the PMAD component used during sizing, in $W \cdot kg^{-1}$.
integrated _circuit_protection[a]	false	Switch whether the selected PMAD design included the circuit protection.
Circuit Protection System Component		
design_data		
max_system_power	3,653,808.8	The maximum amount of electric power which the circuit protection system must be able to protect, in W.
efficiency	0.988	The effective efficiency of the circuit protection system used during sizing.
specific_power	200,000.0	The specific power of the circuit protection system component used during sizing, in $W \cdot kg^{-1}$
Thermal Management System Component		
design_data		
max_electric_power	3,653,808.8	The maximum amount of electric power in the propulsion system for which the TMS must handle the produced heat, in W.
specific_power	36,600.0	The specific power (relating *electric* power in the propulsion system to TMS mass) of the TMS used during sizing, in $W \cdot kg^{-1}$.
Electric Motor Component		

Continued on next page

Table 6.13: (cont.) Overview of the example results output generated by the 'HEPSretro_Components' sizing tool.

Output Parameter Name	Determined Value	Description
design_data		
max_output_power	1,637,417.9	The maximum mechanical output power the electric motor component was sized to deliver, in W.
max_elec_input_power	1,688,059.7	The maximum electrical input power the electric motor component requires to deliver the demanded maximum mechanical output power, in W.
efficiency	0.97	The effective efficiency of the electric motor used during sizing.
specific_power	9000.0	The specific mechanical power of the electric motor component used during sizing, in $W \cdot kg^{-1}$
	Battery Pack Component	
dimensions		
length_x	0.05[c]	The length in x-direction (along fuselage) of the sized battery pack, in m.
available_fuselage _cross_section_area[a]	2.73	The available space in the fuselage cross-section used during the sizing of the battery pack, in m^2.
volume	0.125	The computed volume of the battery pack corresponding to the computed final mass, in m^3.
volume_sized_by	power_requirements	Declares, whether the computed volume of the battery pack was determined by the power requirement or the energy requirement.
design_data		
pack_capacity _usable_Wh	120,258.0	The total amount of usable energy provided by the battery pack, in Wh.
pack_capacity _usable_J	432,928,800.0	The total amount of usable energy provided by the battery pack, in J.
pack_capacity _total_Wh	150,322.5	The total amount of energy stored in the battery pack (ignoring the maximum DoD), in Wh.
pack_capacity _total_J	541,161,000.0	The total amount of energy stored in the battery pack (ignoring the maximum DoD), in J.
max_power_draw _design[a]	521,972.7	The maximum electrical power draw from the battery pack when discharging at the determine optimal max. C-rate, in W.

Continued on next page

Table 6.13: (cont.) Overview of the example results output generated by the ‘HEPSretro_Components‘ sizing tool.

Output Parameter Name	Determined Value	Description
max_power_draw _available[a]	962,064.0	The maximum electrical power draw available from the battery pack when discharging at the max. C-rate as defined in the model settings, in W.
C_rate_max_design	8.0	The maximum C-rate of the battery pack according to the used underlying battery model.
efficiency	0.970	The efficiency of the battery pack used during sizing, according to the underlying battery model.
max_depth_of _discharge[a]	0.8	The maximum depth of discharge of the battery pack used during sizing.
specific_power _max_model[a]	2448.0	The specific power of the battery at pack level when discharging at the maximum C-rate according to the underlying model, in $W \cdot kg^{-1}$.
specific_power _max_design[a]	1328.04	The specific power of the battery at pack level when discharging at the C-rate for max. power determined during sizing, in $W \cdot kg^{-1}$.
specific_energy_Wh	382.5	The specific energy of the battery at pack level according to the underlying battery model, in $Wh \cdot kg^{-1}$.
specific_energy_J	1,377,000.0	The specific energy of the battery at pack level according to the underlying battery model, in $J \cdot kg^{-1}$.
power_density_design	4,187,752.8	The power density of the battery at pack level when discharging at the C-rate for max. power determined during sizing, in $W \cdot m^{-3}$.
energy_density_Wh	1,206,150.0	The energy density of the battery at pack level, in $Wh \cdot m^{-3}$.
energy_density_J	4,342,140,000.0	The energy density of the battery at pack level, in $J \cdot m^{-3}$.
	Transmission Line Component	
parentUIDs	[*Component1uID; Component2uID*][a]	List of the component uIDs of the components connected via the transmission line. Here: battery pack 1 to PMAD.
dimensions		

Continued on next page

Table 6.13: (cont.) Overview of the example results output generated by the 'HEPSretro_Components' sizing tool.

Output Parameter Name	Determined Value	Description
length	2.19	The total length of the sized transmission line corresponding to the determined path, in m.
transmission_line_path		The path determined by the sizing methodology. Coordinates provided as set of three steps between the CoGs of the components being connected in the global CPACS reference frame, in m
x_coordinates	21.76;20.64;20.64;20.64	
y_coordinates	0.00;0.00;0.00;0.00	
z_coordinates	-1.07;-1.07;-1.07;0.00	
design_data		
maximum _transmission_power[a]	962064.00	The maximum amount of electric power transmitted via the transmission line component, in W.
transmission_voltage	1000.00	The voltage used for power transmission as defined in the PMAD, in V.
installation_mass _penalty_factor [a]	0.300	The percent-fraction of the total mass due to installation.
HMS_mass _penality_factor[a]	0.050	The percent-fraction of the total mass due to the health monitoring system.
cable_model	simple_normal_conducting	The cable model used during sizing of the transmission line.
max_allowed _cable_current[a]	360.000	The maximum allowed current per cable according to the underlying cable mode, in A.
cable_linear_density	1.000	The linear density of the cables according to the underlying cable model, in $kg \cdot m^{-1}$.
cable_specific_losses	80.000	The specific losses occurring when transmitting power through the cable, in $W \cdot m^{-1}$.

[a] Parameter is one continuous string, but was separated to fit within the available space in the table.
[b] Due to CPACS internal layout standards, the position in x-, y-, and z-coordinates is supplied as a translation operation within a transformation node, denoted here by the parent-node notation of "transformation/translation".
[c] Note the extreme short length of a sized battery pack. This is caused by a limitation of the current methodology using the total available cross-sectional area and not allowing multiple packs to placed side-by-side.

7

Conceptual Design Workflows

As the devised methodology and sizing tools were created to be included in an overarching design process, their use in the creation of aircraft concepts is highly flexible. For the verification of both the methodology and the created sizing tools, the design process is kept simple to allow a more direct assessment of the individual tools. Sections 7.1 and 7.2 provide the breakdown of the design workflows, detailing the overall process flow, the connection of the design tools, and the various scripts required to adapt the data flow.
Besides the required process flow to create a converged aircraft concept, both workflows contain a "post-convergence" process flow, which is used to generate additional information on the created concept and to demonstrate some additional functionality of the sizing tools that are available but were not properly utilised during the concept iteration. The purpose of this "post-convergence" process flow is explained in Section 7.4. Additionally, the workflows contain a method to estimate the engine mass corresponding to the predicted performance. As the HEPS engine features a smaller engine core and includes an electric motor, traditional regression-based methods are unable to accurately estimate the engine mass. A brief description of the method used for the estimation of the engine masses is provided in Section 7.3.

The workflows themselves were created within RCE, a distributed and workflow-driven integration environment developed by the DLR. It is designed to analyse, optimize, and design complex systems like aircraft and allows the user to easily integrate their own design and analysis tools [a]. RCE was chosen for its ease of implementing and connecting the individual design tools, as well as the inclusion of intermediate scripts to manipulate the transferred data.
Both workflows are essentially identical with the exception that only the workflow for the generation of the HEPS concepts contains the design tool used to size the electric propulsion components, as these are irrelevant for the conventional turbofan. Utilising the same general process flow for both the HEPS and the reference concept substantially increases the usefulness of the subsequent comparison of the concepts, because any difference can be directly linked to the employed sizing tools. This directly effects the verification procedure, and the more accurate the cause of those differences can be identified, the more insight into the validity of both the tools and the underlying methodology can be gained.

Both design workflow layouts follows the same rudimentary process flow of "Concept Synthesis", followed by "Engine Performance Estimation" and "Mission Simulation". In case of the HEPS concepts, this is succeeded by the "Electric Component Sizing" to estimate the additional mass of the HEPS components and their impact on the aircraft balance. The conceptual design process flow is executed as an iteration over the aircraft MTOM and OEM until the design concept is deemed sufficiently converged (prescribed convergence tolerance of 10 kg or 0.012 %).
The "Concept Synthesis" is performed via the OAD tool "openAD", which is currently in active development by the DLR and thus not yet publicly available. It is capable of creating a full conceptually sized aircraft concept of a conventional turbofan aircraft based on only the TLARs, using mostly classical design principles. This tool is used for the generation of the initial concept, as well as to update the concept for the changes in mass, caused by the changed required fuel mass for the design mission and the introduced mass of the HEPS components.

[a] For more information on RCE: `https://rcenvironment.de/`

As can be expected, the function of "Engine Performance Estimation" is provided by the created sizing tool ‘HEPSretro_Performance‘ (see Section 6.3). This tool estimates the resulting engine performance, as well as some other fundamental engine characteristics such as the fan diameter, based on provided origin performance maps for the fan and engine core, and the desired performance at characteristic points in the flight envelope (more information on which characteristic design sizing points were defined for the generated concepts is provided in Section 4.1.2). Although the tool was created for the purpose of estimating the performance of a parallel hybrid-electric engine — supporting either a boosted turbofan or a constant power split ratio —, it can easily predict the performance of a conventional turbofan engine by simply prescribing a desired power split ratio of 0.0 for each design sizing point.
To accurately account for the impact of the changed aircraft mass, the required amount of fuel is computed during each iteration step in the "Mission Simulation" phase. This is achieved via simulating the design mission (more information on the employed design mission definition and its CPACS implementation is provided in Section 4.1.3 and Chapter 8 respectively) using the design tool called "AMC", which is also in active development at the DLR and thus also not yet publicly available. This tool performs a numerically simulated flight of the design mission and computes the required point performance of the aircraft for consecutive sample points. The determined amount of fuel and electric energy is based upon the provided engine performance (in the case of this thesis obtained from the tool ‘HEPSretro_Performance‘), as well as the aerodynamic performance of the aircraft concept. This illustrates one of the advantages of the newly devised methodology: by creating a standalone performance map that captures the performance of the HEPS engine over the entire operational envelope, the designer can choose any existing mission simulation tool. The de-coupling of the engine performance estimation methods and the mission simulation enables the use of dedicated design tools, which usually are not only more advanced and robust than a mission simulation procedure created specifically for the research study, but also readily available.
Finally, in case of the HEPS concepts, the "Electric Component Sizing" is performed by the created sizing tool ‘HEPSretro_Components‘ (see Section 6.4). This tool sizes all electric components required for the hybrid-electric propulsion system, both in terms of mass and position. All implemented sizing methods use physical characteristics instead of relying on empirical relations. As the choice as to the classification of the masses is subjective to each user, only the individual component masses returned by the tool are used. In the case of this study, the mass of the electric motors is considered part of the engine mass, however it is equally valid to include it in the combined mass of the HEPS powertrain. The individual electric component masses and their respective positions within the aircraft layout are then combined into a corresponding combined HEPS mass and CoG position, which is used during the subsequent "Concept Synthesis" phase to adapt the aircraft concept.

The following discussions of the specific workflows in Sections 7.1 and 7.2 will focus mostly on the various scripts inserted between the design tools. These script are critical in the workflows, as they are responsible for the correct data flow between the individual sizing tools. For improved clarity of the workflows, each script is limited to one main purpose, no script is performing two important functions.

7.1. Parallel HEPS Concepts Workflow

Figure 7.1 depicts the workflow for the generation of a parallel HEPS aircraft concept. The four main phases of the convergence iteration are clearly illustrated, however, the post-convergence process flow is excluded. Also indicated in the figure are the "pre-processing" operations for each phase. During these operations, the inputs for the respective design tools are updated with the most recent data, either directly forwarded or computed from the results of the previous iteration. Directly forwarded data includes the fuel and electric propulsion system masses, whereas the design sizing point altitudes and the corresponding required point performances are updated based on the previous mission simulation and the thrust requirements for the updated aircraft mass. The following paragraphs will detail the exact purpose of each integrated script, as well as provide an overview of which parameters are handled or which computations are performed.

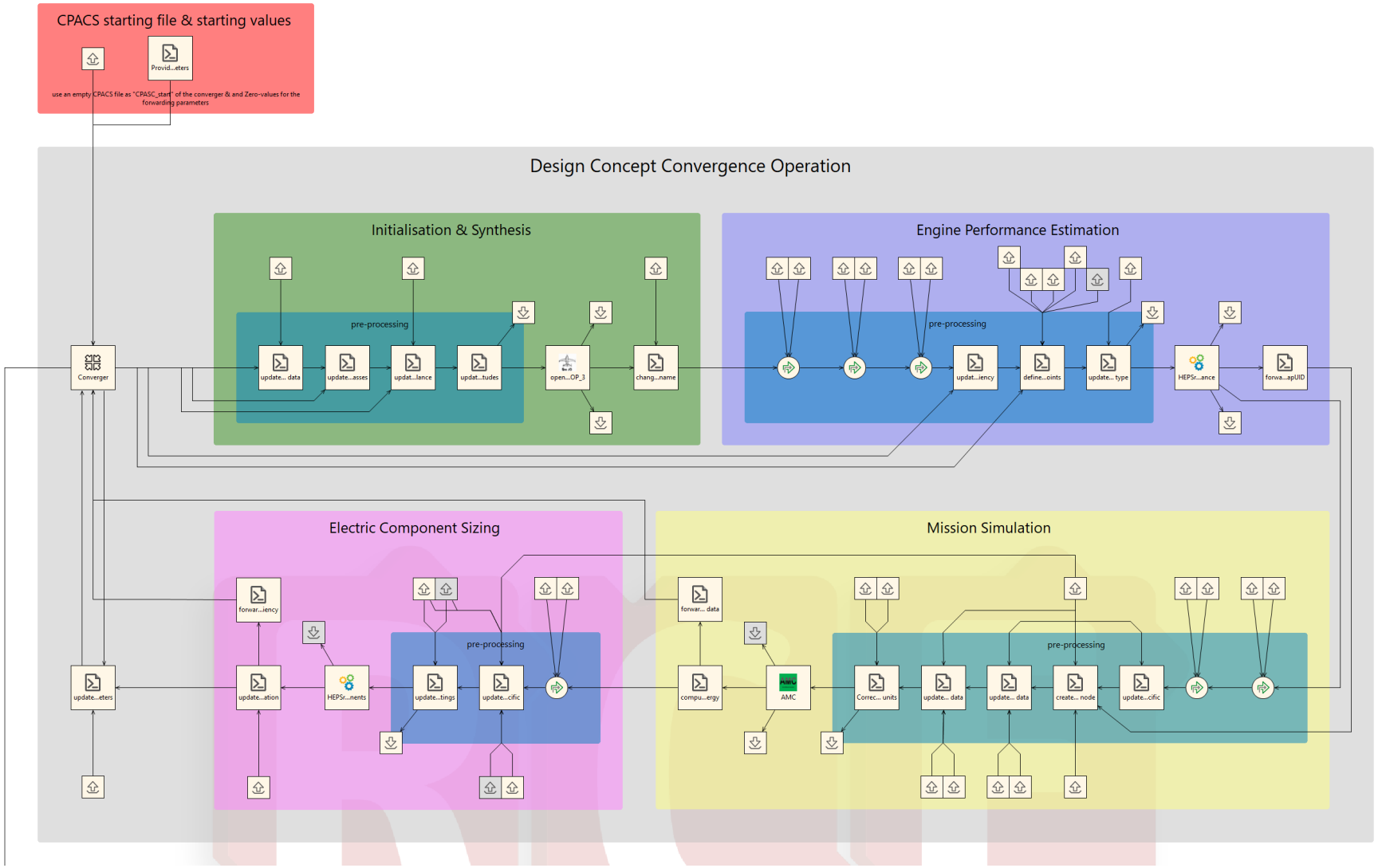

Figure 7.1: Overview of the workflow created within RCE for the generation of a parallel hybrid-electric aircraft concept, showing only the process flow of the aircraft mass convergence iteration.

Initialisation & Synthesis The workflow requires four pre-processing operations before the updated aircraft concept can be synthesised, as well as one script after the sizing tool. The pre-scripts are executed only from the second iteration onwards, as they rely on data forwarded from the previous iteration. Each script corresponds to a specific purpose, in order of execution within the workflow:

Pre-Process Operations:
1. "Update Engine Data"
2. "Update Fuel Masses"
3. "Update Weight & Balance"
4. "Update Design Altitudes"

Post-Process Operations:
1. "Change Engine Name"

A detailed overview over which parameters are updated by each of the above scripts is provided in Table 7.1. All of these parameters are directly taken from the forwarded data of the previous iteration, no computations are performed within the scripts. The purpose of the post-script is simply to change the name assigned to the engine node within the CPACS file, as 'openAD' simply assigns a default name. The script updates the name to properly reflect whether the created engine is conventional or hybrid-electric.

Table 7.1: Overview of all pre-process scripts for the concept initialisation & Synthesis phase of both the HEPS and conventional concept generation workflows.

RCE Script Name	Updated Parameter	Description
Update Engine Data	Engine Mass	The combined total estimated mass of the engines (i.e. $N_{eng} \cdot m_{engine}$; m_{engine} includes electric motor mass), in kg.
	Engine Fan Diameter	The diameter of the engine fan, as estimated by 'HEPSretro_Performance', in m.
Update Fuel Masses	Fuel Mass Taxi-Out	The amount of fuel consumed during the taxi-out phase, in kg.[a]
	Fuel Mass Taxi-In	The amount of fuel consumed during the taxi-in phase, in kg.[a]
	Fuel Mass Takeoff	The amount of fuel consumed during the takeoff phase, in kg.[a]
	Fuel Mass Approach/Landing	The amount of fuel consumed during the approach and landing phase, in kg.[a]
	Fuel Mass Reserve	The amount of fuel required as reserve (includes flight to alternate airport, loiter, and contingency), in kg.
	Fuel Mass Design Mission [b]	The total amount of fuel to be stored on-board for the design mission, in kg.
Update Weight & Balance [c]	HEPS Mass	The total mass of all components of the hybrid-electric system, except for the electric motors (included in engine mass), in kg.

Continued on next page

Table 7.1: (cont.) Overview of all pre-process scripts for the concept initialisation & Synthesis phase of both the HEPS and conventional concept generation workflows.

RCE Script Name	Updated Parameter	Description
	HEPS CoG X-Position	The estimated x-position of the centre of gravity of the combined HEPS components, computed from individual component CoG positions, in m.
	HEPS CoG Z-Position	The estimated z-position of the centre of gravity of the combined HEPS components, computed from individual component CoG positions, in m.
Update Design Altitudes	Altitude ToC	The optimum altitude for top of climb of the design mission, as computed by AMC (mission simulation), in m.
	Altitude Mid-Cruise	The altitude at mid-cruise corresponding to the design mission as simulated by AMC, in m.

[a] Methods used to compute/estimate fuel used during ground segments are detailed in Section 4.1.4.
[b] Includes the fuel computed for the following phases: taxi-out, takeoff, climb, cruise, descent, approach/landing, and reserve.
[c] Only applicable for the HEPS workflow.

Engine Performance Estimation As shown in Figure 7.1, the process flow responsible for predicting the engine performance requires five pre-process operations and one post-process operation. The first three pre-processes are merging operations, wherein pre-defined data is added to the current CPACS file, while the last two operations are again script executions. The purpose of each operations for the "engine performance estimation" is listed below:

Pre-Process Operations:

1. "Add Origin Fan Map"
2. "Add Origin Core Map"
3. "Add Performance Toolspecific"
4. "Update Overall HEPS Efficiency"
5. "Define Design Sizing Points"

Post-Process Operations:

1. "Forward Performance Map UID"

During the merging operations, the origin performance maps that are intended to be used by the sizing tool 'HEPSretro_Performance' for the engine performance prediction, and the pre-defined tool specific settings (see Section 6.3.3), are added to the CPACS file. In the case of this study, the performance maps are added as additional engine nodes — one each for the fan and engine core — while the toolspecific data is added according to the standard of the <toolspecific> node.

The first script simply updates the overall efficiency of the electric powertrain in the hybrid-electric propulsion system, using the value computed by 'HEPSretro_Components' during the previous iteration. The second script is more critical, as it governs the definition of the design sizing points, which are responsible for the performance prediction performed by the sizing tool. The parameters that are defined for each sizing point are listed in Table 7.2, and it should be noted that these parameters have to be defined for each individual design sizing point.

For the creation of the aircraft concepts during this study, it was decided to define the desired engine performance at four important points of the flight envelope:

1. Takeoff: The engine performance at takeoff has long been established as a critical point in the traditional sizing process.
2. Top of Climb: The top of climb is a characteristic point in the design mission, as it reflects on both the climb and the cruise engine performance.
3. Mid-Cruise (2x): The mid-cruise point offers much insight into the cruise performance, which corresponds to the main purpose of any transport aircraft. Defined once for steady cruise without electric boost power, and once for mid-cruise climb performance with electric boost power.

The exact method used for the computation of the desired point performance at each design sizing point is covered in detail in Section 4.1.2. Finally, the post-script is a simple forwarding of the unique ID used to identify the created hybrid-electric engine performance map, which is defined within the added 'HEPSretro_Performance' toolspecifics.

Table 7.2: Overview of all pre-process scripts for the engine performance estimation phase of the HEPS concept generation workflow.

RCE Script Name	Updated Parameter	Description
Update Overall HEPS Efficiency	HEPS Efficiency	The overall HEPS powertrain efficiency.
Define Design Sizing Points	Altitude [a]	The desired altitude of the design sizing point, in m.
	Mach Number [a]	The desired Mach number of the design sizing point.
	Thrust [a]	The desired total thrust per engine of the design sizing point, in N.
	Power-Split Ratio [a]	The desired maximum power split ratio of the design sizing point.
	Max. GT shaft power[b]	The maximum allowed gas turbine output shaft power, used when not prescribing a power-split ratio

[a] Parameter is defined for each design sizing point; choice of number of prescribed design sizing points depends on use case. More information on the methods employed to compute the required performance data at the prescribed design sizing point in Section 4.1.2
[b] Used when defining the "mid-cruise_climb" design sizing point to have to tool compute the required electric boost power-split automatically.

Mission Simulation The workflow phase responsible for simulating the design mission and computing the necessary amount of fuel and electric energy illustrates a key difference between the newly devised and the already existing methodologies. The generation of a cohesive HEPS engine performance map allows the use of an established mission analysis tool with only limited pre-processing, in the form of two data merging and five pre-tool processes. Two additional post-tool operations are required for the aircraft concept mass convergence.

Pre-Process Operations:
1. "Add AMC Toolspecific"
2. "Add Design Mission Definition"
3. "Update AMC Toolspecific"
4. "Create <performanceCase> Node"
5. "Update Mission Segments Data"
6. "Update <missionDefinitions> Design Data"
7. "Convert Energy Units"

Post-Process Operations:

1. "Compute Consumed Electric Energy"
2. "Forward Sizing Points Data"

During the two merging operations, the toolspecific options for the mission simulation tool ‘AMC‘, as well as the definition of the used design mission are added to the CPACS file. The used default toolspecific settings are provided in Listing 7.1, whereas the CPACS implementation of the design mission definition is detailed in Chapter 8.

```
<?xml version="1.0" encoding="UTF-8"?>
<cpacs>
  <toolspecific>
    <tool>
      <name>AMC</name>
      <toolversion>0.2.2</toolversion>
      <AMC>
        <global>
          <performanceCaseUID>perfoUID</performanceCaseUID>
          <aircraftModelUID>AircraftModel</aircraftModelUID>
          <archiveMode>1</archiveMode>
        </global>
        <toolSettings>
          <PayloadRange>0</PayloadRange>
          <trimDrag>0</trimDrag>
        </toolSettings>
        <vehicleSpecificData>
          <designPayload>23750</designPayload>
          <designTOmass>80540.9</designTOmass>
          <nEngines>2</nEngines>
        </vehicleSpecificData>
      </AMC>
    </tool>
  </toolspecific>
</cpacs>
```

Listing 7.1: Toolspecific settings for AMC used during the mission simulation of the aircraft concepts.

As the AMC toolspecifics in Listing 7.1 include data specific to the aircraft concept for which the mission is being simulated — in this study the design payload mass, the maximum takeoff mass, and the number of engines — the first script updates these values for the current state of the concept. It also updates the uIDs used for the aircraft model and the performance case, as the default file used for the merging operation is the same for all created example concepts. The next script creates a <performanceCase> node within the aircraft node, which is required to link the defined design mission to the aircraft concept and the applicable aero and engine performance maps within the CPACS file.
Subsequently, two scripts are employed to update the data in the defined design mission. In the mission segments, the stored values of the consumed fuel and energy for the ground segments (taxi, takeoff, and approach/landing; for both the design mission and reserve) are updated to reflect the most recent predicted engine performance map. The values are computed based on assumed thrust settings at the beginning and end of the respective segment, as stated in Section 4.1.4. The second script updates the values for the desired contingency fuel and the cruise Mach number for the alternate segment. Additionally, it can be used to prescribe a fixed altitude for the top of climb segment, which allows the user to enforce a specific cruise altitude for the mission simulation instead of the "optimal cruise altitude" as determined by AMC.
Finally, the last pre-script is required due to the used version of AMC deviating from the pure SI-unit approach of CPACS by using MJ instead of J for the consumed electric energy in the mission segments. Since the tool is still in active development and this deviation may be removed in later versions of AMC, the conversion between energy units was placed in a separate script and not included in the "Update Mission Segments Data" script.

In the first of the post-tool scripts, the total amount of electric energy used over the entire mission is calculated. The mission simulation tool 'AMC' computes the momentary state and performance of the aircraft for a series of sequential sample points. While storing some global data (e.g. total fuel mass, total duration and distance travelled, performance at mid-cruise point etc.), the main output of 'AMC' is the state and performance at each sample point, stored in the CPACS file in dedicated <trajectory> nodes (for this study, two trajectories nodes are present: the route from origin to target airport, and the reserve phase). The total amount of required electric energy on-board is simply computed via numerical integration of the momentary electric power over the flight time for each trajectory. The last script in the "mission simulation" phase of the workflow simply extracts the parameters required for the definition of the design sizing points (see Section 4.1.2) from the CPACS file and forwards them via the RCE converger to the next iteration loop. A detailed overview of all scripts and which parameters they update/compute is given in Table 7.3.

Table 7.3: Overview of all pre- and post-process scripts for the mission simulation phase of both the HEPS and conventional concept generation workflow.

RCE Script Name	Updated Parameter	Description
Update AMC Toolspecific	Performance Case uID	The uID assigned to the <performanceCase> node created in the subsequent script.
	Aircraft Model uID	The uID corresponding to the aircraft concept used within the CPACS file.
	Design Payload	The prescribed design payload mass of the aircraft, in kg.
	Design Takeoff Mass	The current maximum takeoff mass, in kg.
	Number of Engines	The total number of installed engines (the stored engine performance maps specify the performance per engine).
Create <performanceCase> Node	Mission uID [a]	The uID of the mission as defined within the <missionDefinitions> node, linking the design mission to the aircraft concept.
	Point Performance uIDs [a]	The uIDs of all defined point performances to be included as special points of interest in the flight envelope.
	Default Engine Performance Map uID [a]	The uID corresponding to the engine performance map to be used by AMC. [b]
	Default Aero Performance Map uID [a]	The uID corresponding to the aero performance map to be used by AMC. [b]
Update Mission Segments Data	Consumed Fuel [c]	The total fuel consumed during each segment, in kg.
	Consumed Energy [c]	The total amount of electric energy consumed during each segment, in J.
Update Mission Design Data	Contingency Fuel Fraction	The percentage fraction of fuel to be added as contingency.
	Mach Number Reserve	The Mach number for the cruise segment of the reserve phase.

Continued on next page

Table 7.3: (cont.) Overview of all pre- and post-process scripts for the mission simulation phase of both the HEPS and conventional concept generation workflow.

RCE Script Name	Updated Parameter	Description
	Top of Climb Altitude [d]	The altitude for the top of climb point, essentially the ICA, in m.
Convert Energy Units [e]	Consumed Energy [c]	The total amount of electric energy for each segment, converted for AMC energy unit (here MJ).
Compute Consumed Electric Energy	Electric Energy [f]	The total amount of energy required for the design mission/reserve phase, in J.
Forward Sizing Points Data	Altitude [g]	The characteristic altitude used for the definition of the design sizing points, in m.
	Mach number [g]	The corresponding Mach number for each design sizing point.
	Drag [g]	The corresponding total aircraft drag for each design sizing point, in N.
	TAS [g]	The corresponding true airspeed for each design sizing point, in $m \cdot s^{-1}$.
	Weight$_{A/C}$ [g]	The current weight of the aircraft for each design sizing point, in N.

[a] All updated parameters are located within the created <performanceCase> node under the CPACS path '/cpacs/vehicles/aircraft/-model/performanceRequirements/performanceCases/performanceCase'.
[b] It is possible to additionally define engine/aero performance maps for specific mission segments, but for this study only the default performance maps were used.
[c] The consumed fuel/energy are defined for each "ground segment", as AMC only computes the fuel and energy flow for segments where the aircraft is entirely airborne.
[d] The Top of Climb altitude is an optional parameter; not used for generated example concepts.
[e] Only applicable for the HEPS workflow.
[f] Computed separately for design mission and reserve phases.
[g] Defined for each design sizing point, for purpose see Section 4.1.2

Electric Component Sizing The final phase of the hybrid-electric design workflow is straight forward and requires three pre- and two post-tool operations. Although termed the "Electric Component Sizing", it also includes the updated mass estimation for the engines.

Pre-Process Operations:
1. "Add Components Toolspecific"
2. "Update 'HEPSretro_Components' Toolspecific"
3. "Update Battery Model Settings"

Post-Process Operations:
1. "Update Engine Mass Estimation"
2. "Forward Overall HEPS Efficiency"

Analogous to the previous two phases, the first pre-operation is the merging of the sizing tool's toolspecifics into the main CPACS file. The toolspecifics contain not only many parameters for the internal settings of the sizing tool, but also the design parameters for the required hybrid-electric propulsion system — such as the total amount of electric energy to be stored on-board and which component models to use for the various electric components — as well as all models that govern the performance characteristics of each electric component. Thus, the subsequent script is responsible for updating the added toolspecifics based on the previously determined amount of required electrical energy, as well as the user defined settings on whether to use just one or two types of batteries. An overview of all parameters updated in the toolspecific

node is provided in Table 7.4. Although some of the parameters could simply be defined correctly in the provided default toolspecifics, here they are included in the update script to highlight that this can be used to dynamically adjust the battery model used in the electric component sizing to account for changes in the power- or energy-requirements.
The last script before the sizing tool is executed defines the battery model(s) within the CPACS file, depending on the performance parameters supplied by the user. It was decided to define the battery model(s) directly from user supplied parameters, instead of merging a predefined model setting node into the CPACS file, as this allowed the user to adapt the battery model at the same point where all other design inputs are defined.

Table 7.4: Overview of all pre- and post-process scripts for the electric component sizing phase of the HEPS concept generation workflow.

RCE Script Name	Updated Parameter	Description
Update 'HEPSretro_Components' Toolspecific Node	Main Battery Model UID	The component model uID for the main battery.
	Main Battery Available Energy	The total amount of energy made available to the propulsion system from the main battery, in J.
	Main Battery Max. Power [a]	The maximum amount of electric power that can be provided by the main battery (all packs combined in parallel), in W.
	Secondary Battery Model UID [a]	The component model uID for the secondary battery.
	Secondary Battery Available Energy [a]	The total amount of energy made available to the propulsion system from the secondary battery, in J.
Update Battery Model Settings	Model Energy Unit [b]	What energy unit the battery component model is using.
	Max. Pack Capacity [b]	The maximum amount of energy that can be stored in one battery pack, in J (or Wh).
	C-Rate Max. Power [b,c]	The maximum C-rate at which the battery pack can be discharged (corresponds to max. power output).
	Specific Energy [b]	The specific energy of the battery at pack level, in $J \cdot kg^{-1}$ (or $Wh \cdot kg^{-1}$).
	Energy Density [b]	The energy density of the battery at pack level, in $J \cdot m^{-3}$ (or $Wh \cdot m^{-3}$).
	Max. Discharge [b]	The maximum depth of discharge (DoD), indicating the percentage of stored energy that can be discharged without damaging the battery.
	Efficiency [b]	The efficiency of the battery pack.
	Specific Power [b,c]	The specific power (per mass) of the battery pack. Optional input and must be compatible with the provided maximum C-rate.

Continued on next page

Table 7.4: (cont.) Overview of all pre- and post-process scripts for the electric component sizing phase of the HEPS concept generation workflow.

RCE Script Name	Updated Parameter	Description
Update Engine Mass Estimation	Engine Mass	The estimated mass of the engine, based on the scaled mass of the engine core and the added electric motor.
Forward Overall HEPS Efficiency	HEPS Efficiency	The overall HEPS powertrain efficiency, computed via sized electric component efficiencies.

[a] Only applicable if user decides to include two dedicated battery types in the component sizing.
[b] Defined for each battery model, in case more than one is desired.
[c] Only one is necessary. If both defined simultaneously, the values have to be compatible (will be checked within the sizing tool).

Once the design tool 'HEPSretro_Components' has completed the sizing of the individual electric component masses and positions, the only design parameter left to estimate is the resulting mass of the hybrid-electric engine. To obtain a reasonable prediction of the engine mass for the hybrid-electric engine, the established conceptual mass estimation methods cannot be used. A description of the chosen engine mass estimation method, valid for both HEPS and conventional turbofan engines, is provided in Section 7.3. Ideally, this process would be performed by a dedicated engine mass estimation design tool, potentially combined with the generation of a tailored engine core performance map to be used in the next iteration step. For this study, this was not readily available and a rough mass estimation was deemed sufficient.
Finally, the sized electric components are used to compute the overall efficiency of the hybrid-electric propulsion system. This efficiency is then forwarded via the RCE converger to the "engine performance estimation" phase of the next iteration step, where it is used to compute the amount of electric energy required at each sample point of the performance map.

7.2. Conventional Turbofan Concepts Workflow

The design workflow for the generation of the conventional turbofan concept is based on the workflow created for the HEPS concepts discussed in Section 7.1, and thus very similar. As can be seen in Figure 7.2, the convergence iteration for a conventional aircraft concept consists of only three main phases, as no electric components have to be sized. The remaining phases, discussed in more detail below, are largely identical to their HEPS counterpart, albeit with small alterations to reflect the reduced complexity of the concept.

Initialisation & Synthesis Compared to the synthesis phase of the hybrid-electric workflow, the conventional design only requires three pre-tool script executions, as no additional mass and the corresponding shift in the centre of gravity has to be considered. All other scripts listed below are exactly the same as for the hybrid-electric workflow, and update the same parameters as shown in Table 7.1. Again, once the updated concept has been synthesised, the name of the installed engine is updated to reflect that it is a conventional turbofan engine.

Pre-Process Operations:
1. "Update Engine Data"
2. "Update Fuel Masses"
3. "Update Design Altitudes"

Post-Process Operations:
1. "Change Engine Name"

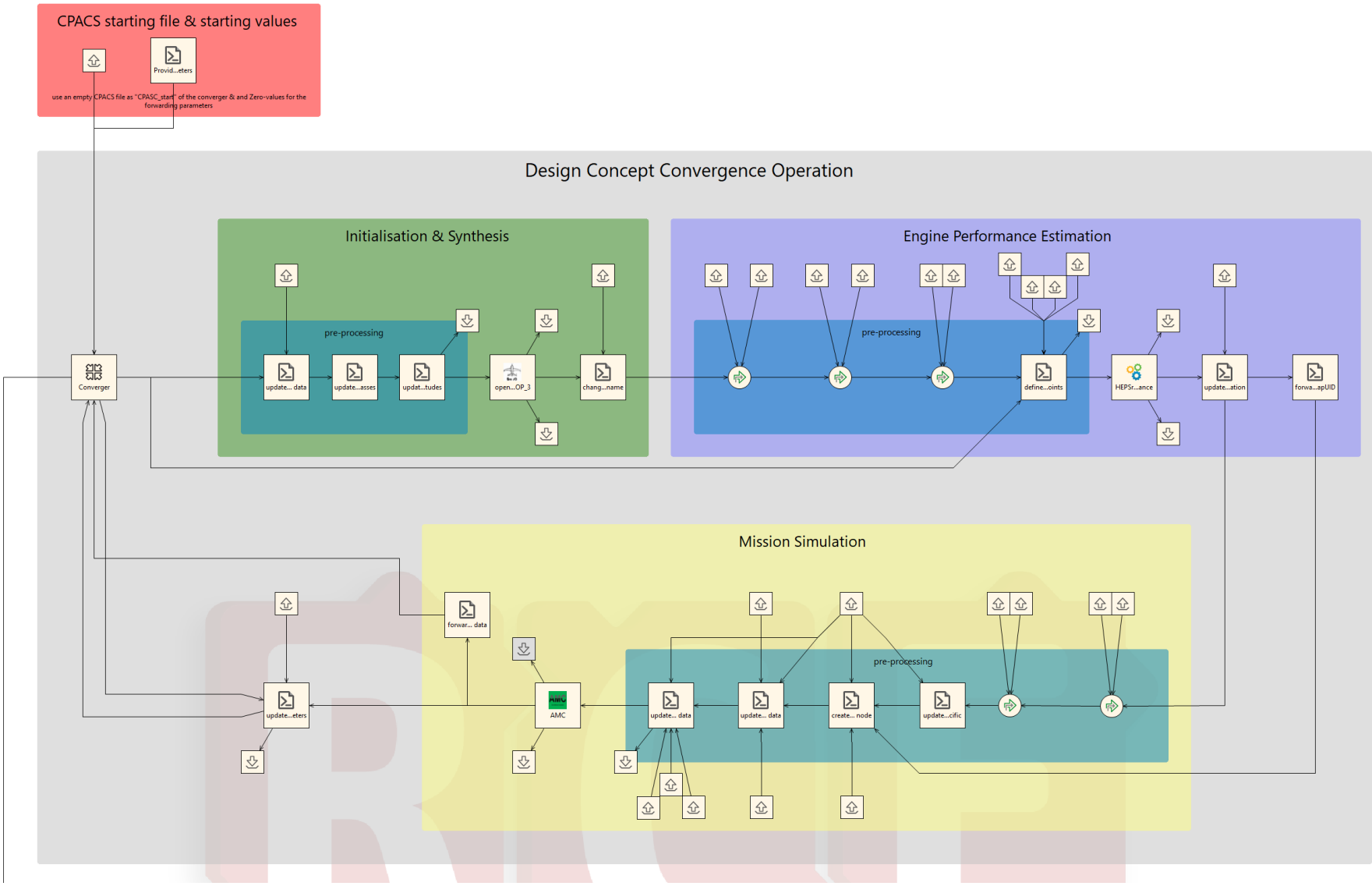

Figure 7.2: Overview of the workflow created within RCE for the generation of a conventional turbofan aircraft concept, showing only the process flow of the aircraft mass convergence iteration.

Engine Performance Estimation The preparation of the data for the estimation of the engine performance of a conventional turbofan aircraft requires the same handling as for the HEPS concept, except the overall efficiency of the hybrid-electric propulsion system no long has to be considered. A conventional engine performance map is created via the same method as an "augmented" hybrid-electric performance map, with the value of the desired maximum allowed power-split ratio at each design sizing point set to zero.

Pre-Process Operations:
1. "Add Origin Fan Map"
2. "Add Origin Core Map"
3. "Add Performance Toolspecific"
4. "Define Design Sizing Points"

Post-Process Operations:
1. "Update Engine Mass Estimation"
2. "Forward Performance Map UID"

A change to the hybrid-electric workflow is that the script for the updated engine mass estimation is now included in this phase. As the method now requires only the engine core mass, since no electric motor is included in the engine design, it's mass can be estimate immediately after the performance prediction. Again, a list of all parameters updated by the scripts of this phase is provided in Table 7.5.

Table 7.5: Overview of all pre-process scripts for the engine performance estimation phase of the conventional concept generation workflow.

RCE Script Name	Updated Parameter	Description
Define Design Sizing Points	Altitude [a]	The desired altitude of the design sizing point, in m.
	Mach Number [a]	The desired Mach number of the design sizing point.
	Thrust [a]	The desired total thrust per engine of the design sizing point, in N.
	Power Split Ratio [a]	The desired maximum power split ratio of the design sizing point.
Update Engine Mass Estimation	Engine Mass	The estimated total mass of the engine, based on the computed mass of the engine core, in kg.

[a] Parameter is defined for each design sizing point; choice of number of prescribed design sizing points depends on use case. More information on the methods employed to compute the required performance data at the prescribed design sizing point in Section 4.1.2

Mission Simulation Similarly to the previous two phases, the mission simulation of a conventional aircraft concept requires less additional data handling. While the pre-tool scripts are essentially identical to the ones in the HEPS workflow (the script converting the units of the consumed energy of the ground segments to account for AMC using MJ instead of J is obviously no longer required), the most notable difference is the absence of the script to compute the total consumed energy. Because the conventional engine performance no longer contains an electrical component, and AMC is internally computing the total consumed fuel instead of simply returning the momentary fuel flow, this script is no longer required. All parameters that are updated during the script executions of the "mission simulation" iteration phase are included in Table 7.3.

Pre-Process Operations:
1. "Add AMC Toolspecific"
2. "Add Design Mission Definition"
3. "Update AMC Toolspecific"
4. "Create <performanceCase> Node"

5. "Update Mission Segments Data"
6. "Update <missionDefinitions> Design Data

Post-Process Operations:

1. "Forward Sizing Points Data"

7.3. Engine Mass Estimation Method

Established engine mass estimation methods for the conceptual aircraft design are typically empirical, and relate basic engine parameters such as the maximum SLS thrust and the BPR to the total engine mass. Parallel hybrid-electric turbofan engines have inherently smaller engine cores compared to conventional turbofan engines of similar thrust performance, which makes the established mass estimation methods unusable for HEPS concepts. Alternative component based weight estimation methods [35, 36] offer significantly more accurate results, especially for novel engine configurations. These methods, however, require much more detailed input data, particularly about the internal engine layout and flow characteristics.

Ideally, the design workflow for the hybrid-electric aircraft design contains an engine sizing phase that is more extensive than in the workflows described in Sections 7.1 and 7.2, including the presented engine performance prediction in combination with a detailed engine mass estimation using a design tool based on a component based method. As such a tool was not readily available, a substitute method based on the verification data of the method by Lolis [36] was created.

The replacement method is rather simple and works on the assumption, that the contribution of the different components to the overall engine mass remains relatively constant. Using the verification data presented in [36, Table 4.3], the percent fraction contribution of the core engine, the fan, the nacelle, the support structure, and the accessories to the total engine mass were estimated as shown in Table 7.6.

Table 7.6: Engine component mass fractions for a conventional turbofan engine, assumed usable for the conceptual mass estimation of a parallel HEPS engine.

	engine core	fan	nacelle	support structure	accessories
Mass Fraction	0.5	0.3	0.1	0.0	0.1

The final engine mass is computed according to Equation (7.1), using the masses for the engine core and electric motors as determined by the HEPS sizing tools, and the component fraction defined in Table 7.6. A more accurate result can be achieved by calibrating the mass fractions using a high-fidelity, component-based engine design tool. This method has been applied during the generation of both the reference conventional and example HEPS aircraft concepts.

$$m_{engine} = \frac{m_{core} + m_{EM}}{1 - \left(f_{fan} + f_{nacelle} + f_{support} + f_{accessory}\right)} \tag{7.1}$$

7.4. Post-Convergence Process Flow

Both the hybrid-electric and the conventional concept workflow contain a "post-convergence" phase, which is performed once the designs are sufficiently converged. Theses additional executions are not strictly necessary for the generation of a usable aircraft concept, but were included to highlight some optional features of the devised sizing tools, as well as produce some additional data such as the payload-range diagrams.

Because the post-convergence process flow of the conventional concept workflow is identical to the one used in the hybrid-electric concept workflow just without the component sizing tool included, only the HEPS concept workflow's post-convergence process flow is depicted in Figure 7.3.

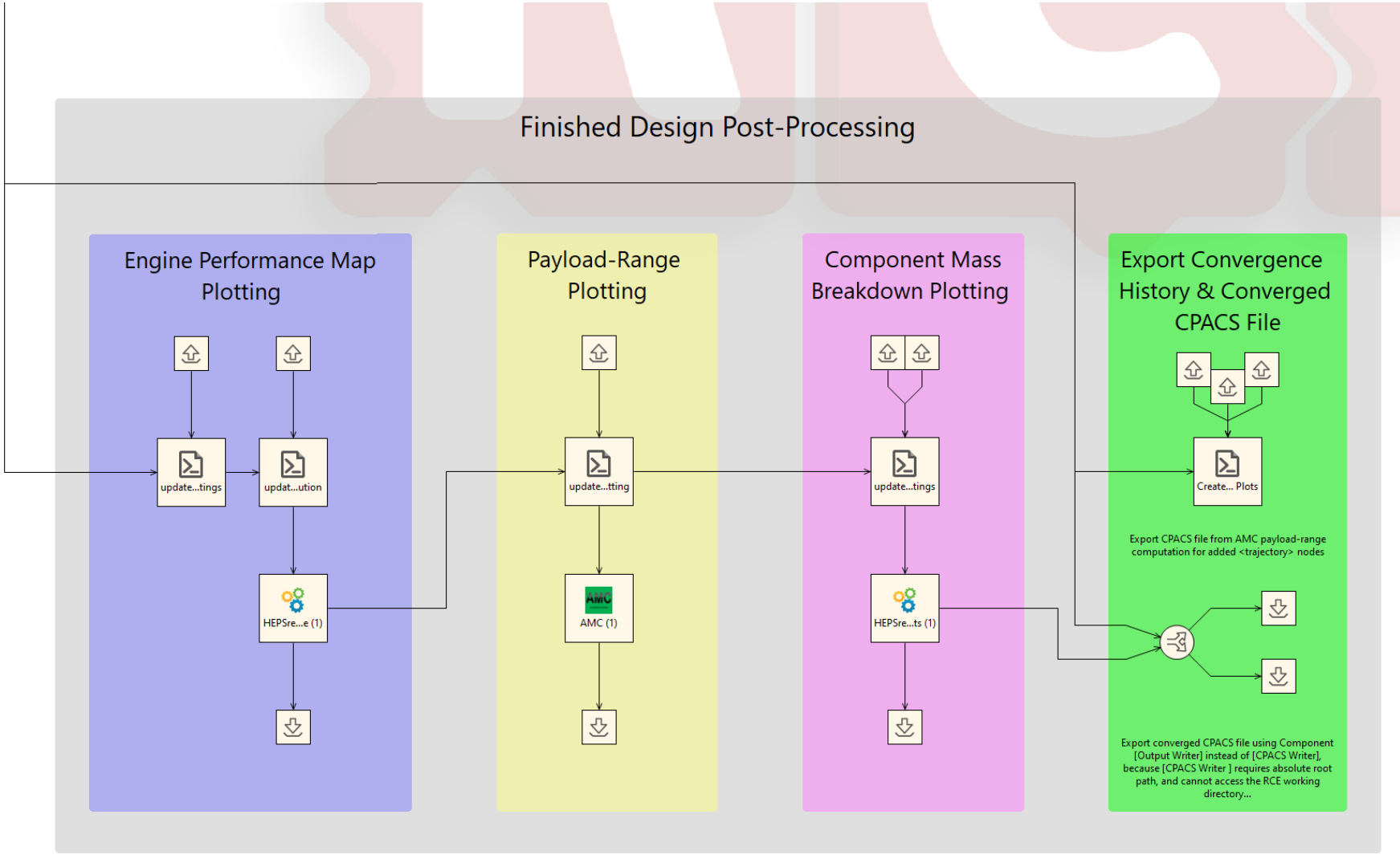

Figure 7.3: Overview of the post-convergence process flow of the hybrid-electric aircraft concept workflow used to highlight additional features of the devised sizing tools. For the generation of conventional aircraft concepts, the "Component Mass Breakdown Plotting" process is removed, as no electric components were sized.

The first process post convergence is an additional execution of the created engine performance prediction tool 'HEPSretro_Performance'. The toolspecifics are altered such, that the tool creates the engine performance map with an increased number of sample points for each combination of altitude & Mach number, generating a higher resolution performance map, and to trigger the internal post-processing option of creating plots of the produced total thrust vs. the engine core power output for each sample Mach number, separated by sample altitude. The increased sample point resolution illustrates the ability of the tool to be used to either generate a rough performance map quickly, or a detailed one at the cost of more time. Additionally the distribution of the sample thrust values within the thrust range can be adjusted, allowing for a higher resolution at more critical thrust values.
Following the generation of the high resolution engine performance map, the mission simulation tool AMC is executed once more to create the payload range diagram of the converged concept, which allows a quick comparison of the mission performance of the various concepts. It is not generated during the iteration due to a significant increase in tool's runtime.
Finally, the component sizing tool 'HEPSretro_Components' is executed again to create mass breakdown plots of the sized electrical propulsion system components, as well as of the main design masses of the concept (for both maximum payload and maximum fuel mass). This enables a quick inspection of the impact of the added mass due to the electric components of the hybrid-electric propulsion system.
The last operations simply create a plot of the convergence history and exports the CPACS file of the final converged aircraft concept into the desired directory.

8

Design Mission CPACS Implementation

The implementation of the selected design mission is an important part in the generation of the example aircraft concepts, as the electric energy requirement calculated during the mission simulation is critical for the design mass convergence. In this chapter, first the structure of a mission definition in CPACS is presented in Section 8.1, before Section 8.2 provides a detailed breakdown of the individual mission constraints and end conditions prescribed.

8.1. CPACS Mission Definition Structure

Although some changes were made to the structure of the mission definitions between CPACS versions 3.2 (used in the generation of the example concepts) and 3.4 (the most recent at time of writing this thesis), those changes address the syntax to allow a more precise definition, not the logic in how a mission is represented. As such, the following description is equally valid for CPACS versions 3.2 and 3.4.

Figure 8.1a, taken from the official CPACS documentation [a], provides an illustration of the build-up of the "missionDefinitions" node of a CPACS file. Each mission defined in the CPACS file is broken down into first a sequence of "segmentBlocks", each of which contains a series of consecutive "segments".

The purpose of the different levels in the hierarchy are is best understood when observing the illustration of a typical example mission profile in Figure 8.1b. The <mission> node includes the entire route, usually beginning and ending with the taxiing to the gate. Besides defining the start condition in terms of velocity (CAS or Mach) and position, it also allows for the prescription of the environment, such as the use of the international standard atmosphere and the desired temperature delta.

The second level of the hierarchy, the <segmentBlocks>, allows the overall mission to be separated into multiple distinct parts, typically reflecting the different reasons for why it is part of the mission. In the example mission in Figure 8.1b, three segment blocks were defined: the "designMission", including everything from taxi out of the gate at the departure, to landing at the destination airport; the "reserves", accounting for a go-around, cruise to an alternate airport, and a loiter phase; and an "endPhase", which includes the taxi in to gate after landing and potentially any contingency fuel. This logical break-up of the overall mission allows for a high degree of flexibility. Should a desired mission contain a stopover for example, this can easily be implemented via an additional segment block. Besides declaring which segments each <segmentBlock> consists of, further constraints and additional information can be defined, such as the total range covered during the segment block, which of the individual <segments> is variable to allow for matching the prescribed total range, or which type of fuel planning the segment block contributes to (design fuel, reserve fuel, etc.).

Finally, the third level of the mission definition hierarchy is the . Each defined <segmentBlock> is separated into distinct <segments>, corresponding to specific phases of the flight. Besides the expected "take-off", "climb/descent", "accelerate/decelerate", "cruise", and "landing", a wide variety of additional segment types are available. Each individual allows for the prescription of type-specific <endCondition> and <constraint> settings. These settings are used to impose the desired design mission, by defining the exact performance for each part of the flight profile. In the example in Figure 8.1b, the "climb" segment defines a final altitude of 10,058.4 m (FL330) and consists of two-step discrete profile, prescribing a speed limit of CAS $\leq 128.61\ \mathrm{m{\cdot}s^{-1}}$ (250 kt) and Mach ≤ 0.78 for altitudes below 3047.7 m (FL100), and CAS $\leq 154.33\ \mathrm{m{\cdot}s^{-1}}$ (300 kt)

[a] https://cpacs.de/pages/documentation.html

and Mach ≤ 0.78 for altitudes up to the defined ICA. The "cruise" segment contains no <endCondition> or <constraint>, as these are handled by the <segmentBlock>, and the "descent" segment simply imposes a final

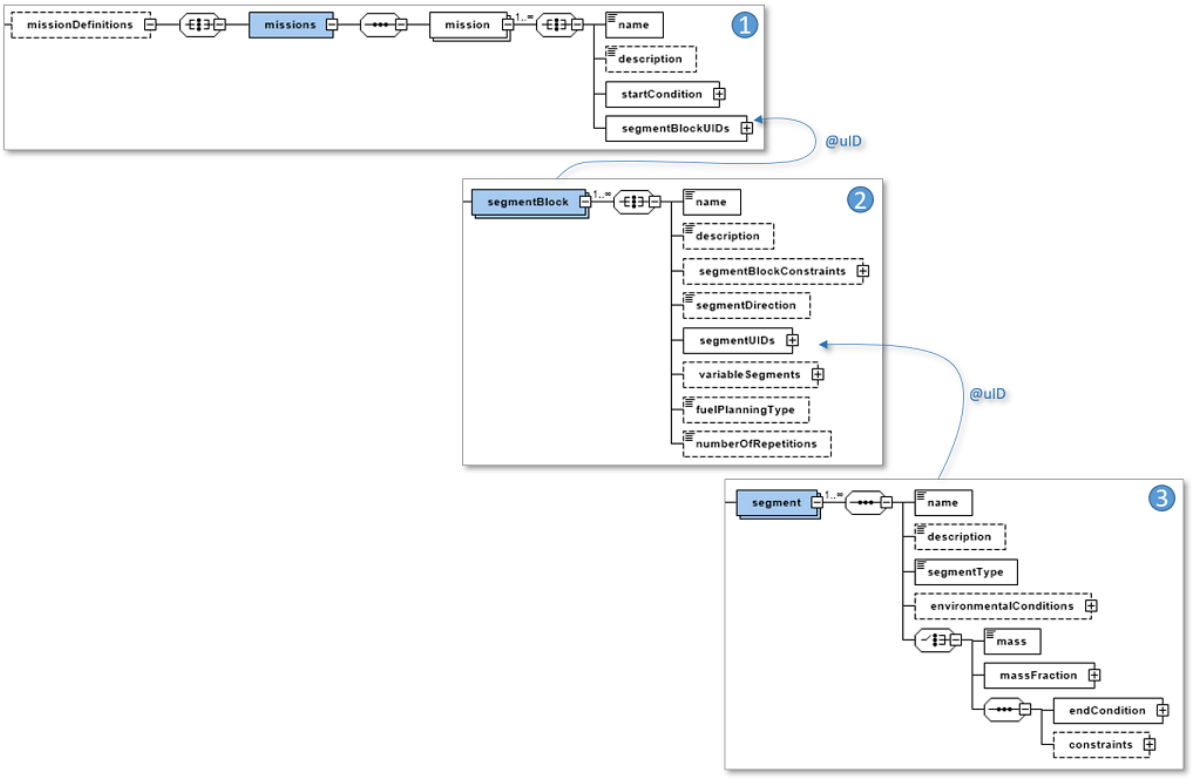

(a) Illustration of the hierarchical breakdown used to define aircraft missions in the CPACS standard.

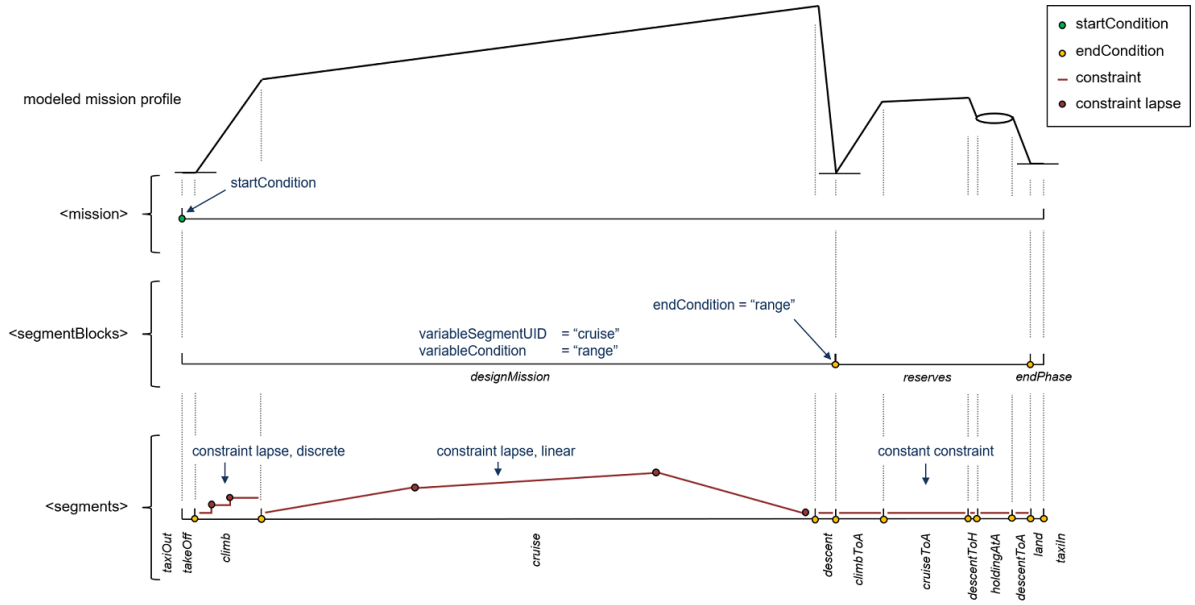

(b) Simplified illustration of an example mission profile for a typical civil aircraft transport mission, including the breakdown into the corresponding hierarchical elements.

Figure 8.1: Illustrations to visualise the structure of the "missionDefinitions" node in the CPACS format. Although taken from the documentation for CPACS version 3.4, the information contained is unchanged from the CPACS version 3.2 used during the generation of the example concepts in Sections 4.2 to 4.5.

Source: `https://www.cpacs.de/documentation/CPACS_3_4_0_Docs/`

altitude at mean sea-level.
Using this approach of break-down, any arbitrary mission can be defined and subsequently used by a dedicated design tool (provided it is compatible with the CPACS standard) to simulate the mission and compute the corresponding fuel mass, and for HEPS compatible tools electric energy, requirements.

8.2. Design Mission CPACS Segment Data

To enable a proper replication of the design workflows, detailed information about the specific constraints and end conditions imposed for the design mission are required. In Table 8.1, the prescribed data for each defined segment is presented. It should be noted that some segments ("taxi out" and "taxi in", "takeoff", and "approach/landing") are not included as a performed simulation, as they are at most only partially airborne. For those segments, the consumed fuel and electric energy are computed based on the engine performance prediction obtained using the devised methodology, as explained in Section 4.1.4.
The entry for the "segment type" for each defined segment in Table 8.1 corresponds to the extended differentiation to the CPACS standard introduced by the used mission simulation tool "AMC". Particularly important new segments types are "acc_dec_auto" and "holding_opti". The former is an acceleration and deceleration segment which determines the final velocity (either as CAS or Mach) depending on the specification of the subsequent segment instead of requiring a numerical value. In case of the latter, the distinction to the standard "holding" segment type is that the Mach number is consistently computed to find the optimum speed for loitering. The endCondition and constraint Mach number entries are re-defined to correspond to upper and lower bounds for these computations.

Table 8.1: Overview of the data prescribed for each individual segment in the definition of the design mission used for the generation of the example aircraft concepts.

Parameter	Value	endCondition/constraint
	Taxi Out	
segment type	taxi_out [a]	
duration	540 s (9 min)	endCondition
fuelConsumed	X.X kg[b]	endCondition
	Takeoff (Main Mission)	
segment type	take_off [a]	
CAS	128.6 $m \cdot s^{-1}$	endCondition
range/z	457.2 m	endCondition
duration	120 s (2 min)[c]	endCondition
fuelConsumed	X.X kg[b]	endCondition
energyConsumed	X.X J[d]	endCondition
thrustSetting	1.0	constraint
	Climb I (Main Mission)	
segment type	climb_cas_mach [a]	
range/z	3048 m (FL100)	endCondition
CAS	128.6 $m \cdot s^{-1}$ (250 kt)	constraint
machNumber	0.76	constraint

Continued on next page

Table 8.1: (cont.) Overview of the data prescribed for each individual segment in the definition of the design mission used for the generation of the example aircraft concepts.

Parameter	Value	endCondition/constraint
thrustSettings	1.0	constraint
	Acceleration I (Main Mission)	
segment type	acc_dec_auto [a]	
CAS	1[e]	endCondition
machNumber	0[e]	endCondition
	Climb II (Main Mission)	
segment type	climb_cas_mach [a]	
range/z	ICA m[f]	endCondition
CAS	144.0 $m \cdot s^{-1}$ (280 kt)	constraint
machNumber	0.76	constraint
thrustSetting	1.0	constraint
stepClimbAltitudeDifference	304.8 m (1000 ft [g]	constraint
rateOfClimb	1.524 $m \cdot s^{-1}$ (300 $ft \cdot min^{-1}$	constraint
	Acceleration II (Main Mission)	
segment type	acc_dec_auto [a]	
CAS	0[e]	endCondition
machNumber	1[e]	endCondition
	Cruise (Main Mission)	
segment type	cruise_step [a]	
altitude	12,192.0 m (FL400)[h]	constraint
machNumber	0.78	constraint
stepClimbAltitudeDifference	609.6 m (2000 ft)[i]	constraint
thrustSetting	0.99	constraint
rateOfClimb	1.524 $m \cdot s^{-1}$ (300 $m \cdot min^{-1}$)	constraint
	Deceleration (Main Mission)	
segment type	deceleration	
CAS	128.6 $m \cdot s^{-1}$ (250 kt)	endCondition
machNumber	0.76	endCondition
thrustSetting	0.001	constraint

Continued on next page

Table 8.1: (cont.) Overview of the data prescribed for each individual segment in the definition of the design mission used for the generation of the example aircraft concepts.

Parameter	Value	endCondition/constraint
	Descent I (Main Mission)	
segment type	descent_cas_mach [a]	
range/z	3048.0 m (FL100)	endCondition
CAS	128.6 $m \cdot s^{-1}$ (250 kt)	constraint
machNumber	0.76	constraint
thrustSetting	0.001	constraint
	Descent II (Main Mission)	
segment type	descent_cas_mach [a]	
range/z	457.2 m (FL15)	endCondition
CAS	128.6 $m \cdot s^{-1}$ (250 kt)	constraint
machNumber	0.76	constraint
thrustSetting	0.001	constraint
	Approach/Landing (Main Mission)	
segment type	approach_landing [a]	
duration	300 s (5 min)	endCondition
fuelConsumed	X.X kg	endCondition
energyConsumed	X.X J[d]	endCondition
	Takeoff (Alternate Mission)	
segment type	take_off [a]	
CAS	128.6 $m \cdot s^{-1}$	endCondition
range/z	457.2 m	endCondition
duration	96 s (1.6 min)[c]	endCondition
fuelConsumed	X.X kg[b]	endCondition
energyConsumed	X.X J[d]	endCondition
thrustSetting	1.0	constraint
	Climb I (Alternate Mission)	
segment type	climb_cas_mach [a]	
range/z	3048 m (FL100)	endCondition
CAS	128.6 $m \cdot s^{-1}$ (250 kt)	constraint
machNumber	0.63	constraint

Continued on next page

Table 8.1: (cont.) Overview of the data prescribed for each individual segment in the definition of the design mission used for the generation of the example aircraft concepts.

Parameter	Value	endCondition/constraint
thrustSettings	1.0	constraint
Acceleration I (Alternate Mission)		
segment type	acc_dec_auto [a]	
CAS	1[e]	endCondition
machNumber	0[e]	endCondition
Climb II (Alternate Mission)		
segment type	climb_cas_mach [a]	
range/z	7620.0 m (FL250)	endCondition
CAS	144.0 $m \cdot s^{-1}$ (280 kt	constraint
machNumber	0.63	constraint
thrustSetting	1.0	constraint
Acceleration II (Alternate Mission)		
segment type	acc_dec_auto [a]	
CAS	0[e]	endCondition
machNumber	1[e]	endCondition
Cruise (Alternate Mission)		
segment type	cruise_const_altitude [a]	
altitude	7620.0 m (FL250)	constraint
machNumber	X.X [k]	constraint
Deceleration (Alternate Mission)		
segment type	acc_dec_auto [a]	
CAS	1[e]	endCondition
machNumber	0[e]	endCondition
Descent I (Alternate Mission)		
segment type	descent_cas_mach [a]	
range/z	3048.0 m (FL100)	endCondition
CAS	128.6 $m \cdot s^{-1}$ (250 kt)	constraint
machNumber	0.63	constraint
thrustSetting	0.001	constraint

Continued on next page

Table 8.1: (cont.) Overview of the data prescribed for each individual segment in the definition of the design mission used for the generation of the example aircraft concepts.

Parameter	Value	endCondition/constraint
	Descent II (Alternate Mission)	
segment type	descent_cas_mach [a]	
range/z	457.2 m (FL15)	endCondition
CAS	128.6 $m \cdot s^{-1}$ (250 kt)	constraint
machNumber	0.63	constraint
thrustSetting	0.001	constraint
	Deceleration (Alternate Holding)	
segment type	acc_dec_auto [a]	
CAS	0[e]	endCondition
machNumber	1[e]	endCondition
thrustSetting	0.001	constraint
	Loiter (Alternate Holding)	
segment type	holding_opti	
duration	1800 s (30 min)	endCondition
machNumber	0.31[m]	endCondition
altitude	457.2 m (FL15)	constraint
machNumber	0.4[m]	constraint
acceleration	1.0 $m \cdot s^{-2}$	constraint
	Approach/Landing (Alternate Holding)	
segment type	approach_landing [a]	
duration	270 s (4.5 min)	endCondition
fuelConsumed	X.X kg	endCondition
energyConsumed	X.X J[d]	endCondition
	Contingency	
segment type	contingency	
fuelFraction	0.05	endCondition
	Taxi In	
segment type	taxi_in [a]	
duration	300 s (5 min)	endCondition

Continued on next page

Table 8.1: (cont.) Overview of the data prescribed for each individual segment in the definition of the design mission used for the generation of the example aircraft concepts.

Parameter	Value	endCondition/constraint
fuelConsumed	X.X kg[b]	endCondition

[a] The mission simulation tool (AMC) extended the standard CPACS segment type definition.
[b] The amount of consumed fuel/electric energy of the ground segments is updated during each design iteration to reflect the changes in the predicted engine performance (see Section 4.1.4).
[c] Includes the initial climb to 1500 ft.
[d] Unit used for consumed electric energy depends on applied convention and the standard used by the mission simulation design tool.
[e] For segments of type acceleration/deceleration, the endCondition for "CAS" and "machNumber" can also be specified as boolean 1/0 (True/False). This indicates, that the segment should accelerate/decelerate to the respective CAS/machNumber as specified in the subsequent segment.
[f] The final altitude of the last climb segment (ICA) is either a fixed input value or computed based on the optimum ICA as determined by the mission simulation tool during the previous design iteration step.
[g] Constraining the altitude variation during the final climb segment to multiples of 1000 ft guarantees cruise at exact flight levels.
[h] Imposing an altitude constraint during cruise prevents the mission simulation tool from potentially attempting to access engine performance data outside the data set in the performance map, thus preventing NaN-errors in the internal calculations.
[i] Prescribing an altitude change of 2000 ft for step-climb during cruise enforces the semicircular/hemispheric rule (see Table 4.4).
[k] Mach number for alternate cruise computed by openAD based on assuming same dynamic pressure as during design mission cruise.
[m] For the segment type "holding_opti" AMC redefined the "machNumber" inputs given for <endCondition> and <constraint> to represent the lower and upper bounds respectively

Bibliography

[1] D. Felix Finger, Cees Bil, and Carsten Braun. Initial sizing methodology for hybrid-electric general aviation aircraft. *Journal of Aircraft*, 57:245–255, 2020. ISSN 15333868. doi: 10.2514/1.C035428.

[2] Jacopo Zamboni, Roelof Vos, Mathias Emeneth, and Alexander Schneegans. A method for the conceptual design of hybrid electric aircraft. American Institute of Aeronautics and Astronautics Inc, AIAA, 2019. ISBN 9781624105784. doi: 10.2514/6.2019-1587.

[3] Reynard de Vries, Malcom T. Brown, and Roelof Vos. A preliminary sizing method for hybrid-electric aircraft including aero-propulsive interaction effects. American Institute of Aeronautics and Astronautics Inc, AIAA, 2018. ISBN 9781624105562. doi: 10.2514/6.2018-4228.

[4] C. Pornet, C. Gologan, P. C. Vratny, A. Seitz, O. Schmitz, A. T. Isikveren, and M. Hornung. Methodology for sizing and performance assessment of hybrid energy aircraft. *Journal of Aircraft*, 52:341–352, 2015. ISSN 0021-8669. doi: 10.2514/1.C032716. URL http://arc.aiaa.org/doi/10.2514/1.C032716.

[5] Tobias Hecken, Xin Zhao, Michael Iwanizki, Max J. Arzberger, Daniel Silberhorn, Martin Plohr, Konstantinos Kyprianidis, Smruti Sahoo, Giorgio Valente, Sharmila Sumsurooah, Micheal Sielemann, Clément Coïc, Andreas Bardenhagen, Annika Scheunemann, and Claire Jacobs. Conceptual design studies of "boosted turbofan" configuration for short range. volume 1 PartF. American Institute of Aeronautics and Astronautics Inc, AIAA, 2020. ISBN 9781624105951. doi: 10.2514/6.2020-0506.

[6] A. W.X. Ang, A. Gangoli Rao, T. Kanakis, and W. Lammen. Performance analysis of an electrically assisted propulsion system for a short-range civil aircraft. *Proceedings of the Institution of Mechanical Engineers, Part G: Journal of Aerospace Engineering*, 233:1490–1502, 2019. ISSN 20413025. doi: 10.1177/0954410017754146.

[7] Michael Iwanizki, Max J. Arzberger, Martin Plohr, Daniel Silberhorn, and Tobias Hecken. Conceptual design studies of short range aircraft configurations with hybrid electric propulsion. American Institute of Aeronautics and Astronautics Inc, AIAA, 2019. ISBN 9781624105890. doi: 10.2514/6.2019-3680.

[8] National Academies of Sciences. *Commercial Aircraft Propulsion and Energy Systems Research*. The Nathional Academies Press, 2016. ISBN 978-0-309-44096-7. doi: 10.17226/23490. URL http://www.nap.edu/catalog/23490.

[9] Ralph Jansen, Cheryl Bowman, and Amy Jankovsky. Sizing power components of an electrically driven tail cone thruster and a range extender. pages 1–9, 2016. ISBN 978-1-62410-440-4. doi: 10.2514/6.2016-3766. URL http://arc.aiaa.org/doi/10.2514/6.2016-3766.

[10] Marty K Bradley and Christopher K Droney. Subsonic ultra green aircraft research: Phase I final report, 2011. URL https://ntrs.nasa.gov/archive/nasa/casi.ntrs.nasa.gov/20110011321.pdf.

[11] Marty K. Bradley and Christopher K. Droney. Subsonic ultra green aircraft research: Phase II – volume II – hybrid electric design exploration, 2011. URL https://ntrs.nasa.gov/search.jsp?R=20150017039.

[12] Stefan Stückl, Jan van Toor, and Hans Lobentanzer. Voltair - the all electric propulsion concept platform – a vision for atmospheric friendly flight. pages 1–11, 2012. ISBN 9781622767540.

[13] Karen Davies, Patrick Norman, Catherine Jones, Stuart Galloway, and Mark Husband. A review of turboelectric distributed propulsion technologies for n+3 aircraft electrical systems. Institute of Electrical and Electronics Engineers, 2013. ISBN 9781479932542. doi: 10.1109/UPEC.2013.6714885.

[14] Charles E. Lents, Larry W. Hardin, Jonathon Rheaume, and Lee Kohlman. Parallel hybrid gas-electric geared turbofan engine conceptual design and benefits analysis. pages 1–12, 2016. ISBN 978-1-62410-406-0. doi: 10.2514/6.2016-4610. URL http://arc.aiaa.org/doi/10.2514/6.2016-4610.

[15] Lorenzo Raffaelli, Jae-Hoon Chung, and Ivan Popovic. Optimisation of a high bypass ratio turbofan engine using energy storage. 10 2016.

[16] Jason Welstead and James L. Felder. Conceptual design of a single-aisle turboelectric commercial transport with fuselage boundary layer ingestion. pages 1–18, 2016. ISBN 978-1-62410-393-3. doi: 10.2514/6.2016-1027. URL http://arc.aiaa.org/doi/10.2514/6.2016-1027.

[17] A. Sgueglia, P. Schmollgruber, N. Bartoli, O. Atinault, E. Benard, and J. Morlier. Exploration and sizing of a large passenger aircraft with distributed ducted electric fans. pages 1–33, 2018. ISBN 9781624105241. doi: 10.2514/6.2018-1745.

[18] Daniel P. Raymer. *Aircraft Design: A Conceptual Approach*. American Institute of Aerodnautics and Astronautics, second edition edition, 1992. ISBN 0-930403-51-7.

[19] Jan Roskam. *Airplane Design*. DARcorporation, 1985.

[20] Egbert Torenbeek. *Advanced Aircraft Design*. John Wiley and Sons, Ltd., 2013. ISBN 9781118568118. doi: 10.1002/9781118568101.

[21] Mark Voskuijl, Joris van Bogaert, and Arvind G. Rao. Analysis and design of hybrid electric regional turboprop aircraft. *CEAS Aeronautical Journal*, 9:15–25, 3 2018. ISSN 18695590. doi: 10.1007/s13272-017-0272-1.

[22] Maurice F.M. Hoogreef, Roelof Vos, Reynard de Vries, and Leo L.M. Veldhuis. Conceptual assessment of hybrid electric aircraft with distributed propulsion and boosted turbofans. American Institute of Aeronautics and Astronautics Inc, AIAA, 2019. ISBN 9781624105784. doi: 10.2514/6.2019-1807.

[23] Benjamin J. Brelje and Joaquim R.R.A. Martins. Electric, hybrid, and turboelectric fixed-wing aircraft: A review of concepts, models, and design approaches. *Progress in Aerospace Sciences*, 104:1–19, 2019. ISSN 03760421. doi: 10.1016/j.paerosci.2018.06.004. URL https://doi.org/10.1016/j.paerosci.2018.06.004.

[24] European Commission. Batteries europe: Strategic research agenda for 2020, 2020. URL https://energy.ec.europa.eu/system/files/2020-12/batteries_europe_strategic_research_agenda_december_2020__1_0.pdf.

[25] Stefan Stückl. Methods for the design and evaluation of future aircraft concepts utilizing electric propulsion systems, 2016. ISSN 0022-3751 (Print). URL https://d-nb.info/1107543258/34.

[26] M. J. Gouge, Jonathan A. Demko, Ben W. Mcconnell, Soumen Kar, and J. M. Pfotenhauer. Cryogenics assessment report related papers implement at ion plan for cryogenic r&d in support of t he ht s program, 2002.

[27] Airbus S.A.S. Customer Services. Airbus a320 - aircraft characteristics, airport and maintenance planning, 12 2020. URL https://www.airbus.com/content/dam/corporate-topics/publications/backgrounders/techdata/aircraft_characteristics/Airbus-Aircraft-AC-A380.pdf.

[28] Z. Berdowski, F. N. van den Broek-Serlé, J. T. Jetten, Y. Kawabata, J. T. Schoemaker, and R. Versteegh. Survey on standard weights of passengers and baggage final report, 2009.

[29] ICAO. *Part I-International Commercial Air Transport-Aeroplanes Operation of Aircraft International Standards and Recommended Practices*. International Civil Aviation Organization, eleventh edition edition, 7 2018.

[30] Sheng Chien Tan. Electrically assisted propulsion & power systems for short-range missions, 4 2018.

[31] E. Tarnowski. A320 family instructor support, 1 2001.

[32] David Kalwar. Integration of turbofan engines into the preliminary design of a high-capacity short-and medium-haul passenger aircraft and fuel efficiency analysis with a further developed parametric aircraft design software, 4 2015.

[33] Gerald Brown. Weights and efficiencies of electric components of a turboelectric aircraft propulsion system. 2011. ISBN 978-1-60086-950-1. doi: 10.2514/6.2011-225. URL http://arc.aiaa.org/doi/10.2514/6.2011-225.

[34] Arvid L Keith Jr. A brief study of the effects of turbofan-engine bypass ratio on short- and long-haul cruise aircraft, 1975. URL https://ntrs.nasa.gov/api/citations/19760004980/downloads/19760004980.pdf.

[35] R. J. Pera, E. Onat, G. W. Klees, and E. Tjonneland. A method to estimate weight and dimensions of aircraft gas turbine engines, 5 1977. URL https://ntrs.nasa.gov/api/citations/19770018227/downloads/19770018227.pdf.

[36] Periklis Lolis. Development of a preliminary weight estimation method for advanced turbofan engines, 2014. URLhttps://core.ac.uk/download/pdf/29409793.pdfhttps://dspace.lib.cranfield.ac.uk/handle/1826/9244.

[37] Gokcin Cinar, Dimitri N. Mavris, Mathias Emeneth, Alexander Schneegans, Carsten Riediger, Yann Fefermann, and Askin Isikveren. Sizing, integration and performance evaluation of hybrid electric propulsion subsystem architectures. 2017. ISBN 978-1-62410-447-3. doi: 10.2514/6.2017-1183. URL http://arc.aiaa.org/doi/10.2514/6.2017-1183.

[38] H Kuhn, A Seitz, L Lorenz, A. T. Isikveren, and A Sizmann. Progress and perspectives of electric air transport. volume 6, pages 4886–4899, 2012. ISBN 9781622767540 (ISBN). doi: 10.13140/RG.2.1.4833.4889. URL http://www.icas.org/ICAS_ARCHIVE/ICAS2012/PAPERS/947.PDF.

[39] C. Pornet and A. T. Isikveren. Conceptual design of hybrid-electric transport aircraft. *Progress in Aerospace Sciences*, 79:114–135, 2015. ISSN 03760421. doi: 10.1016/j.paerosci.2015.09.002. URL http://dx.doi.org/10.1016/j.paerosci.2015.09.002.

[40] Larissa Lorenz, Arne Seitz, H Kuhn, and Andreas Sizmann. Hybrid power trains for future mobility. volume 8785, pages 1–17, 2013.

[41] A. Emadi, Young Joo Lee, and K. Rajashekara. Power electronics and motor drives in electric, hybrid electric, and plug-in hybrid electric vehicles. *IEEE Transactions on Industrial Electronics*, 55:2237–2245, 2008. ISSN 0278-0046. doi: 10.1109/TIE.2008.922768. URL http://ieeexplore.ieee.org/lpdocs/epic03/wrapper.htm?arnumber=4493430.

[42] C. Friedrich and P.A. Robertson. Hybrid-electric propulsion for aircraft. *Journal of Aircraft*, 52:176–189, 2015. ISSN 0021-8669. doi: 10.2514/1.C032660. URL http://arc.aiaa.org/doi/10.2514/1.C032660.

[43] Arne Seitz, Oliver Schmitz, Askin T Isikveren, and Mirko Hornung. Electrically powered propulsion: Comparison and contrast to gas turbines. pages 1–14, 2012. ISBN 9036514444. doi: 281358.

[44] Xiaodong Zhang, K T Chau, and C C Chan. Overview of power networks in hybrid electric vehicles. *Journal of Asian Electric Vehicles*, 8:1371–1377, 2010.

[45] C. C. Chan. The state of the art of electric, hybrid, and fuel cell vehicles. *Proceedings of the IEEE*, 95:704–718, 2007. ISSN 00189219. doi: 10.1109/JPROC.2007.892489.

[46] K.T Chau and Y.S Wong. Overview of power management in hybrid electric vehicles. *Energy Conversion and Management*, 43:1953–1968, 2002. ISSN 01968904. doi: 10.1016/S0196-8904(01)00148-0.

[47] D. Felix Finger, Carsten Braun, and Cees Bil. An initial sizing methodology for hybrid-electric light aircraft. American Institute of Aeronautics and Astronautics Inc, AIAA, 2018. ISBN 9781624105562. doi: 10.2514/6.2018-4229.

[48] Oliver Schmitz and Mirko Hornung. Methods for simulation and analysis of hybrid electric propulsion systems. *CEAS Aeronautical Journal*, 6:245–256, 2015. ISSN 18695590. doi: 10.1007/s13272-014-0137-9. URL http://dx.doi.org/10.1007/s13272-014-0137-9.

[49] A.T. Isikveren, S. Kaiser, C. Pornet, and P.C. Vratny. Pre-design strategies and sizing techniques for dual-energy aircraft. *Aircraft Engineering and Aerospace Technology*, 86:525–542, 2014. ISSN 0002-2667. doi: 10.1108/AEAT-08-2014-0122. URL http://www.emeraldinsight.com/doi/10.1108/AEAT-08-2014-0122.

[50] Gokcin Cinar, Dimitri N. Mavris, Mathias Emeneth, Alexander Schneegans, and Yann Fefermann. Development of parametric power generation and distribution subsystem models at the conceptual aircraft design stage. 2017. ISBN 978-1-62410-447-3. doi: 10.2514/6.2017-1182. URL http://arc.aiaa.org/doi/10.2514/6.2017-1182.

[51] Ioannis Hadjipaschalis, Andreas Poullikkas, and Venizelos Efthimiou. Overview of current and future energy storage technologies for electric power applications. *Renewable and Sustainable Energy Reviews*, 13:1513–1522, 2009. ISSN 13640321. doi: 10.1016/j.rser.2008.09.028.

[52] Xing Luo, Jihong Wang, Mark Dooner, and Jonathan Clarke. Overview of current development in electrical energy storage technologies and the application potential in power system operation. *Applied Energy*, 137:511–536, 2015. ISSN 03062619. doi: 10.1016/j.apenergy.2014.09.081. URL http://dx.doi.org/10.1016/j.apenergy.2014.09.081.

[53] H Kuhn and A Sizmann. Fundamental prerequisites for electric flying. pages 1–8, 2012.

[54] D Linden, T B Reddy, A J Salkind, R O Hammel, A G Cannone, and F A Trumbure. *Handbook of Batteries*. 2002. ISBN 0071359788.

[55] Vinodkumar Etacheri, Rotem Marom, Ran Elazari, Gregory Salitra, and Doron Aurbach. Challenges in the development of advanced li-ion batteries: A review. *Energy and Environmental Science*, 4:3243–3262, 9 2011. ISSN 17545692. doi: 10.1039/c1ee01598b.

[56] Saad Khan, Khawaja Mehmood, Zunaib Haider, Syed Bukhari, Soon-Jeong Lee, Muhammad Rafique, and Chul-Hwan Kim. Energy management scheme for an ev smart charger v2g/g2v application with an ev power allocation technique and voltage regulation. *Applied Sciences*, 8:648, 2018. ISSN 2076-3417. doi: 10.3390/app8040648. URL http://www.mdpi.com/2076-3417/8/4/648.

[57] Taesic Kim and Wei Qiao. A hybrid battery model capable of capturing dynamic circuit characteristics and nonlinear capacity effects. *IEEE Transactions on Energy Conversion*, 26:1172–1180, 12 2011. ISSN 08858969. doi: 10.1109/TEC.2011.2167014.

[58] Ghassan Zubi, Rodolfo Dufo-López, Monica Carvalho, and Guzay Pasaoglu. The lithium-ion battery: State of the art and future perspectives. *Renewable and Sustainable Energy Reviews*, 89:292–308, 2018. ISSN 18790690. doi: 10.1016/j.rser.2018.03.002.

[59] Yoshiki Miyairi, Christopher Perullo, and Dimitri N. Mavris. A parametric environment for weight and sizing prediction of motor/generator for hybrid electric propulsion. pages 1–19, 2015. ISBN 978-1-62410-321-6. doi: 10.2514/6.2015-3887. URL http://arc.aiaa.org/doi/10.2514/6.2015-3887.

[60] Erik Odvářka, Abdeslam Mebarki, David Gerada, Neil Brown, and Cestmír Ondrůšek. Electric motor-generator for a hybrid electric vehicle. *Engineering MECHANICS*, 16:131–139, 2009.

[61] Ralph Jansen, Yaritza De Jesus-Arce, Peter Kascak, Rodger W. Dyson, Andrew Woodworth, Justin J. Scheidler, Ryan Edwards, Erik J. Stalcup, Jarred Wilhite, Kirsten P. Duffy, Paul Passe, and Sean McCormick. High efficiency megawatt motor conceptual design. 2018. ISBN 978-1-62410-570-8. doi: 10.2514/6.2018-4699. URL https://arc.aiaa.org/doi/10.2514/6.2018-4699.

[62] Askin T Isikveren, Arne Seitz, Patrick C Vratny, Clément Pornet, Kay Plötner, and Mirko Hornung. Conceptual studies of universally-electric systems architectures suitable for transport aircraft. *Deutscher Luft- und Raumfahrtkongress 2012*, pages Document–ID: 281368, 2012. ISSN 0002-9394. doi: 10.1038/ismej.2011.177.

[63] Michael Armstrong. Superconducting turboelectric distributed aircraft propulsion rolls-royce products today, 2015.

[64] Michael J. Armstrong, Christine A. H. Ross, Mark J. Blackwelder, and Kaushik Rajashekara. Propulsion system component considerations for nasa n3-x turboelectric distributed propulsion system. *SAE International Journal of Aerospace*, 5:2012–01–2165, 2012. ISSN 1946-3901. doi: 10.4271/2012-01-2165. URL `http://papers.sae.org/2012-01-2165/`.

III

Appendix

A

Background Information

This upcoming chapter presents all required background knowledge for the two main aspects of this project: the concept of hybrid-electric propulsion itself, and the electric component technologies that enable hybrid-electric propulsion.
The concept of using a hybrid-electric system to provide the propulsive power of an aircraft concept can be implemented in numerous ways. As such, hybrid-electric propulsion systems (HEPS) are typically categorised based on the connection order of its components. Different architectures offer different benefits, and accordingly suffer from different drawbacks. Appendix A.1 elaborates on the available HEPS architectures, as well as which metrics can be used to assess the performance of a hybrid-electric propulsion system, compared to a conventional equivalent.
Since clearly any form of propulsion system performance is dependent on it's constituent components, Appendix A.2 will provide an overview of the most important electrical components required. This overview includes a short introduction on the different types available, their characteristic behaviour, as well as the current state of the art performance. It should be noted, that the individual component types are discussed in more detail than required for the models used in the devised methodology.

A.1. Hybrid-Electric Aircraft Propulsion

It is important to understand, that hybrid-electric propulsion has not emerged as a challenge to conventional turbofan technology due to either a superior performance, nor as a complete solution to the problem of climate emissions. The true contender to the conventional turbofan propulsion of aircraft is the all-electric propulsion system. It is not only much more efficient at converting energy into propulsive power, but the specific power of electric motors is already comparable to contemporary turbofan engines, despite being at a significantly earlier stage of technological advancement. However, the energy density of any electric energy source available in the foreseeable future is Table A.2 prohibitively low, negating any advantage of the electric propulsion system. In light of the problems of both the conventional turbofan and all-electric propulsion concepts, multiple studies have identified hybrid-electric propulsion as the best near- to mid-term alternative [37–39].
In literature, a hybrid-electric propulsion system is typically defined as any system that utilises at least two different energy sources and/or energy conversion devices in such a way, that the overall performance exceeds the performance of each individual subsystem [40–42]. The core principle of HEPS is to use the synergy between different systems to improve the overall performance, typically combining the high energy density of hydrocarbon fuel with the efficiency and high power-to-weight ratio of electric components. There are numerous possibilities on how to implement a hybrid-electric propulsion system, and an accurate classification must therefore address the following three aspects:

1. **Constituent components:** What type of energy and power sources are incorporated in the propulsion system.

2. **Relative configuration:** How the constituent components are connected. This choice of architecture influences the working principle of the complete propulsion system (see Appendix A.1.1).

3. **Amount of power per component:** As the propulsion system no longer contains a singular energy and/or power source, the energy flow is no longer characterised by a single parameter (e.g.: fuel flow). The duality within the powertrain enables an individually optimised energy/power draw from each part, depending on the current situation or mission.

The first two aspects are self-explanatory: a HEP system equipped with a battery will behave differently than a system that uses a fuel cell; and a HEP system that is connected in a parallel architecture will display different performance characteristics than a series architecture system. The third aspect however, is the actual reason why hybrid-electric propulsion systems can improve the aircraft's performance (both in terms of a more powerful performance, as well as a reduced fuel consumption [a]). For transport aircraft, knowing the upcoming mission profile in advance allows the computation of the optimum power usage strategy, employing the optimal combination of conventional and electric propulsion to achieve the lowest possible fuel and/or energy consumption. Depending on the motivation of the airline, this translates into, for example, the lowest possible climate emissions or the lowest cost. The final responsibility to manage the power draw from each available source in this determined optimum combination lies not with the pilot but a specific component that is mandatory for any type of HEPS system: the Power Management And Distribution (PMAD) system. This system translates the pilot input (the selected thrust setting) into the desired energy and power draw for each component.

A.1.1. HEPS Architectures

In contrast to contemporary transport aircraft, where the propulsion system is classified as either "turbofan" or "turboprop" [b], hybrid-electric propulsion systems are unique in their immense variety of possible combinations. A generic HEPS architecture can consist of a multitude of different layouts, as illustrated in Figure A.1, and any system combination that can be formed with the various sources of energy and types of power converters is considered a valid HEPS concept [38].

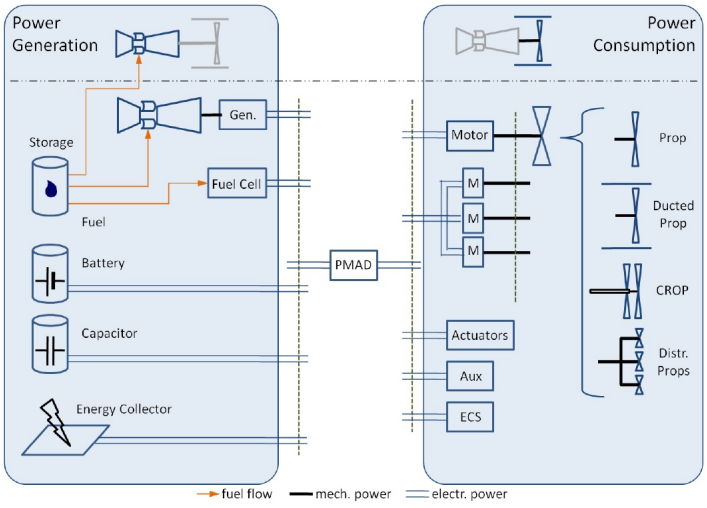

Figure A.1: Overview of all possible combinations of components in a generic HEPS architecture.

Source: [38]

From a quick inspection of Figure A.1, it becomes immediately apparent that the introduction of electric energy in the aircraft propulsion system has significant implications on the overall aircraft design and performance characteristics [43]. Battery-based HEPS systems change how much the aircraft mass reduces as the mission progresses; fuel-cell hybrid systems are likely to be designed to operate on hydrogen to make optimal use of the technology, which requires either a large volume (gaseous hydrogen) or a cryogenic high-pressure (liquid hydrogen) storage tank [8]; and incorporating multiple different power converters, or even distributed propulsion, has a drastic impact on the aerodynamic design of the aircraft concept. Furthermore, Figure A.1 emphasises the vital importance of the Power Mangement And Distribution (PMAD) system. Coordinating the interaction of the individual propulsion systems and enforcing the determined optimum power management strategy is what produces the potential benefits of hybrid-electric propulsion.

[a] One theoretical application of a hybrid-electric propulsion system to increase the performance of a fighter jet is a low-power parallel HEP system, that is not employed during normal operation but instead activates when the pilot requires a swift change in thrust. In this implementation, the electric motor would be used not to boost the produced shaft power, but to overcome the inertia that conventional turbomachinery engines encounter when the desired output power is changed.

[b] While "turbojet" airliner concepts obviously existed in the past, even high performance fighter jets have long since switched to using turbofan powerplants, albeit with low-bypass ratios (as early as the F-14, developed in the 1970s).

Series Hybrid-Electric Configuration

"In the series HEV [(Hybrid-Electric Vehicle)], the electrical energy is converted from the mechanical movement of the ICE [(Internal Combustion Engine)] first, and then, is used to propel the [vehicle]"[44]. This signifies that the power node is purely electrical (all power to the propulsor is provided by an electric motor); and that all energy extracted from the stored fuel is converted into electricity, which is then combined with the electrical power stored in e.g. a battery. The component layout typical for a series hybrid-electric architecture can be seen in Figure A.2: An internal combustion engine powered by a fossil fuel, which drives a generator that converts mechanical into electrical power. This electric power is then fed to the PMAD system, which connects to a secondary energy source (e.g. a battery) and the electric power converter. Depending on the current power requirements, the PMAD manages the energy flow: either drawing power from both sources to produce propulsive power; or using the power generated by the ICE to provide both propulsive power, as well as charge the battery.

The concept of a series hybrid-electric architecture is to extend the range of a fully electrically propelled vehicle, by eliminating the weight penalty imposed by electric energy storage. The series HEPS configuration utilises the high energy density of hydrocarbon fuel to provide the required energy for the mission, and uses the battery as a temporary energy storage to compensate for short-term variations in power draw. This definition can be found in multiple variations throughout literature [41, 45, 46], with a clear description of the defining feature being given by Chau and Wong: "[The] key feature of the series hybrid is to couple the engine with [a] generator to produce electricity for pure electric propulsion"[46]. This implies, that the electric motors have to be sized for the peak power requirement, while the ICE has to be sized for at least the nominal power output, depending on how large the installed battery capacity is.

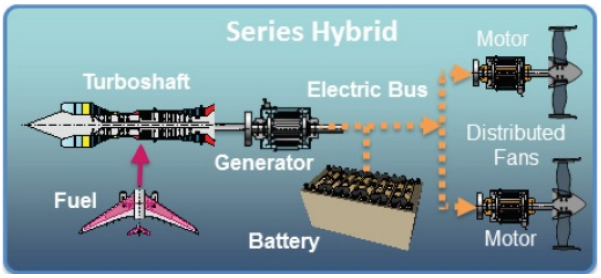

Figure A.2: Illustration of the connection of components in a typical series hybrid-electric architecture for aviation vehicles. Note, that the choice of "Distributed Fans" was made to illustrate the versatility of the architecture, it is equally valid to employ a single fan as propulsive device.

Source: [8, page 52]

A series architecture is considered as the simplest HEPS architecture and gains it's performance improvements from the fact, that the decoupled turbine engine consistently operates at it's highest efficiency point [41]. This provides the best possible use of the hydrocarbon fuel, allowing the maximum amount of energy to be extracted, because any power requirement that deviates from this optimum operating condition is compensated by the installed battery.

Parallel Hybrid-Electric Configuration

"In the parallel HEV, the [internal combustion] engine and the battery can drive the [propulsor] simultaneously. So [a] torque coupler is needed to connect them to the driveshaft" [44].

In contrast to the series configuration, the power node is mechanical, since both the ICE and the electric motor (EM) have to be connected to the propulsion unit. Figure A.3 illustrates the typical component layout of a parallel hybrid-electric propulsion system. The electric motor, purely battery-powered, is connected to the propulsor's driveshaft (here via the LP spool of the turbine engine). This allows it to either add power to the driveshaft, operate as a generator and extract excess power into electricity for later use, or to idle such that the propulsion system is effectively a conventional turbofan.

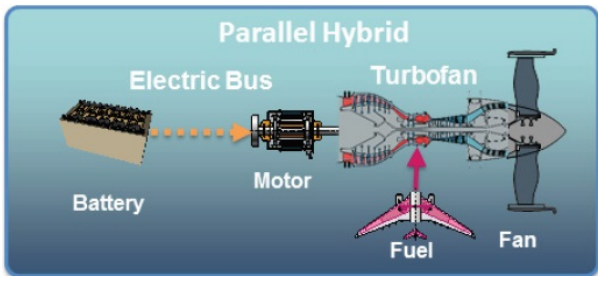

Figure A.3: Illustration of the connection of components in a typical parallel hybrid-electric architecture for aviation vehicles. Note, that some publications consider an aircraft concept that operates a conventional engine and an all-electric engine simultaneously as a parallel HEPS as well [47].

Source: [8, page 52]

Whereas the concept of a series HEPS architecture was to extend the range of an electric vehicle, the principle of a parallel configuration is to augment the conventional internal combustion engine. This concept was the basis for the typical definitions found in literature [45, 46]. Besides reducing the fuel consumption and emissions of the conventional ICEV, a further benefit is that the "total usable power output of

the parallel HEPS is given by the sum of both underlying sub-systems"[48]. This allows a parallel HEPS architecture to use smaller scale electric motors and internal combustion engines than a series HEPS architecture of comparable power output.

Series-Parallel Hybrid-Electric and (Partial) Turbo-Electric configuration

The series-parallel HEPS architectures is, as the name implies, the attempt to combine the series and the parallel configurations into a single system. The component structure is illustrated in Figure A.4, clearly showing the main problem of this architecture (especially for aviation): by combining both major HEPS configurations, this architecture contains more components than the specialised configurations, increasing the weight of the system. Since the added mass is already the driving complication of any hybrid-electric propulsion system, this deficit usually negates any performance improvement over the purely series *or* parallel HEPS architectures.

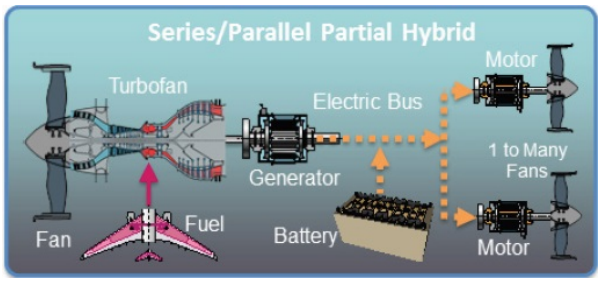

Figure A.4: Illustration of the connection of components in a typical series-parallel hybrid-electric architecture for aviation vehicles.

Source: [8, page 52]

In contrast to the series-parallel architecture's attempt at combing the two systems, the (partial) turbo-electric architecture can be considered a simplification of the two, which is illustrated in Figure A.5. The full turbo-electric configuration is basically a series HEPS powertrain without the battery, while the partial turbo-electric is essentially a parallel HEPS configuration without battery and with extra power extraction.

In a fully turbo-electric architecture as seen in Figure A.5a, not only the electric motor (see series HEPS architecture) but also the ICE have to be sized for the peak power requirement, as no battery is installed to compensate. This already negates the main advantage of a series HEPS system: that the ICE can operate continuously at it's maximum efficiency point. Furthermore, a fully turbo-electric propulsion system is expected to be both less efficient and heavier than the equivalent conventional system using a mechanical link [8].

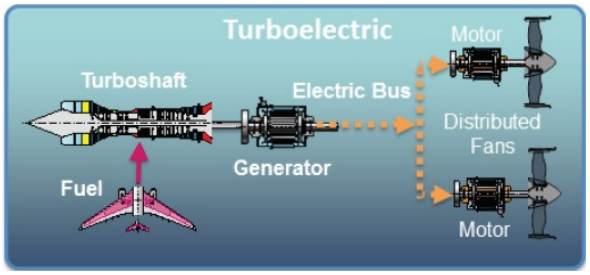

(a) Illustration of the connection of components in a typical turbo-electric architecture for aviation vehicles

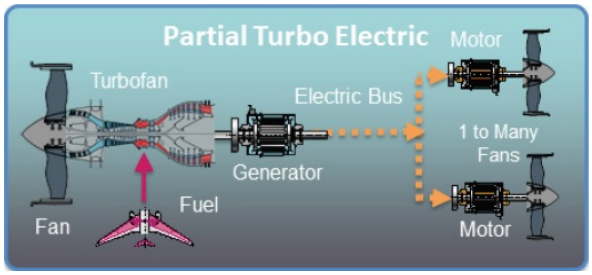

(b) Illustration of the connection of components in a typical partial turbo-electric architecture for aviation vehicles

Figure A.5: Illustrations of the two turbo-electric architectures for application in aviation vehicles found in contemporary literature.

Source: [8, page 52]

A partial turbo-electric architecture features an ICE that is providing power to both the propulsor as well as a generator, as illustrated in Figure A.5b. While it's component layout marks it as similar to a parallel HEPS configuration, the principle behind this architecture is the opposite: instead of augmenting the ICE with electric power, it uses the ICE to extract power to drive an additional electric propulsion system. It is debatable, whether the benefits provided by this auxiliary electric powertrain offset the penalties from the larger ICE[c].

The only real benefit provided by a turbo-electric configuration is the offered flexibility due to the electric part of the propulsion system. This can be used to enable further technologies, such as Boundary Layer Ingestion

[c]The only published study featuring a partially turbo-electric concept is the STARC-ABL. An overview of the concept, as well as a brief discussion on the presented improvements over its reference concept are provided in section 3.6 of the literature review preceding this thesis.

(BLI) or Distributed Propulsion (DP). Whether this flexibility is worth the incurred penalties depends on the offered benefits of the enabled technology.

A.1.2. HEPS Performance Metrics

The term 'performance' is the possibly most ambivalently used expression in the field of aircraft design. Depending on the objective of the performed research, it is used to: discuss the aircraft's physical performance, the maximum speed, acceleration, rate of climb, etc.; how efficient a concept is at performing a given mission, i.e. how much block fuel is used, how much fuel is consumed per passenger over a specific distance, how much climate damaging emissions are created, etc.; or even how cost-effective a certain concept is. Furthermore, different fields might evaluate a concepts performance based on the impact of a single, or a fleet of vehicles.
In this thesis, performance will be evaluated as the capability of a vehicle, and concepts will be directly compared based on the vehicle performance. As the focus is on hybrid-electric concepts, the "three fundamental principles of the feasibility assessment of electric flight", as defined by Kuhn et al. [38], will be used as a basis. These principles describe what is required to enable electric flight, with each consecutive principle adding a more demanding requirement. Below, all three principles are briefly summarised:

1. **Exergy concept:** "The usefulness of an energy carrier for aviation is determined by its specific exergy content, i.e. gravimetric and volumetric exergy density, rather than by its energy content"[38]. This principle specifies a requirement on the power system level (see Appendix A.1.2), and essentially describes that an energy source should be evaluated based on not only the energy density, but also how efficiently this energy can be converted into power.

2. **Specific power:** "The usefulness of an energy carrier in combination with power converter is fundamentally determined by their combined power density and exergy density [...]. These two metrics are the key indicators for electric aircraft feasibility when comparing alternative power sources"[38]. This extends the previous principle on the exergy density; the feasibility of an electrified propulsion system depends on the combined exergy and power density, rather than each individual component's.

3. **Hybridisation degrees of freedom:** "Two or more energy storage and power conversion devices that separately are inadequate for electric flight [...] may constitute an enabling power system when combined into a hybrid system"[38]. The final principle formulates a requirement on the vehicle level, allowing a comparison between vehicle concepts rather than propulsion systems. By combining various energy sources and/or power converters, the hybrid propulsion system uses the synergy between the individual components to achieve an overall performance improvement. The term 'Degree-of-Hybridisation' (DoH) is used as a measure of the electrification of the propulsion system.

Ultimately, the performance of any hybrid-electric propulsion system is determined by two aspects: the design and the operation of the system. During the design aspect, the propulsion system is sized such that it provides the largest performance potential; the choice of architecture and the individual components performance characteristics are the main focus. In contrast, the operational aspect determines how well the potential of the HEPS is realised. The core principle of hybrid-electric propulsion is to obtain a performance improvement by optimally manipulating the interaction of the individual subsystems. Only by operating the HEPS according to the determined optimum interaction can the overall performance, such as fuel burn or energy consumption, be improved [6].
Based on the three fundamental principles of electric flight state above, the parameters used to assess the performance can be categorised as being on either a power system or a vehicle level.

Power System Level Metrics

The metrics on a power system level deal with the performance of the power system as an isolated entity, removed from their interaction with the vehicle. On a conventional turbofan aircraft, the power system is completely defined by three independent types of parameters: the specific power of the engine; the component efficiencies, sometimes combined into a single parameter denoted as the overall efficiency; and the thrust specific fuel consumption (TSFC), adjusting the fuel burn for the developed thrust, to allow a comparison of different sized power systems. It is important to note, that any information on the fuel mass is part of the vehicle level performance. The amount of stored fuel is simply denoting how much energy is available, dictating how long the propulsion system can be operated; it has no impact on the performance of the power system itself [39].

As soon as an additional, electric energy source is introduced, these clear separations of the performance metrics disappear. A battery for example, is a combined energy storage and conversion device, meaning it stores electric *energy* but supplies electric *power* to the propulsion system (for more information on battery technology, refer to Appendix A.2.1). During the design process, the energy and power characteristics can therefore no longer be sized independently [39]. The key performance metrics as established for conventional propulsion system must therefore be extended to include information on the energy source. Referring back to the three fundamental principles, this is achieved via the inclusion of the exergy. Finally, the thrust specific fuel consumption has to be adapted to consider all available energy sources. The equivalent parameter is the thrust specific power consumption (TSPC), as described below.

Exergy and Specific Power As per the first and second of the three fundamental principles of the feasibility of electric flight, the main metrics used to assess the performance of an electrified power system are the exergy density and the specific power.
The official definition of exergy is "the part of the energy that can absolutely be converted into useful work" [38], which includes the effects of the individual subsystem component efficiencies [43]. By using exergy instead of energy for the power system comparison, the losses due to necessary energy conversion (e.g. from heat to mechanical power) are included. A good example of the implication of this effect is the comparison of kerosene fuel and batteries as energy storage. By accounting for the Carnot limitation present in the ICE, the apparent energy density gap is halved, dropping from a factor of 50–60 to only about 20–30 [38]. While this is still a significant deficit for batteries as energy storage, it clearly demonstrates the importance of using exergy over energy densities. It also emphasises, why hybrid-electric propulsion systems are currently considered the only realistic approach to introduce electric propulsion into commercial aviation.
In addition to the exergy density requirement, the second fundamental principle stated that a feasible power system must provide sufficient specific power. The propulsion system must be able to provide the required power output without incurring a prohibitively large weight penalty. For any propulsion system that contains (partial) battery-based electric energy storage, the attainable energy density and specific power are linked. This inherent characteristic of batteries imposes careful consideration during the sizing process, as both exergy and specific power have specified requirements.

Efficiencies The evaluation of the available exergy of any generic propulsion system requires knowledge of the efficiency of the complete system chain. A general definition of the overall efficiency η_{ov} for any motive power system in Equation (A.1) can be found in literature [43, 49]:

$$\eta_{ov} = \frac{P_{thrust}}{P_{supply}} = \eta_{EC} \cdot \eta_{TR} \cdot \eta_{PR} \tag{A.1}$$

The complete chain overall efficiency can be broken down into three sub-efficiencies: the energy conversion efficiency η_{EC}, equivalent to the core efficiency of conventional turbofan engine, covers the complete chain of energy conversion between the on-board sources and the power usable to drive the propulsor; the transmission efficiency η_{TR} relates the usable power to the propulsive jet power; while the propulsive power η_{PR} denotes how efficiently this propulsive jet power is producing thrust. This breakdown is more clearly illustrated in Equation (A.2), taken from [43].

$$\eta_{ov} = \underbrace{\frac{P_{useable}}{P_{supply}}}_{\eta_{ec}} \cdot \underbrace{\frac{P_{jet}}{P_{useable}}}_{\eta_{tr}} \cdot \underbrace{\frac{P_{thrust}}{P_{jet}}}_{\eta_{pr}} \tag{A.2}$$

For any propulsion system utilising two or more distinct energy sources, an analytical definition of the energy conversion efficiency η_{EC} is given in [49] as shown in Equation (A.3):

$$\eta_{EC} = \frac{P_{INS\ tot}}{P_{SUP\ tot}} = \frac{P_{INS_a} + P_{INS_b}}{P_{SUP_a} + P_{SUP_b}} \tag{A.3}$$

Ultimately, the overall efficiency is simply, as the name suggests, the cumulation of all component efficiencies.

Thrust Specific Power Consumption (TSPC) For a conventional power system, the possibly most important performance metric is the thrust specific fuel consumption (TSFC). It intuitively relates how fast fuel is consumed, without requiring any insight into the target vehicle size (since the value is normalised for the produced thrust). Due to the potential for multiple distinct energy sources of hybrid-electric propulsion, the measure of consumed fuel is no longer uniquely descriptive. To maintain the intuitive nature, the TSFC was simply extended to provide information on the power consumed per unit thrust (TSPC), instead of the limiting fuel consumption. This parameter is widely used in the area of hybrid-electric propulsion [4, 6, 43, 48], and easily computed.

$$TSPC = \frac{\sum_i P_{supply,\,i}}{T} = \frac{P_{sup}}{T} = \frac{V_\infty}{\eta_{ov}} \tag{A.4}$$

The definition shown in Equation (A.4) is universally valid, accounting for any combination of energy and power sources used in hybrid-electric propulsion. It is also easily related to the TSFC used in conventional, purely fuel-based propulsion systems (Equation (A.5)), allowing for a direct comparison of conventional and HEPS concepts.

$$TSPC_{conv.} = \frac{P_{sup}}{T} = \frac{\dot{m}_{fuel} \cdot FHV}{T} = TSFC \cdot LHV \tag{A.5}$$

Vehicle Level Metrics
In contrast to the power system level, the vehicle level metrics assess how a propulsion system will impact the performance of the entire vehicle. A common deficit of aircraft concepts using (partially) electric propulsion is a reduction in vehicular efficiency, due to the increase in its weight from the on-board electric energy storage [49]. The two metrics most prominent in literature are the Energy Specific Air Range (ESAR) and the Degree-of-Hybridisation (DoH).

Energy Specific Air Range (ESAR) Analogous to the TSPC, the ESAR is an extension of its conventional equivalent: the Specific Air Range (SAR), which "describes the distance travelled for a given unit quantity of fuel"[4]. It is widely suggested as a metric to assess the vehicle level performance of hybrid-electric concepts, as it describes the vehicle performance independent of the used energy source [4, 43, 48, 49].

$$ESAR = \frac{dR}{dE} = \frac{V \cdot \frac{L}{D}}{TSPC \cdot W_{A/C}} = \frac{\eta_{ov} \cdot \frac{L}{D}}{W_{A/C}} \tag{A.6}$$

As most variables in the definition given in Equation (A.6) are dependent on the aircraft operational conditions (L/D, η_{ov}, $W_{A/C}$, V), the ESAR has to be either treated as an instantaneous performance measure [43], or integrated over the complete mission to obtain the corresponding vehicular efficiency [4].
It is important to realise that the ESAR is not intended as a replacement of the conventional SAR, as they are not equivalent. "When considering a hybrid concept, because of the simultaneous consumption of different energy sources, the optimisation according to SAR and ESAR will lead to different optimums"[4]. Indeed, a key aspect when analysing hybrid-electric concepts, is to distinguish between concepts designed for minimum fuel or minimum energy consumption. Many HEPS concept achieve their lower fuel consumption compared to their reference designs by suffering from a higher energy consumption.

Degree-of-Hybridisation (DoH) The second vehicle level performance metric, the DoH, directly relates to the third fundamental principle on the feasibility of electric flight. It is a measure of the electrification of the propulsion system, and quantifies how much of the system energy and power is supplied by electric components and how much is obtained from the conventional system. As discussed in Appendix A.1, and illustrated in Figure A.1, any hybrid-electric propulsion system is characterised by two distinct aspects: the energy storage and the power production. It follows logically, that two distinct parameters are necessary to properly define the power and energy share of both individual systems. While the exact nomenclature varies throughout literature, the underlying premise is to express the share of the electric power and energy relative to the total propulsion system power and energy respectively [4, 39, 40, 49].

$$H_P = \frac{P_{EM}}{P_{tot}} = \frac{P_{EM}}{P_{EM} + P_{ICE}} \qquad H_E = \frac{E_{el}}{E_{tot}} = \frac{E_{el}}{E_{el} + E_{fuel}} \tag{A.7}$$

Equation (A.7) shows the most common definition of the power-based (H_P) and energy-based (H_E) Degree-of-Hybridisation. The power terms in H_P both refer the the respective *maximum installed* power of the electric motor and the total system, while the energy terms in H_E similarly refer to the *total stored* electric and combined (electric and chemical) energy. For a two-component hybrid-electric system, these two parameters are sufficient to completely define the state of the electrification of the propulsion system; any HEPS employing more than two distinct main components, obviously requires additional parameters to define the interaction of the extra components.
Both definitions for the DoH in Equation (A.7) are constant quantities for a HEPS aircraft design, independent on the chosen power control schedule. Any hybrid-electric concept can thus be assigned to a specific point in the (H_E, H_P) parameter space shown in Figure A.6a. This figure illustrates the available design space for hybrid-electric aircraft, representing all possible propulsion system architectures, including conventional and all-electric. The region corresponding to large H_E and small H_P is deemed "unfeasible", since the small electric power capabilities of such a concept would lack the ability to utilise the large available source of electric energy. The actual shape "is expected to have a more complicated shape, depending on the transport task to which a given system is designed"[40], but the illustration gives a good impression of the available design space.

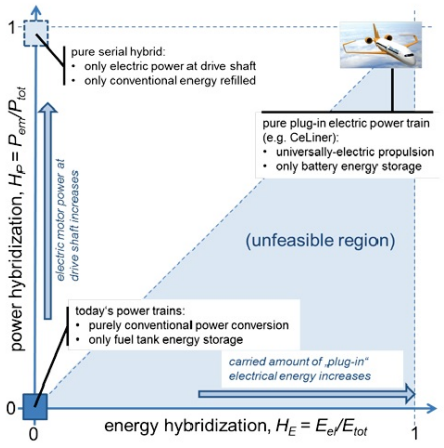

(a) Illustration of the parameter space for any hybrid-electric propulsion system, as defined by the power- and energy-based Degree-of-Hybridisation.

Source: [40]

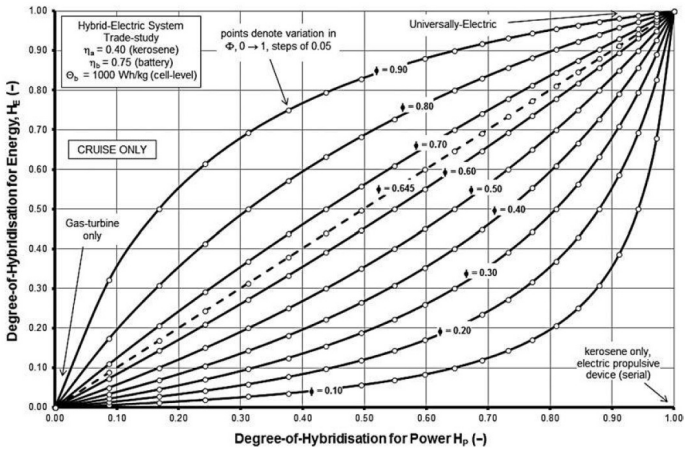

(b) Plot depicting an example trade study of a hypothetical HEPS concept for varying 'supplied power ratios' Φ and 'activation ratios' ϕ.

Source: [49]

Figure A.6: Two illustrations visualising the design space defined by the dependency power- and energy-based Degree-of-Hybridisation.

Figure A.6b explains the cause for the expected complicated shape of the border of the "unfeasible" region: The power-based DoH is directly determined by the 'Supplied Power Ratio' Φ, whereas the energy-based DoH is a function of both the 'Supplied Power Ratio' Φ and the 'Activation Ratio' ϕ [39]. In the figure the same design space as in Figure A.6a is presented, but the axes have been inverted as H_P is a monotonic function. Each displayed curve corresponds to a fixed 'Activation Ratio' ϕ and the full range of the 'Supplied Power Ratio' Φ, illustrating the non-linear relation of the power- and energy-based DoH.

'Supplied Power Ratio' Φ and 'Activation Ratio' ϕ During the discussion of the Degree-of-Hybridisation, two new parameters were introduced: the 'Supplied Power Ratio' Φ and the 'Activation Ratio' ϕ. The 'Supplied Power Ratio' in Equation (A.8) is defined as the ratio of the power supplied by source 'b' (typically the electric source) and the total power supplied by the propulsion system. It is easily understood and indicates how much of the currently supplied power is supplied by the secondary (electric) source.

$$\Phi = \frac{P_{sup,\,b}}{P_{sup,\,tot}} \tag{A.8}$$

$$\phi = \frac{\overline{\omega}_b}{\overline{\omega}_a + \overline{\omega}_b} = \frac{\frac{1}{T}\int_0^T \omega_b dt}{\frac{1}{T}\left(\int_0^T \omega_a dt + \int_0^T \omega_b dt\right)} = \frac{\int_0^T \omega_b dt}{\int_0^T \omega_a + \omega_b dt} \tag{A.9}$$

In contrast, the purpose of the 'Activation Ratio' is harder to understand. It is a notion of how active the specified energy source is over the performed mission, indicating how much of the utilised energy was drawn from source 'b' (again, typically the electric source). The definition in Equation (A.9) clearly implies, that the 'Activation Ratio' is an integrated parameter, and as such unique for each analysed design mission. It is based on the integration of the 'Power Control Parameters' ϖ_a and ϖ_b, which define how much of the maximum possible supplied power of each component is delivered to the propulsion system at a specific point in time. As such, the 'Power Control Parameters' represent the pre-defined power schedule for the analysed mission.

A.2. Electric Components

As the final performance of a hybrid-electric propulsion system is highly dependent on the constituent electric components, a detailed knowledge of different component aspects is required. While limited to the electric components necessary for a *parallel* HEPS architecture, the new methodology is planned to be modular to facilitate easy adaptation and easy the implementation of different component models. As such, the component models implemented into the devised methodology will of a lower level of detail than the information provided here.
The particular electric components detailed in this section cover the three major aspects of an electric propulsion system: the energy storage and power supply, the power conversion, and the distribution network. Energy storage and power supply for this project is limited to batteries, which is discussed in Appendix A.2.1. Power conversion between electrical and mechanical power is achieved using electric motors and generators, discussed in Appendix A.2.2. Finally, the network used to distribute the electric power throughout the propulsion system is discussed in Appendix A.2.3, the power transmission via normal- or super-conducting cables is detailed in Appendix A.2.4, and the thermal management system TMS is presented inAppendix A.2.5.

A.2.1. Energy Source: Battery

Batteries are an electrochemical system, generating DC electricity by converting chemical to electrical energy [37]. Although sometimes used interchangeably, "a battery is actually made up of at least two cells connected in series configuration"[50] , giving the battery a higher voltage than the individual cells. To achieve a desired battery voltage and current combination, a specific combination of cells connected in both series and parallel is required. The actual electrochemical reactions occur inside a cell between between two electrodes submerged in an electrolyte, activated by connecting an external load. These reactions involve a transfer of electrons from the negative electrode (anode) to the positive electrode (cathode) through the applied external circuit. In case of rechargeable batteries, the electrochemical reaction can be reversed by applying an opposite current in the external circuit, forcing electrons to move from the cathode to the anode [51, 52].

Battery Pack Characteristics

For the conceptual design phase of a battery-powered HEPS aircraft, the battery pack characteristics are much more relevant than the more minute cell level characteristics. The most defining characteristic of a battery is that it is a combined energy storage and power delivery devices [53]. The performance of any generic battery pack has to describe both its energy and power capabilities, so to allow for better comparison with other energy storage and power supply options, usually specific parameters are used. In terms of energy storage, a battery is usually defined by its gravimetric energy density, the amount of stored energy per unit mass in $\mathrm{Wh}\cdot\mathrm{kg}^{-1}$, and the volumetric energy density, the amount of stored energy per unit volume in $\mathrm{Wh}\cdot\mathrm{L}^{-1}$ or $\mathrm{Wh}\cdot\mathrm{m}^{-3}$. The power characteristics of a battery pack are assessed using equivalent gravimetric and volumetric power densities in $\mathrm{W}\cdot\mathrm{kg}^{-1}$ and $\mathrm{W}\cdot\mathrm{L}^{-1}/\mathrm{W}\cdot\mathrm{m}^{-3}$ respectively. Together with cycle stability and operational safety, the specific energy and specific power were the key focus of improvements during the last decade [12]. It should be noted, that depending on the publication, the quantity of stored energy per unit mass can be referred to as either specific energy, gravimetric energy density, or simply energy density; similarly the quantity of supplied power per unit mass can be referred to as either specific power, gravimetric power density, or power density. As a general guideline, it can be assumed that for aviation applications, either of those terms refers to the energy/power per unit mass. In case the actual energy/power per unit volume is considered, this is usually explicitly stated.
Another important characteristic of a battery is its current State-of-Charge (SoC). The SoC is the ratio of the remaining energy stored in the battery to the total amount that could be stored. Beyond the obvious information on how much energy is left to be used, this characteristic is especially important as most batteries suffer from degradation when discharged over a certain limit. These degradations are caused by the electrochemical reactions in the battery cells, and just like the energy and power capabilities, the maximum safe

level of discharge depends on the materials used. For current SoA Li-ion batteries, the maximum safe level of discharge is to 20 % of full charge [14].

The best current SoA battery packs are constructed from cells using lithium metal oxides as electrode materials.Such “lithium-ion battery systems with power capabilities greater than 10 MW and energy storage capacity greater than 10 MWh have already been demonstrated in stationary energy storage for electric utility applications" [8, p. 61], however, current SoA battery packs are still limited to specific energies below 300 $Wh \cdot kg^{-1}$ [38, 43]. Contemporary Li-ion batteries with good cycle performance achieve specific energies between 100-200 $Wh \cdot kg^{-1}$ and volumetric energy densities of 250-400 $Wh \cdot L^{-1}$, with a corresponding specific power of 1,800 $W \cdot kg^{-1}$. Experimental lithium-sulphur (Li-S) batteries with limited recharge cycles were able to increase the specific energy up to 350-380 $Wh \cdot kg^{-1}$ [12].

Battery Cell Characteristics
Although the scope of the thesis is limited to the battery pack level performance, it is important to understand the underlying technology. The overall performance of the battery pack is directly determined by the combined battery cell performance, which is a result of the underlying electrochemical reaction and the associated materials.
A battery cell is usually defined by two parameters: the cell voltage and the capacity. The cell voltage is the direct result of the reaction potential of the used materials and the capacity is a measure of how much load current the battery cell can provide over time [50]. The official SI unit is the Coulomb C, but for batteries it is usually given in Ampere-hours Ah, as this is more intuitive since it denotes the combination of how much current can be supplied for a given time. An important battery cell characteristic to note in relation to the capacity is that cell discharge exhibits a non-linear behaviour: "shorter discharge time has a negative effect on capacity due to unwanted side reactions"[50].
Due to this characteristic, battery discharge (also at pack level) is often discussed in terms of ’C-rates’. Every battery cell is usually rated for a specific discharge current, with the capacity being defined as the cell being capable of supplying the specified current for one hour. A "15 Ah" cell usually has a nominal capacity of "$Q = 15A$". Discharging the battery cell at 15 A, the cell is said the be discharged at 1C. Due to the non-linear discharge behaviour, discharging the cell at 1/15C (corresponding to a current of 1 A) would result in over 15 hours of energy supply; however discharging at 2C (or 30 A), the battery cell would be drained in under 30 minutes [50].
The total energy stored in a battery cell can be determined as the product of the cell voltage and the cell capacity. As stated above, the discharge rate influences the capacity, therefore it also influences the available energy. A high current draw on the cell results in a lower available energy. This phenomena is also the reason for the trade-off between specific energy and specific power in batteries. A high output power corresponds to a fast discharge, and the according reduction in available stored energy. The current SoA batteries with the highest specific energy are lithium-ion batteries, due to the lithium-ion cells having the highest capacity of currently available architectures. These cells use lithium metal oxides as cathode (positive electrode) materials and graphite as anode (negative electrode) material. The common lithium metal oxides used are lithium cobalt, lithium manganese, and lithium iron phosphate, all of which exhibit capacities lower than 170 $mAh \cdot g^{-1}$. The SoA anode material graphite performs better at a practical capacity of 350 $mAh \cdot g^{-1}$ [53]. These capacities result in the aforementioned limit of battery specific energies below 300 $Wh \cdot kg^{-1}$.
There are actually many other material options that yield higher capacities today, such as lithium-metal as a negative electrode. In a study investigating different potential combinations of electrode materials [53], lithium-metal anodes consistently obtained the highest specific energies. Unfortunately this material is not suitable to be used in commercial lithium cells due to its poor safety behaviour. Battery cells using lithium-metal anodes are susceptible to a high risk of thermal runaway, a failure mode in which the electrochemical reaction causes a continuously increasing temperature rise until the cell explodes and/or catches fire. A famous case of thermal runaway is the grounding of Boeing B787 aircraft due to battery failures[d]. The study conducted by Kuhn et al. [53] found that with novel combinations of electrode materials (e.g. silicon, germanium, tin, and nano-structured titanium-supported silicon for the negative anode; Sulphur, nano-structured tungsten disulfide (WS_2), and nickel-manganese-cobalt metal oxides ($Ni_yMn_yCo_{1-2y}O_2$) for the positive cathode) higher specific energies are possible. While the electrode combinations are predicted to exceed the current limit of 300 $Wh \cdot kg^{-1}$, they are still estimated to remain below 1,000 $Wh \cdot kg^{-1}$.

[d] see: https://www.scientificamerican.com/article/how-lithium-ion-batteries-grounded-the-dreamliner/, accessed: 15.03.2022, 11:04

Battery Performance Characteristics

The discharge characteristics of different battery types vary in shape, but follow the same principle. In an ideal battery, the discharge occurs at the constant theoretical voltage until the active materials are consumed, fully utilising the battery capacity and causing the voltage to drop to zero.

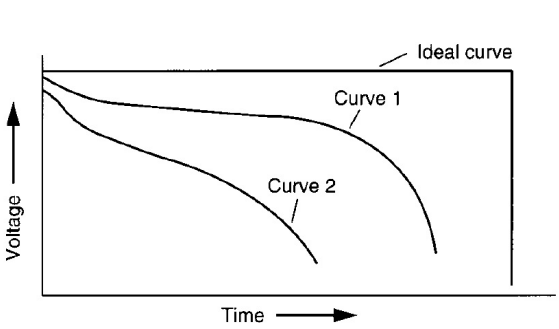

(a) Characteristic discharge behaviour of a general battery

Source: [54]

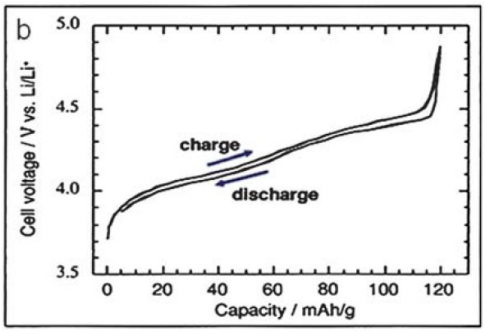

(b) Exemplary charge-discharge behaviour of a $LiMn_2O_4$ battery

Source: [55]

Figure A.7: Examples of battery discharge characteristics, showing the change in battery voltage against discharge time (a) or battery capacity (b)

The voltage of an actual battery will be lower than for the ideal case, as illustrated in Figure A.7a. Due to the internal cell resistance and the resultant *IR* drop and polarisation effects, the initial battery voltage will drop quickly upon start of discharge. During continued discharge the cell resistance will increase due to accumulation of discharge products and other factors, causing the voltage to decrease steadily as clearly shown in Curve 1. This steady decrease is relatively linear, and the battery is considered to operate in the "nominal region" during this time. The actual battery will not be able to utilise the full capacity, causing the voltage to drop off rapidly earlier than in the ideal case [54]. Curve 2 represents a battery with a higher internal resistance and/or a higher discharge rate, illustrating the non-linear correlation between capacity and discharge rate that is discussed in Appendix A.2.1. The curve illustrating a battery's voltage-discharge characteristic is typically displayed as either a dependency of discharge time, or in relation to the battery's capacity, as shown for a $LiMn_2O_4$ battery in Figure A.7b. The curve displays the same characteristic behaviour, albeit mirrored. A quick drop upon start of discharge, a steady decrease in voltage within the nominal region, and a quick drop-off upon depletion.

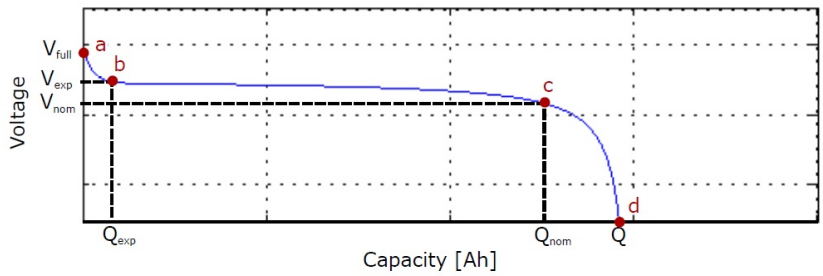

Figure A.8: Sample discharge curve for Li-ion battery, indicating characteristic points used for the Tremblay-Dessaint equivalent circuit model

Source: [50]

Because the general behaviour is the same for all types of batteries, it is possible to easily validate the accuracy of a battery model by comparing the simulated with a measured discharge curve. One approach for Li-ion batteries is an "equivalent circuit model", which can produce accurate results without going into details of the battery chemistry. A popular equivalent circuit model was developed by Tremblay and Dessaint [50], which requires only four characteristic points (see Figure A.8) on a batteries discharge curve to yield and accurate prediction.

An example discharge curved obtained using a Tremblay-Dessaint equivalent circuit model is shown in Figure A.9a. It clearly models the quick drop upon start of discharge, the steady decrease in the nominal region,

and the sudden drop-off upon depletion. The model operates using a single equation based on the characteristic points shown in Figure A.8 and is thus computationally light [56]. The discharge curves in Figure A.9b was generated using a more sophisticated electrical circuit model, where the electrical circuit of each cell is modelled using capacitor and resistor (*RC*) circuits. In addition, an even more complex hybrid battery model is used which replaces one of the *RC* circuits with a module using differential equations to capture the non-linear capacity variations of the battery [57].

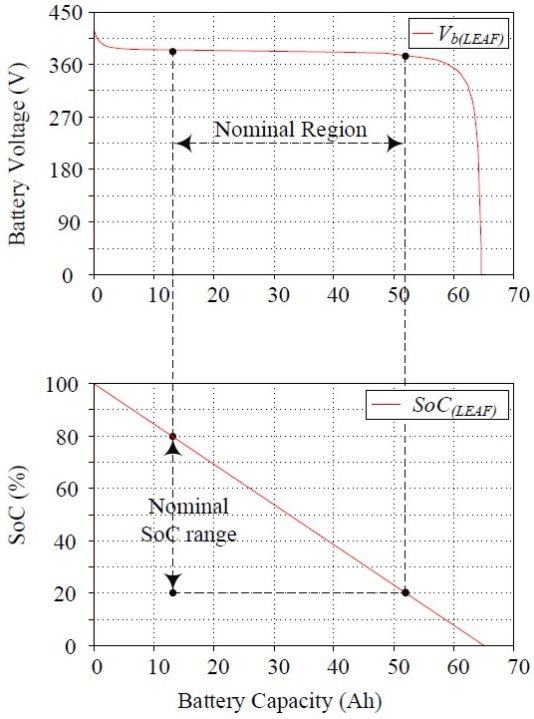

(a) Battery discharge curve and State-of-Charge (SoC) for a Li-ion battery used in a Nissan LEAF EV, simulated using a Tremblay equivalent circuit model.

Source: [56]

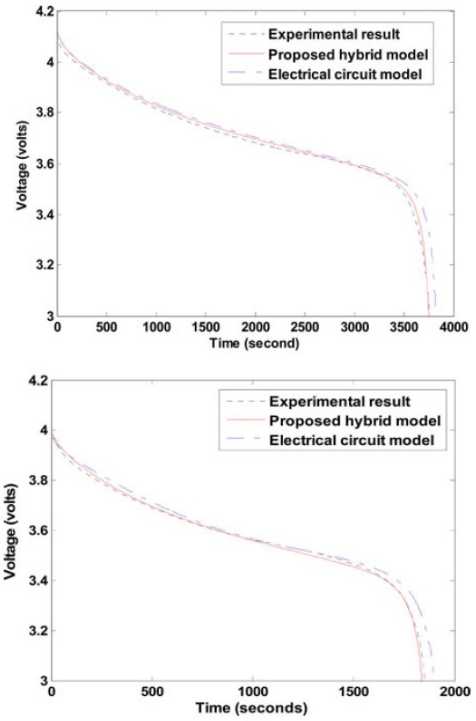

(b) Comparison of experimental and simulated discharge curves with constant discharge currents of 0.93C (above) and 1.86C (below).

Source: [57]

Figure A.9: Examples of simulated discharge curves using an equivalent circuit (a) and a more sophisticated electrical circuit (and enhanced hybrid) model (b).

For the purpose of the ongoing research into the conceptual design of HEPS for aircraft however, more simple battery models are employed. These models operate on battery pack level performance parameters, with the variation in discharge behaviour represented fully via the C-rate. The more sophisticated models were merely presented to give a brief overview of the possibilities on the degree of detail obtainable in battery modelling.

Energy-Power Interdependency

A battery is an integrated energy storage and power delivery device, meaning the energy storage and power supply characteristics are coupled. The charge capacity and charge mobility at a microscopic level in the battery cells determine the overall battery energy content and power performance [53]. The choice of electrode materials influences the cell's capacity, based on the underlying electrochemical reaction, while the power performance is dependent on how quickly these reactions can occur, meaning on how fast the reaction substances can travel between the electrodes.

Batteries experience a strong trade-off between high specific power and specific energy. The faster a battery cell is discharged (higher discharge current/C-rate), the lower the capacity and energy efficiency is [50]. These dependencies however are not linear, and a small reduction in specific energy can yield a large increase in specific power. According to Kuhn et al. [53], current commercial batteries at a discharge rate of 0.2C can achieve a specific energy of 245 $Wh \cdot kg^{-1}$ with an associated specific power of only 49 $W \cdot kg^{-1}$. Discharging the same battery at 1C instead, only slightly reduces the specific energy to 237 $Wh \cdot kg^{-1}$, but creates a significant increase in corresponding specific power to 237 $W \cdot kg^{-1}$. Of course, the 'increased' discharge at a rate of

1C indicates that the battery is actually meant to be discharged at these currents, and further increasing the discharge rate would likely cause a more drastic drop in specific energy.

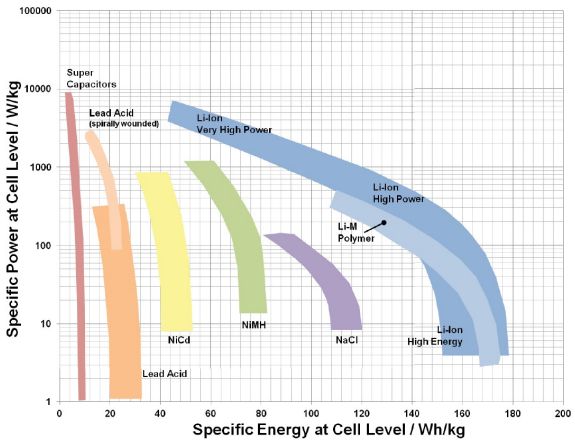

Figure A.10: Visualisation of dependency between specific energy and specific power of different battery technologies using a Ragone diagram. Technology status of 2008.

Source: [53]

A Ragone diagram offers an easy visual comparison of power and energy characteristics and was introduced in 1968 to compare different battery technologies [53]. Figure A.10 shows example Ragone diagrams for the most common current battery types. The diagrams are created conducting several individual measurements of the specific batteries at various discharge currents. It can generally be observed, that at low C-rates (high specific energy end of spectrum) a fast increase in power for a small reduction in energy capacity can be achieved. Only for high power conditions, the specific energy penalty becomes drastic. Today's batteries are optimised for either power or energy performance, limiting the usefulness for aviation purposes. However, Kuhn et al. [53] predict that future nano-structured electrode materials might eliminate this limitation. The nano-structuring allows for shorter diffusion paths of the ions, increasing the charge mobility and thus improving the power performance without encountering the capacity degradation.

Li-Ion Battery Overview

Of currently available batteries, the lithium-ion technology is the most promising for facilitating electrified propulsion. They offer high specific energy and power, which is essential for electro mobility [58]. Figure A.11 shows a comparison of different available devices for electrical energy storage. For aviation, a combination of high specific energy with good specific power capabilities is required. It is immediately apparent, that Li-ion batteries are the best choice of currently available technologies.

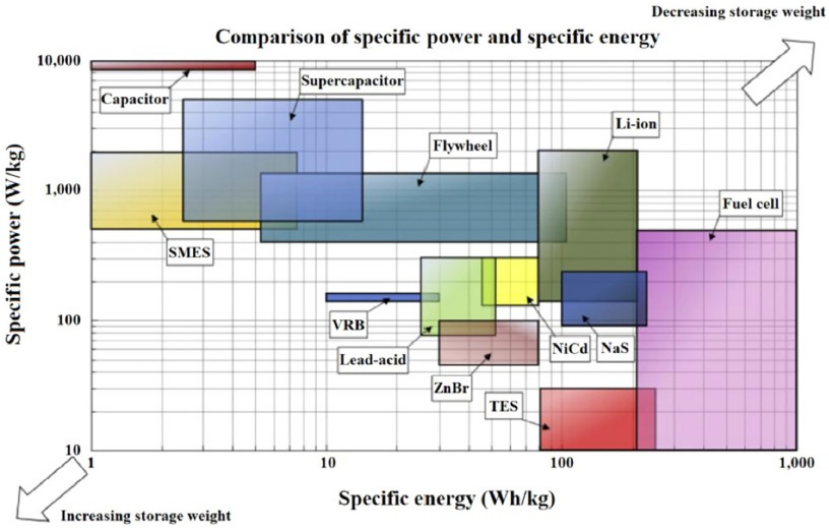

Figure A.11: Comparison of specific energy and specific power of various Electrical Energy Storage (EES) devices. Acronyms: SMES (superconducting magnetic energy storage), VRB (vanadium redox battery), ZnBr (zinc-bromine battery), NaS (sodium-sulphur), TES (thermal energy storage).

Source: [58]

Further reasons for the choice of lithium as main battery component is that it is widely available, non-toxic, and very light and electropositive (higher potential for energy storage). It is also, however, highly reactive, making it difficult to built safe battery cells. For this reason, current lithium cells are not using metallic lithium, but rather compounds that can donate lithium ions (Li+) [58].

The structure of a lithium-ion battery cell consists of four components: the two electrodes, the electrolyte, and a separator. During charging, the lithium ions move from the cathode (positive electrode) to the anode (negative electrode), during discharge the opposite occurs. Simultaneously to the ions moving from anode to cathode (discharging), electrons are moving from the anode to the cathode through the external applied load, generating the output current.

A lithium-ion battery is named after the lithium-ion donor in the cathode. Currently, five distinct lithium-ion

variants are produced: lithium cobalt oxide (LCO), lithium managanese oxide (LMO), lithium iron phosphate (LFP), lithium nickel cobalt aluminium oxide (NCA), and lithium nickel manganese cobalt oxide (NMC). Table A.1 gives a brief overview of the main characteristics of the five different Li-ion variants. Additionally, some individual aspects should be mentioned. LCO variant batteries have a very low inherent safety. The batteries used on the Boeing B787 aircraft that were grounded due to safety hazards were LCO Li-ion batteries [58]. LFP variants offer a wide SoC window with constant voltage between 15–100 % charge. NCA variants are usually produced with a blend of 80% nickel, 15% cobalt, and 5% aluminium. Additionally, Tesla opened a huge factory of NCA variant batteries, creating a cost benefit for NCA Li-ion batteries.

Table A.1: Overview of main characteristics of different lithium-ion battery variants, based on information in [58].

Li-ion variant	Specific energy	Lifetime	Typical application
LCO	150-190 $Wh \cdot kg^{-1}$	500-1,000 cycles	Used on B787 [e]
LMO	100-140 $Wh \cdot kg^{-1}$	1,000-1,500 cycles	E-bikes, power tools, medical devices
LFP	90-140 $Wh \cdot kg^{-1}$	up to 2,000 cycles	-
NCA	200-250 $Wh \cdot kg^{-1}$	1,000-1,500 cycles	Electric vehicles (e.g. Tesla)
NMC	140-200 $Wh \cdot kg^{-1}$	1,000-2,000 cycles	"dominates in EV and PHEV applications" [58]

These variants are a prime example to show how the battery characteristics are directly dictated by the electrode materials. It should be noted that the compounds used have a much higher impedance (AC equivalent to DC resistance) than metallic lithium. This impedance being the reason for both the reduced specific energies and the increased operational safety. The adverse effects of the increased impedance can be partially overcome by finely powdering and blending the lithium compound with a conductive carbon material. The usual cathode manufacturing process consists of powdering the lithium compound, blending it with conductive carbon and mixing the blend with a solvent (e.g. Nmethyl-2-pyrrolidone) and a binder (e.g. Pliy Vinylidene Flouride). The final paste is then applied onto an aluminium foil with leads to the electrode terminal [58].

Future Battery Performance Predictions

When researching the feasibility and fuel saving potentials of (hybrid-)electric propulsion concepts for aircraft, assumptions have to be made on the battery performance that will be available in the target year. These assumptions are often stated to be based on the predicted development in battery technology, however no further explanation is given on which changes are expected to yield these improvements.

Table A.2: Overview of common assumptions on development of battery technology found in hybrid-electric aircraft conceptual design publications, relative to year 2015.

	Time horizon	Specific Energy	Efficiency	Max. Discharge
Lents [14]	Current	200 $Wh \cdot kg^{-1}$	0.95	80%
	10 years	600 $Wh \cdot kg^{-1}$	0.96	85%
	20 years	1,000 $Wh \cdot kg^{-1}$	0.97	90%
Raffaelli [15]	20 years	750 $Wh \cdot kg^{-1}$	0.95	-

A good representation of the general development that is assumed in published papers is given by Lents et al. [14] and summarised in Table A.2. Lents et al. also stated, that battery technology is expected to improve by a factor of 5 to 10, which indicates that the presented 1,000 $Wh \cdot kg^{-1}$ in the 20 year horizon is on the lower end of expected improvements. This is clearly contradicting not only the estimation in other papers such as Raffaelli et al. [15], but also the information presented in the above sections. Clearly, the information obtained in publications dealing with battery technology directly is more likely to present accurate results than pub-

lications investigating aircraft concepts, therefore presented optimistic estimations should be treated with caution.
One source detailing predictions on future development of battery technology is the "Strategic Research Agenda for batteries 2020", published by the European Technology and Innovation Platform for the European Commission [24] . Within this publication, a detailed set of target key performance indicators (KPI) for battery technology for various applications are formulated. For the aviation sector, three distinct types of batteries (energy, power, and high power focussed) are considered, addressing the desired, and considered plausible, state of the technology for the year 2030. The KPIs related to the battery pack performance relevant for conceptual design are summarised in Table A.3.

Table A.3: Overview of the target key performance indicators for future battery development as formulated by the European Technology and Innovation Platform on Batteries [24, 62-64]. Provided data is limited to the battery performance parameters for the three battery types relevant for airborne transport.

Parameter	Operating conditions	Pack/Cell level	Unit	2020	2030
		Energy Battery, 250-100 kWh max. pack capacity			
Cell/Pack weight ratio		Pack	%	70	80-90
Charging time	Back to 80% SoC		minutes		30
Gravimetric energy density	2C discharge - 23 °C	Cell	$Wh \cdot kg^{-1}$		500-600
Cycle life	80% DoD, 23 °, 3C charge, 1C discharge	Cell	cycles	N/A	>3000
		Power Battery, 150 kWh max. pack capacity			
Cell/Pack weight ratio			%	70	80-90
Charging time	Back to 80% SoC		minutes		20
Gravimetric energy density	8C discharge - 23 °C	Cell	$Wh \cdot kg^{-1}$		450
Cycle life	80% DoD, 23 °C, 3C charge, 1C discharge	Cell	cycles	N/A	>3000
		High Power Battery, 100 kWh max. pack capacity			
Cell/pack weight ratio			%	70	80-90
Gravimetric energy density	30C discharge - 23 °C	Cell	$Wh \cdot kg^{-1}$		200
Cycle life	80% DoD, 23 °C, 3C charge, 1C discharge	Cell	cycles	N/A	>3000

A.2.2. Electric Motor and Generator

The general function of an electric motor is to convert supplied electrical power into mechanical power for propulsion [17]. This conversion is achieved through the interaction of a magnetic field and the current running through the conductors; by supplying a current, this interaction is generating a rotating force. Usually, the rotor contains the conductors carrying the current and reacts to the magnetic field generated by the stator, but the reverse is equally possible. The magnetic field of the stator can be created either using permanent magnets or an electric magnet using windings. In the case of a generator, the mechanical force is supplied

to the machine and the interaction with the magnetic field is in turn inducing a current running through the conductors.
While the first working electric motors date in the 1880s-1890s[f], research into compact and low weight machines started only recently with the emergence of e-mobility in the automotive industry [12]. Aviation is unique in its need for machines that simultaneously have high power, high efficiency, and a low mass [9], which caused a special interest in the development of High Temperature Superconducting (HTS) technology due to high promised specific powers and efficiencies [43]. Unfortunately, "power densities for aircraft applications lag the densities of other industrial applications such as automotive and ship, mainly because the stringent operating environment and safety certification requirements unique to aircraft add size and weight to electrical power system components"[8].
Generally, electrical motors are characterised by their high reliability, very high efficiency and their high specific powers. Current SoA motor efficiencies are in the order of 95% which, opposed to internal combustion engines, do not vary with altitude [17]. The performance of an electric motor is determined by the torque and speed characteristics [17, 37], which is discussed in more detail in Appendix A.2.2. Stückl et al. [12] as well as Jansen et al. [9] state that the most important requirements for electric machines in aviation are a high specific power (to minimise the weight) and high efficiency (to minimise losses and cooling requirements). Other requirements concerning safety (such as high reliability and robustness) and less obvious figures of metric such as dynamic and transient electrical performance, as well as the size also have to be considered [8].
One of the biggest problems in producing electric motors to be used in aircraft is the poor scaling behaviour of current machines. A current SoA motor by Siemens has a power capability of around 260 kW with a corresponding specific power of $5\,\mathrm{kW\cdot kg^{-1}}$ [50]. While the specific power is adequate for aviation needs (current gas turbine engines having specific powers in the range of 3–8 $\mathrm{kW\cdot kg^{-1}}$ [13]), power outputs in the MW-range are required for aircraft propulsion. A simple up-scaling of existing machines is infeasible, because the ratio of outer (cooling) surface to internal motor volume is getting worse with increasing size, an effect that hampers efficient heat dissipation. An approach increasing in popularity to solve this problem is the application of superconducting technology. Replacing the conductors on the rotor and/or the windings on the stator with superconducting materials, allows for significantly increased magnetic flux densities, with an associated reduction in weight and almost zero losses. The major disadvantage of this technology is the required cooling to either 5 K (LTS) or about 80 K (HTS). This necessitates the addition of a dedicated cryocooler with the corresponding weight penalty, potentially offsetting the gained benefits. In case a cryogenic fuel such as liquid hydrogen is used, the dedicated cryocooler and its weight penalty can be replaced for HTS materials, the storage of the cryogenic fuel however imposes its own added mass penalty.

Electric Motor Performance Characteristics
As stated above, the performance of an electrical motor is determined by its torque (T) and rotational speed (ω) characteristics. The mechanical output power is defined as the product of torque and the angular velocity, as shown in Equation (A.10), with the rotational speed often given in terms of revolutions per minute (RPM). Equation (A.11) provides the equation for the electrical power consumed in the motor, where I is the current, V the voltage, and η_{EM} the conversion efficiency from electric to mechanical power. Motor control is achieved via variations in the supplied voltage, handled by the Power Management And Distribution system (see Appendix A.2.3).

$$P_{mech} = T \cdot \omega = T \cdot 2\pi \cdot \left(\frac{n_{RPM}}{60}\right) \tag{A.10}$$

$$P_{elec} = I \cdot V = \frac{P_{mech}}{\eta_{EM}} \tag{A.11}$$

A feature that distinguishes electric motors from gas turbine engines, is that its power characteristics are largely independent of the operating condition. In Figure A.12 it clearly shows how the output power remains constant over a wide range of speeds [25]. Electric motors provide the maximum torque at low shaft speeds, with the torque starting to decrease once the maximum output power is achieved. This behaviour can be beneficial to overcome the inertial of turbomachinery parts when the electric motor is incorporated into a parallel-electric hybrid architecture and could also be used to autonomously start the engine. The constant output power for a wide range of shaft speeds is less important for aviation applications, as the engine is

[f] such as the DC motor designed by Sprague for the Chicago metro

mostly operating at constant speeds. A further, more influential, advantage of electric motors is that the power is also independent of altitude and Mach number, resulting in a much less sever power lapse rate compared to classical air-breathing engines [43]. In case of universally-electric configurations, this causes the electric motors to operate in part load conditions during TOC and cruise, since the thrust required for acceleration at takeoff is larger than the required cruise thrust.

The other defining characteristic besides output power is the motor efficiency. Although all types of electric motors, normal- and superconducting, are characterised by high efficiencies, the difference between 95% and 99% efficiency is still substantial. The efficiency is a measure of the losses occurring in the conversion of electrical to mechanical power, with the losses being equivalent to heat production. An increase in efficiency as stated above will result in the motor producing 5 times less heat, which is extremely important in electrical machines. Opposed to conventional internal combustion engines (ICE), where the waste heat leaves in the exhaust and is still contributing to the produced thrust, electrical systems absorb all waste heat locally. This absorption into the powertrain and structure requires active thermal management, adding additional weight and power requirements.

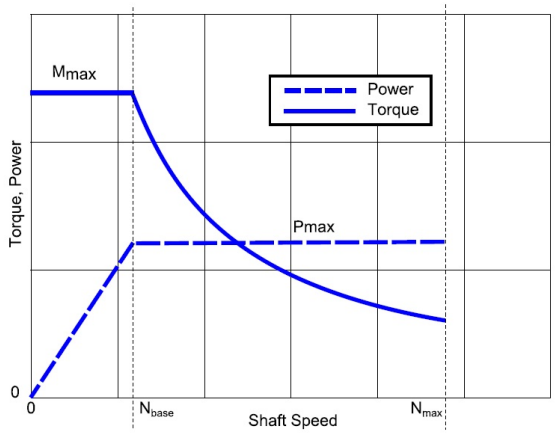

Figure A.12: Typical torque and power characteristics for variations in rotational speed of a generic electric motor

Source: [25]

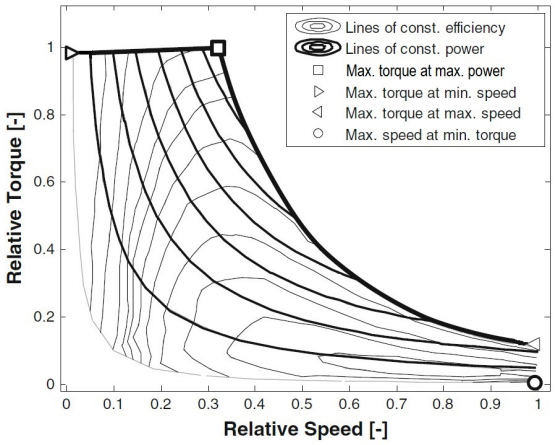

Figure A.13: Representation of a performance map for a generic electric motor.

Source: [48]

The overall performance of an electric motor is typically displayed as efficiency contours in the speed-torque plane [48, 50], sometimes with additional lines indicating constant power. An example of a performance map for a generic electric motor is displayed in Figure A.13. Besides the typical efficiency contours, this map also indicates lines of constant output power, the system boundary due to max. torque and max. power, and the characteristic boundary points. For computations, the performance map is often stored as a table or list, giving the efficiency as a function of rotational speed and torque. It should be noted, that when working with complete powertrain chains instead of isolated electrical machines, it is important for the bookkeeping to check whether the motor performance is already including losses caused by an integrated power inverter device or is for the machine only.

Generally, four main sources for losses in electric motors can be identified: *ohmic/copper losses*, *core/iron losses*, *friction and windage losses*, and other *miscellaneous losses*. The *ohmic losses* occur in the rotor and stator and are caused by energy dissipation into heating due to electrical resistance of the wires. It is proportional to the square of the applied current. This type of loss tends to be the largest contributor to total losses, especially in smaller machines. *Core losses*, mostly consisting of eddy and hysteretic losses, are caused by changing magnetic field effects in the core of the motor. *Friction and windage losses* are caused by the rotational motion, originating from the friction in the shaft bearings and the movement of the rotor through a medium (in conventional machines air), and are thus proportional to the shaft speed. The final *miscellaneous losses* groups all other losses that are independent of either torque or shaft speed. Cinar et al. [50] developed a loss model which can be used to predict the motor efficiency. The model assumes each type of loss to vary with either torque or shaft speed, and defines proportionality constants to predict individual losses. Ohmic and friction losses are assumed proportional to torque, while core and windage losses are assumed proportional to shaft speed. The total losses are the summation of all individual losses as defined in Equation (A.12), and is stated to be valid for all motor types. Proportionality constants are given by the letter k, the symbol T_f denotes the friction torque, and miscellaneous losses are defined as a constant C. Equation (A.13) provides

the corresponding equation to estimate the electric motor efficiency.

$$Total\ Losses = k_{ohm} \cdot T^2 + k_{core} \cdot \omega + T_f \cdot \omega + k_w \cdot \omega^3 + C \tag{A.12}$$

$$\eta_{EM} = \frac{T \cdot \omega}{T \cdot \omega + k_{ohm} \cdot T^2 + k_{core} \cdot \omega + T_f \cdot \omega + k_w \cdot \omega^3 + C} \tag{A.13}$$

It should be noted that the formula as given by Cinar et al. in [50] varies from the equation defined above by excluding the term denoting the friction power ($T_f \cdot \omega$). However, given that the paper contains an inconsistency between the defined total losses and their incorporation into the efficiency formula, and considering that the authors state in the text that "the total loss is given as the sum of all these losses" [50], it is assumed that the friction loss term is meant to be included.

Normal-Conducting Electric Motors
The most mature electric motor technology is using normal conductors, with different designs existing for both DC and AC electric power, whereby current AC machines are generally lighter than comparable DC machines [17]. An example of a current SoA normal-conducting electric motor is the Remy Motors Inc. HVH 250 series motor, as presented by Stückl et al. [12]. It achieves a specific power of 7–8 $kW \cdot kg^{-1}$ (excluding components for cooling and power control), 300 kW peak power capabilities in a speed range of 3000–4000 RPM. An overview of assumptions about the component performance parameters for current electrical motors, as published by various authors, can be found in Table A.4. It should be noted, that the majority of the presented assumptions are based on vehicle studies and are not reflecting existing machines. Only the data from the column "N.A.o.S." (National Academies of Sciences) is presenting their understanding of possible electric motor performance while considering the actual design of the motor, instead of considering it as a component within a vehicle design study.

Table A.4: Comparison of contemporary electrical motor component performance assumptions for various published studies.

Parameter	Unit	Lents et al. [14]	Kuhn et al. [38]	N.A.o.S. [8]	Miyairi et al. [59]	Welstead & Felder [16]	Jansen et al. [1] [9]
$p_{specific}$	$kW \cdot kg^{-1}$	6.6	2-10	2.2	3.3-4.9	13.16	13.0/6.0
Capability	MW	-	-	0.25	6.0	-	2.6/0.15
Efficiency	-	92%	-	-	93%	96%	96% / 96%

[1] Jansen et al. discussed electric machines for two concepts, the STARC-ABL and the NASA SCEPTOR. The first value refers to the STARC-ABL concept components whereas the latter value refers to the NASA SCEPTER concept components.

Chan [45] describes three types of normal conducting motors as being suitable for applications in universally-electric, hybrid-electric, or fuel cell electric vehicles: *Permanent Magnet (PM) motors* (synchronous or brushless), *Induction motors*, and *Switched Reluctance Motors (SRM)*. His paper details their use for automotive applications, however Jansen et al. list the same motor types but extend the list to include *Wound Field Machines*.

PM motors are characterised by exhibiting good performance in efficiency, torque, and power density simultaneously. They do however suffer from inherently short constant power ranges due to their limited field weakening capabilities. Additionally, the occurring back emf can become an issue and the inverter has to be designed to be able to withstand the maximum back emf of the stator winding [45]. These types of electric motors are widespread in traction applications due to their high power densities, compactness, and the availability of power electronics [60].

Induction motors are mostly chosen for their simplicity, robustness, and wide speed range. They do not suffer from back emf and their field-oriented control causes them to behave like DC machines. However, they are generally bigger than comparable PM machines and operate at lower efficiencies [45]. Still, induction machines are a mature technology and are also widely accepted in traction applications [60].

Switched Reluctance Machines are gaining interest in the aerospace industry because of several advantages. They consist of a simple and rugged construction and require only simple control. Additionally, SRM machines are capable of operating hazard-free and at extremely high speeds [45, 59]. According to Miyairi et al. switched reluctance motors are also "the best non-cryogenic motor in terms of power density in any power range"[59].

Figure A.14 shows a qualitative comparison of different types of normal-conducting electric motors. Inspection of the chart in combination with the established mounting interest in SRM systems shows, that while electric motors are typically selected based on their specific power and efficiency, other parameters can be equally important. Amongst those parameters are speed matching with the intended load or source, the ability to shut down a fault condition, thermal management constraints, and electrical system integration considerations [61].

	SR motor	AC motor	SPM motor	IPM motor
Usable in High Temperature	Good	Intermediate	Poor	Poor
High-speed Rotation	Good	Poor	Poor	Intermediate
High Environment Resistance	Good	Intermediate	Poor	Poor
Size and Weight	Intermediate	Intermediate	Good	Good
Vibration and Noise		Good	Intermediate	Intermediate
Efficiency	Intermediate	Poor	Good	Good
Fixed output variation range	Good	Poor	Poor	Intermediate
Startup Torque	Good	Intermediate	Intermediate	Good
Torque Density	Intermediate	Poor	Good	Good
System Cost	Good	Intermediate	Intermediate	Intermediate

AC: Alternating Current / SPM: Surface mounted Permanent Magnet / IMP: Interior Permanent Magnet

Figure A.14: Qualitative comparison of different normal-conducting electrical motors.

Source: [59]

Super-Conducting Electric Motors

Superconducting electrical machines are widely considered as a promising approach to overcome the limitations in specific power of large normal-conducting motors. Superconductors and the components in which they are used are typically differentiated depending on the required critical operating temperature below which they have to be cooled to become superconducting. Generally, materials with critical temperatures below 30 K are termed low-temperature superconductors (LTS), whereas materials that exhibit superconduction at temperatures above 30 K are called high-temperature superconductors (HTS). The discovery of HTS materials allowed for a wider technical usability of the superconducting technology [25]. Nowadays, HTS-based electrical machines are considered the most probable type of electric motor for aviation application, due to the weight-specific power being significantly higher than for normal-conducting machines [48].
Classic HTS motors/generators consist of cryogenic rotors equipped with superconducting coils, while the stator armature is non-cryogenic and operates close to ambient conditions. Because only the the rotor is using superconducting materials, these designs are sometimes considered as being "partially superconducting". Extending the use of superconductors to the stator yields "all-cryogenic", or "fully superconducting" machines, which offer double the power density of classical HTS machines [43]. The advantages of using HTS windings is due to superconducting wires being able to sustain much higher current densities compared to conventional conductors. These high current densities lead to reduced wire cross sections as well as increased magnetic field strength, resulting in weight reductions and larger motor torque respectively [25].
The major disadvantage of superconducting machines is their need for extremely low operating temperatures of some components. The cooling of these components requires a separate cryogenic fluid cooling system, which adds additional mass, volume, and complexity to the motor system, potentially negating the achieved increases in specific power [61]. There are two main options on how to achieve the required cooling. On aircraft concepts operating on cryogenic fuel such as liquid hydrogen, the fuel can be used as a low temperature heat sink (20 K in case of hydrogen) before it is used to power a turbine or fuel cell. In case the aircraft operates on conventional fuel and/or battery power, a dedicated cryogenic cooling device [25, 43] is required. According to publications by Seitz et al. [43], as well as Stückl et al. [12], various HTS machines in the MW class designed for airborne applications have been demonstrated and tested. Stückl et al. refer to a study

Table A.5: Comparison of contemporary component performance assumptions from various published studies for superconducting electric motors.

Parameter	Unit	Stückl et al. [12]	N.A.o.S. [8]	Davies et al. [13]	Miyairi et al. [59]	Stückl [25]
$p_{specific}$	$kW \cdot kg^{-1}$	8.0/>25.0[1]	0.2	3-8	16.4	6.6-7.5
Capability	MW	-	1.5	-	-	0.45-1.5

[1] values correspond to 3000 RPM and 20,000 RPM respectively

indicating that HTS machines can match turbo-shaft engines in terms of specific power, providing $8\,kW \cdot kg^{-1}$ at 3000 RPM and even achieving more than $25\,kW \cdot kg^{-1}$ at 20,000 RPM. An overview of the assumption as to component performance for contemporary superconducting machines from literature is given in Table A.5.

There are four main types of superconducting motors proposed for airborne applications: *Synchronous machines with superconducting excitation coils*, *trapped flux machines*, *superconducting homopolar machines*, and *fully superconducting machines*. The following description of the different systems are adapted from the PhD dissertation of Stückl [25].

Synchronous machines with superconducting excitation coils are possible in two variants: with a stationary normal-conducting armature and the superconducting excitation coils mounted on the rotor, or the reverse. In both variants, the excitation coils are supplied by DC electricity (due to AC problems of superconductors) to generate a magnetic field that is static in the coil-fixed frame. The coils are additionally located within a vacuum vessel containing an eddy current shield, to protect the superconductors from heat radiation and eddy current heat induction. Continuous superconducting operation is guaranteed via a dedicated cryogenic cooling system. To reduce the demands on the cryogenic cooling system, the stator armature which is supplied by AC voltage, is operating at room temperature and consists of resistive copper or aluminium.

Trapped flux machines are similar to the synchronous motor in that it consists of a stationary and resistive armature windings operating at room temperature in combination with a superconducting rotor. This is again generating a magnetic field that is fixed in the excitation coil frame of reference. Opposed to the synchronous motor however, the magnetic field is not generated by continuously supplying DC current to the superconductors, but by turning the HTS bulk material into a permanent magnet using a technique called "flux trapping". One of the defining characteristics of material being in a superconducting state is not only the zero resistance to DC electricity, but also that a magnetic field is unable to penetrate the bulk material. This phenomenon is known as the Meissner-effect. It was discovered however, that when placing a superconductor in its resistive state inside a magnetic field and then cooling it below its critical temperature, the outside magnetic field gets "trapped" in the material, effectively turning it into a permanent magnet. This effect persists until the material looses its superconductivity by heating above the critical temperature. The advantage of this approach is that no continuous current has to be supplied for the generation of the magnetic field during operation, reducing the overall weight, heat leak-in, and complexity of the motor.

Superconducting homopolar machines are tackling one of the fundamental problems caused by HTS materials. Contemporary HTS materials are made from ceramic materials, causing them to be brittle and more sensitive to vibrations. This is especially problematic in motors and generators that are intended to operate at high rotational speeds. The superconducting homopolar machine circumvents this problem by placing both normal-conducting armature windings as well as HTS excitation coils in the stationary part of the motor. The stationary HTS coils are used to magnetise a homopolar steel rotor that has two salient poles. This gives the machine the operational characteristics of a synchronous motor. According to Stückl [25], a 5 MW generator for aviation application using this technology has already been built and tested.

Fully superconducting machines are the final evolution of applying superconducting materials for electrical machines. The previously discussed partially-superconducting machines are limited to applying su-

perconductors to DC components. This is caused by the inability of superconducting materials to efficiently handle AC electricity, instead suffering from increased heat generation. Theoretically it is possible to also replace the conventional copper or aluminium wires in the armature windings with superconducting materials, further improving the weight savings. This does however require the cryogenic cooling system to be capable of continuously removing the heat from AC losses. Stückl states, that for contemporary "state of the art cooler technology and the AC tolerances of available HTS materials, the associated cooler weight would more than offset any weight advantage coming from superconducting materials"[25]. With future advances in HTS AC losses and cryo-cooler technology, it could however be possible to better exploit the potential of fully superconducting machines.

Cryogenic Cooling Systems

Although not being part of the components considered during the development of the sizing methodology — excluding the possibility to roughly account for the added mass when selecting an overall specific power for the HEPS thermal management system component — a brief discussion of a dedicated cryo-cooling system is presented here. The following description is adapted from the PhD thesis of Stückl [25], which contains a detailed but concise overview of this topic.

To achieve a superconductive state, the materials must be operated below their critical temperature, typically in the range of 20–80 K. Although the conductors are thermally isolated, the current running through them is inducting heat due to conduction and, potentially, further AC losses. The most common principle for cryogenic cooling designs are the Stirling-, Gifford-McMahon-, and Brayton cycles. Depending on the intended temperatures, the working fluids are chosen between different gasses with low boiling point. The usual options are hydrogen, helium, argon, neon, or nitrogen.

Cryo-coolers operate by transferring heat from a low temperature medium to a higher temperature medium and their maximum theoretic efficiency is the Carnot-efficiency (ϵ) as stated in Equation (A.14). However, real machines cannot achieve this theoretical efficiency because of mechanical losses and non-optimal thermodynamic cycles. To model this deficiency, an additional efficiency - the component efficiency (η_{comp}) - is defined. Using both efficiency terms, a relation between the mechanical input power (P_{cool}) required and the heat load (Q_{cool}) to be removed from the cryogenic superconductors can be established, as given in Equation (A.15).

$$\epsilon = \frac{T_l}{T_h - T_l} \tag{A.14}$$

$$P_{cool} = \frac{Q_{cool}}{\epsilon \cdot \eta_{comp}} \tag{A.15}$$

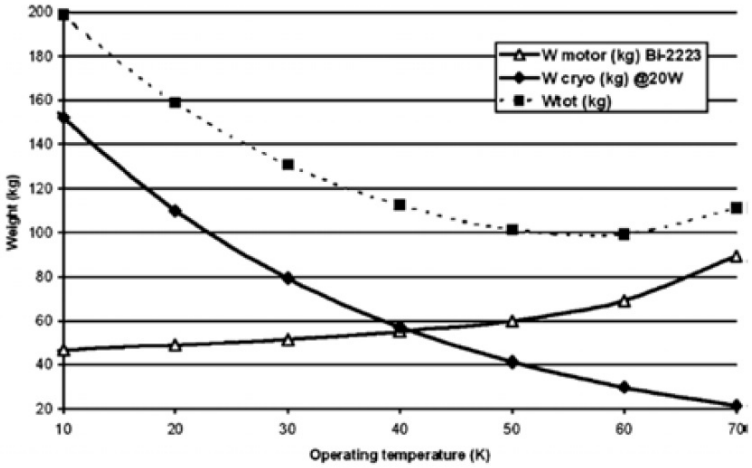

Figure A.15: Overview of dependency of weight on operating temperature of a superconducting motor, the corresponding cryogenic cooler, and the combined system weight.

Source: [25]

The biggest problem with current cryocoolers is their high weight and bulky dimensions. Current SoA ground based systems provide a specific weight of 14 kg · kW^{-1} of heat input power and achieve component efficiencies in the magnitude of η_{comp} = 30%. Optimising the systems specifically for aviation purposes allows for significant weight savings, especially when based on the Brayton cycle, due to the use of a turbo-compressor. Studies working on low-weight designs for aviation applications aim for specific weights of around 3 kg·kW^{-1} at 30% Carnot efficiency. These lightweight designs however are not yet validated, nor have airworthiness requirements for safety and reliability been proven.

It is fairly obvious that the weight dependency of superconducting motors and cryogenic coolers on operating temperature is oppositely proportional. The colder the operating temperature, the lighter the motor design for a given output power, because the current density can be further increased. The cryogenic cooler on the other hand increases in weight because more heat has to be removed from even lower temperatures. Any propulsion system design using superconducting motors with cryogenic cooling should therefore established the system offering the optimal combined weight and performance. The weight variations with selected operating temperature for a 150 kW HTS motor (DC rotor rotating at 3000 RPM) from a study by Masson et al. were used as an example by Stückl, as displayed in Figure A.15. The combined system has a minimum weight in the temperature range of 50–60 K, clearly showing the importance of using a combined optimum approach for the design.

Current Research and Future Predictions

The choice of assumption for the performance of future electric machines is often what determines whether a researched concept is performing well or not. As such it is important to analyse what the common assumption for component performance - primarily specific power and efficiency - used in vehicle studies are, and what the current research for electric machines is indicating as expected realistic improvements. Figure A.16 gives an overview of what size electric machine (measured in mechanical output power capability) is expected to be used in different aircraft classes. It also indicates what is expected to be the largest electrical machine that can be installed on an aircraft for different time horizons.

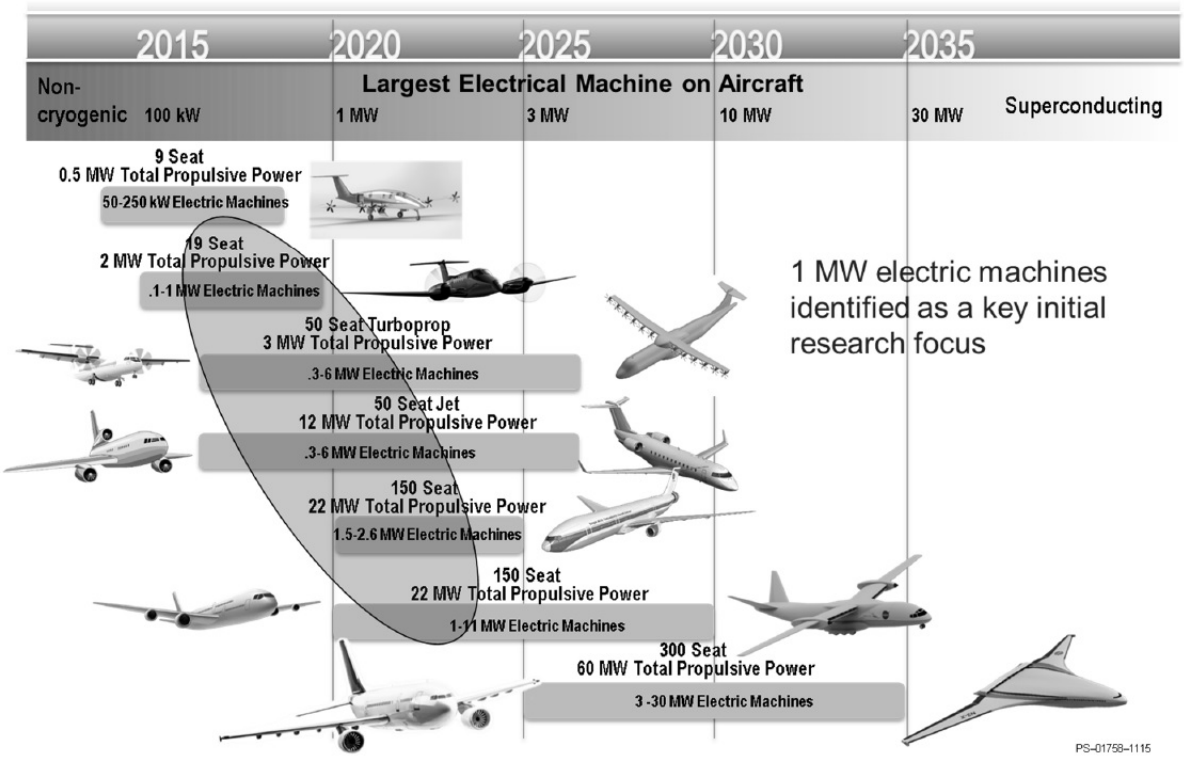

Figure A.16: Predictions on development of electric machine sizes used on future aircraft.

Source: [9]

The figure clearly shows how the trend of electrification is expected to progressively move from small to larger aircraft sizes, mostly due to available power capabilities but also due to weight and safety limitations. While it might appear that the shown information is outdated - currently no electric motors are used in either 50 PAX turboprop or 50 PAX jet aircraft - it should be noted that the figure refers to electric machines rather than electric motors. Especially with the increasing trend towards More Electric Aircraft (MEA), the size of the installed generators is steadily increasing. An example of this is the Boeing 787 aircraft, which employs four generators with a combined electrical power output of 1 MW [8].
Due to the wide spread of applicable electric machine sizes of transport aircraft, Jansen et al. identified 1 MW machines as a key enabler of propulsion electrification [9]. The reason being that this size machine can be used on many different aircraft classes, depending on the approach to electrification taken (providing only boost power, fully hybrid-electric cruise, universally-electric).
Many research programs are currently investigating possibilities of increasing the performance of electric machines, especially in regards to their power capabilities and specific powers. Table A.6 gives an overview of the stated goals of some of the major ongoing electric machine research projects, with an intended time horizon differing between 3 and 20 years. The values stated in the column labelled "N.A.o.S" are what the committee of the National Academy of Sciences considers realistic estimates.

Table A.6: Overview of stated goals of current research programs for normal-conducting electric machines, including the projections of realistic performance from the committee of the National Academies of Sciences (N.A.o.S.). Adapted from [8, see table 4.3].

	Unit	NASA		U.S. Air Force [1]	Ohio State Univ.		Airbus	N.A.o.S.
Horizon		10 year	20 year	20 year	3 year	5 year	15 year	20 year
Capability	MW	1–3	5–10	1	0.3	2	-	1–3
Specific Power	$kW \cdot kg^{-1}$	13.0	16.0	5.0	15.0	15.0	10.0–15.0	~ 9

[1] Stated goal for specific power includes required packaging for use on an aircraft

Besides research in normal-conducting machines, the improvement of superconducting motors and generators is also being investigated. According to Jansen et al. [9], this research is currently more focused on completing a 1 MW demonstration of a fully superconducting motor, rather than investigating means of increasing the performance of existing machines. The stated machine is an advancement over current SoA motors in that is uses superconducting materials on both the rotor and stator. The distinction is the application of novel superconducting wire that is expected to enable the use of AC currents in the stator, which was not possible before due to the limiting AC losses of conventional superconducting wires. Another study investigating fully superconducting machines is the NASA URETI program. According to Davies et al. [13], the study predicts that specific powers of $40\,kW \cdot kg^{-1}$ and $66\,kW \cdot kg^{-1}$ are achievable in the N+3 timeframe for fully superconducting motors and generators respectively.
The information available for current research in normal- and partially-superconducting machines is a bit more extensive. One such effort is the Advanced Air Transport Technology (AATT) project by NASA, which is the successor of the NASA Subsonic Fixed Wing Project. It defined a subproject called the Hybrid Gas Electric subProject (HGEP) which extends the research in advanced motors without application of superconduction. The goal of the program is the demonstration of a MW class electric motor with efficiency >96% and a specific power of $13.2\,kW \cdot kg^{-1}$. According to Jansen et al. two projects are being conducted under this program, each following a different approach: Using a Permanent Magnet Synchronous design versus an induction motor design. Both projects however are required to deliver a hardware and performance demonstration at 1 MW level, as well as a scalability study to the 10 MW scale [9].
The other major research project is also funded by NASA and is developing a High Efficiency Megawatt Motor (HEMM). The key objective of this program is to establish a motor with simultaneously high specific power ($>16\,kW \cdot kg^{-1}$) and high efficiency (>98%). A detailed description of the developed motor can be found in the paper by Jansen et al. [61], but a general overview is given in the following paragraphs. The requirements established for the motor design are based on the NASA STARC-ABL concept [9]: the rated output power should be 1.4 MW or grater; the specific power should exceed $16\,kW \cdot kg^{-1}$; the machine efficiency should exceed 98%; the operating speed should be 6800 RPM; and the thermal management should be based on fluid cooling designed for an inlet temperature of 60 °C. A comparison of the stated requirements and the estimate performance of the final design can be found in Table A.7.

The design of the HEMM is a wound field type machine, combining a superconducting rotor and a normal-conducting stator operating at ambient temperature. The rotor is cryogenically self-cooled, thus preventing the weight penalty of an external cooler, and the stator is semi-slotless using a typical fluid or air cooling loop. In the prototype presented, the stator cooling was designed using dielectric oil with an input temperature of 60 °C. Because of the self-cooling characteristic of the superconducting rotor, the HEMM "essentially operates like any traditional (non-superconducting) motor when viewed externally as a system" [61]. The choice for a wound field type machine was based on trade studies for balanced performance, but it offers the additional benefit of being able to be shut down by de-energising the field winding. This allows the motor to remove force from the drive shaft without any mechanical decoupling.

Table A.7: Comparison of formulated requirements and final estimate performance for the HEMM partially-superconducting motor, including additional estimate performance characteristics for the motor and incorporated cryogenic cooler.

	Parameter	Unit	Requirement	Estimate Performance
Motor Design	Operating Power	MW	1.4	1.42
	Specific Power	$kW \cdot kg^{-1}$	>16.0	17.4
	Efficiency	-	>98%	98.9%
	Operating speed	RPM	6800	6800
	Thermal management		fluid cooling (60 °C inlet temperature)	
	Torque	$N \cdot m$	-	2,000 (constant for 0–7500 RPM)
	Mass	kg	-	81.9 (74.4 estimate + 10% margin)
	Losses	kW	-	26.2 (13.5 losses + 20% margin)
Cryocooler	Cooling power (heat)	W	-	50
	Cold tip temperature	K	-	50
	Rejection temperature	K	-	300
	Mass	kg	-	<10
	Diameter	mm	-	<100
	Allowable rotation	RPM	-	6800 [1]

[1] required for integration into motor shaft

As stated above, the cryo-cooler required for the superconductors in the rotor is integrated into the rotor itself, with the cold tip of the cryo-cooler being connected to the superconducting coils via conduction. This removes the need for external cryogenic fluids or other equipment. The design of the cryogenic cooler to be incorporated allows 50 W of heat to be lifted from a 50 K cold tip with a subsequent rejection to a 300 K ambient temperature. Further important design features are the planned low weight and small diameter, as well as the ability to withstand the required 6800 RPM about its central axis. The last is a necessity to be able to incorporate the cryogenic cooler into the motor design, such that the motor will interface with the aircraft as essentially a normal-conducting machine. An overview of the intended cry-ocooler performance is also given in Table A.7.

Finally, a quick summary of the commonly assumed future electric motor performance is given in Table A.8. It can be seen that while the predictions pertaining to efficiency are relatively similar, the estimations on the development in specific power are vastly different. Lents at al. predict a specific power for the year 2026 that is twice as high as what Rafaelli and Chung predict for the year 2035. This underlines the inaccuracy introduced in any vehicle study that assess the potential of a future concept based on assumed electrical component performances.

Table A.8: Overview of predicted development in electric motor specific power and efficiency for various timeframes, based on selected research papers.

Parameter	Unit	Rafaelli & Chung [15]	Lents et al. [14]	Kuhn et al. [38]		
horizon/year		2035	10 year	20 year	2035+	HTS [1]
$p_{specific}$	$kW \cdot kg^{-1}$	6.3 [2]	13.1	26.3	20	40
Efficiency	-	98%	96%	98%	99%	-

[1] No timeframe provided for HTS technology prediction
[2] based on torque density of 12 Nm/kg provided by Rafaelli and Chung, converted using Equation (A.10)

A.2.3. Electric Power Management and Distribution

The component PMAD is usually a simplification of multiple electric components working as a unit to regulate the flow of the electric power through the distribution network. It controls when to use the various electric components and is thus responsible for executing the pre-defined power and energy control strategy, as it is very unlikely that hybrid-propulsion systems will be designed such, that the pilot has to manually set the power share between the conventional engine and the electric motor. To control the power output of the electric motor, the input voltage is varied, as mentioned in Appendix A.2.2. These variation in motor input voltage are set by the PMAD system [50].

For a (partially-) electric vehicle concept in the conceptual phase, the design of the PMAD focusses on the "voltage type (AC or DC), voltage level, and conductor materials [...] to match safety requirements at minimum weight"[12]. These consideration also include that the overall powertrain architecture incorporates sufficient redundancy. The PMAD can be impacted by the design of the redundancy because it has to also manage the re-routing of power in case of failure. For example, if the subsystems of the aircraft are also electrically powered, a possible choice for redundancy might be to cross-link the different system levels (operating at different voltages), instead of installing a redundant network for each level [62].

To enable the use of electrical power for propulsion purposes, MW level power electronics are required. Modern components have replaced silicon with a silicon carbide (SiC), which provides some important advantages over the earlier silicon devices. The efficiency is increased, the components have better high voltage performance characteristics, and the technology is more reliable [8]. All three advantages are very important for the electrification of aircraft propulsion, by either enabling the introduction of electric propulsion or by guaranteeing the safety of this new approach. An example of the device that is used for the PMAD in the CeLiner concept is a cryogenic Solid-State Power Controller (SSPC). These SSPC devices were incorporated to provide two functions: switching and fault detection. Switching allows to connect and disconnect a load from the distribution network, and fault detection identifies if faulty currents occur within a system component.

Normal-conducting SSPCs are already relatively efficient and light, and are well developed for ground applications. Typical efficiencies are around 95% with typical specific powers for traction applications of around $8\,kW \cdot kg^{-1}$. The highest specific power according to Brown is around $16.4\,kW \cdot kg^{-1}$ [33]. Brown also stated that cryogenic cooling of power controllers would allow better performance. A goal of $33\,kW \cdot kg^{-1}$ at 99.8% efficiency for the controller was set in a baseline study. Including the corresponding cryo-cooler, a specific power of $16.4\,kW \cdot kg^{-1}$ at 98.8% efficiency was stated. Further predictions based on models developed by the NASA SBIR study, estimate a specific power of $25\,kW \cdot kg^{-1}$ for the combined controller–cryo-cooler system, with controller efficiencies around 99.5%.

Power Distribution & System Operating Voltage

The power distribution on board of an aircraft, especially the modern MEA or future concepts including electric propulsion, is one of the major challenges in electric aircraft design. The difficulty lies in minimising the losses during transmission of large amounts of power without compromising on safety. According to the Committee of the National Academy of Sciences [8], a distribution system using $\pm 270\,V$ AC($540\,V$ peak-to-peak) is the limit for the foreseeable future, which is stipulated based on a physical phenomenon referred to as Paschen's curve limit.

Paschen's curve, also called Paschen's law, "describes the breakdown voltage in a homogeneous electric field depending on the gas pressure and the electrode spacing"[25]. Essentially, it states the maximum safe voltage for a conductor placed in a certain medium at a certain distance to the nearest conducting material. For

voltages above Paschen's curve, the risk of electric arcing exists. Figure A.17 shows the variation in breakdown voltage for various distances within dry air. Since the medium is not changed, a variation in the pressure-distance (p d [Pa m]) corresponds to an increase in spacing. A change of medium, either by submerging the conductor or simply by changes in air density due to increasing altitude, will change the curve, but the general shape will remain. As can be seen for dry air, the maximum allowable voltage without any danger of electric arcing is 327 V DC, which corresponds to a sinusoidal RMS voltage of 231 V AC [25].

To minimise losses however, it is beneficial to increase the system voltage above the current limit into the region of potential electric arcing. This requires the introduction of new types of insulation systems and electrical conductor spacing rules and practices. Furthermore, MW-class circuit breakers required for the circuit protection of an electric propulsion system currently only exist for ground-based applications. For an adaptation to use on aircraft, it has to be verified that the requirements for weight and volume, voltage, safety, etc. are fulfilled. According to the Committee of the National Association of Sciences [8], there are currently no ongoing developments for MW-level circuit protection devices for aircraft power systems.

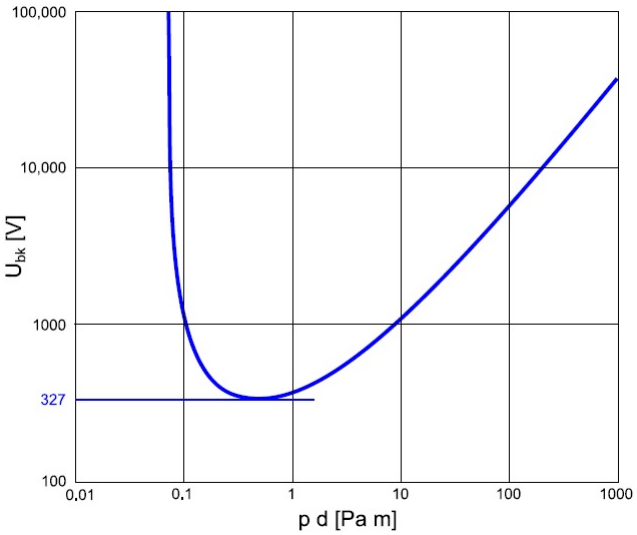

Figure A.17: Illustration of Paschen's curve for a dry air environment, relating the breakdown voltage u_{bk} to the pressure-gap length product pd.

Source: [25]

Another important aspect to consider in the power distribution system is redundancy. The distribution system is essential for the aircrafts airworthiness, as a failure in the distribution system could lead to an "all engines out" situation (depending on the propulsion architecture). Applying current CS 25 requirements to electrical power distribution for propulsion, the requirement for a standard configuration, twin-engine aircraft dictates at least two independent power lines, with each line being capable of transmitting sufficient power for continued flight and safe landing [25]. The redundancy requirement is obviously increasing system mass, and Isikveren et al. [62] thus proposed an integrated redundancy approach for a universally-electric system architecture. In their proposed universally-electric system architecture, the distribution network can be categorised into three distinct levels, each operating at different voltages and transmitting different power levels. These levels correspond to a high voltage – high power level for aircraft propulsion, a medium voltage – medium power level for on-board consumer systems, and a low voltage – low power level for the avionics equipment. Their proposal for integrated redundancy is to cross-link these levels, enabling a power transfer via one of the other system levels in case of failure. This approach eliminates the need for a dedicated redundancy system for each of the distribution system levels.

The system operating voltage is an important design parameter and aspects to consider when choosing a voltage level are: the stead state regulation; the transient behaviour; the fault tolerance and recovery; and the distortion and harmonics. A fundamental problem with electrical systems in aviation is, that the governing standards have not been designed to optimise the system. Current certified voltage levels for aircraft are still based on early airplanes, which used car batteries whose cell voltages were multiples of 6 V, resulting in the initial choice for aircraft voltage of 24 V DC [63].

The selection of the nominal system voltage type and level is usually based on the resulting system mass and the expected system losses [63]. Generally, opposed to the high voltage AC distribution used in terrestrial power transmission, a DC voltage system is stated as the more beneficial choice for power transmission in aircraft. This is due to DC systems minimal Electro-magnetic Interference (EMI) and the compatibility with other devices such as batteries and fuel cells without the need of a converter [62]. A further advantage over an AC network connecting AC devices is that no synchronisation of the different components is required. In case the AC power output of the generator is transmitted as AC electricity to the motor, the phases of those machines have to be synchronised. This effectively couples the systems, introducing a dependency of component speeds. Finally, for normal-conducting wires, DC networks result in lower conductor weights, due to the larger required cable cross-sections of AC voltage [25].

PMAD Performance Assumptions in Literature

The Committee of the National Academy of Sciences published some useful data about the performance of contemporary silicon-based power electronics as well as expected performance of silicon carbide (SiC) devices in the next 20 years. Current silicon-based electronics have a specific power of about 2.2 kW/kg, with the integral circuit protection limited to 25 A at 270 V DC (corresponding to 7 kW). For higher powered circuits, mechanical breakers are required which are capable of handling up to 500 A at 270 V DC (corresponding to 135 kW). Future SiC devices are expected to achieve a specific power of $9\,\mathrm{kW\cdot kg^{-1}}$ with an integral circuit protection capability of 200 A at ±270 V AC (essentially 540 V peak-to-peak; resulting in a power capability of 108 kW). Using mechanical breakers, this can be extended to 1000 A at ±270 V AC (effectively 540 kW) [8].
Advanced performance assumptions using superconducting PMAD components are detailed by Isikveren et al. [62]. This paper estimates converter and controller specific powers of $20\,\mathrm{kW\cdot kg^{-1}}$ at 99.5% efficiency, with Solid-State Power Controllers (SSPC) achieving $44\,\mathrm{kW\cdot kg^{-1}}$ at 99.5% efficiency. Finally, Table A.9 shows the goals of various research efforts on the future power electronics performance. It can be seen, that there is little consistency in the provided data with the U.S. Air Force goals being much lower than for Ohio State University, despite being considered for a much larger horizon. The column "N.A.o.S." presents what the Committee of the National Academy of Sciences considers realistic component performance within the next 20 years.

Table A.9: Overview of research goals for power electronics for various institutions. Adapted from [8]

Parameters	Unit	NASA		U.S. Air Force	Ohio State Univ.	McLaren [1]	N.A.o.S.
horizon		10 year	15 year	20 year	5 year	-	20 year
Specific Power	$\mathrm{kW\cdot kg^{-1}}$	15.0	19.0	5.0	23.0	50.0	~ 9.0
Capability	MW	1–3	5–10	1.0	2.0	0.25	~ 1–3

[1] Data relates to automotive application

Power Converters and Inverters/Rectifiers

The most common components typically comprising the power management and distribution system are power converters, inverters, and rectifiers. Power converters change the voltage of the incoming transmitted power to a new desired level. This change is often required because electrical devices such as motors or non-propulsive subsystems operate at a different voltage than what is required for optimal power transmission. Because the conversion cannot be perfect, a device efficiency is defined as the ratio of power output to power input (computed via the incoming and outgoing combination of voltage and current) [37]. The component performance is relatively high, with existing liquid cooled power converters achieving around $8\,\mathrm{kW\cdot kg^{-1}}$, but SoA technology would allow specific powers as high as $26\,\mathrm{kW\cdot kg^{-1}}$ according to Armstrong et al. [64]. This assumption is validated by Raffaelli and Chung, who assumed a specific power of $25\,\mathrm{kW\cdot kg^{-1}}$ at 99% efficiency. The typical step of introducing superconducting technology was also applied to power converters, and while the expected power densities are estimated at $40\,\mathrm{kW\cdot kg^{-1}}$, the efforts are still in early stages of development [64].
Power converters are a component that is often used in combination with inverters/rectifiers to achieve the required voltage levels of the connected components. Inverters and rectifiers are essentially performing the same operation but in reverse. While an inverter converts DC to AC electricity, rectifiers convert AC to DC. Both components are essential for AC–DC combined networks, as is favoured for power distribution on electrified propulsion aircraft using a series architecture (AC power generation, DC power transmission, AC or DC power usage). Current inverters/rectifiers have specific powers up to $11\,\mathrm{kW\cdot kg^{-1}}$ [25] at only 90% efficiency [17], however the introduction of semiconductor materials and cryogenic cooling is expected to yield a factor three weight reduction [12].
The AATT projects HGEP is funding "investments in 1 MW sized inverters with the objective to design, build, and test a technology demonstrator for high efficiency/high specific power MW-class inverter intended to meet the anticipated needs of aircraft electric propulsion drives" [9]. The developed configuration uses a 1000 V DC bus input and produces a three phase AC output, being compatible with a range of electric motor designs (PM, induction, switched reluctance, etc.). While sized for around 1 MW, the evaluation of the

scalability to 10 MW is to be assessed as well. An overview of the targeted inverter performance is given in Table A.10.

Table A.10: Performance targets of the AATT HGEP MW-class inverter design, adapted from [9].

	Specific power	Efficiency
Minimum	$12\,\mathrm{kW \cdot kg^{-1}}$	98%
Goal	$19\,\mathrm{kW \cdot kg^{-1}}$	99%
Stretch	$25\,\mathrm{kW \cdot kg^{-1}}$	99.5%

A.2.4. Power Transmission

Power transmission is achieved via electrical cables that transport current at a given voltage between the devices [17]. Since the move towards electrification in aircraft started only recently, there are no methods for high power conductor modelling available in common aircraft design literature [25]. The choice of cable type is typically based on the highest current occurring in the system, which has to be below the maximum allowable current of the cable. Since the voltage is dictated by the choice of system voltage discussed earlier, the cables are sized to carry the required current at minimum weight. As stated by Armstrong et al. [64], the optimal voltage of a system has to be determined by considering all components including the wires. An increase in nominal voltage can lead to significant weight savings in the cables, as was demonstrated by Cinar et al. [50]. A doubling of the system voltage from 270 V to 540 V allowed a different choice of cable due to the lower occurring currents. This in turn resulted in a reduction in cable weight of 38.7%. The weight of the cables of a power distribution system in conceptual design is usually calculated using the expected required length and the cables linear density in $\mathrm{kg \cdot m^{-1}}$. It should be stressed, that in the determination of the length the available paths and the requirements pertaining to redundancy have to be considered, usually requiring an increase in total cable length by a factor 2 or 3.

Normalconducting Cables

A simple model to estimate the weight introduced due to normalconducting electrical transmission cables was proposed by Sgueglia et al. [17]. The model requires three cable performance assumptions: the max. allowable current, the operating voltage, and the linear density. In the published paper, the following values were stated for the required assumptions: 360 A maximum current at 2160 V and a cable linear density of $1.0\,\mathrm{kg \cdot m^{-1}}$. From the required transmission power and the assumed nominal voltage, the transmission current is calculated. The required number of cables is then determined via this transmission current and the defined max. allowable current in the cable via Equation (A.16). Using the location of the other system components (battery, electric motor, etc.) the total required cable length is calculated, including the redundancy factor as required. Finally, the total cable mass is determined using Equation (A.17).

$$N_{cable} = \left\lceil \frac{I}{I_{max}} \right\rceil \tag{A.16}$$

$$m_{cable} = N_{cable} \cdot \rho_{cable} \cdot L_{cable} \tag{A.17}$$

The model additionally includes a simple percentage based estimation of weight increase from cable installation and the required health monitoring system (HMS). The stated impact according to Sgueglia et al. was given as a 30% increase due to installation and a further 5% increase for the HMS.

A much more detailed but still computationally lightweight model was presented in the PhD thesis of Stückl [25]. The model was presented using Copper and Aluminium, being the most common conductor materials. Copper excels in terms of low resistance, having the highest conductivity of all technically relevant materials at $\sigma = 56\,\mathrm{m \cdot \Omega^{-1} \cdot mm^{-2}}$. However, copper has a relatively high specific weight at $8.9\,\mathrm{g \cdot cm^{-3}}$. Aluminium as a conductor exhibits the opposite excellence, having a conductivity of only $\sigma = 35\,\mathrm{m \cdot \Omega^{-1} \cdot mm^{-2}}$, but also being significantly lighter at a specific weight of $2.8\,\mathrm{g \cdot cm^{-3}}$. Traditionally, copper has been wider spread due to benefits in ductility, corrosive characteristics, and smaller cross-sections. However, with increasing

electrification of aircraft, weight reduction efforts are putting more importance on aluminium as conductor material of DC wires [25].
The model of Stückl assumes that the cable cross-section of normal-conducting DC cables is mainly dependent on the current load. Ohmic losses within the cable (depending on ohmic resistance of material and the square of the current) generate heat. Once this heat generation is in equilibrium with the heat dissipation to the surroundings, the cable has reached its stable operating temperature. Based on a fixed cable material and cross-section a maximum operating temperature can thus be used to define the limiting current load and current density.
To build a simple model for high power/high voltage normal-conducting cables existing DIN norms were taken as a basis. The cables modelled consist of a circular conductor (in the provided example copper or aluminium), an electric insulation layer (cross-linked polyethylene (XLPE) or ethylene propylene rubber (EPR/HEPR) for better fire protection), and a protective covering sheath (PVC or Ethylene-vinyl acetate (EVA), again for improved fire protection). Stückl stated that "only marginal difference in specific cable weight are found"[25] when choosing the improved fire protection materials. The model computes the final cable specific mass by determining the individual component size and mass from the inside out, based on a provided regression of variation in conductor area with current load. It does require more input data than the model from Sgueglia et al., but all required data is either a material property or a characteristic of the power distribution network such as the voltage.
One important aspect of Stückls model is that it incorporated the effect of increasing altitude. Using a simple altitude-depending correction factor, the current used in the cable component sizing is correct to represent the reduction in maximum allowable current rating. Finally, the losses in the cables can be determined via the conductor resistivity. Considering that the resistivity is temperature depending, a simple calculation using a temperature coefficient yields the resistivity corresponding to the operating temperature.

Superconducting Cables
As with any previously discussed electric component, a popular approach to decrease the occurring losses and reduce the cable weight is the introduction of superconducting technology. According to Davies et al., data from Armstrong et al. [64] shows that "the expected power densities associated with superconducting cables and protection devices are greater than the corresponding power densities associated with with superconducting generators and propulsion motors"[13]. Considering the discussed expected power densities of electric machines of 10–16 $\mathrm{kW \cdot kg^{-1}}$ (see Table A.6), this would result in a very lightweight distribution network, provided the required cryogenic cooling devices are not too heavy. These high power densities are achieved because superconducting cables enable DC power transmission with zero ohmic losses. Because no losses occur, superconducting cables are able to "withstand enormous current densities compared to conventional conductor materials"[25], resulting in significantly smaller conductors cross-sections and thus potential weight savings. With the recent advances in HTS materials, a typical superconducting cable operates at around 77 K, where a cryogenic cooling device has to continuously remove a certain amount of heat generated by imperfections in the thermal insulation of the cable and losses introduced at the terminals connecting the superconducting cable to a normal-conducting device [25].
A simple model to estimate the losses of a SoA 77 K HTS cable are presented by Stückl in [25]. The cryostat losses due to imperfect insulation is estimated to be around $0.5\,\mathrm{W \cdot m^{-1}}$, which is based on a paper by Haugan et al. The losses occurring in the terminals are distinguished in a current-dependent and a constant part, as shown in Equation (A.18). For each current lead (two at each terminal for a standard co-axial cable) a heat load of $45\,\mathrm{W \cdot kA^{-1}}$ is expected, based on a 77 K HTS cable and around 300 K ambient temperature. The additional 200 W loss are additional isolation losses in the terminal.

$$Q_{term}[\mathrm{W}] = 45[\mathrm{W/kA}] \cdot N_e \cdot I_e[\mathrm{kA}] + 200[\mathrm{W}] \tag{A.18}$$

Today's SoA superconducting cable weight is dominated by the masses of the thermal isolation and the cryogenic cooling medium. The highest achieved specific masses are around $10\,\mathrm{kg \cdot m^{-1}}$ for ground based applications. Optimising superconducting cables for aircraft applications is expected to improve on this specific mass. According to Stückl, Brown et al. stated a goal of $5\,\mathrm{kg \cdot m^{-1}}$ and also presented a conceptual 270 V DC HTS cable design aboard aircraft, again featuring $5\,\mathrm{kg \cdot m^{-1}}$ [25].

A.2.5. Thermal Management System

With the increasing amounts of on-board power of modern aircraft and the aspired introduction of electrified propulsion systems, the ability of the aircraft to manage heat will be an essential part of the design process.

The design of the Thermal Management System (TMS) is part of the electrical system sizing process, because it has to be capable of removing all generated heat at minimum weight, but has itself a power demand to be considered in the offtakes [8].
A TMS is required for both normal- and superconducting system architectures. In a conventional internal combustion engine, the waste heat is expelled in the exhaust, often even contributing to the produced thrust. Waste heat of electrical components on the other hand radiate heat locally, which is then absorbed by the surrounding structure and equipment, requiring active control. Superconducting networks do not generate heat because the electric losses are effectively zero, however the conductors have to be continuously cooled to operate below their critical condition, again requiring an active thermal management [23, 61].
Another difference between conventional ICE and electrified propulsion that impacts the design of the thermal management relates to the component hot spot temperatures. Opposed to the conventional turbine engines, hot spot temperatures of electric components are significantly lower. Electrical machines are typically in the range of 105–220 °C and common converters even as low as 85–150 °C. The usual approach to cooling electrical components is via air or liquid (oil or water/glycol) cooling. These cooling cycles require a minimum temperature difference of 10–50 °C, for the hottest day condition this corresponds to the system collecting heat from 75–170 °C and rejecting it to 60 °C. Generally, two different heat sinks can be considered: an ambient air stream or the stored fuel. Using the air stream as a heat sink will result in an increase in overall drag, whereas the stored fuel is a finite sink which in some designs is already close to its maximum heat capacity [61].
A few examples of TMS from different vehicle studies are presented by Brelje and Martins in [23]. The TMS of the ECO-150R was sized to remove 1.5 MW of heat at its critical TOC condition. Employing a recirculating liquid cooling loop with a ram-air radiator, the design used the heated air to generate thrust via the Meredith effect (as used on the P-51 Mustang). The resulting system was found to be responsible for 2-3% of the generated cruise thrust with the TMS accounting for 20% of the overall power electronics and motor mass. Two recent NASA studies (on the X-57 and the STARC-ABL) state the TMS mass as 5% and 6% of the overall power electronics weight respectively. In the former case, this includes the mass of the installed batteries, whereas the latter excludes the battery weight.
Finally, a parallel hybrid-electric vehicle study by Lents et al. [14] contains a detailed overview of their approach for a conceptual TMS design. Based on an assumed TMS architecture, the study performed a detailed analysis of the heat and power transfer, as well as the resulting component temperatures. The assumed architecture consisted of two cooling loops: a coolant loop rejecting heat via a ram-air cooler to provide temperature regulation for the battery and motor drive; and an oil loop removing the propulsion system heat loads. The oil loop operated using two heat sinks. Initial heat rejection occurred into the stored fuel with the remaining heat being rejected at an air oil cooler in the fan air flow. The initial rejection into the fuel presented two advantages. It increased the engine efficiency and reduced the required air oil cooler size, thus limiting the adverse impact of the TMS. Using the presented TMS masses, the provided required power output of the battery, and the component efficiencies, the corresponding specific powers of the TMS were determined. According to Lents et al., the TMS specific powers correspond to 14.26 $\mathrm{kW \cdot kg^{-1}}$, 36.6 $\mathrm{kW \cdot kg^{-1}}$, and 64.22 $\mathrm{kW \cdot kg^{-1}}$ for current, 10 year, and 20 year time horizons.